TECHNISCHE UNIVERSITÄT MÜNCHEN
Lehrstuhl für Technische Chemie II

Investigation into the reaction of toluene methylation to p-xylene over acidic zeolites

John Hyung-Joon Ahn

Vollständiger Abdruck der von der Fakultät für Chemie der Technischen Universität München zur Erlangung des akademischen Grades eines

Doktor-Ingenieur (Dr.-Ing.)

genehmigten Dissertation.

Vorsitzende: Univ.-Prof. Dr. Moniek Tromp

Prüfer der Dissertation:

1. Univ. -Prof. Dr. Johannes A. Lercher
2. Univ. -Prof. Dr.-Ing. Hartmut Spliethoff

Die Dissertation wurde am 04.04.2013 bei der Technischen Universität München eingereicht und durch die Fakultät für Chemie am 21.06.2013 angenommen.

"We imagine that when we are thrown out of our accustomed grooves that all is lost, but it is only then that what is new and good begins. While there is life there is happiness. There is much, so much before us. I say this to you."

Pierre, War and Peace

Leo Tolstoy

(1828-1910)

"No, I don't like work. I had rather laze about and think of all the fine things that can be done. I don't like work—no man does—but I like what is in the work, the chance to find yourself. Your own reality—for yourself, not for others—what no other man can ever know. They can only see the mere show, and never can tell what it really means."

Heart of Darkness
Joseph Conrad
(1857-1924)

Acknowledgements

So finally, I see a light at the end of the tunnel. After all the thinking and sweating, breaking and fixing, reading and writing, that were filled with many joys and pains, satisfactions and disappointments, smiles and cusses in the midst of this ugly green-grey building, during the early mornings and late nights, cold winter snowstorms and refreshing summer thunderstorms (I found out that it is a bit less sunnier here in Germany than the golden California), over many sunsets and sunrises, I have arrived, at last. From the beloved and comfortable place of the sunshine State that I left behind to this strange and foreign place that I came to take on the scientific challenges and to develop into whom I was born to become... The journey of my life somehow led me into this unique and unusual path to TC II (Lehrstuhl für Technische Chemie II) of TUM (Technische Universität München) and has now come to an end; it is time again to continue onto another road, a new, unknown and an exciting chapter of my life. For all these years that I spent in TC II of TUM, I am deeply humbled and grateful for the people that enabled me to build and mature my character into whom I am today. With that being said, I would like now to thank:

Johannes Lercher for giving me an once-in-a-lifetime opportunity to be part of this world-class laboratory. He has provided me with scientific freedom and the almost unlimited resources that I needed to excel on a challenging research project.

Andy Jentys for supervising this project and helping me to write more clearly than I was able to.

Robin Kolvenbach for helpful technical discussions and support throughout the project. I was able to learn many valuable things about diffusion from Robin, whom I would consider to be one of the top experts in his field.

Oliver Gutiérrez for his friendship, encouragements, helpful technical and life discussions, and all the times that were spent with and for me. It is hard to imagine what my life in Germany and in TC II would have been like, without my fellow “American”. Also Minerva and our Hilda (whom I befriended, I think and hope, since she was 6 days old) for extra joy and friendship that they provided us with.

Anastasia Pashigreva, Bo Peng and Jeongnam Kim for their friendship, being my travelling companions, giving me food, love, souvenirs and their time spent together. Without these special friends, I would have found that my life in München much less fun.

My elite officemates: Monica Pop, Jennifer Hein, Stefanie Reiner, Robin Kolvenbach and Stefan Schallmoser for precious times that we spent together inside 46 303. They were a young, energetic and fun group of people, and we shared together (intentionally or unintentionally) many of the joys, frustrations, sweet and bitter things of our everyday life experiences in TC II. I felt privileged to be a member of this lively office and to share my precious two or three years of life with them.

My diverse and interesting lunch-mates over the years (some of the vivid memories written inside parenthesis): André Santos (always leftover food on the Mensa trays), Murat Küçükdişli (I copied and pasted his name from the Facebook), André Van Veen (discussion about how Europe is better than the second-class America), Erika Ember, Elena Wuttke (sorry that Mensa food was so nasty-tasting), Francisco Gonzalez, Marie-Cruz Sanchez, for interesting conversations and listening to my silly humors. It was good to have friends to eat and enjoy with.

Some of the other kind and generous colleagues that I interacted with: Xuebing Li (found me a nice place to live in Garching), Daniela Hartmann (picked me up from Neufahrn S-Bahn station on my first arrival in Germany), Yongzhong Zhu and Michael Salzinger (gave me the momentum to start with zeolite synthesis), Despina Tzoulaki (swapped our places in LSAC-TC II of TUM), Sarah Maier, Sonja Wyrzgol, Baoxiang Peng, Hui Shi, Xianyong Sun (helpful discussions in methylation chemistry), Linus Schulz (for the shooting, which evolved somehow into a poking game because he always lost), Elizabeth Hanrieder (had a great patience to talk in German with me), Sebastian Müller (allowed me to use his “state-of-the-art” Berty reactor), Wenji Song, Maximilian Hahn (only one who spoke proper English in the group) and Stanislav Kasakov.

Our talented and all-knowing secretaries and technicians: Helen Lemmermöhle, Stefanie Maier, Karen Schulz, and Bettina Federmann for helping and supporting me with various paper works (some unnecessary, but forced by law) in *unserem* full-of-bureaucracy Deutschland over the years. Xaver Hecht for his demonstration of almost magical “Chuck-

Norris" like skills in the laboratories (he unfortunately could not cure cancer with his tears nor could he cut scissors with papers) and Martin Neukamm for consistently providing me wonderful zeolite images and their corresponding elemental compositions. These were the people behind the scenes of our everyday life in TC II and they deserve big thanks from me.

The valuable mentors during my research career: Enrique Iglesia and Mirosław Derewiński. My research career started under Enrique's supervision and it was in his lab, that I began to develop and mature into a scientist that I am today. I am proud to say that I was part of LSAC laboratory and that he was my great mentor. He was also the one who has recommended me to Johannes and I was able to begin my training at TC II in TUM as a result (and also my short-lived career at Symyx). I began with zero zeolite synthesis and modification background as I came to TC II and through Mirek's boundless optimism and countless encouragements, I was able to learn few things about zeolite synthesis and ultimately, was able to succeed here. I am very grateful for the contribution of his wisdom and philosophy into my life.

Finally my family for always supporting and loving me as who I am. Without them, I do not know where I would be in my life. All in all, thanks.

John H. Ahn

March 2013

Abstract

The reaction of toluene methylation was investigated over acidic zeolites to better understand limitations of this reaction and to improve the catalyst yield and selectivity towards p-xylene. A significant fraction of methanol was utilized to form products other than xylenes, e.g., light hydrocarbons, tri- and tetramethylbenzenes, during the reaction of toluene methylation, because the aromatic products of toluene methylation were readily methylated further inside the zeolite pores. The hierarchical materials derived from MFI (H-ZSM-5) by a series of modifications, i.e., desilication, dealumination and chemical liquid deposition of tetraethyl orthosilicate (TEOS) onto the zeolite surface, increased the toluene consumption rate (per Brønsted acid site) and p-xylene selectivity simultaneously. The reaction rate increased because desilication/dealumination decreased the diffusion length and consequently increased the diffusivity of reactant and product molecules. The p-xylene selectivity increased because deposition of TEOS increased the diffusivity of p-xylene, while it decreased for the bulkier o- and m- xylene isomers. This differences in diffusivities of xylenes played more significant role in determining p-xylene selectivity as the reactions became faster at higher reaction temperatures.

Die zeolithkatalysierte Toluolmethylierungsreaktion wurde hinsichtlich der Verbesserung der Ausbeute und der Selektivität untersucht und insbesonders die reaktionslimitierenden Faktoren evaluiert. Es konnte gezeigt werden, dass ein signifikanter Anteil des Methanols in Nebenprodukte, z.B. leichte Kohlenwasserstoffe, Tri- und Tetrabenzolisomere, umgesetzt wurde, da die primären Produkte der Toluolmethylierung (Xylole) innerhalb der Pore weiter methyliert wurden. Durch postsynthetische Modifizierung der zeolithischen Katalysatoren, durch Desilizierung, Dealumierung und Abscheidung von Tetraethylorthosilikat auf der äußeren Oberfläche, konnte eine Steigerung der Reaktionsrate (pro Brønsted Säurezentrum) als auch der p-Xylol Selektivität erreicht werden. Die Steigerung der Reaktionsrate kann hierbei auf die Verkürzung der Diffusionswege sowohl für die Reaktant, als auch für die Produktmoleküle zurückgeführt werden. Die Erhöhung der p-Xylol Selektivität wurde durch eine Optimierung der Transporteigenschaften durch die Oberflächenmodifizierung mit Tetraethylorthosilikat hervorgerufen, wobei die Diffusivität von p-Xylol selektiv erhöht und jene von o- und m-Xylol verringert wurde.

Table of Contents

Chapter 4:

Influence of the reaction temperature on p-xylene selectivity in toluene methylation over medium pore-sized zeolites.....107

Chapter 5:

Chapter 1

Introduction

1.1. Introduction

Aromatics are valuable raw materials for the chemical and petrochemical industries. The global consumption of aromatic molecules is more than 85 million tons per year (as of 2006) [1]. The primary sources of these compounds are produced from catalytic reforming or thermal cracking of naphtha [2,3]. Among the aromatics, benzene, toluene and xylenes (BTX) are the most important precursors for chemical commodities, e.g., for polyesters and plasticizers. Some of the most relevant intermediates and products from BTX are shown in Figure 1.1 [2].

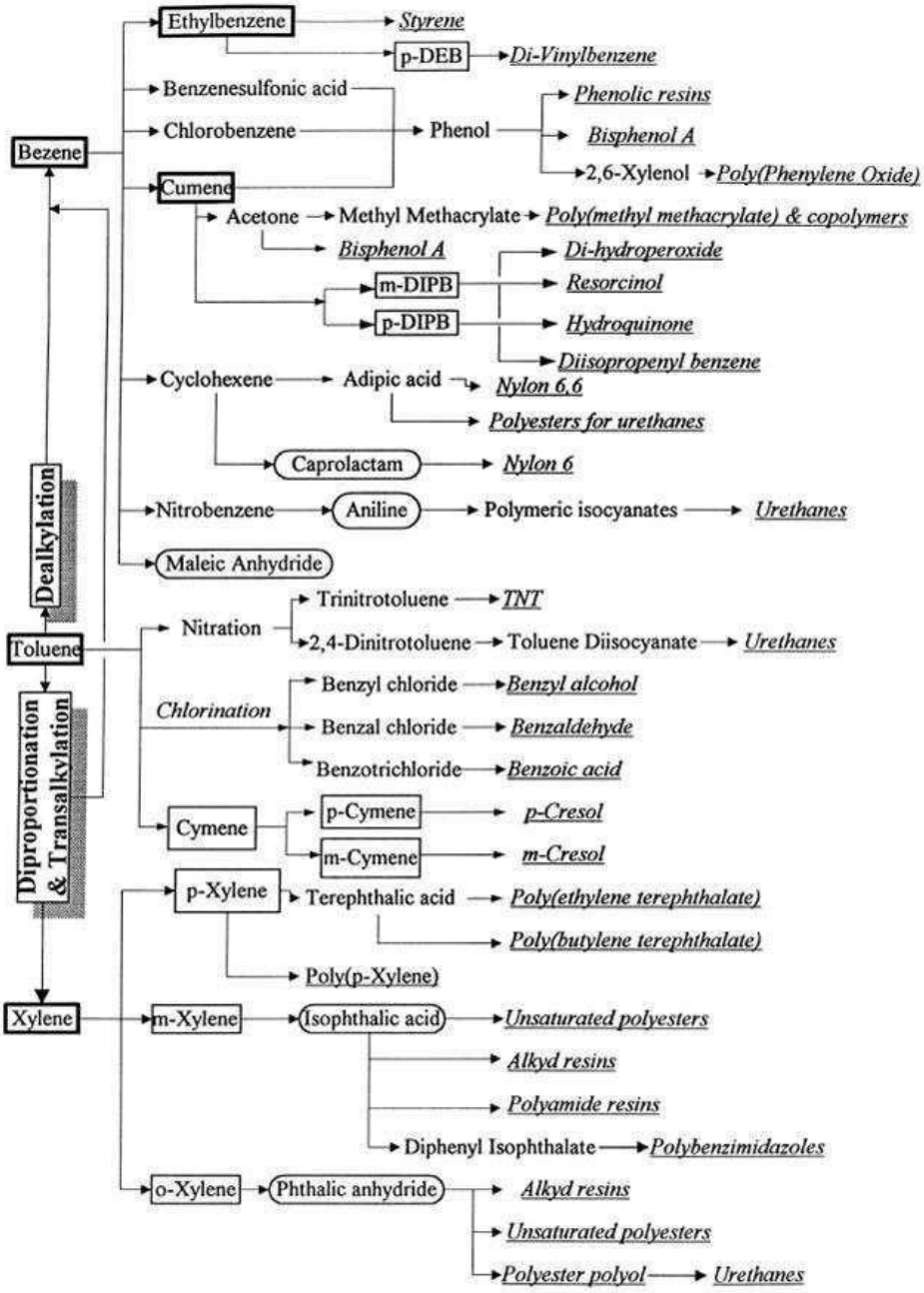

Figure 1.1: Transformation of benzene, toluene and xylenes into various chemical commodities [2].

The global market production and demand of BTX indicates that toluene is produced in excess relative to the market demand (Figure 1.2 [2]). The conversion of the surplus toluene into benzene and xylenes by disproportionation (to produce benzene and xylene) [4,5,6] or methylation with methanol (to produce xylenes) [7,8,9] is therefore a potential way to balance the deficiency of aromatic production in chemical industries. Methylation of toluene with methanol, however, could be an even more attractive process than disproportionation of toluene because methylation can be operated at lower temperatures than disproportionation [10,11] and moreover, methanol can be synthesized from the widely available and abundant natural gas (especially by the emergence of new extraction technologies, e.g., fracking, to recover natural gas from unconventional sources). A potential increase in methanol production for variety of uses in the chemical industry is also expected in the future [12,13] (see also Figure 1.3 [14]).

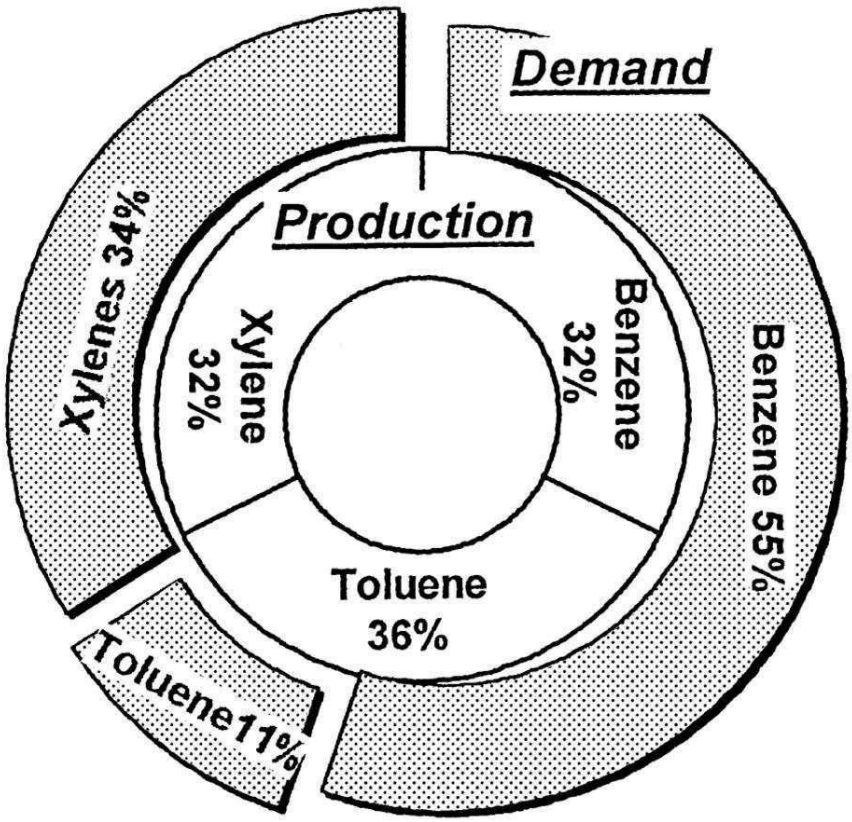

Figure 1.2: Worldwide production and demand of benzene, toluene and xylenes [2].

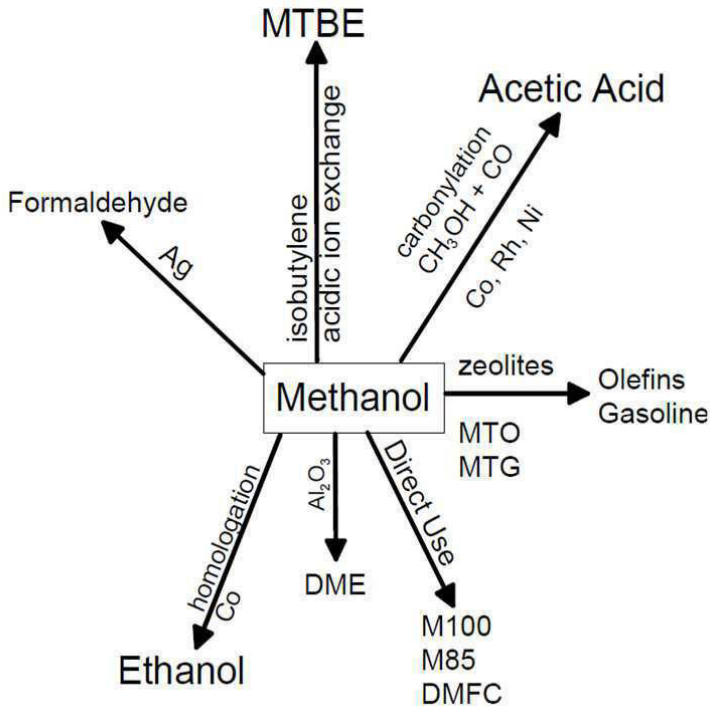

Figure 1.3: Possible transformation of methanol into chemical intermediates and products [14].

Among the three xylene isomers, p-xylene has the highest demand in industry, i.e., ~ 26 million tons per year [15] or ~ 80 % of the xylenes (Figure 1.4), as the precursor for the production of terephthalic acid (Scheme 1.1, via oxidation of the two methyl groups) [2,15]. Polyethylene terephthalate (PETE), a material used for the production of plastics (e.g., for soft drink bottles), can then be produced from terephthalic acid by polymerization with ethylene glycol (Scheme 1.1) [2,15]. Unfortunately, m-xylene is thermodynamically favored and is typically the main product from the major xylene production routes [3,15] (Figure 1.4, close to thermodynamic distribution, i.e., ortho : meta : para xylene ratio of ~22 : 53 : 25 at 650 K [16]).

The boiling points of xylenes are very similar, whereas the differences in melting points between the isomers differ by more than 20 K (Table 1.1). Consequently, more expensive and energy intensive processes, e.g., adsorption or crystallization processes, are required for xylene separation [17], or alternatively, highly para-selective catalysts would be necessary to avoid the separation step. Some of the ways to increase the selectivity to p-xylene in the toluene methylation reported in the literature are increasing the zeolite crystal size [10,11,18], impregnation of the zeolite with phosphorous or boron compounds [7,10,19,20], or chemical

vapor (CVD) [21,22] or liquid deposition (CLD) [23,24,25] of tetra-alkyl orthosilicate onto the zeolite surfaces.

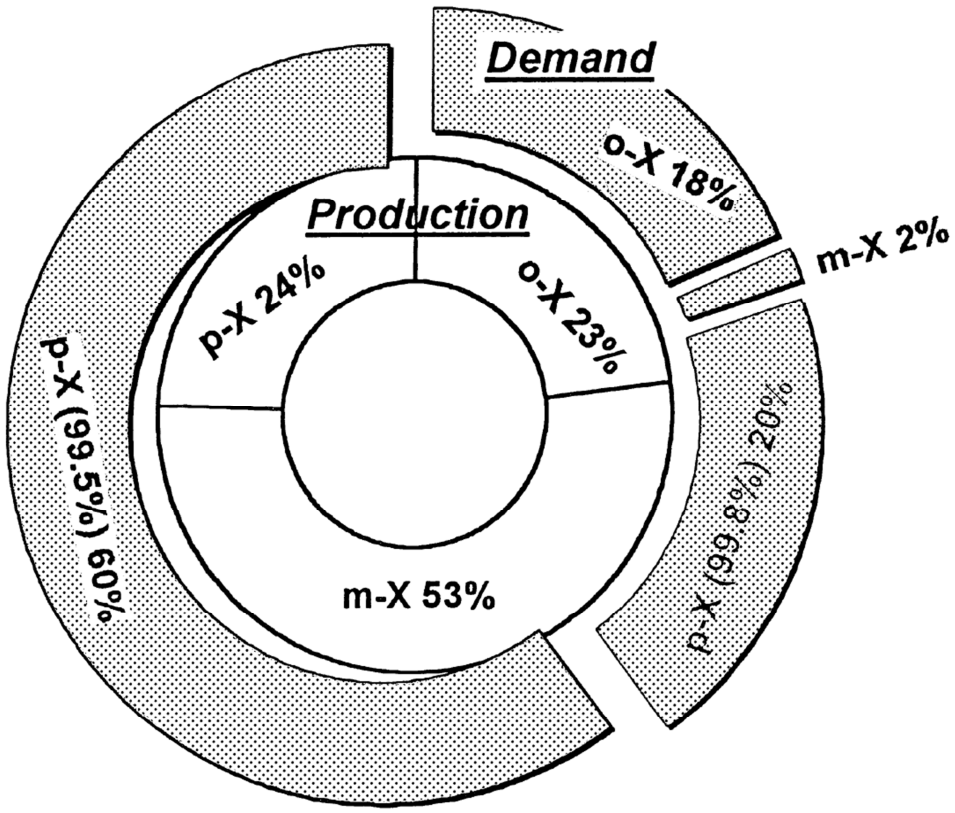

Figure 1.4: Worldwide production and demand of p-, m- and o-xylenes [2].

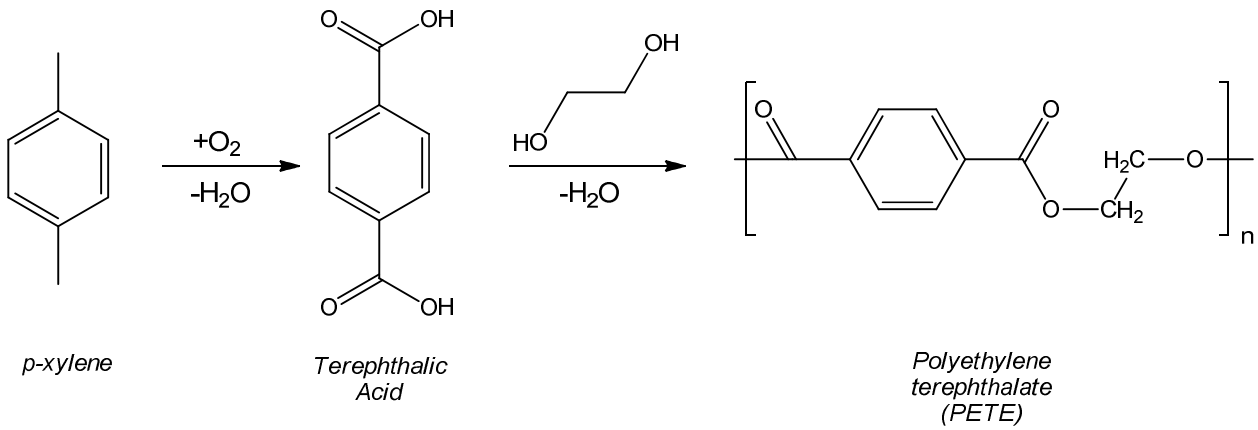

Scheme 1.1: Production of polyethylene terephthalate (PETE) from p-xylene. Terephthalic acid is first synthesized as an intermediate by oxidation of the methyl groups on a p-xylene and subsequently polymerized with ethylene glycol to produce PETE.

Table 1.1: Boiling and melting points of o-, m- and p-xylenes [3].

	Boiling point (K)	Melting Point (K)
o-Xylene	417	248
m-Xylene	412	225
p-Xylene	411	286

1.2. Chemistry of toluene methylation

The most feasible mechanism for the methylation of toluene with methanol over acidic zeolite is shown in Scheme 1.2. The methanol first forms a methylating species, either a methoxy [26,27,28] or a protonated methanol [29,30,31] on the Brønsted acid site of a zeolite (shown as methoxy for simplicity in Scheme 1.2). The nucleophilic toluene then reacts with the methylating species on the surface via carbenium ion like transition state [32,33] and forms an alkoxide intermediate [34,35]. After deprotonation, the product (xylene) leaves from the surface, the Brønsted acid site is restored and the catalytic cycle is closed. A similar methylation reaction mechanism applies to the methylation of other aromatics and alkenes, e.g., of xylenes to trimethylbenzenes or of propene to butenes, which are also produced as byproducts during the reaction of toluene methylation [36,37]. Note that the methanol can readily form dimethyl ether (DME) by dehydration [38,39] under these conditions, which can also methylate unsaturated aromatic and alkene molecules via similar mechanism [30,40,41]. The major difference between them is that a water and a methanol molecule is released when methanol and DME is used as a methylating species, respectively.

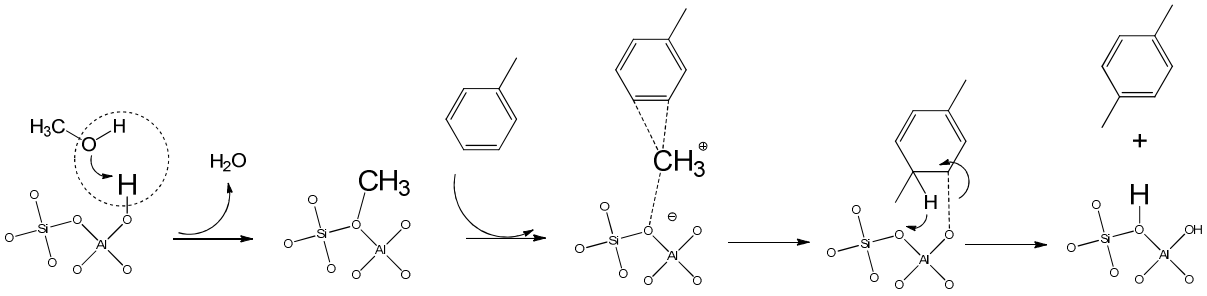

Scheme 1.2: Toluene methylation with methanol with an acidic zeolite (shown as a small cluster) via carbenium ion transition state and alkoxide intermediates. The methylating species are represented as methoxy species for simplicity.

The goal of toluene methylation is to selectively generate xylenes and in particular, p-xylene. The reaction pathways during toluene methylation are shown in Scheme 1.3. The difficulty of achieving a high p-xylene selectivity arises from several major side reactions during toluene methylation. The reactants can directly react via toluene disproportionation (two molecules of toluene react to form a benzene and xylene) [4,5,6] or via methanol to hydrocarbons reactions (leading to the formation of light hydrocarbons) [13,39]. When the reactants, toluene and methanol, react together, o- and p-xylene are most likely formed as a primary products [29,42,43], but they can readily isomerize in acidic zeolites and significantly lower the selectivity of p-xylene. In addition, the aromatic products, e.g., xylenes, can be further methylated to form tri- and tetra-methylbenzenes [7,11,44,45]. In medium pore zeolites, these bulky multi-methylated aromatics cannot leave the zeolite pores and eventually form lower-methylated aromatics, e.g., xylenes and tri-methylbenzenes, with light hydrocarbons as byproducts (hydrocarbon pool cycle [11,13,46]). This lowers the efficiency of methylation, i.e., methanol used to form xylenes, but increases the xylene selectivity within aromatics in medium pore-sized zeolites [47]. It was also concluded that the light hydrocarbons observed in the toluene methylation are most likely not generated from the direct coupling of methanol and/or DME [48,49] nor from alkene methylation-cracking cycle [50,51], but from further methylation and subsequent elimination of light hydrocarbons (and less-methylated aromatic molecules, such as xylenes) [47].

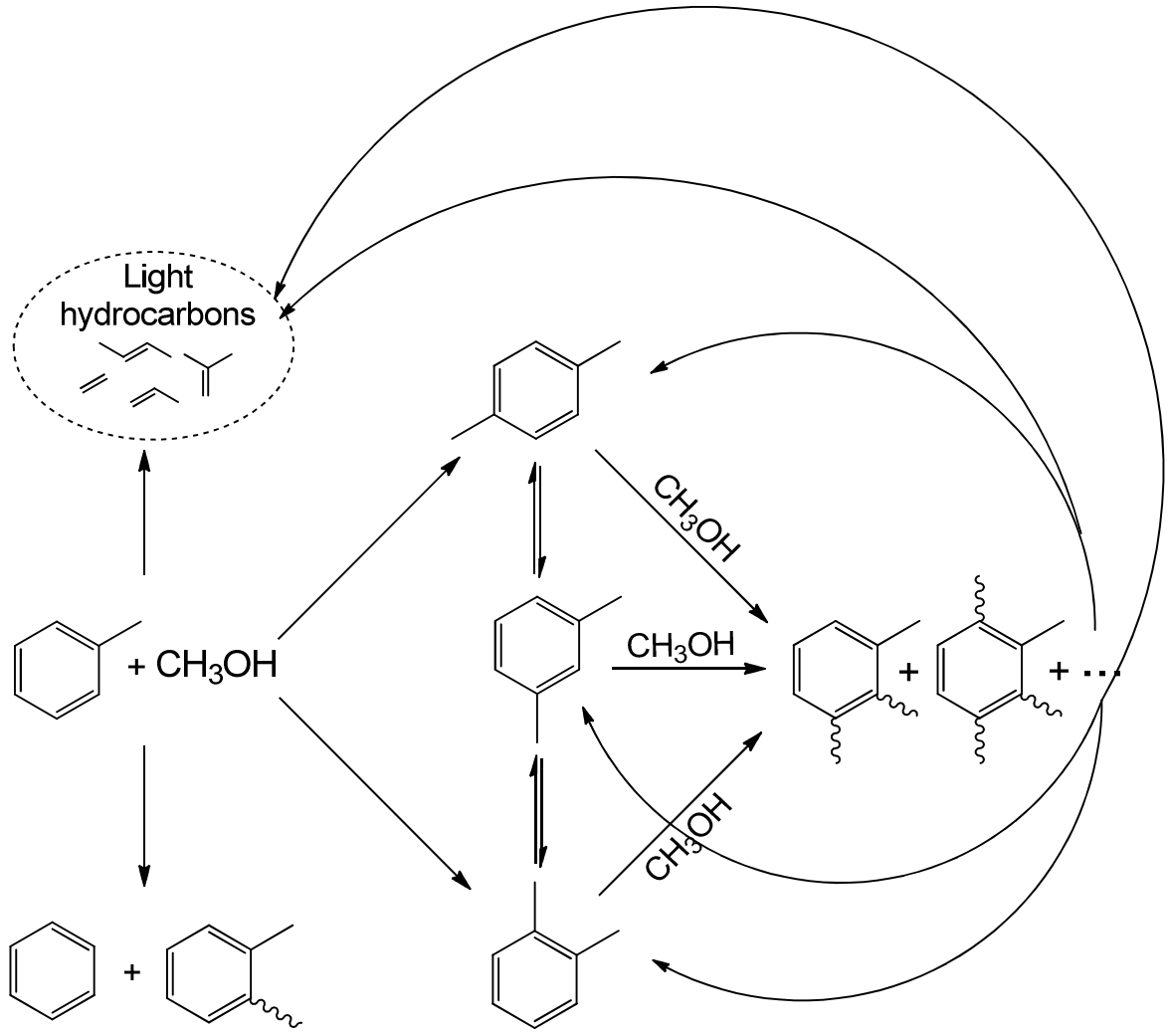

Scheme 1.3: Reaction pathways during the reaction of toluene with methanol inside a medium pore-sized zeolite [47]. The reaction of disproportionation, methanol to hydrocarbons, toluene methylation, isomerization, further methylation and elimination as xylenes (light hydrocarbons as byproducts) are shown.

1.3. Catalysts

Alkylation is a reaction that involves transfer of an alkyl group from one molecule to another. Methylation of toluene is a specific type of alkylation in which the methyl from methanol or DME is a transferred. The alkylation reactions were initially carried out in the industry with liquid acid catalyst, such as Friedel-Crafts catalysts (e.g., $AlCl_3$) [52], sulfuric and hydrofluoric acid [53]. Although these catalysts have been optimized and operated efficiently to produce high quality products, most of them are toxic, volatile, corrosive, difficult to separate after the reaction and are unable to be regenerated. The solid acids for

various alkylation processes, consequently, have been developed to replace the existing liquid acid catalysts (e.g., alkylation of isobutane and butenes from using sulfuric or hydrofluoric acid to trifluoromethanesulfonic acid (F_3CSO_3H) on a porous support [53]) and some of the possible candidates for alkylation reaction (at least proven in the laboratory scale) were polyoxometalates [54,55,56], perfluorosulfonic acid resins (Nafion) [57,58], sulfated zirconia [59,60] and zeolites [59,61]. The synthetic zeolites in particular, have attracted much attention in the industry since their discovery [62], because of their high surface area, the size of the micropores (molecular dimension of the pores, i.e., shape selectivity) and the possibility of modulating the electronic properties of the active sites [61].

As of 2001, ~ 1.6 million tons of synthetic zeolites are annually produced as laundry detergents, catalysts and absorbents [63]. There are currently over 200 known structures (2012) [64], but only about dozen are commercially used in the industry as listed in Table 1.2. Note that each structure is labeled by three capital letters, e.g., FAU for faujasites or MOR for mordenites, which represents the framework type code defined by the IUPAC (International Union of Pure and Applied Chemistry) in 1978 [65]. The nomenclatures used in parenthesis are the original names that were first given at the time of discovery, which typically used the names of minerals (if the natural analogs exist), e.g., FER (ferrierite), letters of the Latin and Greek alphabets, e.g., Zeolite Y, or the acronyms that indicate the names of industrial or university laboratory with a consecutive numbering system e.g., ZSM-5 (Zeolite Socony Mobil-five) [64,66].

Table 1.2: Zeolite used in commercial and emerging catalytic processes [63].

Structural type (zeolite or zeotype)	Catalytic process
FAU (Y)	Catalytic cracking, Hydrocracking, Aromatic alkylation, NO_x reduction, Acetylation
MOR (Mordenite)	Light alkanes hydroisomerisation, Hydrocracking, Dewaxing, NO_x reduction, Aromatic alkylation and transalkylation, Olefin oligomerization
MFI (ZSM-5, TS-1, Silicalite)	Dewaxing, Methanol to gasoline, Methanol to olefins and products, FCC additive, Hydrocracking, Olefin cracking and oligomerisation, Benzene alkylation, Xylene isomerization, Toluene disproportionation, Aromatization, NO_x reduction, Oxidations, Hydration, Amination, Beckmann rearrangement, Cyclodimerisation
BEA (Beta)	Benzene alkylation, Aliphatic alkylation, Acetylation, Baeyer-Villiger reaction, FCC additive, Etherification
LTL (KL)	Alkane aromatization
MWW (MCM-22)	Benzene alkylation
CHA (SAPO-34)	Methanol to olefins
AEL (SAPO-11)	Long chain alkane hydroisomerisation, Beckmann rearrangement
FER (Ferrierite)	Olefin skeletal isomerization
ERI (Erionite)	Selectoforming
RHO (Rho)	Amination
TON (Theta-1, ZSM-22)	Long chain alkane hydroisomerisation

Zeolites are microporous crystalline structures composed of aluminosilicates. Most of the zeolites frameworks are made from rings consisting of 8, 10 or 12 silicon (or aluminum) and oxygen atoms with pore size of ~ 0.3 - 0.7 nm and are typically referred as small, medium or large pore-sized zeolites, respectively (also as 8, 10 or 12 membered-ring (MR) zeolites). Few frameworks, such as DON (UTD-1) [67], however, can be somewhat larger (14-MR zeolite with pore opening of ~ 0.8 nm [64]). These materials can have variety of shapes, sizes and frameworks depending on the synthesis conditions [68]. For example, TON (NU-10) has a straight, 1-dimensional and nonintersecting channel systems (Figure 1.5) with long needle like crystal structures and MFI (ZSM-5) has a 3-dimensional structure comprised of two types of intersecting channels (one sinusoidal and the other straight) with cauliflower shaped crystals (Figure 1.6). Furthermore, different crystal size with same framework can be synthesized by changing the template, e.g., MEL (H-ZSM11) is also 3-dimensional structure comprised of straight intersecting channels and synthesis with tetrabutylammonium hydroxide or 1,8-diamino-octane as the organic templates results in small and large crystal zeolites, respectively (Figure 1.7) [69,70]. It is also interesting to note that the same synthesis gel can be used for both TON (H-NU10) and MEL (H-ZSM11, large crystal) synthesis, i.e., only by

changing the rotation condition of the autoclaves (60 rpm for TON and static for MEL (synthesis), different framework zeolites are crystalized [70].

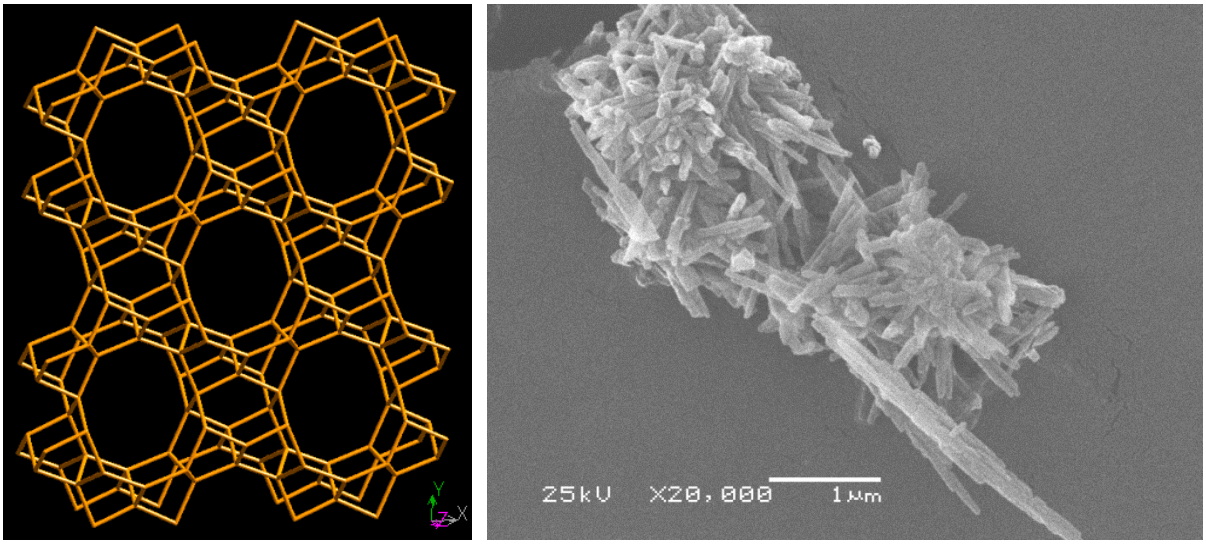

Figure 1.5: Zeolite framework of TON (NU-10) on the left [64] and a scanning electron microscope (SEM) image on the right.

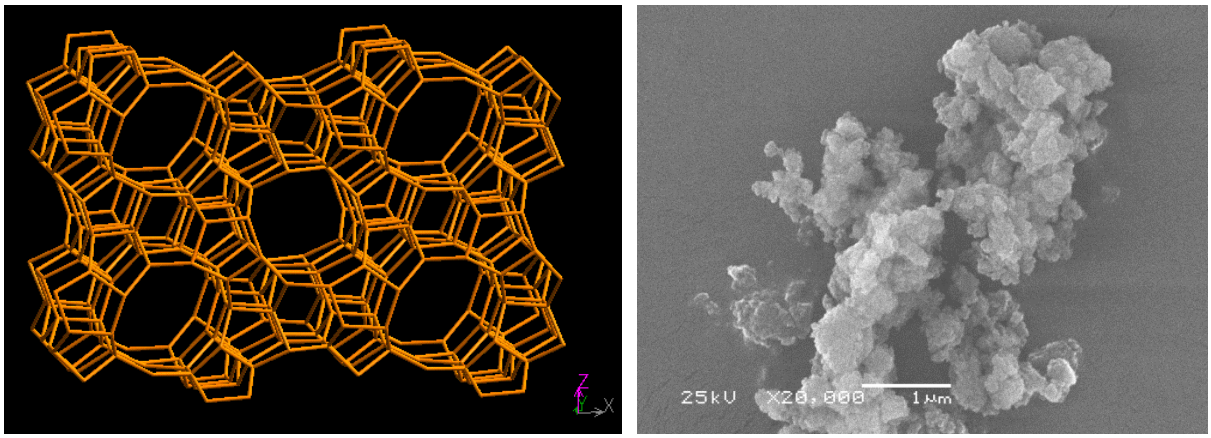

Figure 1.6: Zeolite framework of MFI (ZSM-5) on the left [64] and a scanning electron microscope (SEM) image on the right.

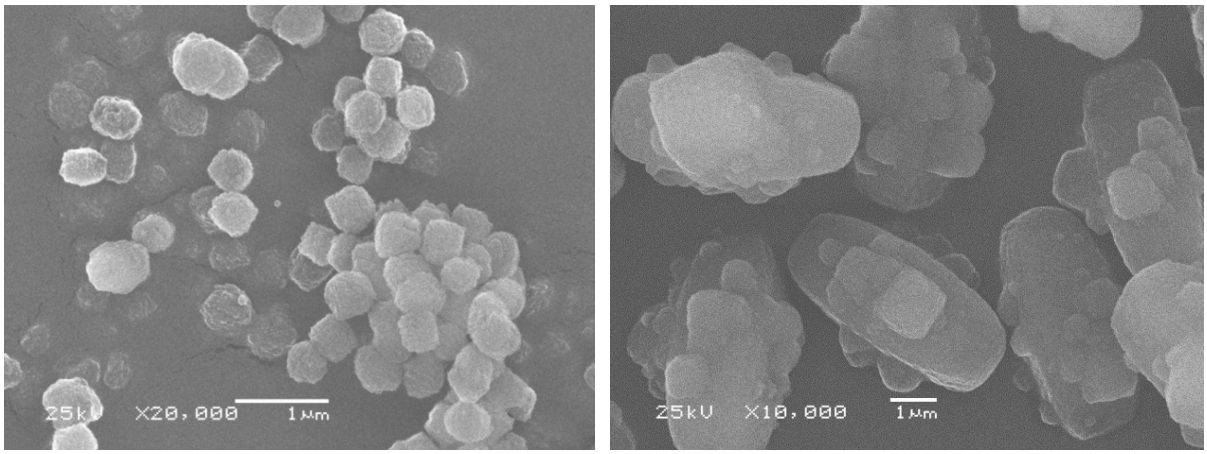

Figure 1.7: Scanning electron microscope image of MEL (ZSM-11) synthesized with tetrabutylammonium hydroxide (left, small crystal) and 1,8-diamino-octane (right, large crystal).

To generate sites for acid catalyzed reactions, e.g., alkylation, a negative charge must be created in a zeolite by substituting the Si^{4+} atom of SiO_4 tetrahedra in the framework with Al^{3+} during the synthesis. The charge on the framework is balanced by a cation (usually with sodium or other alkaline metals [63,71]), but when the substituted cation is exchanged with a hydrogen (by ammonium exchange and heating the sample to release ammonia and to leave hydrogen on the surface), a Brønsted acid site is formed (Figure 1.8). The Si^{4+} atoms in SiO_4 tetrahedra can also be substituted with other metals such as gallium, iron and boron to tailor the strength of the acid in the zeolite [72,73]. It has been reported that decrease in acid strength can enhance the catalyst selectivity in some reaction e.g., in butene isomerization and propene acylation reactions, higher isobutene [74,75] and acetate products selectivities [76], respectively, were observed with weaker acids.

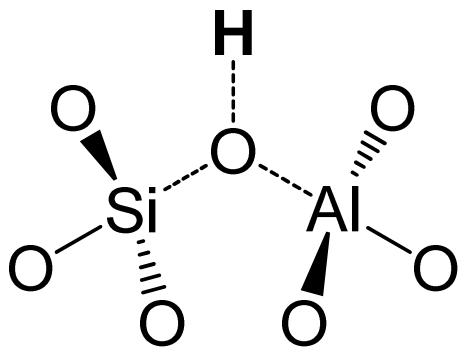

Figure 1.8: Brønsted acid site in a zeolite is generated by substitution of Si^{4+} atom of SiO_4 tetrahedra in the framework with Al^{3+}. When the charge deficiency is balanced by hydrogen, a Brønsted acid site is generated.

One of the first zeolite commercially synthesized was LTA (zeolite A), in the Linde division of Union Carbide Laboratories, followed by FAU (zeolite X and Y) [77]. These zeolites were synthesized based on small alkali cations, but in 1960's, the researchers discovered that new types of zeolites could be synthesized by using an organic cations as templates, e.g., MFI (ZSM-5, with tetrapropylammonium ions) and BEA (Beta, with tetraethylammonium ions) [63]. Further investigation with new elemental compositions led to the discovery of other zeotype (zeolite related materials that are not aluminosilicates) materials, such as aluminophosphate molecular sieves, known as $AlPO_4$ [78] (formed by alternating AlO^{4-} and PO^{4+} tetrahedra) and silicoaluminophosphates (SAPO, by replacing a fraction of PO^{4+} by SiO_4 tetrahedra) [79]. The major milestones in the field of synthesis of zeolites and the related materials are summarized in Table 1.3.

Table 1.3: Landmarks in the history of zeolites and related materials [63].

Year	Description	Inventor
1948	syntheses of mordenite and chabazite	R.M. Barrer
1949	syntheses of zeolites A and X	Union Carbide
1954	application of zeolites for gas drying	Union Carbide
1959	application of zeolites for paraffin separation	Union Carbide
1959	application of clinoptilolite for cation exchange	Ames
1961	organic cations as templates	Barrer and Danny
1962	zeolites as FCC catalysts	Mobil Oil
1967	syntheses of zeolite beta and ZSM-5	Mobil Oil
1974	zeolites as detergent builder	Henkel
1978	synthesis of silicalite	Union Carbide
1982	aluminophosphate molecular sieves	Union Carbide
1983	incorporation of titanium in the TS- 1	Eniricerche
1992	micelle-templated mesoporous silicates	Mobil
1994	micelle-templated mesoporous oxides	G.D. Stucky
1999	mesoporous carbons by silica replica	R. Ryoo
1999	microporous metal-organic frameworks	Yaghi and O'Keeffe

Toluene methylation was first carried out on variety of cation-exchanged zeolite Y (large pore-sized) as catalysts [80], but as the principles of shape selectivity were recognized (Figure 1.9) [81,82,83], the reaction started to be investigated in various medium pore-sized zeolites, e.g., MFI (ZSM-5) [7], EUO (EU-1) [6], TON (ZSM-22), MTT (ZSM-23) [8]. The reasoning behind this was that the transition-state or product shape selectivity (Figure 1.9b), i.e., not

allowing the m- and o-xylenes to form or to leave because of larger kinetic diameter relative to p-xylene, would hinder the formation of m- and o-xylenes and therefore increase selectivity of p-xylene. The high selectivity of p-xylene (> 90 %), however, was only achieved after modification of the medium pore-sized zeolites, e.g., by deposition of tetraethyl orthosilicate (TEOS) on the zeolite surface [21,22] or by impregnation with a boron, phosphorous or manganese [84,85,86].

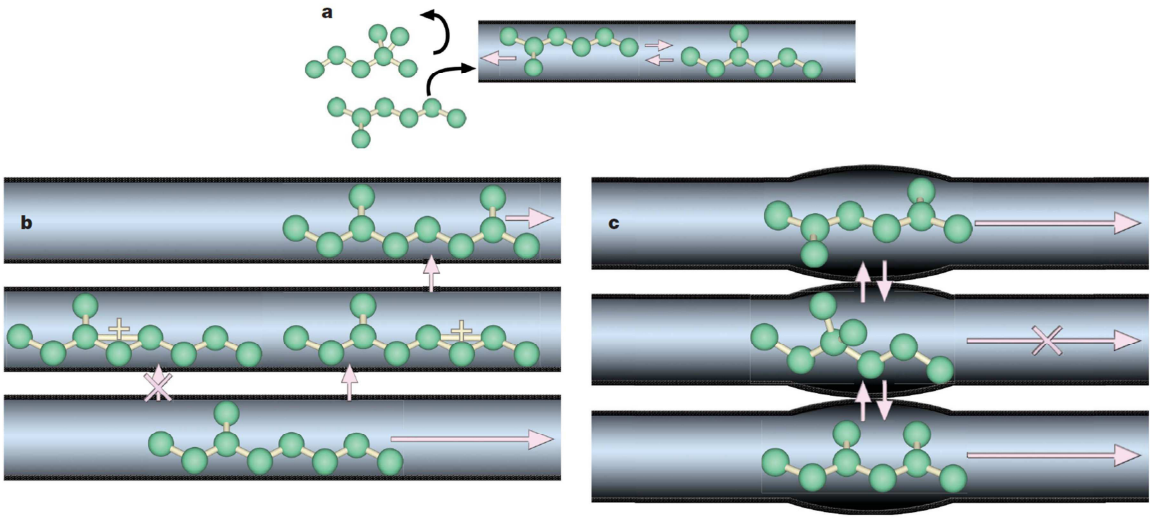

Figure 1.9: Illustrations depicting the concepts of reactant (a), transition-state (b) and product (c) shape selectivity [83].

1.3.1.Zeolite characterization

A variety of experimental techniques is available for characterization of zeolites and most reported below are described in more details in literature, e.g., 77,87. Here, the theoretical background of the methods that are used in this work will be discussed briefly.

- *Atomic absorption spectroscopy (AAS)*

The AAS was used to determine the elemental composition of the zeolites, e.g., silicon, aluminum, iron and sodium. Typically, the solids are first dissolved with a boiling mixture of hydrofluoric/nitro-hydrofluoric acid before they are vaporized and the absorbance measured (the concentrations are then determined based on the Beer-Lambert Law). The molar ratio of

silicon and aluminum (or iron) indicates the acid concentration of a zeolite, i.e., the higher the silicon content relative to the aluminum, the lower the acid concentration is.

- *Dynamic light scattering (DLS)*

The dynamic light scattering (DLS) technique can be used to determine the average crystal size and its distribution of zeolites. In DLS, the intensity of the light, scattered by the sample particles in a solution is measured as a function of time. The intensity of the light fluctuates with time because the sample diffuses in a Brownian motion relative to the detector and this constantly causes constructive/destructive interferences (consequently there is change in the light intensity). The faster the sample diffuses, the faster the intensity changes and this is dependent on the temperature, solvent viscosity and size of the zeolite crystals. The first two are constant and known and, therefore, the variation in the intensity of the scattered light is proportional to the size of the zeolite crystals. An example of a DLS measurement result of a zeolite sample is shown in Figure 1.10.

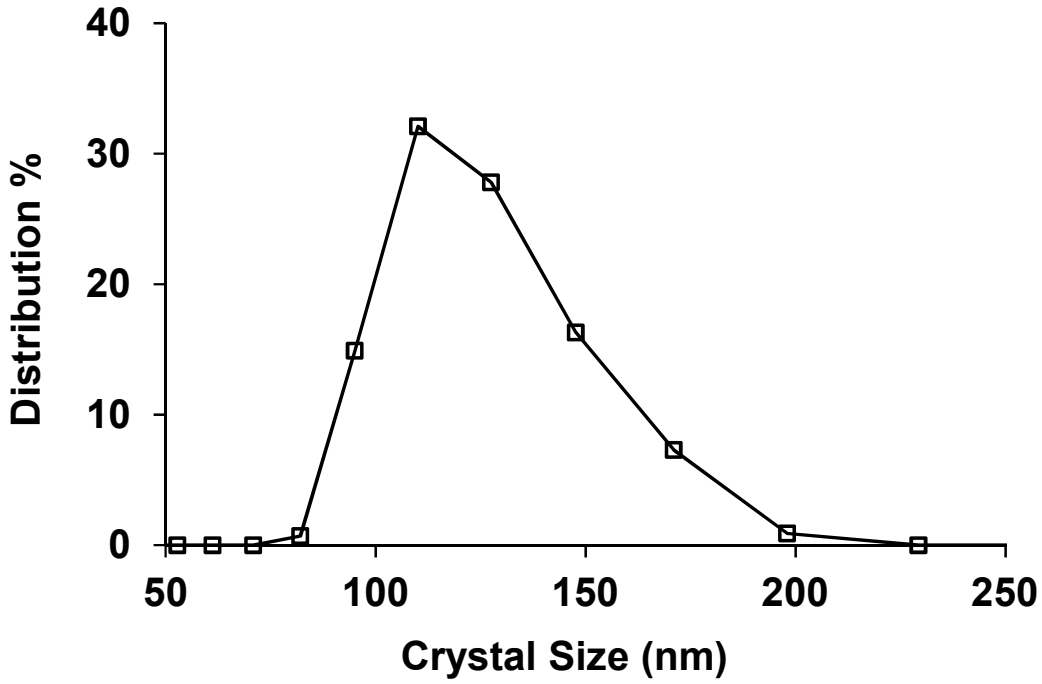

Figure 1.10: Crystal size distribution of MFI (ZSM-5) zeolite from dynamic light scattering (DLS) measurement.

- *Infrared (IR) spectroscopy*

The IR spectroscopy was used to determine the concentration and relative strength of acid sites of the zeolites. During the experiment, infrared light passes through a sample (typically in a self-supporting wafer) and the transmitted light at different wavenumbers (~ 4000 – 400 cm^{-1}) is recorded. If the frequency of the IR beam matches the vibrational frequency, i.e., resonant frequency, of a bond in the sample or the molecule that is adsorbed, absorption occurs. The position, shape and intensity of the transmitted light spectrum thus reveal how much energy was absorbed at various wavenumbers and consequently, the characteristics of the molecular structure of the sample and its interactions with the adsorbed species.

An IR spectrum of acidic zeolites (MFI (ZSM-5)) before adsorption of a probe molecule is shown in Figure 1.13. Typically, two distinct bands at ~3745 cm^{-1} and 3610 cm^{-1}, characteristic for the O-H vibration of terminal silanol groups and Brønsted acid sites, respectively, are observed [88,89]. The location of the Brønsted acid site band reveals information on the relative acid strength because increase in the O-H bond strength (from higher deprotonation energy) of weaker acids causes increase in the wavenumbers, e.g., O-H vibration of Brønsted acid sites shifted from ~3610 to 3630 cm^{-1}, when the aluminum in the framework of MFI (stronger acid) is isomorphously substituted with iron (weaker acid).

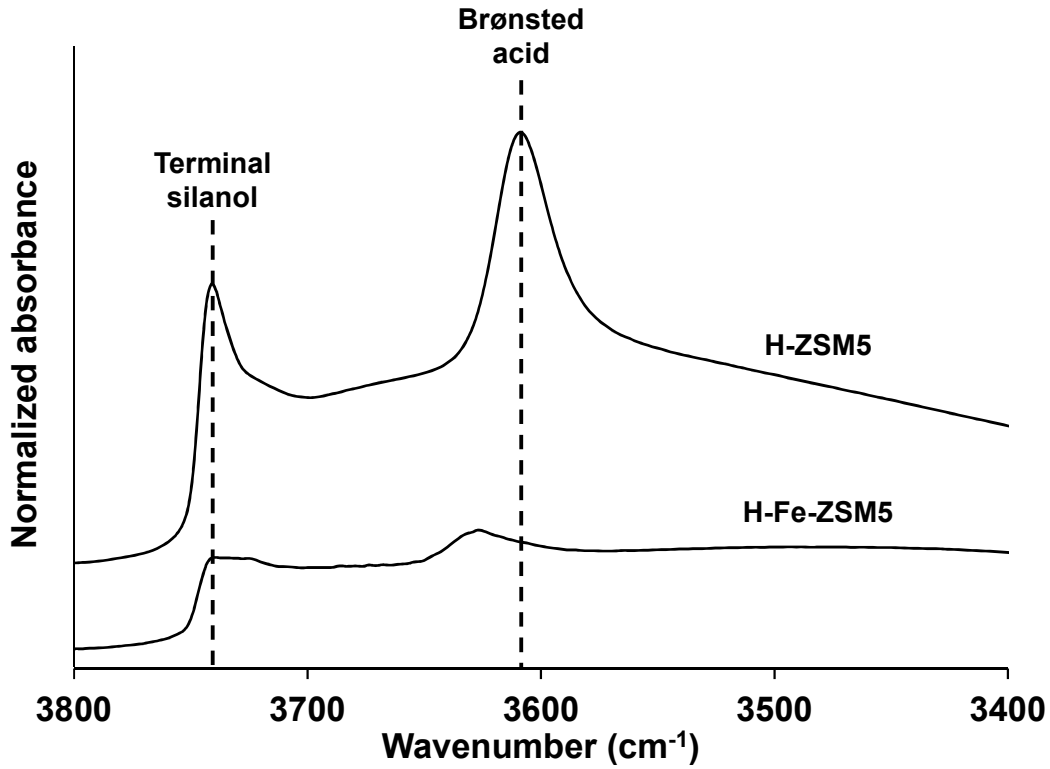

Figure 1.11: Infrared (IR) spectra of activated samples (MFI; heated to 723 K for 1 hour) measured at 423 K under vacuum. The bands at 3745 cm^{-1} and 3610 cm^{-1} represents O-H vibration of the terminal silanol groups and the Brønsted acid sites, respectively.

Variety of molecules, such as ammonia, carbon monoxide, benzene, pyridine and its derivatives [90], are used in literature to probe the acid characteristics (concentration and strength of Brønsted and Lewis acid sites) of a zeolite. Pyridine, in particular, was used as probe molecules in this work to determine the total concentration of Brønsted and Lewis acid sites and an IR spectrum of samples after adsorption of pyridine is shown in Figure 1.12. The band at ~1545 cm^{-1} represents the ring deformation vibration of pyridinium ions formed on Brønsted acid sites and the band at ~1450 cm^{-1} coordinately bonded pyridine molecules on Lewis acid sites [91]. The total number of Brønsted and Lewis acid sites can thus be determined by integrating the bands at ~ 1546 and 1455 cm^{-1}, respectively [92].

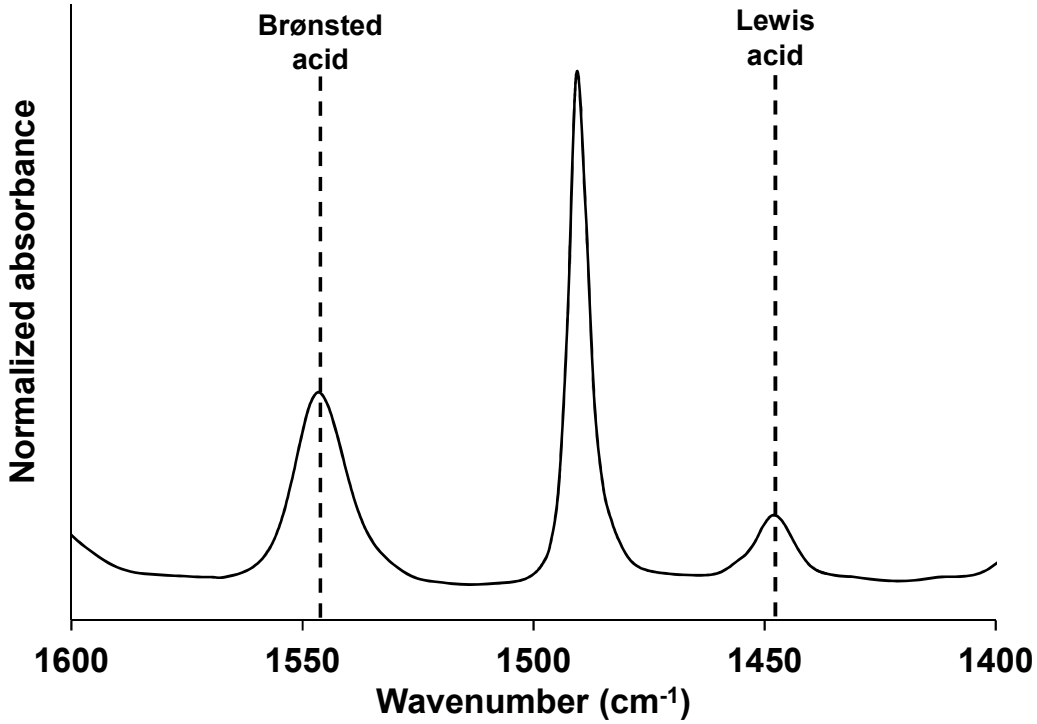

Figure 1.12: Infrared (IR) spectra of MFI (H-ZSM-5) after adsorption of pyridine at 423 K, 0.01 kPa and outgassing for 1 hour under vacuum (spectra of the activated sample subtracted). The bands at 1545 cm^{-1} and 1450 cm^{-1} represents Brønsted and Lewis acid site, respectively.

The concentration of Brønsted acid sites located in the pore mouth regions, which may be of importance in shape selective reactions, can be determined by using 2-6-di-tert-butyl-pyridine (2,6-DTBPy) as a probe molecule for medium pore-sized (10-MR, ~ 4 - 6 nm) zeolites [93] because the kinetic diameter of 2,6-DTBPy (1.05 nm) is much larger than the pores. Two major characteristic bands from the adsorption of 2,6-DTBPy are observed, i.e., at 3367 cm^{-1} ($N\text{-}H^{+}$ stretching of protonated 2,6-DTBPy) and 1616 cm^{-1} (C=C bond in an aromatic ring of adsorbed 2,6-DTBPy) [93], as shown in Figure 1.13 (with MFI (ZSM-5)). The larger area of the bands at 3367 cm^{-1} and 1616 cm^{-1} of the desilicated (DS) material indicates that the concentration of the Brønsted acid sites accessible by 2,6-DTBPy is higher in DS sample than the parent ZSM-5. These areas can also be integrated to calculate the number of Brønsted acid sites interacting with 2,6-DTBPy (sites located in the pore mouth regions).

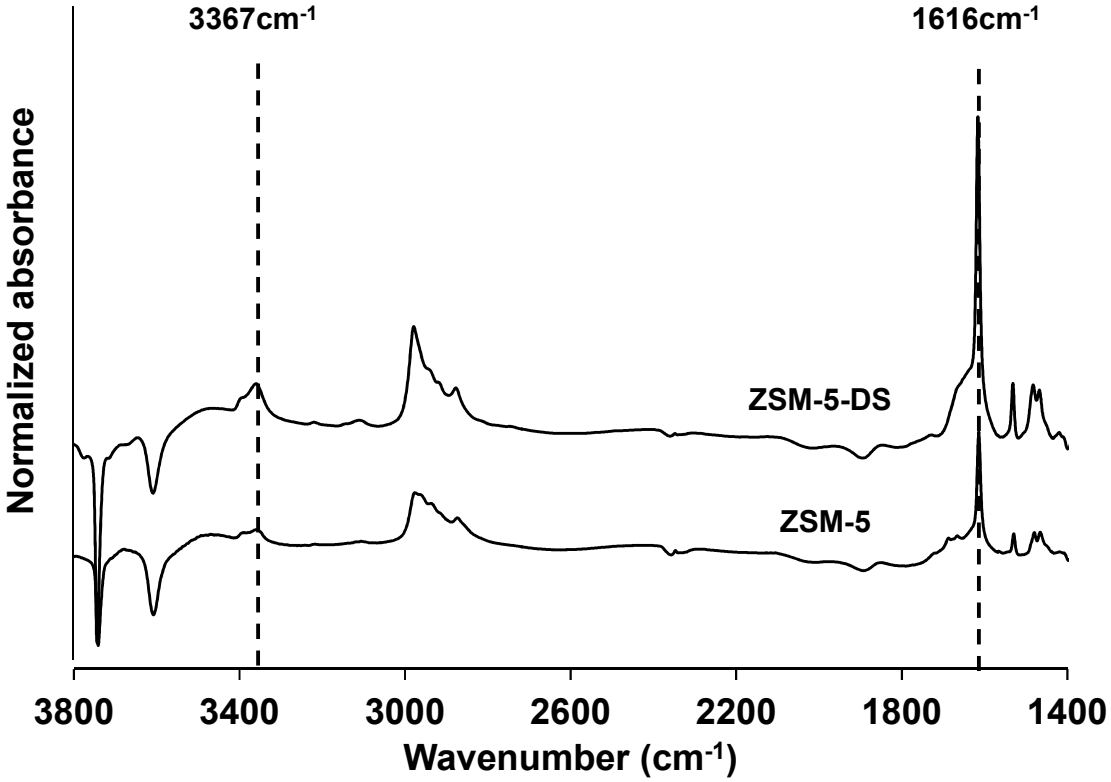

Figure 1.13: The IR spectra of MFI samples after adsorption of 2,6-di-tert-butyl-pyridine (2,6-DTBPy, spectra of activated samples are subtracted). The characteristic bands at 3367 cm^{-1} and 1616 cm^{-1} appear due to the 2,6-DTBPy interaction with the zeolite.

- *Nitrogen adsorption*

The nitrogen (N_2) physisorption was measured to determine the pore volumes (micro- and meso-), pore size distributions, Brunauer-Emmett-Teller (BET) [94] and external surface areas of the zeolites. The measurement is typically carried out by adsorbing-desorbing (by equilibration) nitrogen over certain pressure ranges at liquid nitrogen temperature (77 K), after the samples are outgassed. There are several methods to calculate the pores volumes and external surface areas from the measurement and some of the common methods used in the literature are t-plot [95,96] and α_s-plot methods [97,98]. These methods are based on empirical models, in which the volume of N_2 adsorbed is plotted versus the statistical thickness (t-plot) or an adsorption isotherm of an appropriate nonporous, reference material (α_s-plot). The pore size distributions can be evaluated by density functional theory (DFT; based on principles of statistical mechanics) or Barrett, Joyner and Halenda (BJH; based on

modified Kelvin equation) methods [97,99,100]. An example of N_2 physisorption isotherm of a microporous zeolite is shown in Figure 1.14.

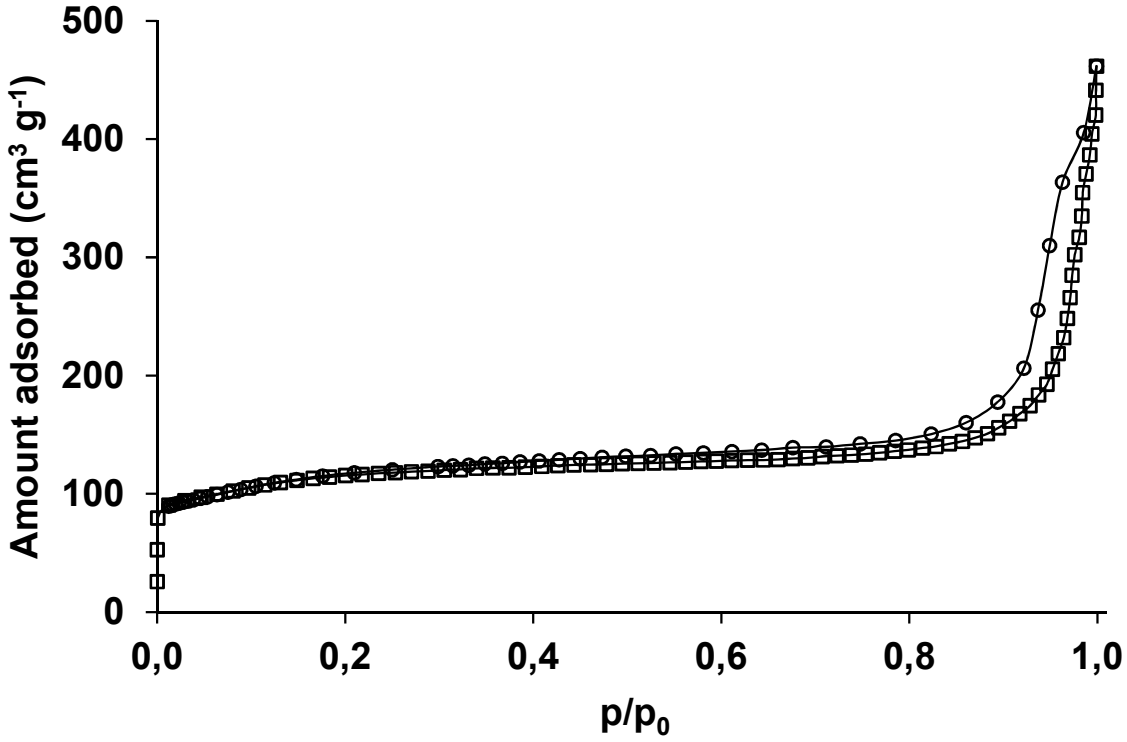

Figure 1.14: Nitrogen physisorption isotherms (□ = adsorption, ○ = desorption) of the MFI (ZSM-5).

- *Scanning electron microscopy (SEM)*

The scanning electron microscopy (SEM) images were taken to determine the morphology and the size of zeolite particles. SEM is carried out by sending a focused beam of electrons over the sample and the images are visualized by detecting the secondary and/or backscattered electrons as a function of the position of the primary beam. The surface facing the detector appears brighter than the surface pointing away and examples of SEM images are shown in Figure 1.5 - Figure 1.7.

- *Temperature programmed desorption (TPD) of ammonia*

The TPD of ammonia (NH_3) was used to determine the total acid concentration and to compare relative acid strengths of the zeolites. Typically, the sample is activated under vacuum before NH_3 is adsorbed and degassed. The temperature is then ramped and desorption

of NH_3 is monitored by mass spectroscopy. The concentration of acid can be calculated by integrating the area under the desorption maxima and comparing it with a standard. The temperature, where the maximum desorption occurs, reflects the strength of ammonia adsorbed on a material and therefore, the relative acid strength of a material. An example of TPD of NH_3 is shown in Figure 1.15 and it shows that the acid concentration and the strength of MFI with iron in the framework is lower and weaker, respectively, compared to the aluminum in the framework (this is also confirmed by IR spectroscopy) because the lower polarizability of iron in the framework increases the deprotonation energy [101].

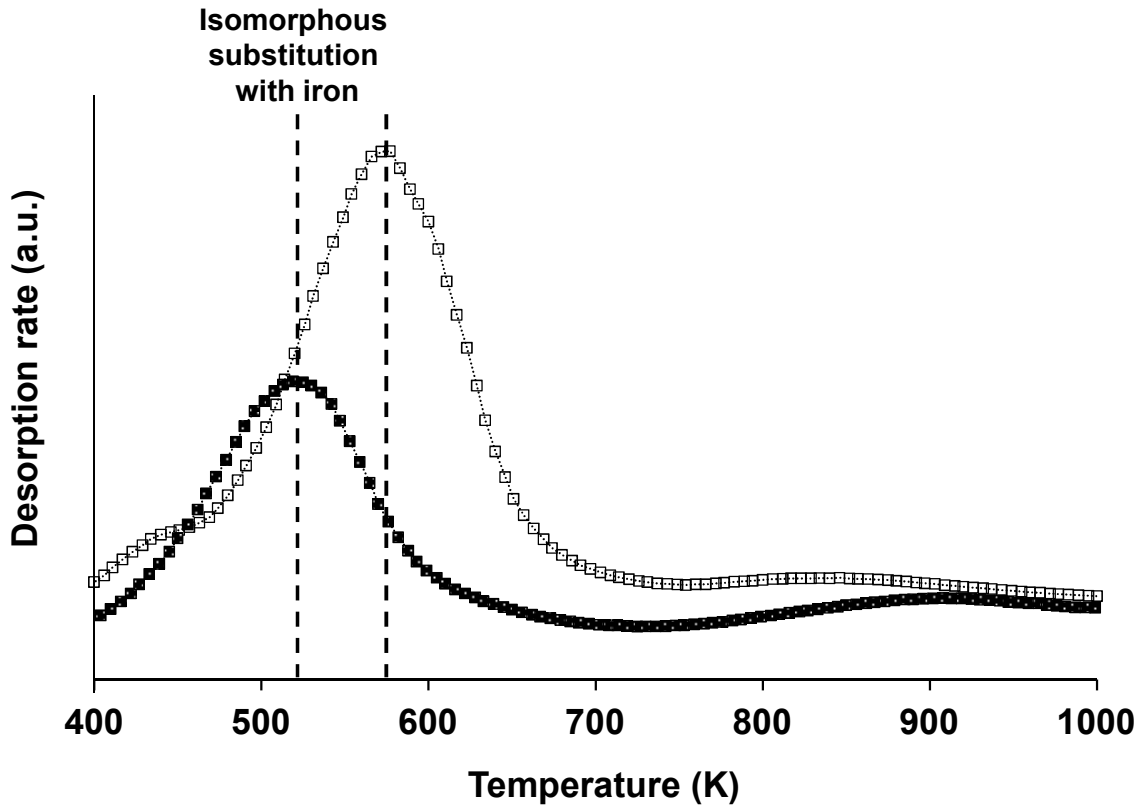

Figure 1.15: Temperature programmed desorption (TPD) of ammonia with MFI (H-Al-ZSM5 (□), and H-Fe-ZSM5 (■)). The first and second vertical dashed line is placed at ~520 and 580K, respectively.

- *X-ray diffraction (XRD)*

The XRD patterns were recorded to determine the purity, crystallinity and the size (inversely proportional to the peak width of the diffraction patterns) of the zeolite crystals. During the XRD measurement, the X-ray beam hits the powder sample and scattering pattern is detected, only if the atoms are arranged in a regular pattern (crystalline). The Bragg's law

for constructive (in-phase) interferences is not fulfilled in an amorphous material due to lack of ordering and the diffraction signals, consequently, are not detected. Each XRD pattern of a pure sample has a specific diffraction patterns and is therefore, a fingerprint of the substance. An example of XRD patterns recorded is shown in Figure 1.16.

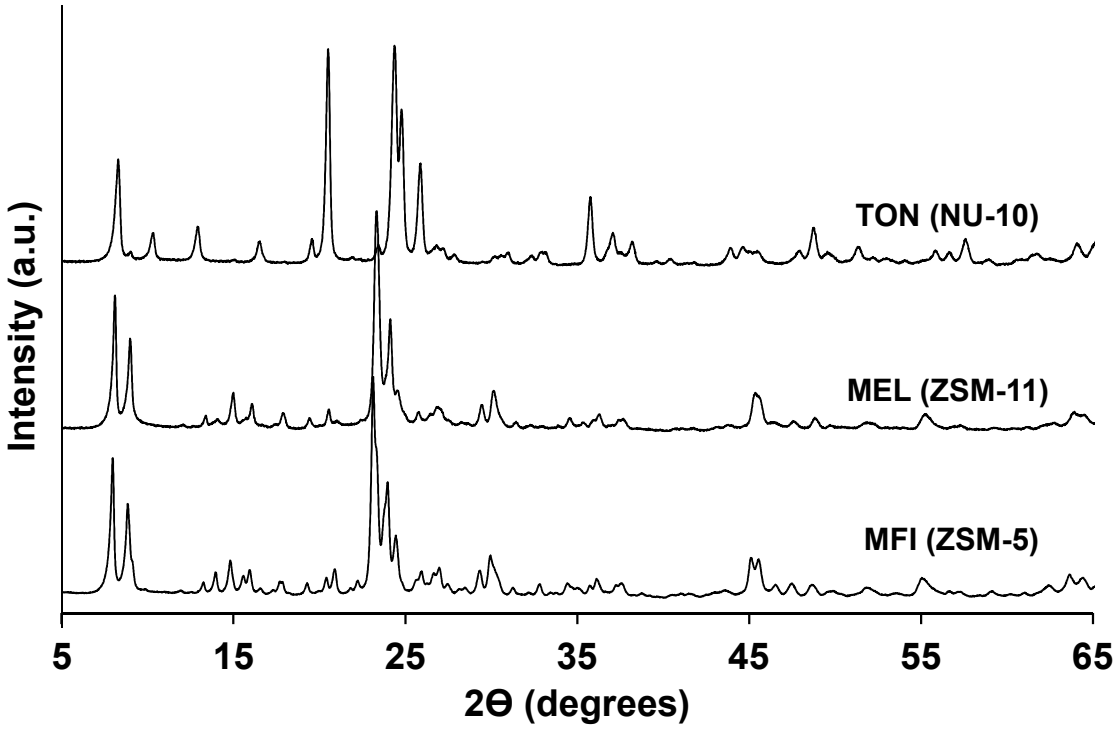

Figure 1.16: Powder X-ray diffraction (XRD) patterns of MFI (ZSM-5), MEL (ZSM-11) and TON (NU-10) samples.

1.4. Motivation and scope of the thesis

The reaction of toluene methylation is a potential industrial process that can increase the production of p-xylene. There are several technical hurdles, however, that first need to be resolved before commercial viability is realized and the purpose of this investigation was to gain deeper insight into some of the limitations of the reaction. A better understanding would ultimately enable us to design and develop a more selective, active and stable catalyst than previously reported in literature, i.e., a catalyst that would yield higher p-xylene selectivity, less methanol consumed for the formation of light hydrocarbons and multi-methylated aromatics, e.g., trimethylbenzenes, (selective), more toluene and xylene molecules converted and produced per active sites (active), respectively, and a catalyst with slower deactivation

and therefore longer lifetime (stable). In this work, we have focused in three different major topics.

- *Utilization of methanol in toluene methylation*

One molecule of methanol reacts with one molecule of toluene to form one molecule of xylene in toluene methylation, according to the stoichiometry. Despite of using an excess of toluene relative to methanol by many research groups in the past [19,21,103,102], the reaction is accompanied by many undesired side-products (i.e., non-xylenes), such as light hydrocarbons [6,42,85,103] and multi-methylated aromatics, e.g., trimethyl- and tetramethyl-benzenes [7,11,42,43]. Inefficient usage of methanol, i.e., methanol not being used to form xylenes only, even in excess of toluene relative to methanol is one of the major drawbacks for the process commercialization [15] and this issue has not been discussed in details so far in the literature. In Chapter 2, the utilization of methanol in toluene methylation was investigated therefore, using medium (H-ZSM-5 and H-ZSM-11) and large pore-sized (H-MOR and H-BETA) zeolites. The results presented here highlight the significance of the hydrocarbon pool cycle [104,105] and of the product shape selectivity [106,107], rather than the transition state selectivity, and the challenges in an efficient usage of methanol in the toluene methylation reaction.

- *Hierarchical zeolites and the catalytic properties in toluene methylation*

The hierarchical zeolites were first prepared from H-ZSM-5 by desilication and subsequent dealumination. The first method generated mesopores within microporous crystals and the latter removed significant amount of extra-framework aluminum species formed from desilication procedure. These methods shorten the diffusion path length and thus increased the transport rates of all molecules [108,109,110]. Consequently, the catalysts were generally more active (relative to the parent materials) [111,112,113], albeit there was some loss in the shape selective behavior (lower p-xylene selectivity [113]). These zeolites were further modified by chemical liquid deposition of TEOS to compensate for the lower selectivity of p-xylene. The TEOS deposition on a zeolite surface selectively reduced the number of unselective Brønsted acid sites in the pore mouth region (because kinetic diameter of TEOS is larger than the size of the H-ZSM-5 micropores) and partially blocked the pore openings [21,22,25]. This modification method changed the transport properties of product molecules

to favor high p-xylene selectivity, i.e., the diffusivity of o- and m-xylene decreases, while the p-xylene slightly increases [24]. In chapter 3, we combine these concepts of zeolite modification to demonstrate that the toluene consumption rate (per Brønsted acid site) and p-xylene selectivity can be enhanced simultaneously over these novel hierarchical zeolites. Furthermore, all these catalysts are also extensively characterized by AAS, SEM, N_2 adsorption and IR spectroscopy using pyridine and 2,6-di-tert-butyl-pyridine as probe molecules to understand the consequence of these modifications on the catalytic activity and p-xylene selectivity.

- *Influence of the reaction temperature on p-xylene selectivity in toluene methylation*

There are three major reaction pathways for the formation of p-xylenes during toluene methylation, i.e., methylation of toluene, isomerization of xylenes, further methylation and subsequent elimination of less-methylated aromatic molecules as xylenes (and light hydrocarbons) from multi-methylated aromatics [11,13,44,45]. In chapter 4, the influence of these reactions on the selectivity of p-xylene during toluene methylation was investigated with medium pore-sized zeolites at different reaction temperatures. Increase in the reaction temperature consistently resulted in higher p-xylene selectivity because the differences in diffusivities of xylenes i.e., between p-xylene and o-, m-xylenes [24], became dominant in determining p-xylene selectivity from fast reactions. These results suggest that toluene methylation to p-xylene reaction should be operated at relative high temperatures because it enables both the formation rate of xylenes and the selectivity of p-xylene to increase simultaneously.

1.5. References

[1] International Energy Agency, Energy Technology Perspectives, France, 2006.

[2] T. Tsai, S. Liu, I. Wang, Applied Catalysis A: General 181 (1999) 355-398.

[3] W. Vermeiren, J.P. Gilson. Topics in Catalysis 52 (2009) 1131-1161.

[4] W.W. Kaeding, C. Chu, L.B. Young, S.A. Butter, J. Catal. 69 (1981) 392-398.

[5] Y. Xiong, P.G. Rodewald, C.D. Chang, J. Am. Chem. Soc. 117 (1995) 9421-9431.

[6] G.N. Rao, R. Kumar, P. Ratnasamy, Appl. Catal. 49 (1989) 307-318.

[7] W.W. Kaeding, C. Chu, L.B. Young, B. Weinstein, S.A. Butter, J. Catal. 67 (1981) 159-174.

[8] R. Kumar, P. Ratnasamy, J. Catal. 116 (1989) 440-448.

[9] H. Nishi, K. Nowinska, J. B. Moffat, J. Catal. 116 (1989) 480-487.

[10] L.B. Young, S.A. Butter, W.W. Kaeding, J. Catal. 76 (1982) 418-432.

[11] O. Mikkelsen, P.O. Rønning, S. Kolboe, Micropor. Mesopor. Mater. 40 (2000) 95-113.

[12] G.A. Olah, Angew. Chem. Int. Ed. 44 (2005) 2636-2639.

[13] U. Olsbye, S. Svelle, M. Bjørgen, P. Beato, T.V.W. Janssens, F. Joensen, S. Bordiga, K.P. Lillerud, Angew. Chem. Int. Ed. 51 (2012) 2-24.

[14] P.L. Spath, D.C. Dayton, Preliminary Screening-Technical and Economic Assessment of Synthesis Gas to Fuels and Chemicals with Emphasis on the Potential for Biomass-Derived Syngas, National Renewable Energy Laboratory, USA, 2003.

[15] S. Kulprathipanja, Zeolites in Industrial Separation and Catalysis, Wiley-VCH, Germany, 2010.

[16] R. D. Chirico, W.V. Steele, J. Chem. Eng. Data 42 (1997) 784-790.

[17] R.A. Meyers, Handbook of Petroleum Refining Processes, McGraw-Hill, USA, 2003.

[18] Y.S. Bhat, J. Das, K.V. Rao, A.B. Halgeri, 159 (1996) 368-374.

[19] J.P. Breen, R. Burch, M. Kulkarni, D. McLaughlin, P.J. Collier, S.E. Golunski, Appl. Catal. A: General 316 (2007) 53-60.

[20] H. Vinek, G. Rumplmayr, J.A. Lercher, J. Catal. 115 (1989) 291-300.

[21] T. Hibino, M. Niwa, Y. Murakami, J. Catal. 128 (1991) 551-558.

[22] H.P. Röger, M. Krämer, K.P. Möller, C.T. O'Connor, Micropor. Mesopor. Mater. 21 (1998) 607-614.

[23] S. Zheng, H.R. Heydenrych, H.P. Röger, A. Jentys, J.A. Lercher, Top. Catal. 22 (2003) 101-106.

[24] S. Zheng, A. Jentys, J.A. Lercher, J. Catal. 241 (2006) 304-311.

[25] J. Čejka, N. Žilková, B. Wichterlová, G. Eder-Mirth, J.A. Lercher, Zeolites 17 (1996) 265-271.

[26] Y. Jiang, M. Hunger, W. Wang, J. Am. Chem. Soc. 128 (2006) 11679-11692.

[27] T.R. Forester, R.F. Howe, J. Am. Chem. Soc. 109 (1987) 5076-5082.

[28] J. Rakoczy, T. Romotowski, Zeolites, 13 (1993) 256-260.

[29] A.M. Vos, X. Rozanska, R.A. Schoonheydt, R.A. van Santen, F. Hutschka, J. Hafner, J. Am. Chem. Soc. 123 (2001) 2799-2809.

[30] I.I. Ivanova, A. Corma, J. Phys. Chem. B 101 (1997) 547-551.

[31] G. Mirth, J.A. Lercher, J. Phys. Chem. 95 (1991) 3736-3740.

[32] M.V. Frash, V.B. Kazansky, A.M. Rigby, R.A. van Santen, J. Phys. Chem. B 102 (1998) 2232-2238.

[33] A.M. Rigby, G.J. Kramer, R.A. van Santen, J. Cat. 170 (1997) 1-10.

[34] J.F. Haw, B.R. Richardson, I.S. Oshiro, N.D. Lazo, J.A. Speed, J. Am. Chem. Soc. 111 (1989) 2052-2058.

[35] V. Kazansky, Acc. Chem. Res. 24 (1991) 379-383.

[36] S. Svelle, B. Arstad, S. Kolboe, O. Swang, J. Phys. Chem. B 107 (2003) 9281-9289.

[37] B. Arstad, S. Kolboe, O. Swang, J. Phys. Chem. B 106 (2002) 12722-12726.

[38] S.R. Blaszkowski R.A. van Santen, J. Am. Chem. Soc. 118 (1996) 5152-5153.

[39] C.D. Chang, Catal. Rev.-Sci. Eng. 25 (1983) 1-118.

[40] S. Svelle, S. Kolboe, O. Swang, U. Olsbye, J. Phys. Chem. B 109 (2005) 12874-12878.

[41] T. Maihom, B. Boekfa, J. Sirijaraensre, T. Nanok, M. Probst, J. Limtrakul, J. Phys. Chem. C 113 (2009) 6654-6662.

[42] P.B. Venuto, L.A. Hamilton, P.S. Landis, J.J. Wise, J. Catal. 4 (1966) 81-98.

[43] A.M. Vos, K.H.L. Nulens, F. De Proft, R.A. Schoonheydt, P. Geerlings, J. Phys. Chem. B 106 (2002) 2026-2034.

[44] Z. Zhu, Q. Chen, Z. Xie, W. Yang, C. Li, Micropor. Mesopor. Mater. 88 (2006) 16-21.

[45] A.M. Prakash, S.V.V. Chilukuri, R.P. Bagwe, S. Ashtekar, D.K. Chakrabarty, Micropor. Mater. 6 (1996) 89-97.

[46] D.M. McCann, D. Lesthaeghe, P.W. Kletnieks, D.R. Guenther, M.J. Hayman, V. Van Speybroeck, M. Waroquier, J.F. Haw, Angew. Chem. Int. Ed. 47 (2008) 5179-5182.

[47] J. H. Ahn, R. Kolvenbach, S. S. Al-Khattaf, A. Jentys, J. A. Lercher, in preparation.

[48] W. Song, D.M. Marcus, H. Fu, J.O. Ehresmann, J.F. Haw J. Am. Chem. Soc. 124 (2002) 3844-3845.

[49] D. Lesthaeghe, V. Van Speybroeck, G.B. Marin, M. Waroquier, Ind. Eng. Chem. Res. 46 (2007) 8832-8838.

[50] M. Bjørgen, S. Svelle, F. Joensen, J. Nerlov, S. Kolboe, F. Bonino, L. Palumbo, S. Bordiga, U. Olsbye, J. Catal. 249 (2007) 195-207.

[51] D.A. Simonetti, J.H. Ahn, E. Iglesia, J. Catal. 277 (2011) 173-195.

[52] R.H. Allen, L.D. Yats, J. Am. Chem. Soc. 83 (1961) 2799-2805.

[53] J. Weitkamp, Y. Traa, Catal. Today 49 (1999) 193-199.

[54] H. Nishi, K. Nowinska, J.B. Moffat, J. Catal. 116 (1989) 480-487.

[55] S. Kamiguchi, S. Nishida, H. Kurokawa, H. Miura, T. Chihara, J. Mol. Catal. A 226 (2005) 1-9.

[56] M.J. Janik, R.J. Davis, M. Neurock J. Catal 244 (2006) 65-77.

[57] G.A. Olah, D. Meidar,R. Malhotra, J.A. Olah, S.C.Naranc, J. Catal. 61 (1980) 96-102.

[58] P. Botella, A. Corma, J.M. López-Nieto, J. Catal. 185 (1999) 371-377.

[59] A. Corma, Chem. Rev. 95 (1995) 559-614.

[60] G.D. Yadav, J.J. Nair, Micropor. Mesopor. Mater. 33 (1999) 1-48.

[61] A. Corma, J. Catal. 216 (2003) 298-312.

[62] R.M. Barrer, D.W. Riley, J. Chem. Soc. (1948) 133-143.

[63] F. Di Renzo, F. Fajula, Stud. Surf. Sci. Catal. 157 (2005) 1-12.

[64] Database of Zeolite Structures (http://www.iza-structure.org/databases/).

[65] R.M. Barrer, Pure. Appl. Chem. 51 (1979) 1091-1100.

[66] Ullmann's Encyclopedia of Industrial Chemistry, Wiley-VCH, Germany, 2011.

[67] C.C. Freyhardt, M. Tsapatsis, R.F. Lobo, K.J. Balkus, M.E. Davis, Nature 381 (1996) 295-298.

[68] C.S. Cundy, P.A. Cox, Micropor. Mesopor. Mater. 82 (2005) 1-78.

[69] P. De Luca, F. Crea, R. Aiello, A. Fonseca, J.B. Nagy, Stud. Surf. Sci. Catal. 105 (1997) 325-332.

[70] M. Derewinski, M. Machowska, Stud. Surf. Sci. Catal. 154 (2004) 349-354.

[71] E.M. Flanigen, Stud. Surf. Sci. Catal. 137 (2001) 11-35.

[72] C.T.W. Chu, C.D. Chang, J. Phys. Chem. 89 (1985) 1569-1571.

[73] R. Szostak, Molecular Sieves: Principles of Synthesis and Identification, Thomson Science, United Kingdom, 1998.

[74] P. Mériaudeau, V.A. Tuan, L.N. Hung, V.T. Nghiem, C. Naccache, J. Chem. Soc., Faraday Trans. 94 (1998) 467-471.

[75] R. Byggningsbacka, N. Kumar, L.E. Lindfors, Catal. Lett. 58 (1999) 231-234.

[76] O. Kresnawahjuesa, R.J. Gorte, D. White, J. Mol. Catal. A 212 (2004) 309-314.

[77] A.W. Chester, E.G. Derouane, Zeolite Characterization and Catalysis, Springer Science, Germany, 2009.

[78] S.T. Wilson, B.M. Lok, C.A. Messina, T.R. Cannan, E.M. Flanigen, J. Am. Chem. Soc. 104 (1982) 1146-1147.

[79] B.M. Lok, C.A. Messina, R.L. Patton, R.T. Gajek, T.R. Cannan, E.M. Flanigen, J. Am. Chem. Soc. 106 (1984) 6092-6093.

[80] T.Yashima, H. Ahmad, K. Yamazaki, M. Katsuta, N. Hara, J. Catal. 16 (1970) 273-280.

[81] P.B. Weisz, Pure Appl. Chem. 52 (1980) 2091-2103.

[82] S.M. Csicsery, Zeolites 4 (1984) 202-213.

[83] B. Smit, T.L.M. Maesen, Nature 451 (2008) 671-678.

[84] J. Breen, R. Burch, M. Kulkarni, P. Collier, S. Bolunski, J. Am. Chem. Soc. 127 (2005) 5020-5021.

[85] Y. Zhao, H. Wu, W. Tan, M. Zhang, M. Liu, C. Song, X. Wang, X. Guo, Catalysis Today 156 (2010) 69-73.

[86] N.Y. Chen, W.W. Kaeding, F.G. Dwyer, J. Am. Chem. Soc. 101 (1979) 6783.

[87] J. W. Niemantsverdriet, Spectroscopy in Catalysis, Wiley-VCH, Germany, 2007.

[88] N. Tøpsoe, K. Pedersen, E.G. Derouane, J. Catal. 70 (1981) 41-52.

[89] P.A. Jacobs, R. Von Ballmoos, J. phys. Chem. 83 (1982) 3050-3052.

[90] J.A. Lercher, C. Gründling, G. Eder-Mirth, Catal. Today 27 (1996) 353-376.

[91] E.P. Parry, J. Catal. 2 (1963) 371-379.

[92] C.A. Emeis, J. Catal. 141 (1993) 347-354.

[93] A. Corma, V. Fornes, L. Forni, F. Marquez, J. Martinez-Triguero, D. Moscotti, J. Catal. 179 (1998) 451-458.

[94] S. Brunauer, P. H. Emmett, E. Teller, J. Am. Chem. Soc. 60 (1938) 308-319.

[95] B.C. Lippens, B.G. Linsen, J.H. de Boer, J. Catal. 3 (1964) 32-37.

[96] G. Halsey, J. Chem. Phys. 16 (1948) 931-937.

[97] M. Kruk, M. Jaroniec, J. Choma, Carbon 36 (1998) 1447.

[98] S. J. Gregg, Adsorption Surface Area and Porosity, 2nd ed.; Academic Press Inc.: New York, 1982.

[99] E.P. Barrett, L.G. Joyner, P.P. Halenda, J. Am. Chem. Soc. 73 (1951) 373-380.

[100] K. Sing, Colloids Surf., A 187-188 (2001) 3-9.

[101] A. Chatterjee, T. Iwasaki, T. Ebina, A. Miyamoto, Micropor. Mesopor. Mater. 21 (1998) 421-428.

[102] G. Mirth, J.A. Lercher, J. Catal 147 (1994) 199-206.

[103] R. Kumar, P. Ratnasamy, J. Catal 118 (1989) 68-78.

[104] U. Olsbye, M. Bjørgen, S. Svelle, K. Lillerud, S. Kolboe, Catal. Today 106 (2005) 108-111.

[105] D. Lesthaeghe, A. Horré, M. Waroquier, G.B. Marin, V. Van Speybroeck, Chem. Eur. J. 15 (2009) 10803-10808.

[106] B. Smit, T.L.M. Maesen, Nature 451 (2008) 671-678.

[107] T.F. Degnan, J. Catal 216 (2003) 32-46.

[108] J.C. Groen, W. Zhu, S. Brouwer, S.J. Huynink, F. Kapteijn, J.A. Moulijn, J. Pérez-Ramírez, J. Am. Chem 129 (2007) 355-360.

[109] F.C. Meunier, D. Verboekend, J.P. Gilson, J.C. Groen, J. Pérez-Ramírez, Micropor. Mesopor. Mater. 148 (2012) 115-121.

[110] R. Kolvenbach, J. H. Ahn, S. S. Al-Khattaf, A. Jentys, J. A. Lercher, in preparation

[111] C.H. Christensen, K. Johannsen, E. Törnqvist, I. Schmidt, H. Topsøe, C.H. Christensen, Cat. Today 128 (2007) 117-122.

[112] C.H. Christensen, K. Johannsen, I. Schmidt, C.H. Christensen, J. Am. Chem 125 (2003) 13370-13371.

[113] C. Fernandez, I. Stan, J.P. Gilson, K. Thomas, Aurélie Vicente, A. Bonila, J. Pérez-Ramírez, Chem. Eur. J. 16 (2010) 6224-6233.

Chapter 2

Methanol usage in toluene methylation with medium and large pore zeolites

The reaction of toluene methylation was investigated with four acidic zeolites of different pore geometries, i.e., the medium pore zeolites H-ZSM5 and H-ZSM11 as well as the large pore zeolites H-MOR and H-BEA. The methylation, methanol consumption, light hydrocarbon formation and disproportionation rates for the reaction of toluene, p-xylene and 1,2,4-trimethylbenezene with methanol were determined. The products of toluene methylation, e.g., xylenes and trimethylbenzenes, were readily methylated further in both medium and large pore zeolites. Considerably higher fraction of methanol was used to form light hydrocarbons with the medium pore zeolites than with large pore zeolites. This was related to the fact that the dealkylation of light hydrocarbons from highly methylated aromatics became more favorable relative to methylation at an earlier stage, i.e., after fewer methyl groups were added to the aromatic ring. Increasing the effective residence time of bulky aromatic molecules with medium pore zeolites, modified either by coating the surface with tetraethyl orthosilicate or by increasing the intra-crystal pore length, converted a larger fraction of methanol to light hydrocarbons via methylation and subsequent dealkylation of light hydrocarbons.

2.1. Introduction

Benzene, toluene and xylenes, are important raw materials for variety of petrochemical commodities [1,2,3]. The majority of these molecules are generated via catalytic reforming or as byproducts of naphtha cracking [2,3]. Among the three, toluene is produced in excess relative to the market demand [1] and methylation of toluene to xylenes would, therefore, be a potential way to balance the deficiency of xylene production.

In toluene methylation, methanol (MeOH) reacts with a toluene to form a xylene (Scheme 2.1). Under typical reaction conditions, this reaction is accompanied by several side reactions leading to light hydrocarbons (LH) [4,5,6,7] and further methylated aromatics, e.g., trimethylbenzene (TriMB) and tetramethylbenzene (TetraMB) [5,8,9,10]. Many research groups have, thus, used an excess of toluene relative to methanol [6,11,12,13] to avoid formation of these side products, albeit with the drawback of lower maximum toluene conversions and relatively high selectivity to light hydrocarbons, nevertheless. Inefficient methanol usage, even in excess of toluene relative to methanol is, thus, one of the major drawbacks for the process commercialization [3] and has not been resolved.

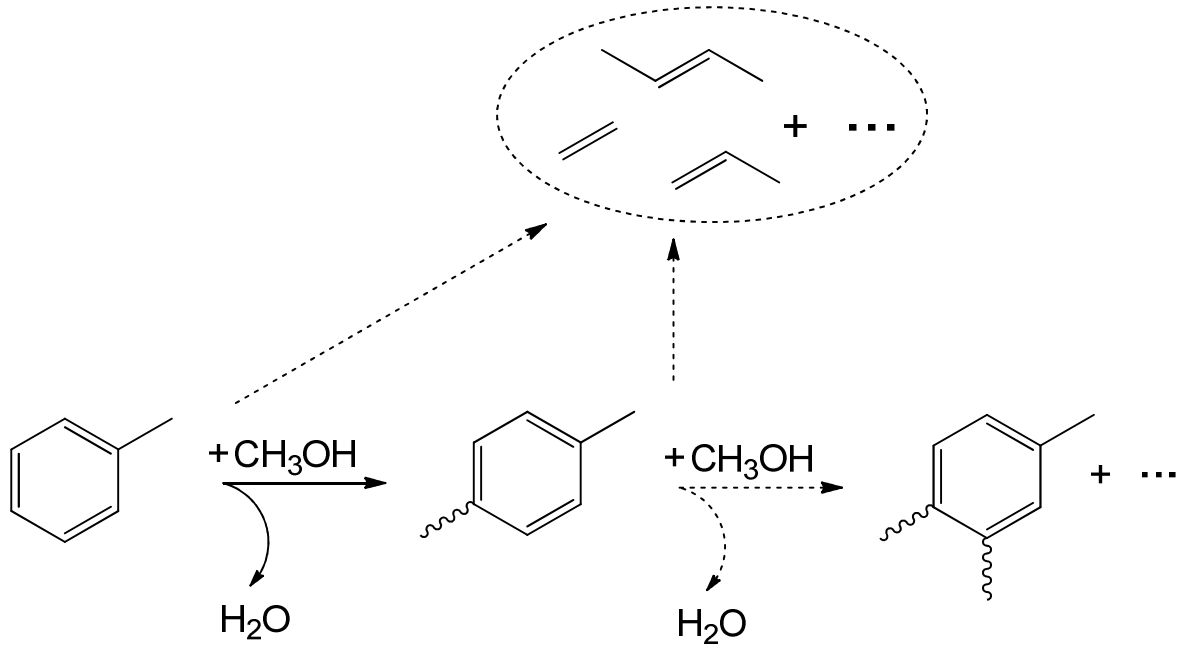

Scheme 2.1: The reaction of toluene methylation with methanol. The formation of undesired side products during the reaction such as light hydrocarbons and trimethylbenzenes are indicated by dashed arrows.

Thus, we selected four different acidic zeolites to gain insight into the methanol usage during toluene methylation, i.e., H-ZSM5, H-ZSM11, H-MOR and H-BEA; the first two are medium pore-sized zeolites (10-membered ring (MR)) and the latter two large pore-sized zeolites (12-MR). The data here indicated that most of the methanol was used for methylation of toluene and its aromatic products, e.g., xylenes and TriMBs, but the dealkylation of light hydrocarbons from highly methylated aromatic molecules eventually became more favorable relative to methylation because of product shape selectivity [14]. The multiple aromatic methylation and the subsequent dealkylation is a well-discussed reaction pathway for the formation of light hydrocarbons during methanol-to-hydrocarbons reactions [9,15,16,17]. The formation of ethene as well as some propene [18] is likely to occur by side chain methylation (via methylation of methyl group of an aromatic ring) or by a paring mechanism (via aromatic ring contraction and expansion) [19,20]. In this work, we provide clear evidence that such a reaction route also plays an important role in the methanol usage during the toluene methylation reaction.

2.2. Experimental

2.2.1. Materials

The materials H-ZSM5 (Si/Al = 36), H-MOR (Si/Al = 45) and H-BEA (Si/Al = 75) were provided by Süd-Chemie and H-ZSM11 was synthesized by using tetrabutylammonium hydroxide (TBAOH; ≥99.0 %, 30-hydrate, Sigma Aldrich) and 1,8-diamino-octane (DAO; 98 %, Sigma Aldrich) as the organic templates for small (SC) and large crystal (LC) zeolites, respectively [21,22]. Aluminum nitrate (≥98 %, nona-hydrate), fumed silica (Cab-O-sil M-5) and sodium hydroxide (≥98 %) were used for SC H-ZSM11 synthesis and aluminum sulphate (99.99 %), potassium hydroxide (99.99 %) and silica sol (Ludox AS-30) for LC H-ZSM11 synthesis (all purchased from Sigma Aldrich). The gel composition for SC H-ZSM11 was 9TBAOH: Al_2O_3: 90SiO_2: 1065H_2O: 6.5Na_2O. The uniform mixture was aged overnight and transferred into Teflon liners and sealed inside autoclaves. The crystallization time was 18 hours at 448 K under rotation (60 rpm). The gel composition for LC H-ZSM11 was 26DAO: Al_2O_3: 90SiO_2: 3580H_2O: 12K_2O. This mixture was aged for ~1 hour before it was transferred

into Teflon liners and sealed inside autoclaves. The crystallization time was 72 hours at 433 K under static conditions.

After the desired crystallization time, the autoclaves were cooled under water, the solids separated by centrifugation and washed three times with deionized water. The samples were dried in an oven at 353 K, ground and treated at 823K (heating rate of 0.05 K s^{-1}) for 10 hours in synthetic air (flowing at 1.67 cm^3 s^{-1}; 20.5% O_2 in N_2, Westfalen) to remove the organic templates.

After the template removal, ammonium ion exchange was carried out at 353 K under stirring for 6 hours in a 0.2 M NH_4Cl solution (30 cm^3 per gram of zeolite). This procedure was repeated three times. After the third ammonium exchange, the zeolites were separated by centrifugation, washed, dried and treated in synthetic air (flowing at 1.67 cm^3 s^{-1}) for 10 hours (heating rate of 0.05 K s^{-1}) at 823 K to obtain the protonic form of the zeolite.

The surface modified (SM) sample of H-ZSM5 was prepared by heating 10 g of zeolite in 250 cm^3 of hexane (>97 %, Sigma Aldrich) containing 1.5 cm^3 of tetraethyl orthosilicate (TEOS; 4 weight% SiO_2 relative to the zeolite; >99.0 %, Sigma Aldrich) at 353 K under stirring for 1 hour [23]. Hexane was removed by a rotary evaporator under vacuum and the sample was dried at 353 K and subsequently treated in a synthetic air (flowing at 1.67 cm^3 s^{-1}) at 353 K (0.083 K s^{-1}) for 2 hours, at 453 K (0.033 K s^{-1}) for 3 hours and finally at 823 K (0.033 K s^{-1}) for 5 hours. This procedure was repeated three times before the material was characterized and tested (total deposition amount of 12 wt % SiO_2).

2.2.2. Catalyst characterization

The elemental composition of the zeolites was determined by atomic absorption spectroscopy (AAS; Unicam M Series Flame-AAS equipped with an FS 95 auto-sampler and a GF 95 graphite furnace) and the purity and crystallinity of the samples were examined by X-ray diffraction (XRD; Philips X'Pert Pro system, $\lambda_{CuK\alpha}$ = 0.154056 nm, 40 kV/40 mA) recorded between 2 θ angles of 5-70° (step size of 0.017° and a scan speed of 115 seconds per step). Nitrogen physisorption measurements were carried out at 77 K on PMI automated sorptometer after outgassing the samples under vacuum at 523 K for 2 hours. The BET surface area [24] was calculated from the nitrogen adsorption data over a relative pressure

range from 0.01-0.1 p/p_0. The pore volumes and external surface areas were evaluated by using the t-plot method [25] according to Halsey [26]. The scanning electron microscopy (SEM) images of all samples were recorded on a JEOL JSM 5900LV microscope operating at 25 kV. The characteristic diffusion time of medium pore zeolites were determined by measuring o-xylene uptake rates by flowing 2.1 $cm^3\ s^{-1}$ of helium to a self-supporting wafer in a cell (1.5 cm^3), using infrared spectroscopy (Thermo Nicolet 6700 FT-IR spectrometer, resolution of 4 cm^{-1}). The sample was activated at 523 K (heating rate of 0.17 K s^{-1}) under flowing helium for 12 hours before switching to a second helium stream (2.1 $cm^3\ s^{-1}$) with saturated o-xylene (0.05 kPa). The spectra were measured every 60s at 403 K and were normalized to the integral of the overtone lattice band between 2105 and 1740 cm^{-1} of the activated H-ZSM5 sample. The characteristic ring vibrations of o-xylene at 1496 and 1466 cm^{-1} [27] were integrated and normalized to the steady state integral to determine the characteristic diffusion time (L^2/D_{app}) with the equation below:

$$\frac{m}{m_\infty} = 1 - \sum_{n=1}^{\infty} \frac{6}{n^2\pi^2} \exp\left(\frac{-n^2\pi^2 D_{app} t}{L^2}\right) \quad (2.1)$$

Here, m and m_∞ are the uptake at time t and after equilibration, respectively, D_{app} the apparent diffusion coefficient and L the average crystal size of a zeolite.

Infrared spectroscopy (Thermo Nicolet 5700 FT-IR spectrometer, resolution of 4cm^{-1}) with pyridine (99.8 %, Sigma Aldrich) as probe molecule was used to determine the total concentration of Brønsted and Lewis acid sites. The spectrum of an activated sample (pressed into a self-supporting wafer with density of ~0.01 g cm^{-2}) was measured at 423 K, after evacuating for 1 hour at 723 K (heating rate of 0.17 K s^{-1}). Pyridine was adsorbed on the zeolite at 0.01 kPa, 423 K for 0.5 hour and outgassed for 1 hour under vacuum to desorb weakly bound species. The total concentration of Brønsted and Lewis acid sites was determined by integrating the peaks at 1546 and 1455 cm^{-1}, respectively.

2.2.3. Catalytic testing

The catalysts (180-250 μm particle size) and silicon carbide (7 times the weight of the catalyst; F46, ESK-SiC GmbH), held in place by quartz wool inside a quartz plug flow reactor (0.4 cm ID), were activated at 823 K (heating rate of 0.17 K s^{-1}) under flowing He (1.7 $cm^3\ s^{-1}$; 99,996%, Westfalen) prior to the reaction. The temperature was measured by a

thermocouple in external contact to the reactor and was maintained constant by a stainless steel furnace connected to a Eurotherm controller (Series 2416). The catalysts were tested at 673 K at 101 kPa by flowing premixed feed of toluene (>99.9 %, Sigma Aldrich) or p-xylene (>99 %, Sigma Aldrich) or 1,2,4-trimethylbenzene (98 %, Sigma Aldrich) with methanol (>99.8 %, Sigma Aldrich) into a vaporizer filled with silicon carbide. The total flow rate was 2.3 cm^3 s^{-1} and the aromatic to methanol molar ratio was 4 with $p_{aromatic}$ = 1.2-6 kPa and $p_{methanol}$ = 0.3-1.5 kPa. The reactor effluent was sampled ~0.75 hour after the start of the reactant flow into the reactor and was analyzed by on-line gas chromatography (Agilent 7820A) using a DB-WAX column (30 m x 0.32 mm x 0.5 μm) and a flame ionization detector. The product selectivities did not change significantly with the reaction time (time-on-stream behavior of a medium (H-ZSM5) and large (H-BEA) pore zeolites is summarized in Table 2.S1).

The rates of methylation (toluene, p-xylene and 1,2,4-TriMB; based on consumption) were calculated by multiplying the aromatic feed rate per gram of zeolite in the reactor (mol g^{-1} s^{-1}) by the conversion of the reactant aromatic molecule (%; the isomers, e.g., o- and m-xylene when p-xylene was co-fed with methanol, were treated as reactants) and dividing it by the concentration of Brønsted acid sites (mol H^+ g^{-1}), determined by the adsorption of pyridine. The formation rates of light hydrocarbon were calculated by multiplying the rate of total carbons in the feed per gram of zeolite in the reactor by the carbon selectivity of light hydrocarbons formed and dividing it by the concentration of Brønsted acid sites.

2.3. Results

2.3.1. Catalyst characterization

The micropore structure and dimensions, the chemical compositions, textural properties and acid site concentration of all zeolite samples derived from atomic absorption spectroscopy, nitrogen physisorption and IR spectra of adsorbed pyridine are summarized in Table 2.1. The total concentration of acid sites (Brønsted and Lewis) determined by adsorption of pyridine agreed well with the calculated values from Si/Al ratios (within ±10%). The Brønsted acid site concentration of H-BEA sample was lower than the others used here,

but the lower acid site concentration of H-BEA did not significantly affect the fraction of methanol usage calculated (section 3.3; see also Table 2.S2-2.S3).

Table 2.1: The channel size and dimensions, chemical compositions, textural properties and acid site concentrations of all zeolite samples tested.

Catalyst	H-ZSM5	H-ZSM11-SC[a]	H-MOR	H-BETA	H-ZSM5-SM[b]	H-ZSM11-LC[c]
Channel size (10^{-1} nm)	{5.1 x 5.5 5.3 x 5.6}***	5.3 x 5.4***	{6.5 x 7 2.6x 5.7}***	6.6 x 6.7** 5.6 x 5.6*	{5.1 x 5.5 5.3 x 5.6}***	5.3 x 5.4***
Si/Al ratio[d]	36 (36)	34 (33)	43 (40)	79 (82)	42 (39)	33 (30)
S_{BET}[e] (m^2 g^{-1})	435	445	584	718	434	427
S_{ext}[f] (m^2 g^{-1})	55	110	81	189	74	2
V_{mi}[g] (cm^3 g^{-1})	0.16	0.13	0.18	0.20	0.13	0.16
Brønsted acid (μmol g^{-1})	380	387	307	175	336	424
Lewis acid (μmol g^{-1})	67	100	98	24	73	112

[a]SC = small crystal. [b]SM = surface modified sample with TEOS. [c]LC = large crystal. [d]Si/Al ratio calculated from the acid concentration from the pyridine adsorption is shown in parenthesis. [e]S_{BET} = BET surface area. [f]S_{ext}, and [g]V_{mi} are external surface area and micropore volume, respectively, calculated from t-plot method (Halsey).

The XRD of synthesized H-ZSM11 (small and large crystals) indicated that both materials are free of crystalline impurities (Figures 2.S1 and 2.S2). Narrower XRD peaks of large crystal sample suggest that the primary crystal size is significantly larger than that of small crystal H-ZSM11. The SEM images of all samples are shown in the supporting material (Figures 2.S3-2.S8). The particle for all samples was around 0.5 μm or less, except for the large crystal H-ZSM11 sample (~6 μm).

2.3.2. Methylation of toluene in medium and large pore zeolites

The reactant (C_1 and toluene) conversions, selectivity of xylenes in aromatics, toluene methylation and light hydrocarbon formation rates on both medium and large pore zeolites are shown in Table 2.2. Here, the C_1 refers to methanol and dimethyl ether (DME) and we treat them as one reactant (accounting for the fact that DME has twice as many carbon atoms as MeOH), because methanol can reversibly dehydrate to DME under typical reaction conditions and DME can be used to methylate unsaturated aromatic/alkene molecules via similar mechanisms [28,29]. The reaction order of toluene methylation was between zero and first

with respect to methanol and first with respect to toluene under the reaction conditions used (see Figure 2.S9-2.S10). Small crystal H-ZSM11 was used for all catalytic tests, unless indicated otherwise and the catalyst amount was adjusted to keep the C_1 conversion (the limiting reactant) at a comparable range. The rate of toluene methylation was similar for all zeolites, but the xylene selectivity was somewhat higher and the light hydrocarbon formation rates significantly higher for the medium compared to the large pore zeolites.

Table 2.2: C_1 and toluene conversion, xylene selectivity, toluene methylation and light hydrocarbon formation rates[a] with medium[b] and large[c] pore zeolites in toluene methylation

Catalyst	H-ZSM5	H-ZSM11	H-MOR	H-BETA
C_1 conversion[d] (%)	55	64	55	53
Toluene conversion (%)	6.4	7.9	9.4	8.7
Xylenes in aromatics (%)	88	86	77	74
Toluene methylation rates[e] [10^{-2} mol (mol H s)$^{-1}$]	16	17	15	15
Light hydrocarbon formation rates [10^{-2} mol C (mol H s)$^{-1}$]	10	10	2.0	0.3

[a]Reaction rates are measured at $p_{toluene}$ = 6 kPa, $p_{methanol}$ = 1.5 kPa, 673 K, 6-20 mg catalyst and 2.3cm^{3}s^{-1} total flow rate. [b]H-ZSM5 and H-ZSM11. [c]H-MOR and H-BEA. [d]C_1 is methanol and DME (both are treated as the same reactant because methanol can be transformed into DME during the reaction and DME can also be used for methylation). [e]Calculated based on the toluene consumption.

2.3.3. Methanol usage in methylation of toluene

To better define methanol usage during the methylation of toluene, three different fractional use of reactant (based on C_1 usage) were calculated, i.e., *MeOH for toluene alkylation*, *MeOH for aromatics alkylation*, *MeOH for LH formation*, and the definitions are shown below:

$$\textit{Fraction of MeOH for toluene alkylation} = \frac{\mathrm{Toluene_{in} - Toluene_{out} - 2\ x\ Benzene}}{\mathrm{Methanol_{in} - (Methanol + 2 \times DME)_{out}}} \quad (2.2)$$

$$\textit{Fraction of MeOH for aromatics alkylation} = \frac{\mathrm{1\ x\ Xylenes + 2\ x\ TriMB + 3\ x\ TetraMB + \ldots}}{\mathrm{Methanol_{in} - (Methanol + 2 \times DME)_{out}}} \quad (2.3)$$

$$\textit{Fraction of MeOH for LH formation} = \frac{2\ x\ C_2 + 3\ x\ C_3 + 4\ x\ C_4 + \ldots}{\mathrm{Methanol_{in} - (Methanol + 2 \times DME)_{out}}} \quad (2.4)$$

The subscripts “in” and “out” indicate the rate of reactant (toluene or methanol/DME) going in and out of the reactor, respectively. Each term in the numerator of equations 3-4, as well as

"Benzene" in equation 2, is the formation rate measured (mol [s mol H]$^{-1}$). Equation 2 (*MeOH for toluene alkylation*) describes the fraction of methanol (and DME) that is used for the methylation of toluene. If the fraction is equal to 1, all of methanol is used for the methylation of toluene and this would be the ideal case. Equation 3 (*MeOH for aromatics alkylation*) describes the fraction of methanol used for alkylating the aromatic ring of toluene. If the fraction is equal to 1, methanol selectively reacts with aromatic molecules and does not form light hydrocarbons. In the numerator, the moles of xylenes formed is multiplied by one because one mole of C_1 is added to the starting aromatic molecule (toluene), the moles of TriMBs formed is multiplied by two because two moles of C_1 are added to toluene. Equation 4 (*MeOH for LH formation*) describes the fraction of methanol used for the formation of light hydrocarbons. If the fraction is 1, methanol only forms light hydrocarbons and is not used for the methylation of aromatics. In the numerator, the moles of C_2 (ethene and ethane) formed is multiplied for example by two, because two moles of C_1 are used to generate C_2 species.

The methanol usage in medium pore (H-ZSM5 and H-ZSM11) and large pore (H-MOR and H-BEA) zeolites are summarized in Figure 2.1. With H-MOR and H-BEA (large pore zeolites), the fraction of *MeOH for toluene alkylation* was only ~0.65-0.7 (Figure 2.1, left) but the fraction of *MeOH for aromatics alkylation* was very high (>0.9; Figure 2.1 right) and the *MeOH for LH formation* low (<0.1; Figure 2.1 right). A high fraction of *MeOH for aromatics alkylation* indicates that most of methanol was utilized to methylate toluene and the products of toluene methylation, e.g., xylenes and TriMBs, in large pore zeolites. The fraction of *MeOH for toluene alkylation* was somewhat lower (~0.55; Figure 2.1 left) with H-ZSM5 and H-ZSM11 (medium pore zeolites) and unlike the large pore zeolites, the fraction of *MeOH for aromatics alkylation* was only slightly higher than the fraction of *MeOH for toluene alkylation* (~0.65; Figure 2.1 right) with a relatively high fraction of *MeOH for LH formation* (~0.35; Figure 2.1 right). This indicates that a considerable amount of methanol was used for the formation of light hydrocarbons in the medium pore zeolites.

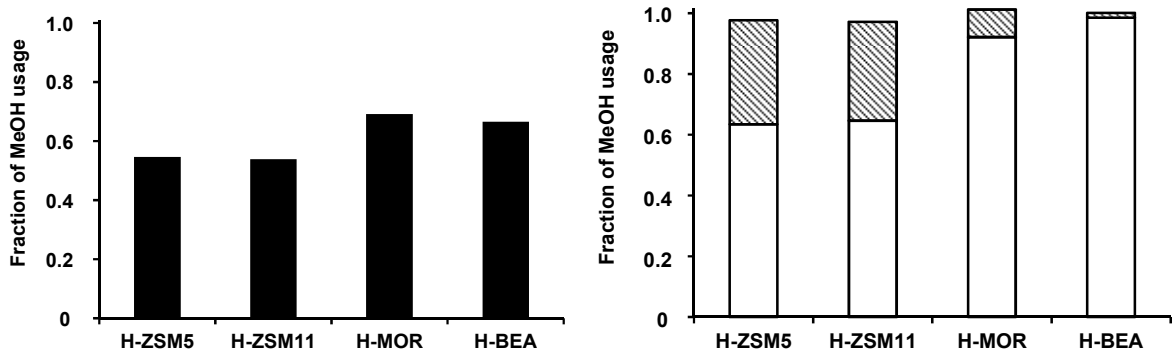

Figure 2.1: Fraction of MeOH used for the methylation of toluene (*MeOH for toluene alkylation*; left, filled), methylation of aromatics (*MeOH for aromatics alkylation*; right, empty) and formation of light hydrocarbons (*MeOH for LH formation*; right, striped) calculated for both medium (H-ZSM5 and H-ZSM11) and large pore zeolites (H-MOR and H-BEA) at $p_{toluene}$ = 6 kPa, $p_{methanol}$ = 1.5 kPa, 673 K, 6-20 mg catalyst, 2.3 cm^3s^{-1} total flow rate, and C_1 conversion = 53-64 %.

2.3.4. Reaction of toluene, p-xylene and 1,2,4-trimethylbezene with methanol

The rate of methylation (measured at the same partial pressures and similar C_1 conversion levels) of toluene, p-xylene and 1,2,4-TriMB with large pore zeolites increased as the number of methyl substitutions in the aromatic ring increased. This trend was especially pronounced with H-BEA (Figure 2.2). An opposite trend was observed with medium pore zeolites (H-ZSM5 and H-ZSM11). The rates of light hydrocarbon formation, as well as the methanol usage towards light hydrocarbons (Fraction of *MeOH for LH formation*) in large pore zeolites increased systematically with number of methyl substitutions (Figure 2.3 and Figure 2.4). The same trends were observed with medium pore zeolites except that the light hydrocarbon formation rate decreased, when the number of methyl groups increased from p-xylene to 1,2,4-TriMB (Figure 2.3).

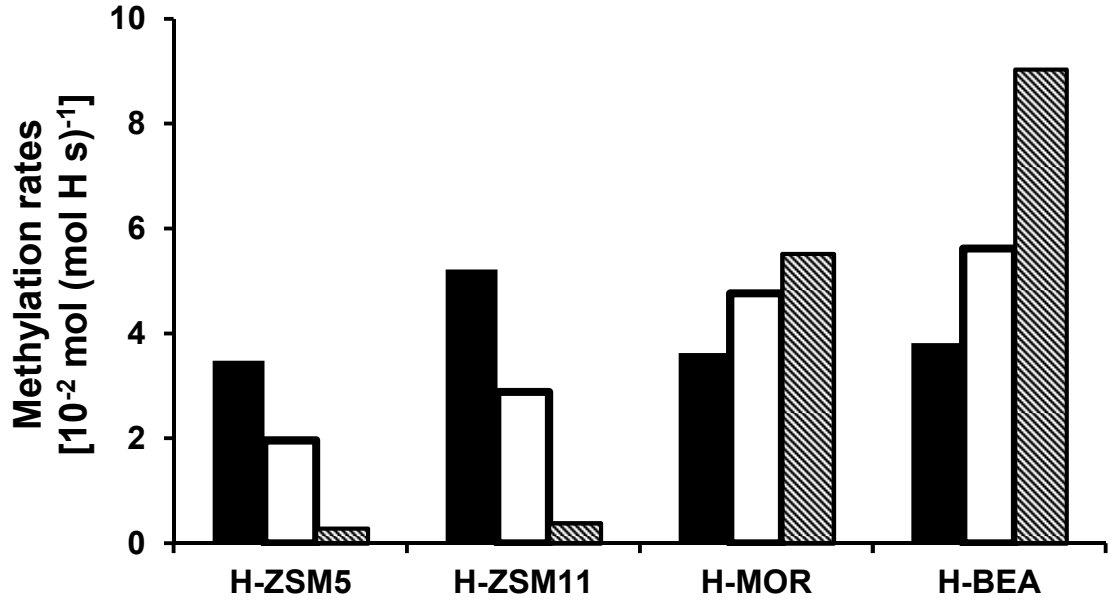

Figure 2.2: Rate of methylation when toluene (filled), p-xylene (empty) or 1,2,4-trimethylbenzene (striped) reacted with methanol in both medium (H-ZSM5 and H-ZSM11) and large pore zeolites (H-MOR and H-BEA) at $p_{aromatic}$ = 1.2 kPa, $p_{methanol}$ = 0.3 kPa, 673 K, 5-12 mg catalyst, 2.3 cm^3s^{-1} total flow rate, C_1 conversion = 51-58 % (H-ZSM5 and H-ZSM11) and 45-50 % (H-MOR and H-BEA).

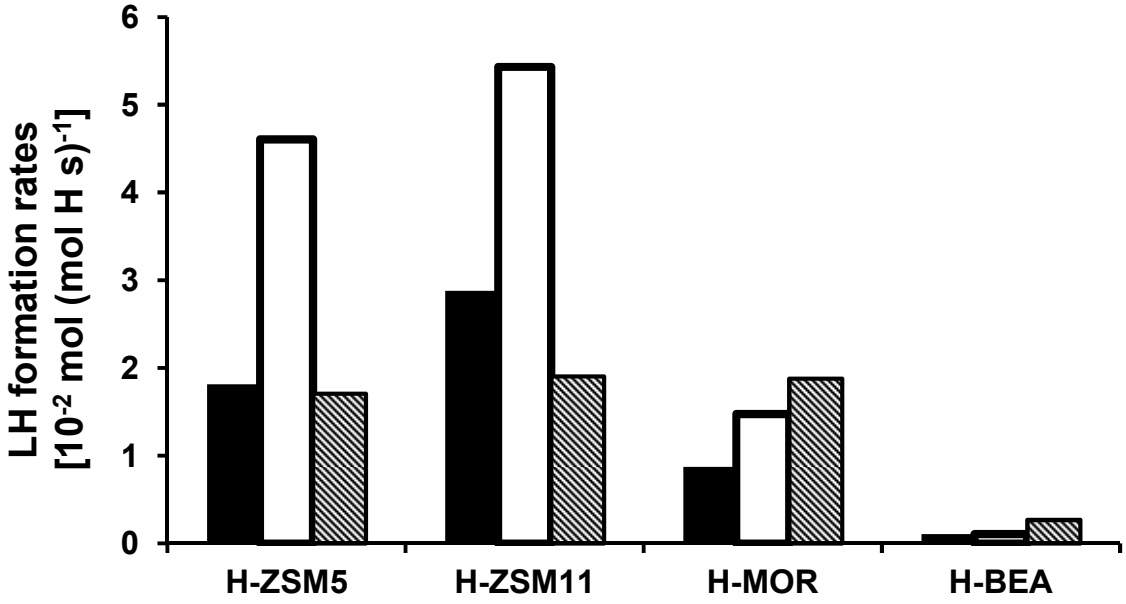

Figure 2.3: Rate of light hydrocarbon (LH) formation when toluene (filled), p-xylene (empty) or 1,2,4-trimethylbenzene (striped) reacted with methanol in both medium (H-ZSM5 and H-ZSM11) and large pore zeolites (H-MOR and H-BEA) at $p_{aromatic}$ = 1.2 kPa, $p_{methanol}$ = 0.3 kPa, 673 K, 5-12 mg catalyst, 2.3 cm^3s^{-1} total flow rate, C_1 conversion = 51-58 % (H-ZSM5 and H-ZSM11) and 45-50 % (H-MOR and H-BEA).

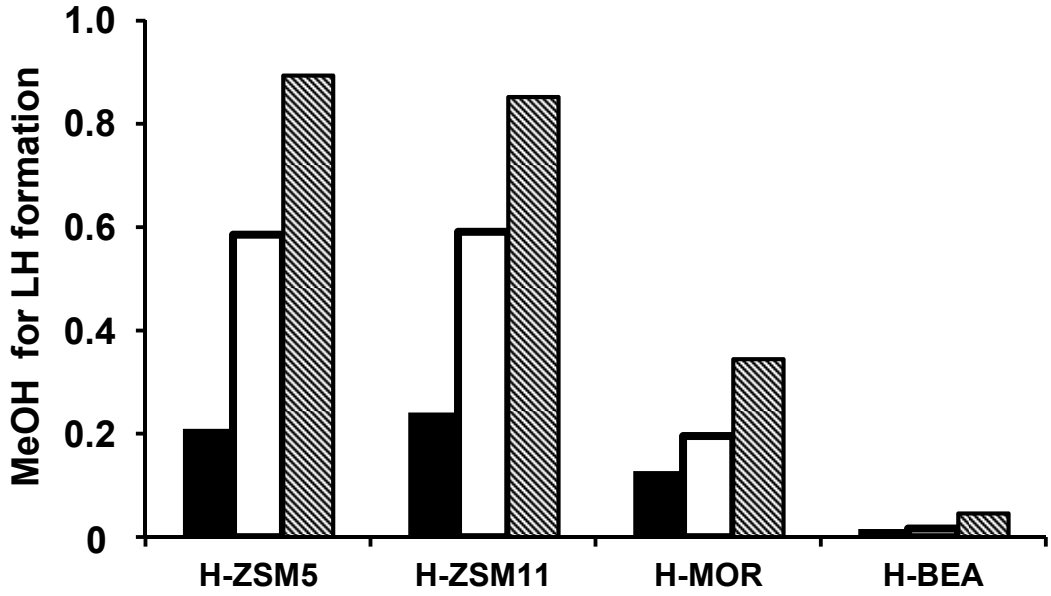

Figure 2.4: Fraction of methanol used for the formation of light hydrocarbons (*MeOH for LH formation*) when toluene (filled), p-xylene (empty) or 1,2,4-trimethylbenzene (striped) reacted with methanol in both medium (H-ZSM5 and H-ZSM11) and large pore zeolites (H-MOR and H-BEA) at $p_{aromatic}$ = 1.2 kPa, $p_{methanol}$ = 0.3 kPa, 673 K, 5-12 mg catalyst, 2.3 cm^3s^{-1} total flow rate, C_1 conversion = 51-58 % (H-ZSM5 and H-ZSM11) and 45-50 % (H-MOR and H-BEA).

2.3.5. Effect of residence time on methanol usage in toluene methylation

Two additional medium pore zeolites were used in order to investigate the relationship between the residence time of bulky methylated aromatics and the methanol usage in toluene methylation. One was prepared by coating the outer surface of H-ZSM5 with tetraethyl orthosilicate. This method partially blocked access to the pore system and increased the overall tortuosity [11, 30, 31], thereby, increasing the effective residence time of bulky aromatics molecules, such as o- and m-xylenes [31]. The second sample was a large crystal H-ZSM11 zeolite (SEM image is shown in Figure 2.S7), for which the longer channel length should increase the effective residence time of molecules inside the micropores. For both modified samples, higher fraction of methanol was converted into light hydrocarbons and less was utilized for the methylation of aromatic molecules (Figure 2.5).

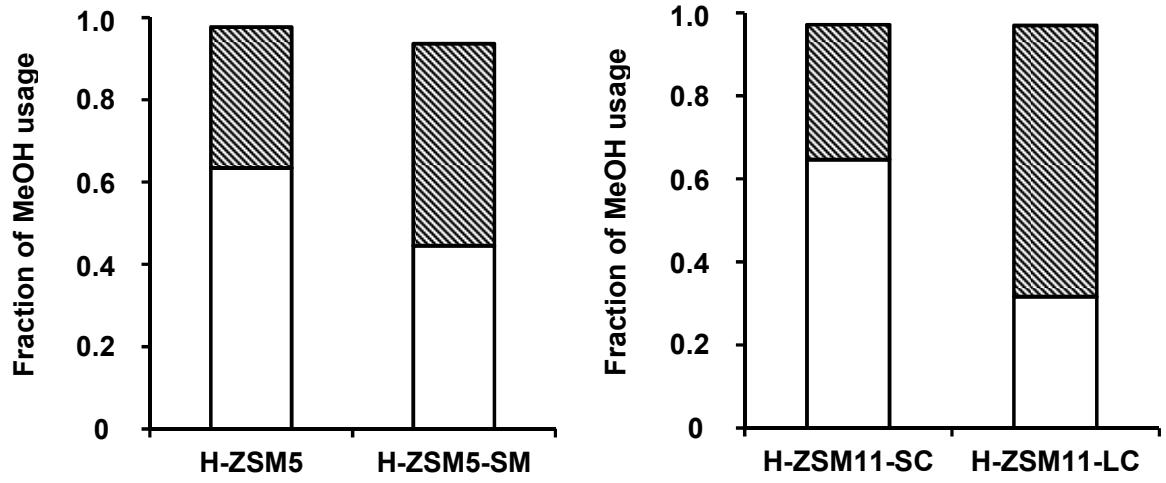

Figure 2.5: Fraction of methanol used for methylation of aromatics (*MeOH for aromatics alkylation*; empty) and for formation of light hydrocarbons (*MeOH for LH formation*; striped) for H-ZSM5 (left, parent and surface modified (SM) with TEOS) and H-ZSM11 (right, small (SC) and large crystal (LC)) at $p_{toluene}$ = 6 kPa, $p_{methanol}$ = 1.5 kPa, 673 K, 5-10 mg catalyst, 1.7-2.3 cm^3s^{-1} total flow rate, C_1 conversion = 53-63 %.

2.4. Discussion

2.4.1. Methanol usage in toluene methylation with large pore zeolites

In the reaction of toluene methylation, one mole of toluene and one mole of methanol (or 0.5 mole of DME) are required to form one mole of xylene (Scheme 2.1). The methanol usage towards methylating toluene in H-MOR and H-BEA (large pore zeolites) is however, only ~0.65, i.e., *MeOH for toluene alkylation* fraction (Figure 2.1, left), despite the fact that toluene is present in four times (molar) excess relative to methanol. Methanol that is not used for the methylation of toluene reacts mostly in methylating the primary aromatic products from toluene methylation, e.g., xylenes and TriMBs, indicated by high *MeOH for aromatics alkylation* fraction (Figure 2.1, right). About 2 mol% with respect to the total concentration in aromatics was observed as hexamethylbenzene over both large pore zeolites.

More than 20 % of the C_1 converted in large pore zeolites is used for methylation of aromatics heavier than toluene, i.e., xylenes to TriMBs, TriMBs to TetraMBs, even though

the toluene concentration is >90 % of the aromatics in the gas phase. One of the reasons for the secondary methylation is related to the fact that the activation energy for methylation decreases with increasing methyl substitution of the aromatic ring, in the absence of steric hindrances [32,33]. The methyl groups are electron donating and increasing the number of methyl groups increases in the base strength of aromatic molecules. The rate of methylation indeed increases as the number of methyl substitution increases from toluene to p-xylene to 1,2,4-TriMB (Figure 2.2) and this most likely contributes to further methylation of methylated products from toluene, as well as lower xylene selectivity within aromatics (relative to medium pore zeolites; Table 2.2).

2.4.2. Methanol usage in toluene methylation with medium pore zeolites

The methanol usage towards toluene methylation is less efficient (~0.55; *MeOH for toluene alkylation* fraction in Figure 2.1, left) with H-ZSM5 and H-ZSM11 (medium pore zeolites) compared to the large pore zeolites, and a substantial fraction of methanol is converted into the light hydrocarbons (Figure 2.1 right). This is unexpected at first, especially because toluene is fed in a four times (molar) excess compared to methanol. Thus the formation of light hydrocarbons from methanol [34,35] is expected to play a minor role relative to the toluene methylation. Only a slight increase in *MeOH for aromatics alkylation* from *MeOH for toluene alkylation* fractions are observed (~0.65 from 0.55, see Figure 2.1), indicating that the bulky xylenes and TriMB is not methylated further or able to exit the micropores very slowly due to the relatively large size of these molecules. Note that only a very small amount of TetraMB (<2 mol %) and no penta- or hexamethylbenzenes were detected in the gas phase.

The kinetic results for H-ZSM5 and H-ZSM11 (Figure 2.2) show that the methylation rates of aromatics decrease, as the number of methyl substitutions increases, which is in contrast to the theoretical simulations reported in ref. [16]. The calculations using a 46 T-atom ZSM5 cluster, which accounts for the steric hindrances, indicates that the reaction rate constants for methylation increases from toluene to p-xylene and 1,2,4-TriMB by an order of magnitude at 673 K (the activation energy of methylation also decreased) [16]. Furthermore, the intersection diameter of H-ZSM5 (~0.9 nm) is larger than the kinetic diameter of the

bulkiest TetraMB (0.86nm for 1,2,3,5-TetraMB [36]). Thus, the methylation rate of aromatics in the medium pore zeolites probably does not decrease due to steric hindrances, at least for the methylation reaction occurring on Brønsted acid sites located at the intersections with the aromatic molecules tested here (1,2,4-TriMB methylates to TetraMB). The highly methylated aromatic molecules most likely methylate further, but leaves the zeolite pores as less-methylated aromatics, e.g., as xylenes and TriMBs, by splitting off light hydrocarbons (vide infra).

The fraction of methanol used for the formation of light hydrocarbons increases as the number of methyl groups increases in the aromatic ring (Figure 2.4). It is unlikely that the majority of the light hydrocarbons is generated from the direct coupling of methanol and/or DME because of high activation barriers [37,38] or from alkene methylation-cracking cycle [39,40], because the aromatics concentration is much higher compared to that of alkenes under the reaction conditions used (>50:1 in the gas phase). Therefore, we expect that most of the light hydrocarbons are formed by the methylation of aromatics followed by ring contraction-expansion (paring mechanism) or by side chain methylation with subsequent cracking [19,20].

It is difficult to unequivocally conclude, however, that all of the light hydrocarbons are generated via this route because alkene methylation has slightly lower energy of activation relative to the aromatic methylation [29,41]. Moreover, 1,2,4-TriMB diffuse slower than p-xylene to active sites in the micropores [31] and consequently, the local concentration ratio of alkenes to aromatics inside the micropores with 1,2,4-TriMB as an aromatic feed relative to p-xylene or toluene, may be higher during the reaction. Thus, the alkene methylation-cracking cycle could play a more significant role for the formation of light hydrocarbons and increase the *MeOH* for *LH formation* fraction (Figure 2.4), when 1,2,4-TriMB reacts with methanol compared to the reaction with p-xylene. The diffusivities of toluene and p-xylene, however, are similar [42,43], but a significant increase in the fraction of *MeOH for LH formation* is observed from toluene to p-xylene, as the reactant in the feed (Figure 2.4). The steady increase in methanol usage towards formation of light hydrocarbons with increasing methyl substitution and the similar diffusivities of toluene and p-xylene, therefore, indicate that most light hydrocarbons are generated from the highly methylated aromatics.

Figure 2.3 shows that the formation rate of light hydrocarbons increases significantly, when p-xylene (instead of toluene) is co-fed with methanol, suggesting that the overall generation of the light hydrocarbons is limited by the rate of sequential methylation of aromatics. The computational results also show that the light hydrocarbon dealkylation step is at least by an order of magnitude faster than the methylation step in MFI (H-ZSM5) framework [16]. When 1,2,4-TriMB is used as an aromatic in the feed instead of p-xylene, the light hydrocarbon formation rate decreases (Figure 2.3) most likely because the rate coefficient of 1,2,4-TriMB methylation decreases slightly relative to p-xylene methylation [16]. The intra-particle diffusion of bulkier TriMB to the active sites is also much slower than for p-xylene and less aromatic molecules are, thus, available for methylation and subsequent dealkylation of light hydrocarbons [31]. Methanol, nevertheless, is used more effectively for the light hydrocarbon formation, when reacting with 1,2,4-TriMB (higher methylated aromatics) compared to the less-methylated molecules such as p-xylene and toluene (Figure 2.4), because TriMB is closer to the point at which dealkylation is favored over methylation.

The methylation of the xylenes to TriMBs and TetraMBs continues in the zeolite pores, but it cannot be stated at which point the dealkylation to light hydrocarbons becomes more favorable, i.e., how many times toluene methylates, before the rate of dealkylation becomes faster than that of methylation. We speculate that 1,2,3,5-TetraMB can be formed in medium pore zeolites and methylated further at the geminal carbon position to 1,1,2,4,6-pentamethylbenzene, because the corresponding pentamethyl-benzenium cation (Figure 2.6) has been observed by NMR spectroscopy (formed most likely in the channel intersections) when toluene reacts with methanol [44]. Note that it is possible for penta- and hexamethylbenezene also to form inside the zeolite pores but these species were only indirectly detected, i.e., by dissolving the used zeolite in HF [45].

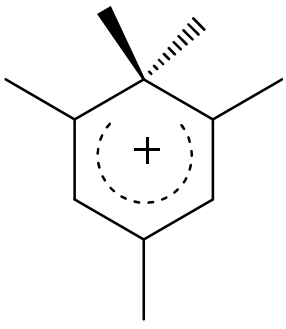

Figure 2.6: 1,1,2,4,6-petamethylbenzenium cation.

The dealkylation reactions from highly methylated aromatic molecules increase the selectivity of light hydrocarbon molecules (undesired byproducts) in toluene methylation. The comparison of disproportionation and methylation rates for toluene, p-xylene or 1,2,4-TriMB when co-fed with methanol, is shown in Table 2.3. The disproportionation rates are calculated as the equations shown below:

$$\textit{Disproportionation rate of toluene} = 2 \times \textit{formation rate of benzene} \quad (2.5)$$

$$\textit{Disproportionation rate of p-xylene} = 2 \times \textit{formation rate of toluene} \quad (2.6)$$

$$\textit{Disproportionation rate of 1,2,4-TriMB} = 2 \times \textit{formation rate of all xylenes} \quad (2.7)$$

The contribution to the products from disproportionation (e.g., benzene from toluene), increases, as the number of methyl groups in the aromatic ring increases (% reacted aromatic consumed for disproportionation in Table 2.3). These products result either from the disproportionation or demethylation or from a reaction involving the cleavage of a light hydrocarbon from a highly methylated aromatic molecule.

Table 2.3: C_1 conversion, methylation and disproportionation rates[a], percent of reacted aromatic molecule consumed for disproportionation, and xylene isomer selectivity with H-ZSM5 and H-ZSM11.

Catalyst	H-ZSM5			H-ZSM11		
Aromatic molecule in feed	Toluene	p-xylene	1,2,4-TriMB	Toluene	p-xylene	1,2,4-TriMB
C_1 conversion[b] (%)	54	51	53	57	51	58
Methylation rates[c] [10^{-2} mol (mol H s)$^{-1}$]	35	22	3.7	52	33	4.9
Disproportionation rates[d] [10^{-2} mol (mol H s)$^{-1}$]	0	1.1	1.6	0	1.3	1.8
% reacted aromatic consumed for disproportionation	0	4.8	31	0	3.7	26
% p-xylene within xylenes	59	93	54	55	92	47
% m-xylene within xylenes	23	6	36	27	7	41
% o-xylene within xylenes	18	1	10	18	1	12

[a]Reaction measured at $p_{toluene}$ = 1.2 kPa, $p_{methanol}$ = 0.3 kPa, 673 K, 5-12 mg catalyst and 2.3 cm^3s^{-1} total flow rate. [b]C_1 is methanol and DME. [c]Calculated based on the consumption of aromatic reactant in the feed. The isomers are treated also as a reactant. [d]Calculated as the equations 2.5-2.7.

Only a minor quantity of disproportionation products, i.e., benzene and toluene, relative to methylation products are observed, when toluene or p-xylene reacts with methanol, but the contribution of the disproportionation increases significantly for the reaction with 1,2,4-TriMB, as indicated by a large decrease and a slight increase in the rates of methylation and disproportionation, respectively, relative to the rates observed during toluene or p-xylene conversions (Table 2.3). Note that the disproportionation should not be significant [46,47,48] and de-methylation rates very slow compared to methylation rates [16,41] under the present reaction conditions in medium pore zeolites.

This suggests that a considerable fraction of the "disproportionation" products is formed from the dealkylation of light hydrocarbons from highly methylated aromatics. Some of these less-methylated aromatic molecules are most likely generated as p/m-xylenes because ~90% of xylenes from the reaction between methanol and 1,2,4-TriMB are observed as p/m-isomers (Table 2.3). A drastic decrease in the methylation rate of 1,2,4-TriMB compared to toluene or p-xylene in the feed may also indicate that TriMBs are formed as a major product in this reaction pathway and decreases, consequently, the overall conversion of 1,2,4-TriMB. The apparent rate of methylation, thus, decreases with increasing number of methyl groups on an aromatic ring (from toluene to p-xylene to 1,2,4-TriMB; Table 2.3) because the aromatic reactant, e.g., xylenes and especially TriMBs, are formed as a product after dealkylation of light hydrocarbons from highly methylated aromatics. For example, the lower conversion of 1,2,4-TriMB and in consequence, lower methylation rates during the reaction of 1,2,4-TriMB with methanol are observed compared to methylation with toluene, because the converted 1,2,4-TriMB in the feed forms the same reactant molecule again after aromatic methylation-dealkylation cycle.

In addition, the primary products of higher methylated aromatic reactants (e.g., TetraMBs from 1,2,4-TriMB) have higher probability to methylate further and dealkylate light hydrocarbons, because their diffusion rate is slower than that of the primary products of lower methylated aromatic reactants (e.g., xylenes from toluene). Note that only very small amounts of TetraMB and no penta- or hexamethylbenzenes are able to exit through the zeolite pores. Thus, the lower rate of methylation with an increase in number of methyl groups on the aromatic ring is also observed, because the primary products of p-xylene methylation are larger than the products of toluene methylation (likewise, the primary products of 1,2,4-TriMB methylation than p-xylene methylation).

The reaction network for toluene methylation with medium pore zeolites is described in Scheme 2.2. From the product distribution observed, we speculate that the methylation of toluene continues at least up to TetraMB, before the dealkylation of light hydrocarbons becomes more favorable relative to methylation. The stage at which the dealkylation reaction is favored over methylation is reached earlier for the medium pore than for the large pore zeolites, i.e., the light hydrocarbons are dealkylated as a less-methylated aromatic molecule, because of less available space in the micropores [39,45].

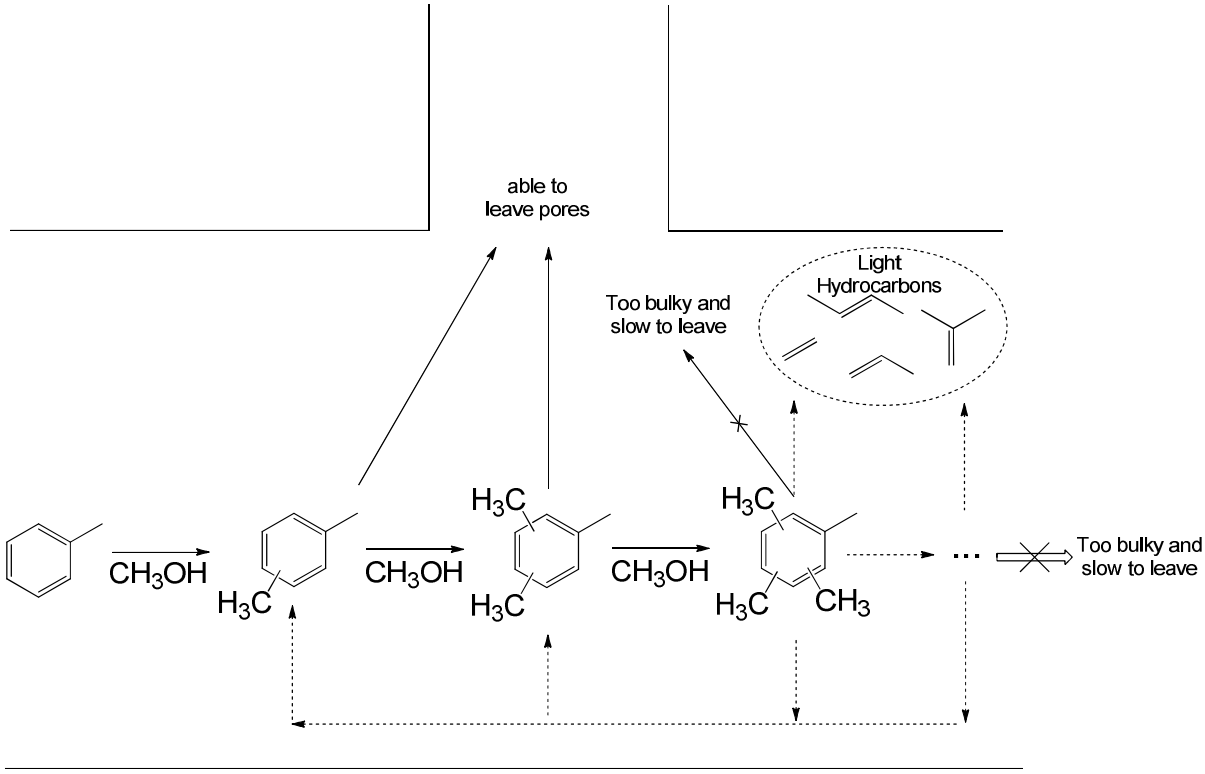

Scheme 2.2: The reactions occurring during the reaction of toluene methylation in medium pore zeolites.

2.4.3. Effect of residence time on methanol utilization in toluene methylation

With increasing the residence time of aromatic molecules inside the medium pore zeolites, i.e., with H-ZSM5-SM and H-ZSM11-LC, the methanol usage increases towards the formation of light hydrocarbons (*MeOH for LH formation*, Figure 2.5, striped) and decreases towards methylation of aromatics (*MeOH for aromatics alkylation*, Figure 2.5, empty). The increase in methanol usage to light hydrocarbons, observed with surface modified and large crystal samples, agrees with the hypothesis that most light hydrocarbons are formed via

methylation and dealkylation from highly methylated aromatic molecules. Longer residence time of aromatic molecules in H-ZSM5-SM and H-ZSM11-LC provide a higher chance for methylation and dealkylation pathway. In parallel, the *MeOH for aromatics alkylation* fraction decreases, because methanol is used for methylating higher methylated aromatics for dealkylation reactions instead of reacting with unreacted aromatic reactant (toluene). This agrees well with the observation that a higher fraction of methanol is incorporated into the aromatic ring of p/m-xylenes with larger crystals [9].

The fraction of methanol used for the formation of light hydrocarbons (*MeOH for LH formation*) and the characteristic diffusion time of o-xylene (relatively bulky aromatic molecule) with medium pore zeolites are shown in Table 2.4. The methanol usage to light hydrocarbons increases with the characteristic diffusion time. This suggests strongly that the highly methylated aromatic molecules act as an intermediate to generate light hydrocarbons under these experimental conditions and that increasing the effective residence time of these aromatic molecules shifts the selectivity towards light hydrocarbon formation in medium pore zeolites.

Table 2.4: Fraction of methanol used for the formation of light hydrocarbons with medium pore zeolites.

Catalyst	H-ZSM11-SC[c]	H-ZSM5	HZSM5-SM[d]	H-ZSM11-LC[e]
LH to C_1[a](%)	32	34	49	64
Characteristic diffusion time[b] (s)	1110	2430	6100	30640

[a]Fraction *of MeOH for LH formation,* defined in equation 4. The data obtained from Figure 2.5. [b]L^2/D determined by o-xylene uptake measurement at 403 K using IR spectroscopy. [c]SC = small crystal. [d]SM = surface modified sample with TEOS. [e]LC = large crystal.

Therefore, a more efficient use of methanol for methylation of toluene is conceivable, if the residence time of the bulky aromatic molecules inside the zeolite pores decreases. The increase in diffusivity of the highly methylated aromatic molecules with the large pore zeolites is, thus, expected to enhance the utilization of methanol towards toluene methylation. Yet the decrease in the activation energy with increasing methyl substitution and the lack of product shape selectivity results in a lower xylene selectivity than for the medium pore zeolites. Conceptually, smaller crystal sizes could also enhance methanol usage with medium pore zeolites. Considering the very small crystals (~100 nm) of H-ZSM5 sample used here, however, it may be challenging to achieve high methanol efficiency towards toluene methylation.

2.5. Conclusions

The present results show that significant fraction of C_1 was utilized to form undesired side-products, such as light hydrocarbons, tri- and tetramethylbenzenes, in toluene methylation reaction. The analysis suggests that the products of toluene methylation, e.g., xylenes and trimethylbenzenes, are readily methylated further in the zeolite pores. These highly methylated aromatic molecules eventually dealkylate light hydrocarbons. With medium pore zeolites (H-ZSM5 and H-ZSM11), the rate of these dealkylation reactions becomes kinetically competitive relative to methylation at an earlier stage, i.e., as less-methylated aromatics compared to the large pore zeolites (H-MOR and H-BEA). This pores size effect increases the xylene selectivity within aromatics and the methanol usage towards undesired light hydrocarbons in medium pore zeolites. Likewise for large pore zeolites, the lack of product shape selectivity decreases the selectivity of xylenes, but also the selectivity to light hydrocarbons. Therefore, the inefficiency of methanol converted during toluene methylation is caused by the further methylation of, e.g., xylenes and trimethylbenzenes (aromatic products of toluene), and eventual dealkylation as light hydrocarbons from product shape selectivity. Modest improvements are foreseen for catalytic materials with smaller zeolite crystals.

2.6. Acknowledgments

The financial support from the King Fahd University of Petroleum and Minerals (KFUPM) is acknowledged. Helpful technical discussions with André van Veen, Xianyong Sun and Oliver Gutiérrez, as well as the N_2 physisorption measurements by Xaver Hecht, SEM images and AAS measurements by Martin Neukamm are also acknowledged.

2.7. Supplementary material

Table 2.S1. C_1 and toluene conversion, xylene selectivity, toluene methylation and light hydrocarbon formation rates, and fraction of methanol usage at different time-on-stream.[a]

Catalyst	H-ZSM5		H-BEA	
Time-on-stream (hours)	0.75	2.8	0.75	1.3
C_1 conversion[b] (%)	67	67	54	50
Toluene conversion (%)	8.8	8.7	8.4	7.9
Xylenes in aromatics (%)	88	88	75	77
Toluene methylation rates[c] [10^{-2} mol (mol H s)$^{-1}$]	14	14	15	14
Light hydrocarbon formation rates [10^{-2} mol C (mol H s)$^{-1}$]	8.1	8.0	0.34	0.30
MeOH for toluene alkylation[d]	0.57	0.57	0.66	0.68
MeOH for aromatic alkylation	0.65	0.66	0.98	0.98
MeOH for LH[e] *formation*	0.33	0.33	0.02	0.01

[a]Reaction rates are measured at $p_{toluene}$ = 6 kPa, $p_{methanol}$ = 1.5 kPa, 673 K, 10-20 mg catalyst and 2.3 cm^3s^{-1} total flow rate. [b]C_1 is methanol and DME (both are treated as same reactant because methanol can be transformed into DME during the reaction and DME can also be used for methylation). [c]Calculated based on the toluene consumption. [d]Definitions of fraction of methanol (MeOH) usage are given in equations 2-4, in the manuscript. [e]LH = light hydrocarbons

The scanning electron microscope (SEM) image of H-BETA-150 (used above in chapter 2) and H-BETA-35 can be found in Figure 2.S6 below and in ref. [49], respectively.

Table 2.S2: The chemical compositions, textural properties and acid site concentrations of H-BEA[a].

Catalyst	H-BETA-150	H-BETA-35
Si/Al ratio	79	18
S_{ext} (m^2 g^{-1})[b]	189	135
V_{mi} (cm^3 g^{-1})[c]	0.20	0.21
Brønsted acid (μmol g^{-1})	175	427
Lewis acid (μmol g^{-1})	24	402

[a]H-BEA-150 was used in the manuscript for the catalytic testing. [b]S_{ext} and [c]V_{mi} are external surface area and micropore volume, respectively, calculated from t-plot method (Halsey).

Table 2.S3: C_1 and toluene conversion, xylene selectivity, toluene methylation and light hydrocarbon formation rates, and fraction of methanol usage on H-BEA[a].

Catalyst	H-BETA-150	H-BETA-35
C_1 conversion[b] (%)	53	58
Toluene conversion (%)	8.7	9.8
Xylenes in aromatics (%)	74	74
Toluene methylation rates[c] [10^{-2} mol (mol H s)$^{-1}$]	15	25
Light hydrocarbon formation rates [10^{-2} mol C (mol H s)$^{-1}$]	0.3	1.6
MeOH for toluene alkylation[d]	66	68
MeOH for aromatic alkylation	99	97
MeOH for LH[e] *formation*	1.5	4.1

[a]Reaction rates are measured at $p_{toluene}$ = 6 kPa, $p_{methanol}$ = 1.5 kPa, 673 K, 6-20 mg catalyst and 2.3 cm^3s^{-1} total flow rate. [b]C_1 is methanol and DME (both are treated as same reactant because methanol can be transformed into DME during the reaction and DME can also be used for methylation). [c]Calculated based on the toluene consumption. [d]Definitions of fraction of methanol (MeOH) usage are given in equations 2.2 - 2.4. [e]LH = light hydrocarbons.

The X-ray diffraction (XRD) patterns indicate that both materials are pure and do not contain any impurities. Typical impurity present during MEL (H-ZSM11) synthesis is MFI phase and the peak at ~45^o (2Θ) usually splits into two; Figures 2.S1 and 2.S2 have no splitting at this position. The SEM images also confirm this (Figure 2.S4).

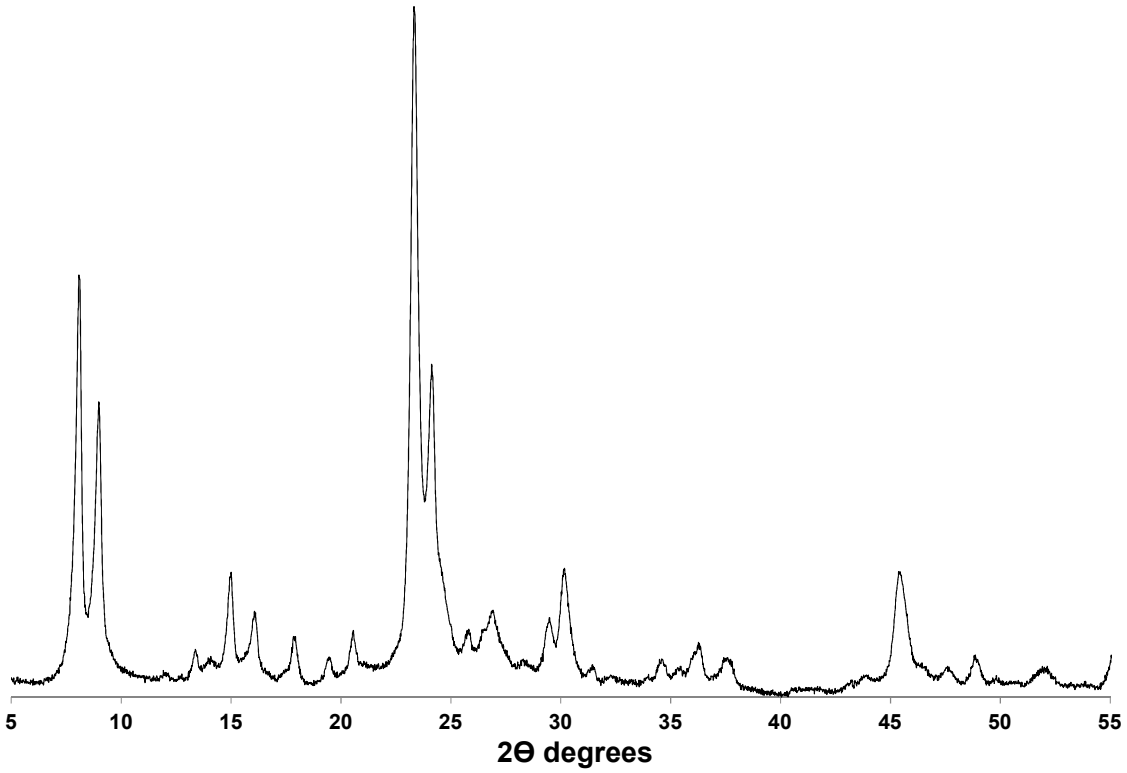

Figure 2.S1: Powder X-ray diffraction patterns of small crystal H-ZSM11.

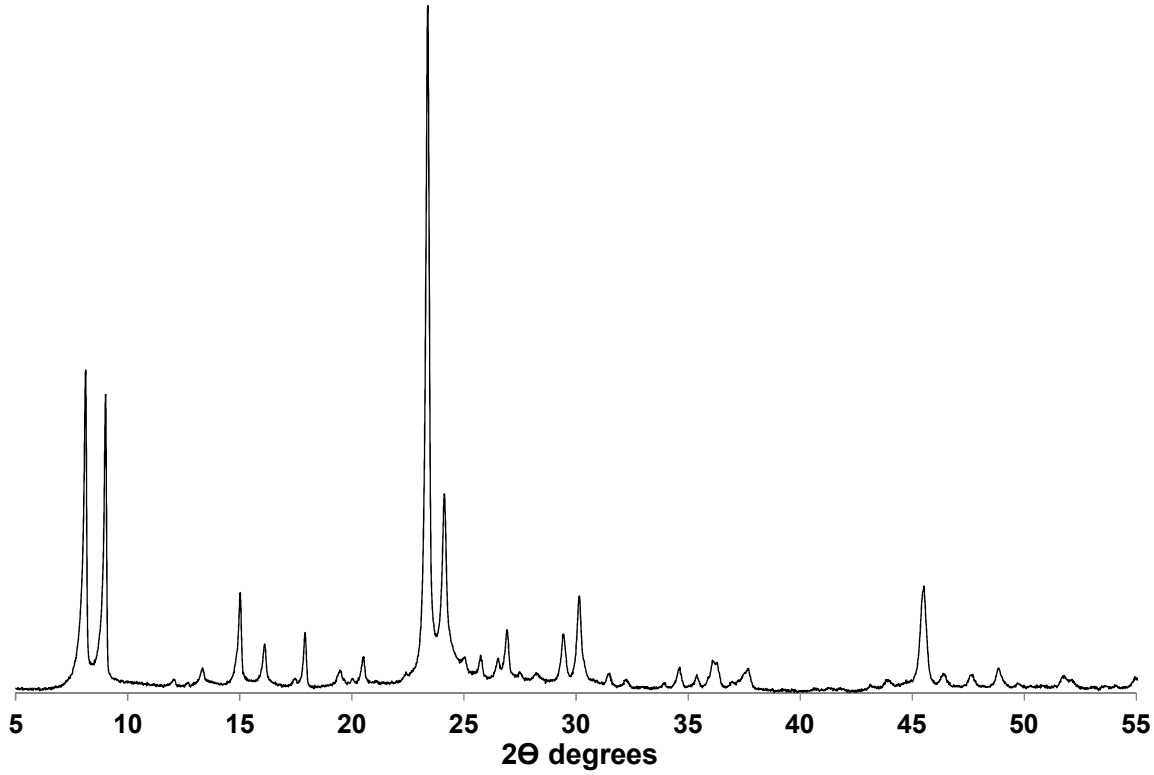

Figure 2.S2: Powder X-ray diffraction patterns of large crystal H-ZSM11.

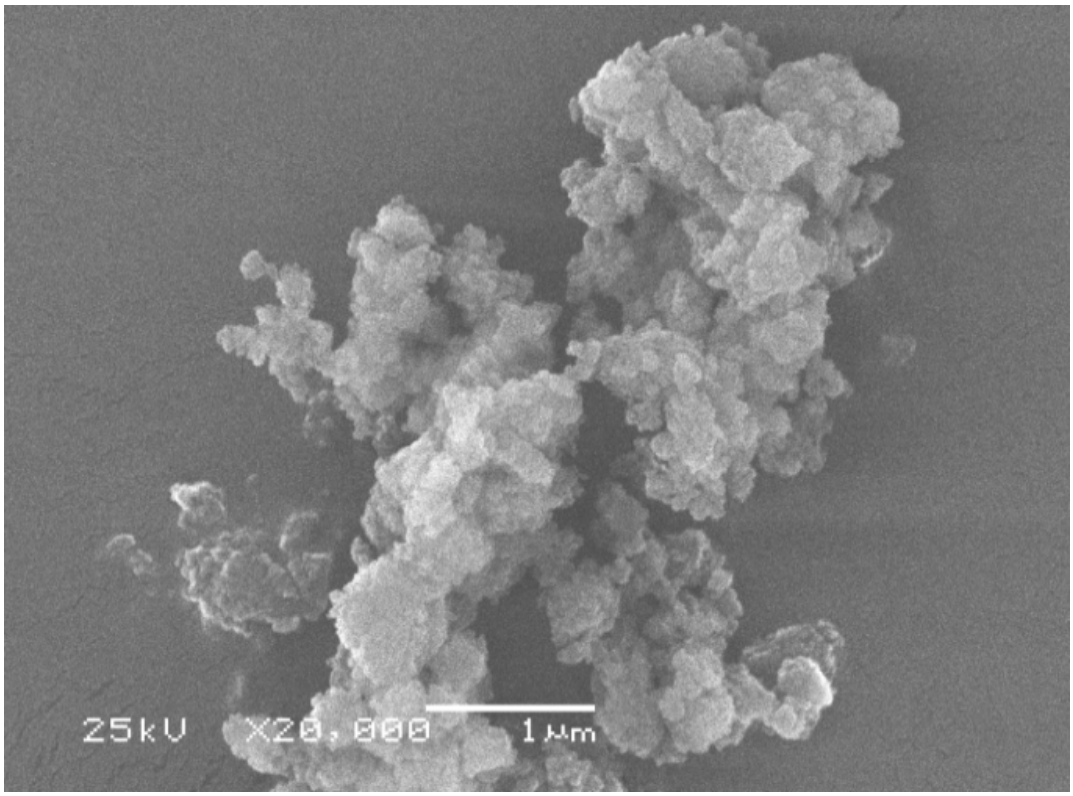

Figure 2.S3: Scanning electron microscope images of H-ZSM5 zeolite.

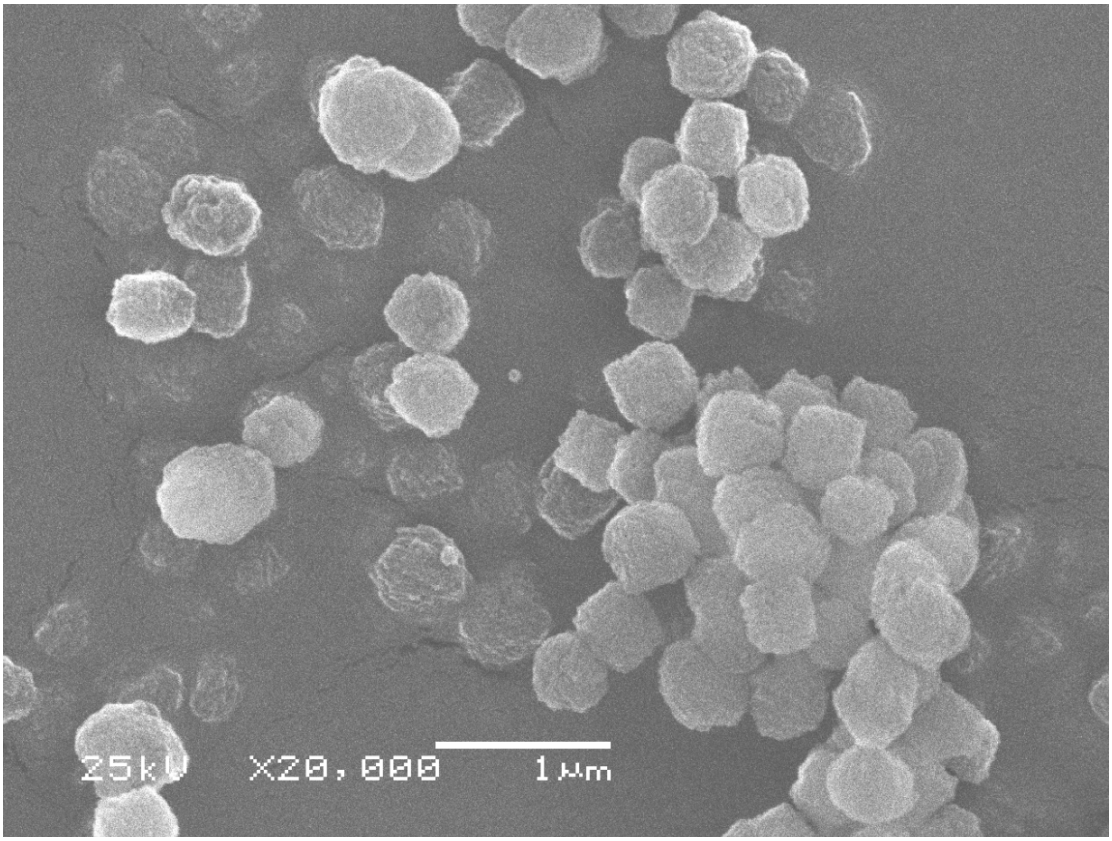

Figure 2.S4: Scanning electron microscope images of H-ZSM11 (small crystal) zeolite.

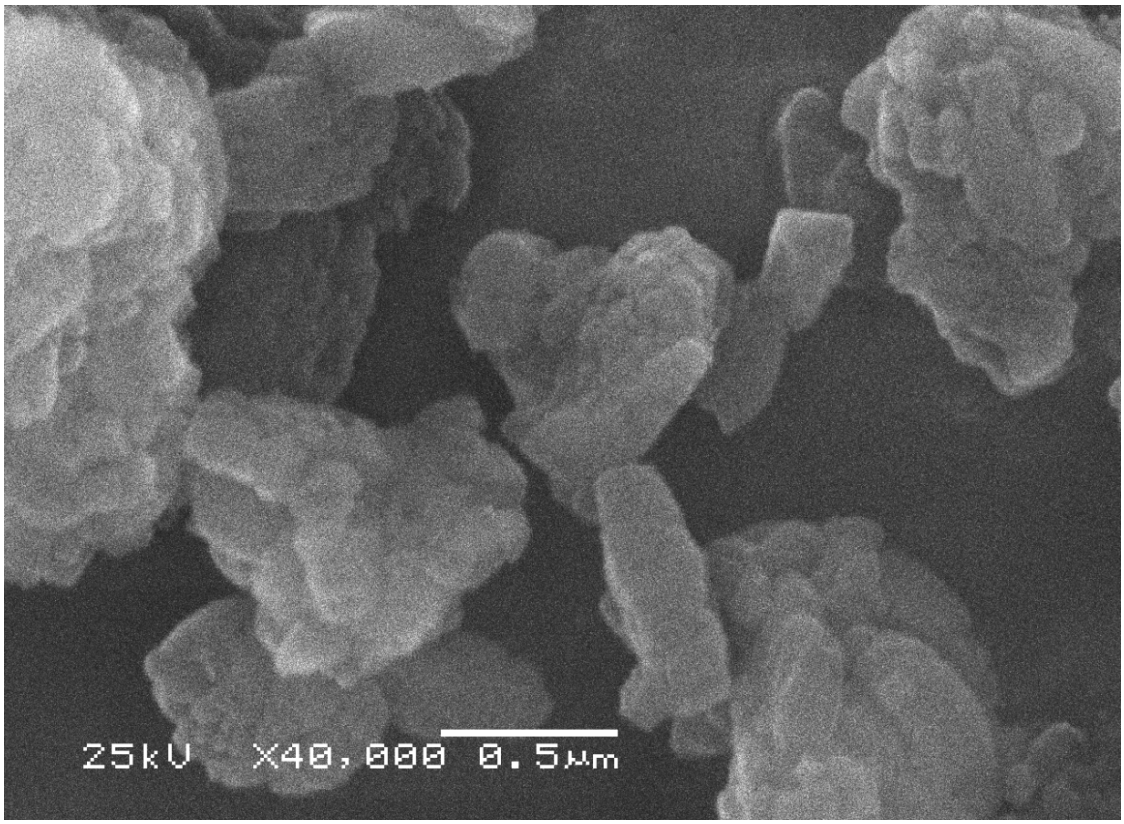

Figure 2.S5: Scanning electron microscope images of H-MOR zeolite.

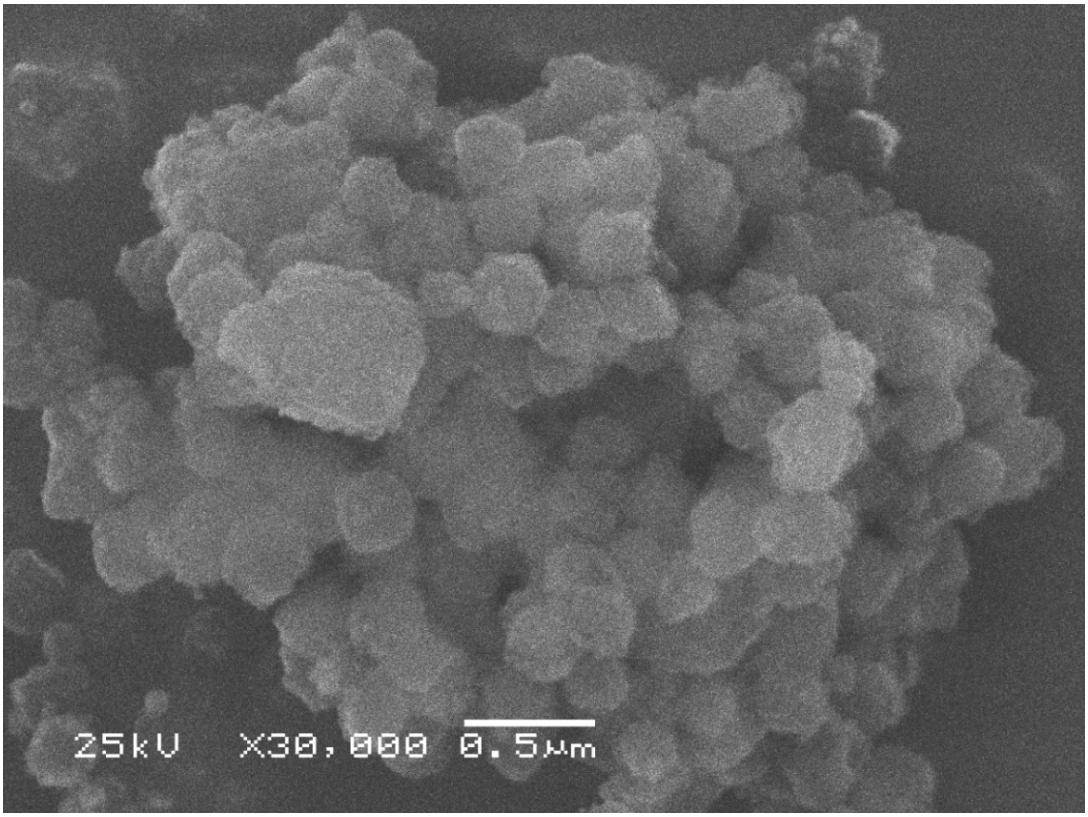

Figure 2.S6: Scanning electron microscope images of H-BETA zeolite.

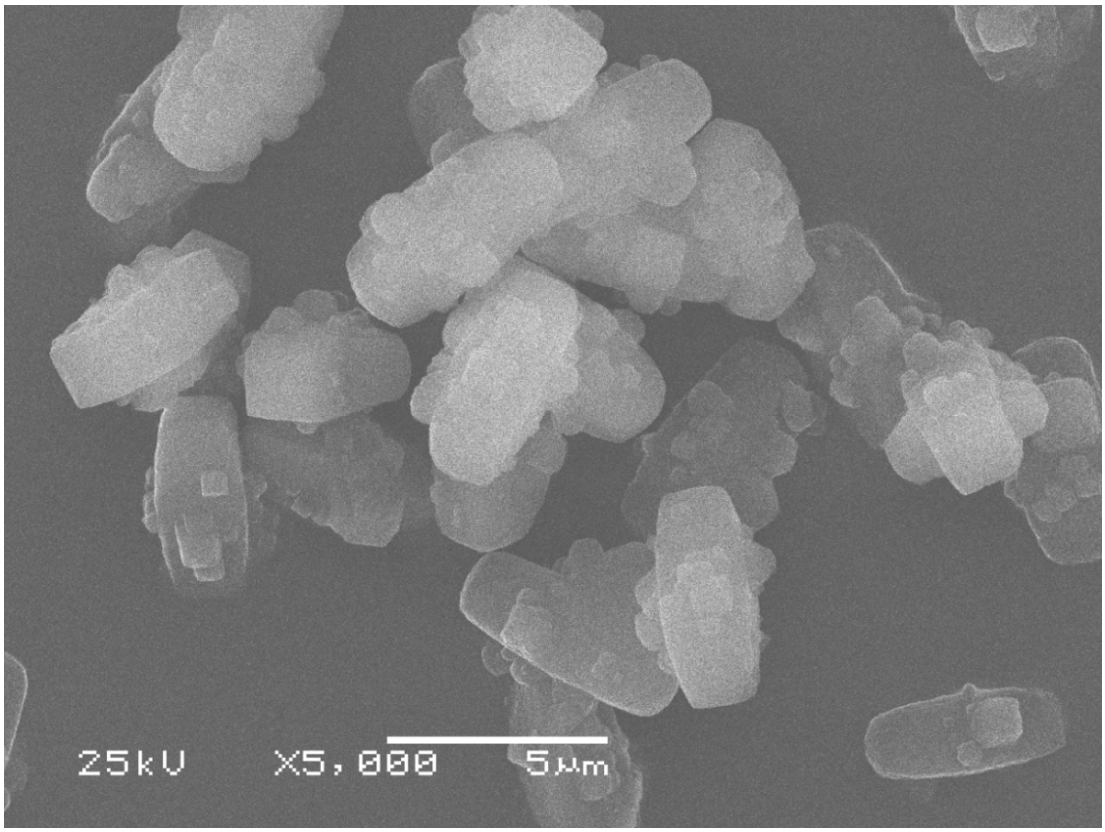

Figure 2.S7: Scanning electron microscope images of H-ZSM11 (large crystal) zeolite.

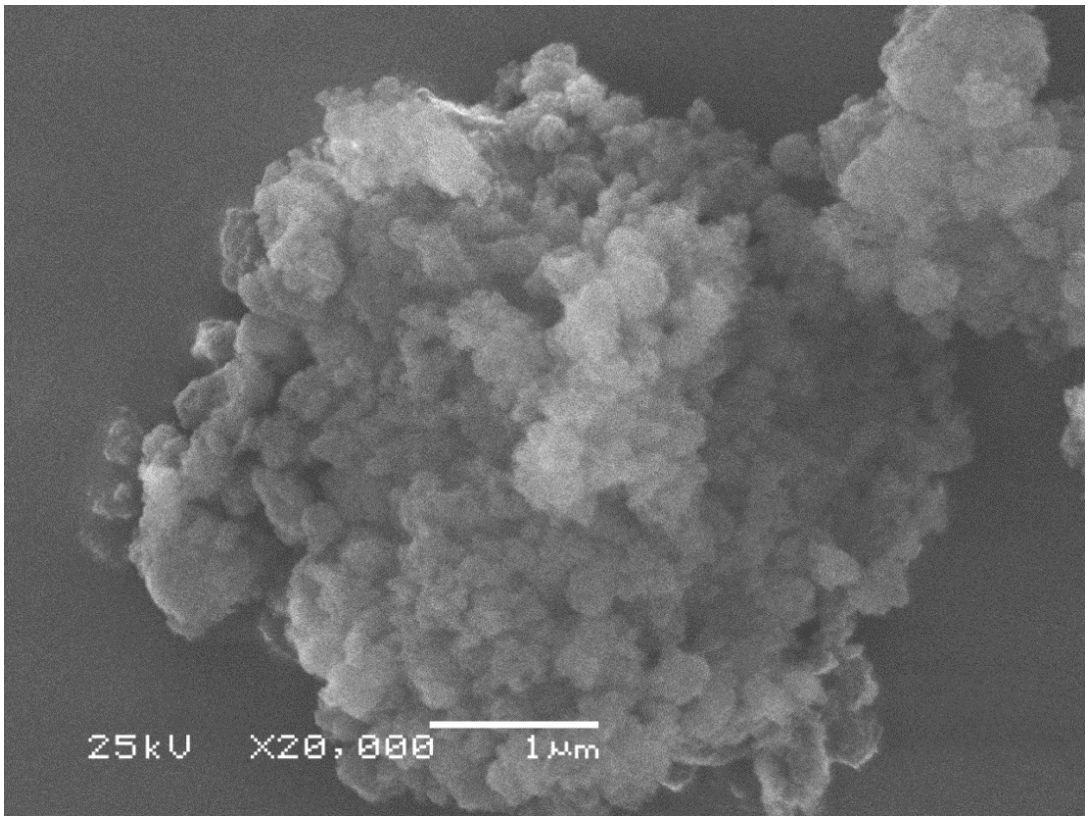

Figure 2.S8: Scanning electron microscope images of H-ZSM5-SM (surface modified by TEOS deposition) zeolite.

The reaction order with respect to methanol is close to zero at 623 K and approaches one at 723 K, while the reaction order with respect to toluene is one at both temperatures (Figure 2.S9), with the partial pressures tested here. The fraction of *MeOH for aromatic alkylation* is ~ 0.5, thus, the rate of toluene consumption slope is close to this fraction, i.e., increasing the toluene pressure by four fold increases the toluene consumption rate by two. Note that the slope is higher for the reaction at higher temperatures because methanol is used more efficiently for methylating aromatics and less for the formation of light hydrocarbons (Figure 2.S10).

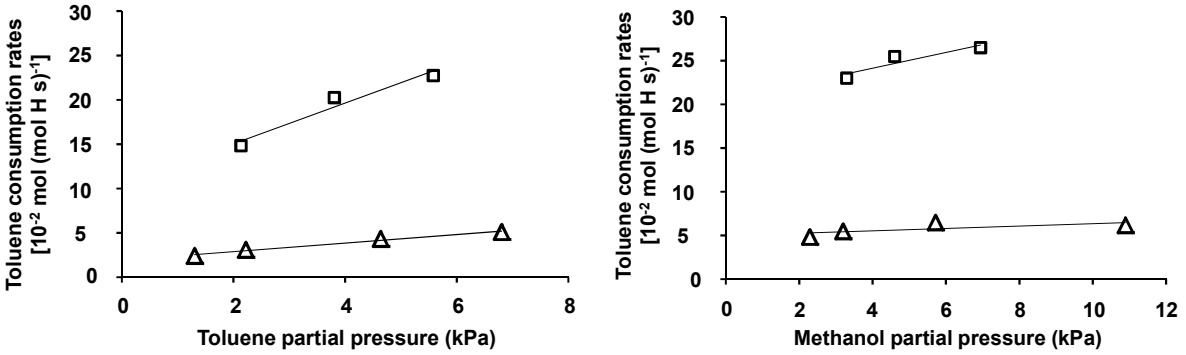

Figure 2.S9. Rate of toluene consumption as a function of toluene (left) or methanol partial pressure (right; □ = 723 K and Δ = 623 K) with 8-20 mg of H-ZSM5 and 2.3 cm^3s^{-1} total flow rate. The partial pressure of methanol and toluene was kept constant at 2.5 kPa (left) and 7 kPa (right), respectively.

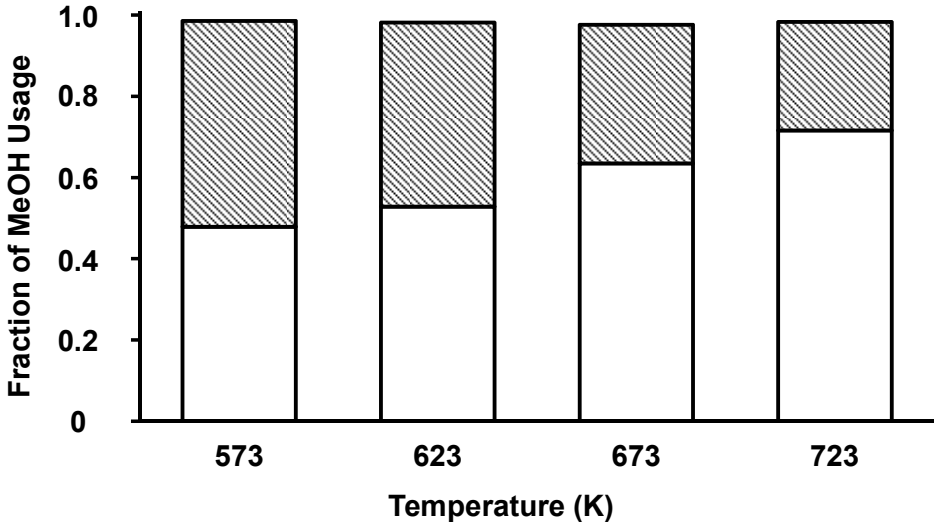

Figure 2.S10. Fraction of methanol used for methylation of aromatics (*MeOH for aromatics alkylation*; empty) and for formation of light hydrocarbons (*MeOH for LH formation*; striped) at $p_{toluene}$ = 6 kPa, $p_{methanol}$ = 1. 5kPa, 5 - 15 mg of H-ZSM5, 1.7-2.3 cm^3s^{-1} total flow rate, C_1 conversion = 47 - 55 %.

2.8. References

[1] T. Tsai, S. Liu, I. Wang, Applied Catalysis A: General 181 (1999) 355-398.

[2] W. Vermeiren, J.P. Gilson. Topics in Catalysis 52 (2009) 1131-1161.

[3] S. Kulprathipanja, Zeolites in Industrial Separation and Catalysis, Wiley-VCH, Weinheim, 2010.

[4] Y. Zhao, H. Wu, W. Tan, M. Zhang, M. Liu, C. Song, X. Wang, X. Guo, Catalysis Today 156 (2010) 69-73.

[5] Z. Zhu, Q. Chen, Z. Xie, W. Yang, C. Li, Micropor. Mesopor. Mater. 88 (2006) 16-21.

[6] R. Kumar, P. Ratnasamy, J. Catal 118 (1989) 68-78.

[7] G.N. Rao, R. Kumar, P. Ratnasamy, App. Catal. 49 (1989) 307-318.

[8] W.W. Kaeding, C. Chu, L.B. Young, B. Weinstein, S.A. Butter, J. Catal. 67 (1981) 159-174.

[9] O. Mikkelsen, P.O. Rønning, S. Kolboe, Micropor. Mesopor. Mater. 40 (2000) 95-113.

[10] A.M. Prakash, S.V.V. Chilukuri, R.P. Bagwe, S. Ashtekar, D.K. Chakrabarty, Micropor. Mater. 6 (1996) 89-97.

[11] T. Hibino, M. Niwa, Y. Murakami, J Catal. 128 (1991) 551-558.

[12] J.P. Breen, R. Burch, M. Kulkarni, D. McLaughlin, P.J. Collier, S.E. Golunski, Appl. Catal. A: General 316 (2007) 53-60.

[13] G. Mirth, J.A. Lercher, J. Catal 147 (1994) 199-206.

[14] B. Smit, T.L.M. Maesen, Nature 451 (2008) 671-678.

[15] S. Svelle, F. Joensen, J. Nerlov, U. Olsbye, K. Lillerud, S. Kolboe, M. Bjørgen, J. Am. Chem. Soc. 128 (2006) 14770-14771.

[16] D.M. McCann, D. Lesthaeghe, P.W. Kletnieks, D.R. Guenther, M.J. Hayman, V. Van Speybroeck, M. Waroquier, J.F. Haw, Angew. Chem. Int. Ed. 47 (2008) 5179-5182.

[17] B. Arstad, S. Kolboe, J. Am Chem. Soc. 123 (2001) 8137-8138.

[18] M. Bjørgen, F. Joensen, K. Lillerud, U. Olsbye, S. Svelle, Catal. Today 142 (2009) 90-97.

[19] U. Olsbye, M. Bjørgen, S. Svelle, K. Lillerud, S. Kolboe, Catal. Today 106 (2005) 108-111.

[20] D. Lesthaeghe, A. Horré, M. Waroquier, G.B. Marin, V. Van Speybroeck, Chem. Eur. J. 15 (2009) 10803-10808.

[21] P. De Luca, F. Crea, R. Aiello, A. Fonseca, J.B. Nagy, Stud. Surf. Sci. Catal. 105 (1997) 325-332.

[22] M. Derewinski, M. Machowska, Stud. Surf. Sci. Catal. 154 (2004) 349-354.

[23] S. Zheng, H.R. Heydenrych, A. Jentys, J.A. Lercher J. Phys. Chem. B 106 (2002) 9552-9558.

[24] S. Brunauer, P. H. Emmett, E. Teller, J. Am. Chem. Soc. 1938, 60, 308-319.

[25] B.C. Lippens, B.G. Linsen, J.H. de Boer, J. Catal. 3 (1964) 32-37.

[26] G. Halsey, J. Chem. Phys. 16 (1948) 931-937.

[27] G. Mirth, J. Cejka, J.A. Lercher, J. Catal. 139 (1993) 24-33.

[28] I.I. Ivanova, A. Corma, J. Phys. Chem. B 101 (1997) 547-551.

[29] S. Svelle, S. Kolboe, O. Swang, U. Olsbye, J. Phys. Chem. B 109 (2005) 12874-12878.

[30] H.P. Röger, M. Krämer, K.P. Möller, C.T. O'Connor, Micropor. Mesopor. Mater. 21 (1998) 607-614.

[31] S. Zheng, A. Jentys, J.A. Lercher, J. Catal. 241 (2006) 304-311.

[32] D. Lesthaeghe, B. De Sterck, V. Van Speybroeck, G.B. Marin, M. Waroquier, Angew. Chem. Int. Ed. 46 (2007) 1311-1314.

[33] B. Arstad, S. Kolboe, O. Swang, J. Phys. Chem. B 106 (2002) 12722-12726.

[34] C.D. Chang, Catal . Rev. Sci. Eng. 25 (1983) 1-118.

[35] M. Stöcker, Micropor. Mesopor. Mater. 29 (1999) 3-48.

[36] H.P. Röger, K.P. Möller, C.T. O'Connor, Micro. Mater. 8 (1997) 151-157.

[37] W. Song, D.M. Marcus, H. Fu, J.O. Ehresmann, J.F. Haw J. Am. Chem. Soc. 124 (2002) 3844-3845.

[38] D. Lesthaeghe, V. Van Speybroeck, G.B. Marin, M. Waroquier, Ind. Eng. Chem. Res. 46 (2007) 8832-8838.

[39] M. Bjørgen, S. Svelle, F. Joensen, J. Nerlov, S. Kolboe, F. Bonino, L. Palumbo, S. Bordiga, U. Olsbye, J. Catal. 249 (2007) 195-207.

[40] D.A. Simonetti, J.H. Ahn, E. Iglesia, J. Catal. 277 (2011) 173-195.

[41] D. Lesthaeghe, J. Van der Mynsbrugge, M. Vandichel, M. Waroquier, V. Van Speybroeck, ChemCatChem 3 (2011) 208-212.

[42] R. Kolvenbach, J.H. Ahn, S.S. Al-Khattaf, A. Jentys, J.A. Lercher, in preparation.

[43] S.J. Reitmeier, O.C. Gobin, A. Jentys, J.A. Lercher, J. Phys. Chem. C 113 (2009), 15355-15363.

[44] T. Xu, D.H. Barich, P.W. Goguen, W. Song, Z. Wang, J.B. Nicholas, J.F. Haw, J. Am. Chem. Soc. 120 (1998) 4025-4026.

[45] S. Svelle, U. Olsbye, F. Joensen, M. Bjørgen, J. Phys. Chem. C 111 (2007) 17981-17984.

[46] W.W. Kaeding, C. Chu, L.B. Young, S.A. Butter, J. Catal. 69 (1981) 392-398.

[47] Fernandez, C.; Stan, I.; Gilson, J.; Thomas, K.; Vicente, A.; Bonilla, A.; Pérez-Ramírez, J. Chem. Eur. J. 16 (2010) 6224-6233.

[48] Cheng, X.; Wang, X.; Long, H. Micropor. Mesopor. Mater. 119 (2009) 171-175.

[49] S.M. Maier, A. Jentys, J.A. Lercher, J. Phys. Chem. C 115 (2011) 8005-8013.

Chapter 3

Characterization and catalytic impact of hierarchically structured H-ZSM5 for toluene methylation

Hierarchical zeolites based on H-ZSM5 were designed, synthesized and characterized as catalysts for highly active and shape selective methylation of toluene. Desilication, followed by dealumination and chemical deposition of a mesoporous SiO2 overlayer were investigated as rational pathways for modifying the mesoporosity, diffusion and acid site concentration of the catalysts. Desilication and subsequent dealumination decreased the effective diffusion length of zeolite crystals and increased the turnover rate of toluene, albeit with some loss in p-xylene selectivity. Deposition of a mesoporous SiO2 overlayer decreased the toluene turnover rate due to the longer residence time of large aromatic methylation products inside the pores. This modification, however, significantly increased the p-xylene selectivity by selectively enhancing the diffusivity of p-xylene, while decreasing it for o- and m-xylenes. The design strategy allowed simultaneous increase of the toluene turnover rate and p-xylene selectivity.

3.1. Introduction

The reaction of toluene with methanol to xylenes has great potential to become an important process in the chemical industry [1]. Among the three xylene isomers, p-xylene has the highest demand as a key intermediate for the production of terephthalate, which itself is an intermediate product for polyesters [2]. Methylation of toluene over commercially available medium pore zeolites, however, typically yields thermodynamic mixtures of the xylene isomers [3,4,5] (i.e., ortho : meta : para xylene ratio of ~22:53:25 at 650 K [6]). As the xylene isomers have similar boiling points, they have to be separated by energy intensive processes, such as adsorption or fractional crystallization [1,2].

The para-selectivity with H-ZSM5 has been reported to be enhanced by increasing the zeolite crystal size [7,8,9], by impregnating with phosphorous or boron compounds [4,8,10,11], and by chemical vapor (CVD) [12] or liquid deposition (CLD) [13,14] of tetraethyl orthosilicate (TEOS). In particular, TEOS deposition on the zeolite particle surface is an attractive method to increase the shape selectivity by partially blocking the pore openings as well as by reducing the concentration of (unselective) Brønsted acid sites in the pore mouths [3,12,14]. The modification decreased the diffusivity of o- and m-xylene, while it increased for p-xylene [15]. On the other hand, the desilication and subsequent dealumination of H-ZSM5 shortened the diffusion path length and increased the transport rates of all molecules [16,17,18], which led to enhanced activity [19,20,21], albeit with some loss in shape selectivity [21].

In this work, a novel strategy of synthesizing small crystal zeolites with high shape selectivity via a sequence of modification steps was explored. The sequence includes desilication, subsequent dealumination and surface modification by deposition of SiO_2 overlayer by repeated grafting and oxidizing of TEOS onto the zeolite surface. We combine these concepts of zeolite modification with H-ZSM5 to demonstrate that the toluene turnover rate and the p-xylene selectivity can be increased simultaneously.

3.2. Experimental

3.2.1. Materials

Zeolite H-ZSM5 (Si/Al = 36; Süd-Chemie) was used as parent material and five different hierarchical samples were prepared by desilication (DS), subsequent dealumination (DS-DA) and by surface modification (SM) by CLD of TEOS, as shown in Scheme 3.1.

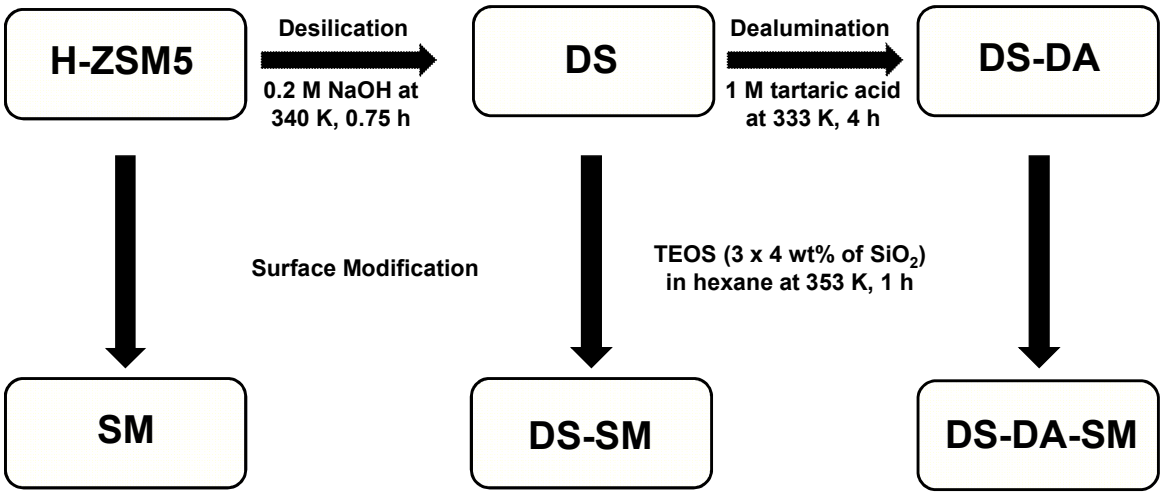

Scheme 3.1: Hierarchical samples prepared from the parent H-ZSM5 zeolite. DS = desilicated H-ZSM5, DS-DA = dealuminated DS sample, SM = surface modified sample by chemical liquid deposition of tetraethyl orthosilicate (TEOS).

The desilicated DS sample was prepared by heating the parent H-ZSM5 in a 0.2 M NaOH (>98 %, Sigma Aldrich) solution (30 cm^3 per gram of zeolite) at 340 K under stirring for 0.75 hour [22]. The solution was transferred into vials and the solid phase was centrifuged at 4000 rpm for ~0.5 hours and washed with deionized water. The washing procedure was repeated three times. The sodium form of the DS zeolite was exchanged into the ammonium form in 0.2 M NH_4Cl (>99.5 %, Sigma Aldrich) solution (30 cm^3 per gram of zeolite) at 353 K under stirring for 6 hours. The solid was separated and the ion exchange with fresh 0.2 M NH_4Cl solution was repeated three times in total. After the third ammonium exchange, the zeolites were separated by centrifugation, washed and dried (at 353 K) before the sample was treated in a synthetic air (flowing at 1.7 $cm^3\ s^{-1}$; 20.5 % O_2 in N_2, Westfalen) at 823 K (heating rate of 0.05 K s^{-1}) for 10 hours to obtain protonic form of the zeolite.

The desilicated-dealuminated DS-DA sample was prepared from the DS sample in a 1 M 2,3-dihydroxybutanedioic acid (L-tartaric acid; >99.5 %, Sigma Aldrich) solution (20 cm^3 per gram of zeolite) at 333 K under stirring for 4 hours [23]. This solution was separated, washed and dried in an oven as described above, before the sample was treated in a synthetic air (flowing at 1.7 $cm^3\ s^{-1}$) at 823 K (0.05 K s^{-1}) for 10 hours.

The surface modified SM samples were prepared by heating the parent H-ZSM5, the DS or the DS-DA sample in hexane (25 cm^3 per gram of zeolite; 97 %, Sigma Aldrich) with TEOS (4 weight % SiO_2 per gram of zeolite; >99.0 %, Sigma Aldrich) at 353 K under stirring for 1 hour [13]. Hexane was removed with a rotary evaporator under vacuum and the materials were dried at 353 K, before the treatment in a synthetic air (flowing at 1.7 $cm^3\ s^{-1}$) at 353 K (0.083 K s^{-1}) for 2 hours, 453 K (0.033 K s^{-1}) for 3 hours and finally at 823 K (0.033 K s^{-1}) for 5 hours. This procedure was repeated three times for all samples (i.e., H-ZSM5, DS and DS-DA) before the catalysts were characterized and tested (total deposition amount of 12 weight % of SiO_2).

3.2.2. Catalyst characterization

The elemental composition of the materials was determined by atomic absorption spectroscopy (AAS; Unicam M Series Flame-AAS equipped with an FS 95 auto-sampler and a GF 95 graphite furnace). The powder X-ray diffraction (XRD; Philips X'Pert Pro system, $\lambda_{CuK\alpha}$ = 0.154056 nm, 40kV/40mA) patterns were recorded between 2θ angles of 5-70° (step size of 0.017° and a scan speed of 115 seconds per step). The signals between ~5-10^o and 22-25^o after background correction was integrated and compared to the parent H-ZSM5 to estimate the relative crystallinity of the hierarchical samples (see Table 3.S1). The crystal size distribution was determined by dynamic light scattering (DLS) using a Malvern Zetasizer Nano ZS system.

The nitrogen physisorption measurements were carried out at 77 K on PMI automated sorptometer after outgassing the samples under vacuum at 523 K for 2 hours. The Brunauer-Emmett-Teller isotherm [24] was used to calculate the apparent surface area from the adsorption data over a relative pressure range from 0.01-0.1 p/p_o. The micro- and meso-pore volumes were evaluated by using the α_s comparative plot [25] with nonporous hydroxylated silica [26] as the reference adsorbent. The macro-pore volume was calculated by subtracting

micro- and meso-pore volumes from the total pore volume determined at $p/p_o = 0.95$. The pore size distribution of the zeolites was evaluated by the DFT method (cylindrical pore, NLDFT equilibrium model).

Infrared (IR) spectroscopy (Thermo Nicolet 5700 FT-IR spectrometer, resolution 4 cm^{-1}) with pyridine (99.8 %, Sigma Aldrich) and 2,6-di-tert-butyl-pyridine (2,6-DTBPy; >97 %, Sigma Aldrich) as probe molecules was used to determine the total concentration of Brønsted and Lewis acid sites as well as of Brønsted acid sites located in the pore mouth regions [27], respectively. 2,6-DTBPy was used as a probe molecule to determine the concentration of Brønsted acid sites located in the pore mouth regions because the kinetic diameter of 2,6-DTBPy (1.05 nm) is much larger than the size of the H-ZSM5 micropores (0.51 x 0.55 and 0.53 x 0.56 nm [28]). All samples were pressed into self-supporting wafers (density ~0.01 g cm^{-2}) and activated under vacuum (<10^{-7} kPa) for 1 hour at 723 K (heating rate of 0.17 K s^{-1}) before the spectra of the activated samples were collected. The samples were then exposed to pyridine or 2,6-DTBPy at 0.01 kPa and 423 K for 0.5 hour and outgassed for 1 hour under vacuum to desorb weakly bound species. The bands at ~1545 cm^{-1} and ~1450 cm^{-1} in the IR spectra of pyridine adsorbed were integrated to determine the total concentration of Brønsted and Lewis acid sites, respectively. Pyridine adsorbed on Lewis acid sites resulted in two bands, i.e., one centered at 1447±1 cm^{-1} and the other at 1455±1 cm^{-1}, which were deconvoluted with two Gaussian functions without baseline correction (R^2 values were larger than 0.98 in all cases). This sample was subsequently heated to 723 K (0.17 K s^{-1}) for 0.5 hour in vacuum to determine the concentration of strong Brønsted and Lewis acid sites. In order to calculate the concentration of Brønsted acid sites interacting with 2,6-DTBPy, the change of 3610 cm^{-1} area of the parent H-ZSM5 sample was correlated to the integrated area of the N-H^+ stretching band of protonated 2,6-DTBPy at 3367 cm^{-1} [27]. This ratio was used to relate the area of the band at 3367 cm^{-1} to the concentration of Brønsted acid sites interacting with 2,6-DTBPy for the hierarchical samples. All spectra were collected at 423 K and normalized to the overtone lattice vibration bands at 1990 and 1870 cm^{-1} for comparison of the IR spectra of different samples. Note that the acid site concentrations were normalized to the weight of zeolite and the materials with SiO_2 overlayer deposited were multiplied by 1.12 (g of material per g of zeolite) because the total SiO_2 (TEOS) deposition amount was 12 weight % of the zeolite.

3.2.3. Catalytic testing

The catalyst samples (4-25 mg, 180-250 μm) diluted with silicon carbide (7 times the weight of the catalyst; F46, ESK-SiC GmbH) were held in place by quartz wool inside a quartz plug flow reactor (0.4 cm ID). All catalysts were treated at 823 K (0.17 K s^{-1}) under flowing helium (1.7 cm^3 s^{-1}; 99,996%, Westfalen) for 0.5 hour prior to the reaction. The temperature was measured by a type K thermocouple in external contact to the reactor. It was maintained constant by a stainless steel furnace controlled by an Eurotherm controller (Series 2416). The toluene methylation was carried out at temperatures between 548-723 K at atmospheric pressure by flowing premixed toluene (> 99.9 %, Sigma Aldrich) and methanol (MeOH; >99.8 %, Sigma Aldrich) feed ($p_{toluene}$ = 6 kPa, $p_{methanol}$ = 1.5 kPa) into a vaporizer filled with silicon carbide. The total flow rate was varied between 1.2 and 2.3 cm^3 s^{-1}. The reactor effluent was analyzed by on-line gas chromatography (Agilent 7820A) equipped with a DB-WAX column (30 m x 0.32 mm x 0.5 μm) and a flame ionization detector. All the rates were normalized by the total concentration of Brønsted acid sites determined by the adsorption of pyridine.

3.3. Results and discussion

3.3.1. Chemical composition and structural characterization of hierarchical materials

The chemical composition and the textural properties of the parent and hierarchical materials are compiled in Table 3.1 [18]. The Si/Al ratios indicate that desilication selectively removed Si, while the dealumination selectively removed Al from the zeolite. The surface modification by TEOS led to the deposition of a SiO_2 overlayer on the zeolite, increasing the nominal Si/Al ratio.

Table 3.1: Chemical composition and textural properties of the parent and hierarchical materials derived from H-ZSM5.

Catalyst	Si/Al ratio	S_{BET}[a] ($m^2\ g^{-1}$)	S_{ext}[b] ($m^2\ g^{-1}$)	V_{mi}[c] ($cm^3\ g^{-1}$)	V_{meso}[c] ($cm^3\ g^{-1}$)	V_{macro}[c] ($cm^3\ g^{-1}$)
H-ZSM5	36	435	57	0.12	0.03	0.17
DS	27	482	96	0.12	0.05	0.23
DS-DA	39	484	99	0.12	0.05	0.24
SM	42	434	24	0.09	0.08	0.13
DS-SM	36	348	41	0.06	0.08	0.14
DS-DA-SM	47	435	84	0.08	0.06	0.20

[a]S_{BET} = specific surface area analyzed according to Brunauer-Emmett-Teller, [b]S_{ext} = external surface area, [c]V_{mi}, V_{meso} V_{macro} correspond to the micro-, meso- and macro-pore volume of the zeolite.

The BET and external surface areas, as well as the meso- and macropore volumes increased considerably after desilication, but only marginally after subsequent dealumination. The increase in the pore volume with diameters of approximately 4-6 nm for the DS sample in Figure 3.1 confirmed the generation of mesopores by desilication, while significant change in the pore volumes after subsequent dealumination was not observed. The deposition of the SiO_2 overlayer decreased the micropore volume, but increased the mesopore volume with pore diameters <2 nm (Table 3.1 and Figures 3.S1-3.S3).

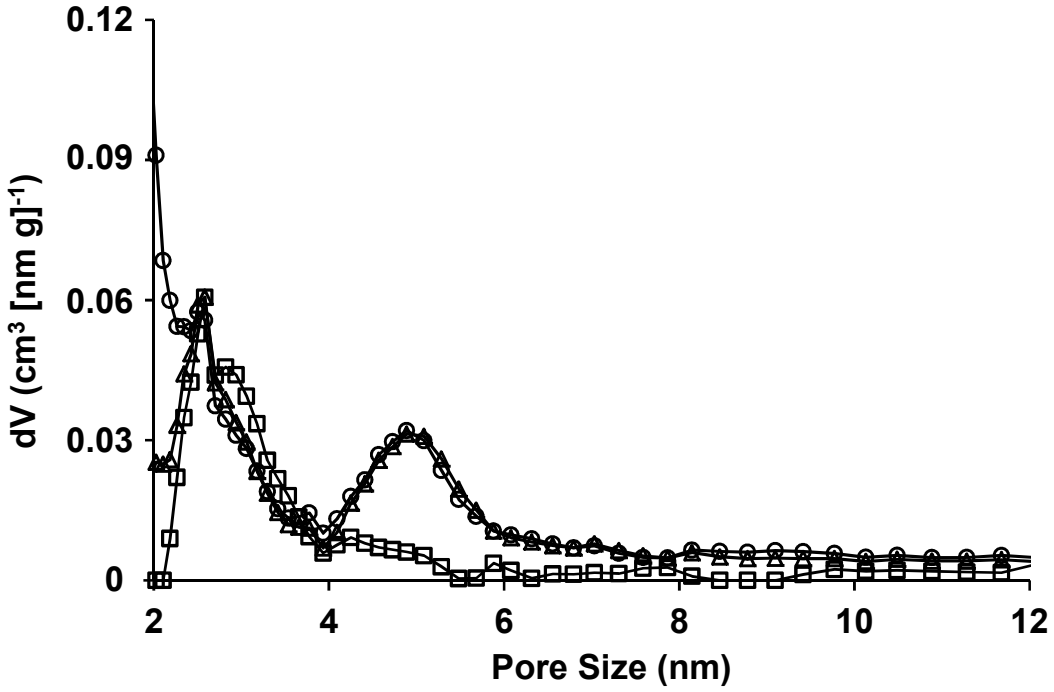

Figure 3.1: Pore size distribution of the parent (H-ZSM5; □), desilicated (DS; Δ) and subsequently dealuminated (DS-DA; ○) samples, analyzed by DFT method (cylindrical pore, NLDFT equilibrium model).

The XRD patterns and the relative crystallinity shown in Figure 3.2 confirmed that the parent and hierarchical H-ZSM5 samples maintained good crystallinity throughout the modification procedures. Note that the relative crystallinity of SM sample decreased to 88 % from H-ZSM5 because the SiO_2 overlayer deposited is amorphous (12 weight %). The slight increase in the average crystal size from 120 to 140 nm (Figure 3.3) after desilication and dealumination resulted presumably from the removal of some fraction of the smallest crystals after centrifugation (slightly cloudy solution even after 0.5 hours of centrifugation at 4000 rpm).

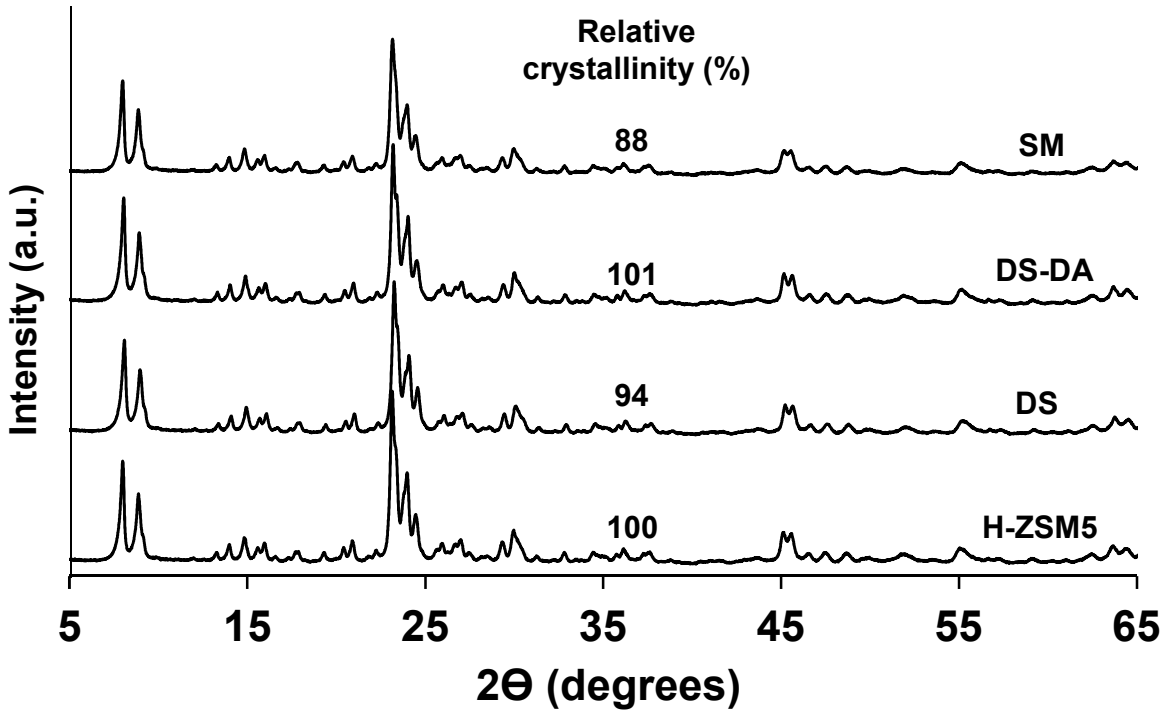

Figure 3.2: Powder X-ray diffraction (XRD) patterns and relative crystallinity of the parent H-ZSM5 and its hierarchical materials.

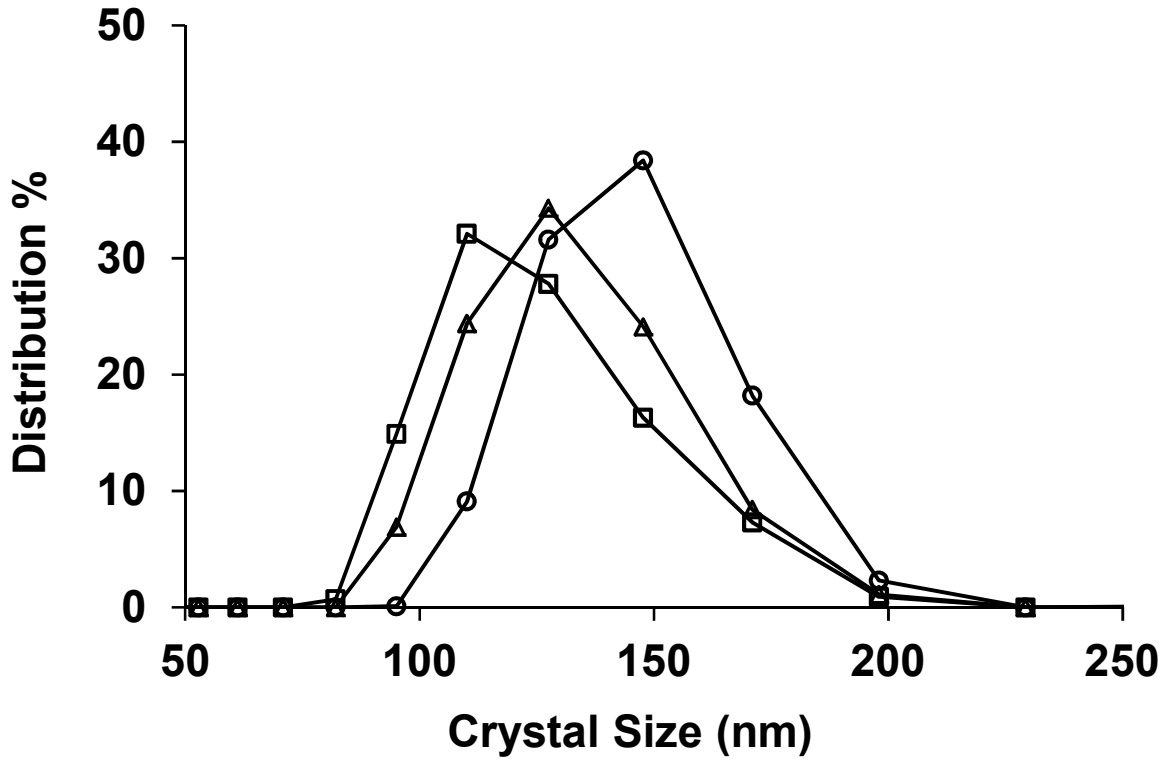

Figure 3.3: Crystal size distribution of the parent (H-ZSM5; □), desilicated (DS; Δ) and subsequently dealuminated (DS-DA; ○) samples measured by dynamic light scattering (DLS) method.

3.3.2. Acid site characterization of hierarchical materials

The stacked and superimposed IR spectra of activated samples are shown in Figure 3.4 and Figures 3.S4-3.S5 (see also Figure 3.S6). Two distinct bands were observed at 3745 cm^{-1} and 3610 cm^{-1}, characteristic for the O-H vibration of terminal silanol groups and Brønsted acid sites, respectively [29,30]. Desilication of the parent H-ZSM5 significantly increased the external surface area (Table 3.1) and consequently the concentration of terminal silanols (3745 cm^{-1}) increased [30]. A band at ~3670 cm^{-1} appeared after desilication resulting from the formation of extra-framework aluminum (EFAl) species [31] and decreased the broad band centered ~3500 cm^{-1} [32], as a result of the removal of the silanol nest (see superimposed spectra in Figure 3.S4, left) [33]. The decrease in intensity of the band at 3670 cm^{-1} showed that subsequent dealumination of the desilicated sample removed EFAl species and the simultaneous re-appearance of a broad band centered at ~3500 cm^{-1} indicated that the removal of aluminum atoms from the zeolite lattice led to formation of silanol nests (Figure 3.S4, left) [34]. Deposition of a mesoporous SiO_2 overlayer decreased both the bands at 3745 cm^{-1} and 3610 cm^{-1} (terminal silanol groups and Brønsted acid sites), while the intensity of

the broad band ~3660 cm^{-1} increased due to the hydrogen bonding of the silanol groups in the amorphous silica layer [35].

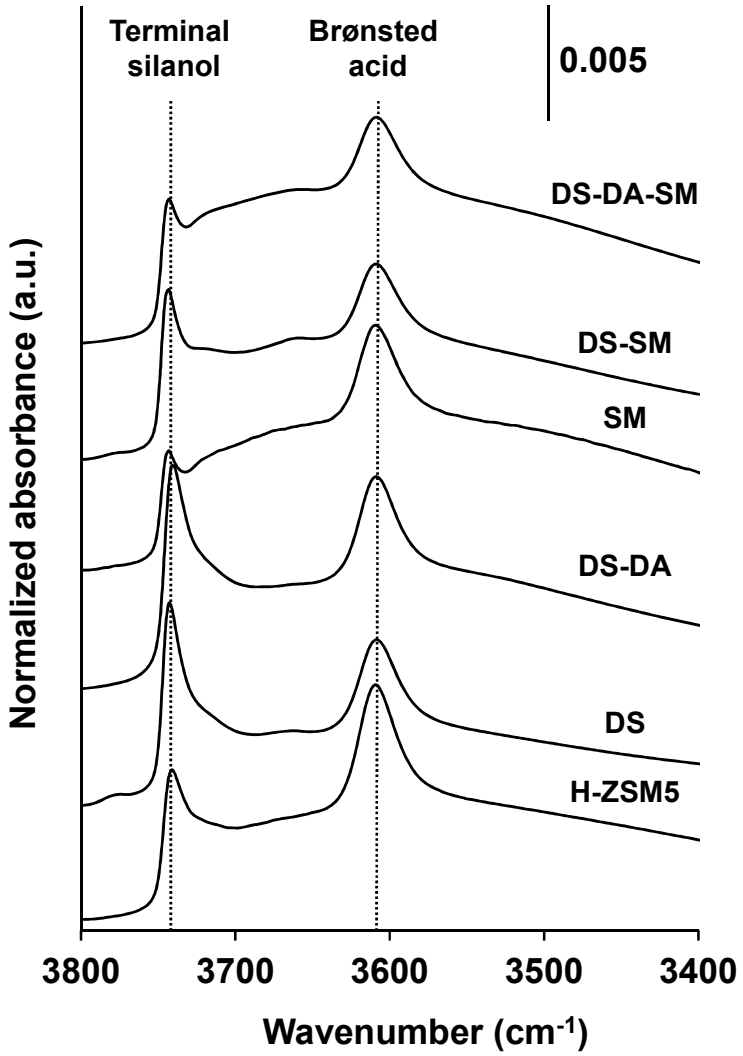

Figure 3.4: Infrared (IR) spectra of activated samples (heated to 723 K for 1 hour) measured at 423 K under vacuum (< 10^{-7} kPa). The bands at 3745 cm^{-1} and 3610 cm^{-1} represents O-H vibration of the terminal silanol groups and the Brønsted acid sites, respectively. The spectra were normalized to the lattice vibrations.

The stacked IR spectra after adsorption of pyridine (after subtracting the spectra of activated sample) are shown in Figure 3.5. The bands at 1447 and 1455 cm^{-1} represent the ring deformation vibrations of coordinately bonded pyridine molecules on Lewis acid sites with and without hydrogen bond interactions, respectively, and the band at 1545 cm^{-1} from the pyridinium ions formed on Brønsted acid sites [36,37]. These two bands from Lewis acid sites were deconvoluted and the distribution of the Lewis acid sites calculated by assuming similar extinction coefficient are summarized in Table 3.S2 (further discussion and the deconvoluted IR spectra of H-ZSM5 and DS are shown as an example in Figure 3.S7).

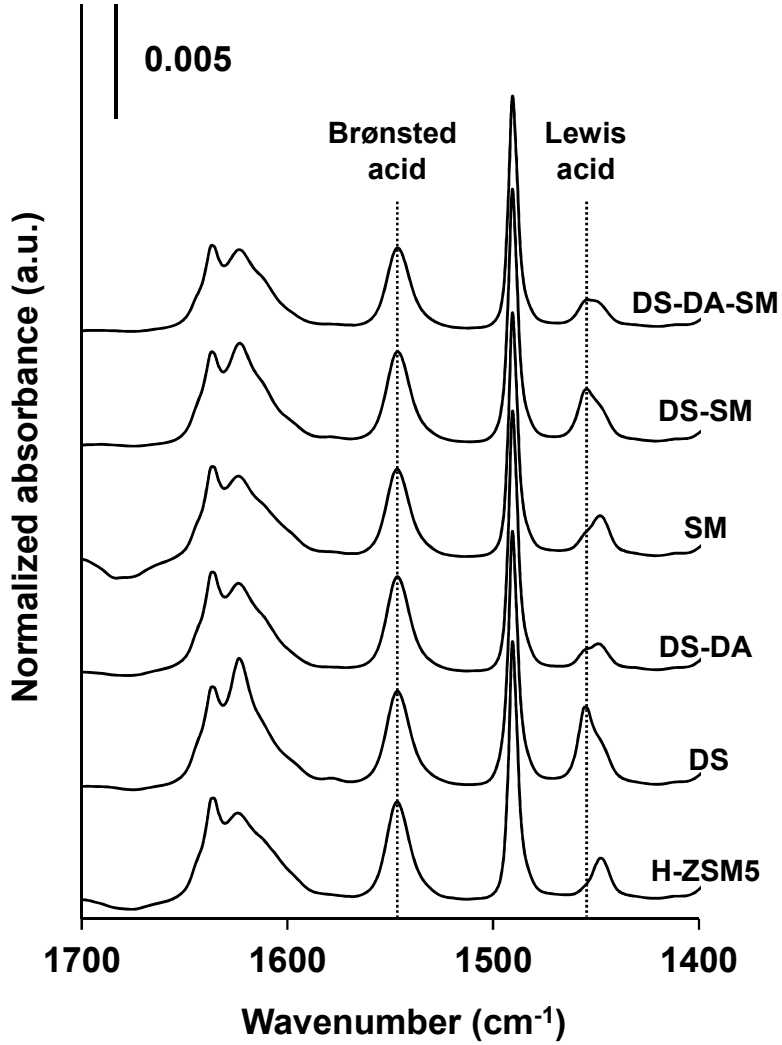

Figure 3.5: IR spectra after adsorption of pyridine at 423 K, 0.01 kPa and outgassing for 1 hour under vacuum (spectra of the activated sample subtracted). The bands at 1447 and 1455 cm^{-1} represent the coordinately bonded pyridine molecules on Lewis acid sites with and without hydrogen bond interactions, respectively, and the band at 1545 cm^{-1} the ring deformation vibrations of pyridinium ions formed on Brønsted acid sites.

The IR spectra of the samples after 2,6-DTBPy adsorption are shown in Figure 3.6. The fraction of terminal silanol groups (3745 cm^{-1}) and Brønsted acid sites (3610 cm^{-1}) interacted with 2,6-DTBPy, as shown by the decrease in the intensity of both bands. New bands appeared at 3367 cm^{-1} and 1616 cm^{-1}, which are assigned to the $N\text{-}H^+$ and C=C stretching vibrations of 2,6-$DTBPyH^+$, respectively. The linear correlations between these vibrational bands shown in Figure 3.S9 indicate that both bands can be used for quantification of these acid sites probed. After desilication, the bands at 3367 cm^{-1} and 1616 cm^{-1} in Figure 3.6 increased compared to the parent H-ZSM5 because a significant concentration of mesopores was formed (therefore increased the external surface area, Table 3.1) and a substantial fraction

of Brønsted acid sites became accessible to 2,6-DTBPy, i.e., the concentration of Brønsted acid sites in the pore mouth region increased. These Brønsted acid sites were primarily removed from the pore mouth region during subsequent dealumination with tartaric acid, whose kinetic diameter (0.68 nm) is slightly larger than the size of the H-ZSM5 micropores (~0.55 nm). The decrease of intensities of the bands at 3367 cm^{-1} and 1616 cm^{-1} compared to DS sample indicated the loss of Brønsted acid sites in the pore mouth region.

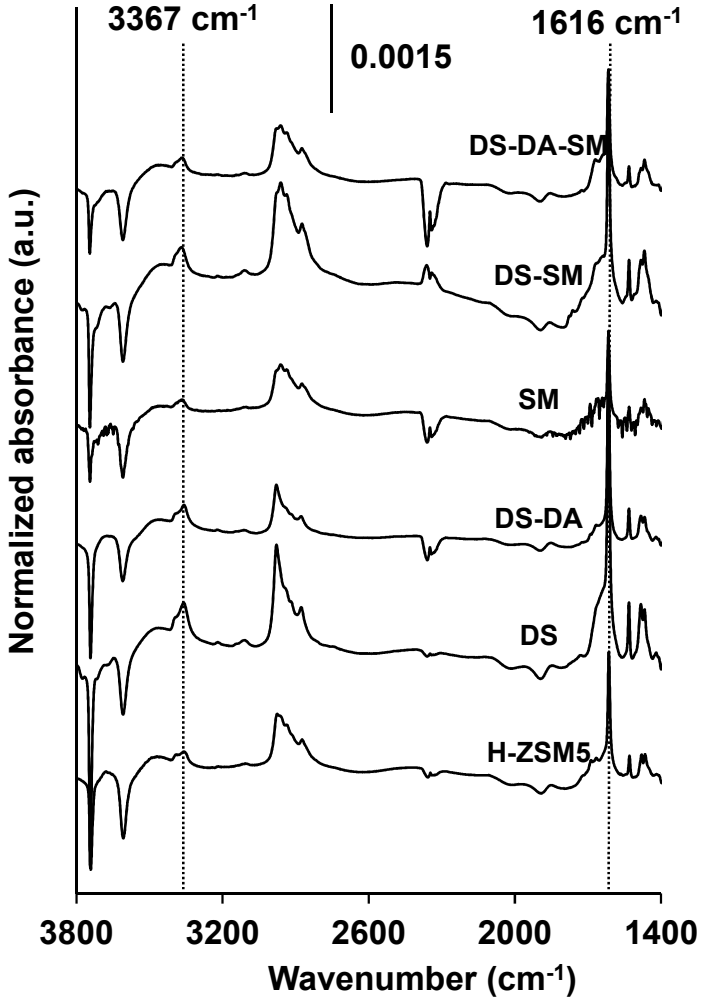

Figure 3.6: Changes in IR spectra after adsorption of 2,6-di-tert-butyl-pyridine (2,6-DTBPy) at 423 K, 0.01 kPa and outgassing for 1 hour in vacuum (spectra of activated samples are subtracted). The characteristic bands at 3367 cm^{-1} ($N\text{-}H^+$ vibration) and 1616 cm^{-1} (C=C vibration) appear from 2,6-DTBPy interaction with the zeolite.

The concentration of Brønsted and Lewis acid sites determined by pyridine and 2,6-DTBPy adsorption are summarized in Table 3.2 and Figure 3.7 (plotted for visualization). The concentration of Lewis acid sites increased significantly by desilication, because the removal of tetrahedrally coordinated silicon atoms from the zeolite led to a breakage of O-Al bonds

and formation of EFAl species [31]. Desilication generated mesopores and the larger external surface area allowed a higher concentration of the Brønsted acid sites to become accessible by 2,6-DTBPy. The total concentration of acid sites increased significantly (from 447 to 573 μmol [g zeolite]$^{-1}$), consistent with decrease in Si/Al ratio (Table 3.1), while the total number of acid remained nearly constant (from 447 to 430 μmol, see Figure 3.S10) if the weight loss after desilication (~25 %) was accounted for. This indicates that the silicon atoms were removed selectively as $Si(OH)_4$ while the aluminum atoms, contributing to the acidity of zeolite, remained in the material. Subsequent dealumination from DS sample by tartaric acid decreased both the concentration of Lewis and Brønsted acid sites because the aluminum atoms were selectively removed in this step. The dealumination treatment, however, decreased only the Brønsted acid sites that were accessible by 2,6-DTBPy because tartaric acid has a slightly larger diameter (0.68 nm) than the H-ZSM5 pores (0.55 nm). A slight increase in the concentration of Brønsted acid sites that are not accessible by 2,6-DTBPy was observed because the weight loss after desilication (~5 %) was not accounted for in Figure 3.7 (see Figure 3.S10).

Table 3.2: Concentration of Brønsted and Lewis acid sites determined by adsorption of pyridine and 2,6-di-tert-butyl-pyridine (2,6-DTBPy).

	Brønsted Acid sites (μmol g zeolite^{-1})				Lewis Acid Sites (μmol g zeolite^{-1})	
	Total[a]	Strong[b]	2,6-DTBPy accessible[c]	% 2,6-DTBPy interaction[d]	Total[a]	Strong[b]
H-ZSM5	380	371	90	24	67	26
DS	398	370	204	51	175	131
DS-DA	345	332	131	38	55	30
SM	351	327	62	18	76	38
DS-SM	366	331	170	47	129	88
DS-DA-SM	312	293	92	29	74	41
Δ_{SM} H-ZSM5[e]	29	44	28	-	-9	-12
Δ_{SM} DS[e]	32	39	34	-	46	43
Δ_{SM} DS-DA[e]	33	39	39	-	-19	-11

[a]After adsorption of pyridine at 423 K and outgassing for 1 hour under vacuum. [b]After subsequently heating the samples to 723 K for 0.5 hour. [c]Total concentration of Brønsted acid sites (both strong and weak) located in the pore mouth region. After adsorption of 2,6-DTBPy at 423K and outgassing for 1 hour under vacuum. [d]Defined as % of 2,6-DTBPy interacting with total Brønsted acid site. [e]Difference between before and after the deposition of SiO_2 overlayer.

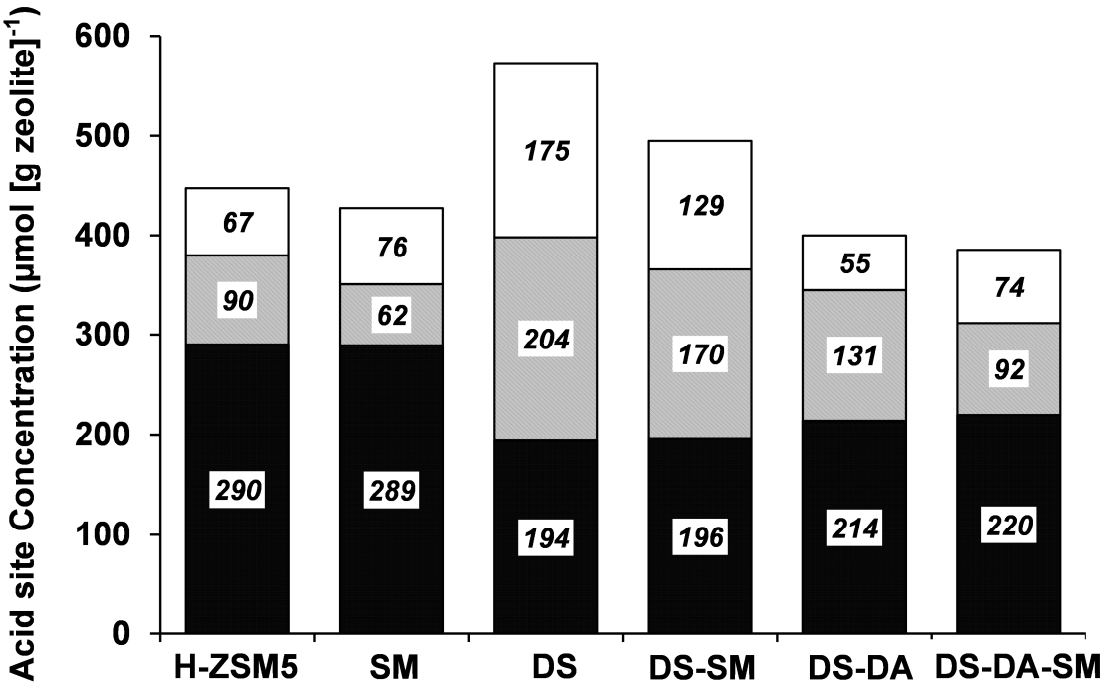

Figure 3.7: Concentration of Brønsted and Lewis acid sites per gram of a zeolite. White represents Lewis acid sites, grey and black the Brønsted acid site accessible and not accessible by bulky 2,6-DTBPy, respectively.

The surface modification by an external SiO_2 overlayer deposition decreased only the fraction of Brønsted acid sites accessible by 2,6-DTBPy because the kinetic diameter of TEOS (0.96 nm) is larger than the size of the H-ZSM5 micropores and, consequently, only Brønsted acid sites at the pore mouth region were affected (Figure 3.7). The concentration of Brønsted acid sites decreased to a similar extend, whether the sample was treated by desilication or subsequent dealumination prior to deposition of SiO_2 overlayer (Δ_{SM} in Table 3.2; loss of 30-40 µmol of Brønsted acid sites per g zeolite). Note that most of the Brønsted acid sites were strong and more than 90 % of pyridine was still adsorbed on all the materials even after the samples were heated to 723 K.

Deposition of mesoporous SiO_2 overlayer onto the DS sample significantly decreased the Lewis acid site concentration, whereas it slightly increased for the H-ZSM5 and DS-DA. The surface modification procedure presumably affects the concentration of Lewis acid sites in two ways, (i) removal of Lewis acid sites by reacting with SiO_2 deposition or (ii) generation of Lewis acid sites by breaking O-Al bonds during hydrolysis and/or condensation. Thus, the Lewis acid site concentration decreased on the DS-SM sample because high fraction of the Lewis acid sites formed during desilication (DS sample) were accessible by TEOS molecules

and concentration of the sites passivated by SiO_2 deposition was much higher than the concentration of additional Lewis acid sites formed (Δ_{SM} DS, Table 3.2; see also Figure 3.S11). On the other hand, the concentration of Lewis acid sites of SM and DS-DA-SM slightly increased from H-ZSM5 and DS-DA samples, respectively, because the formation of Lewis acid sites by breaking O-Al bonds were greater than the ones passivated by SiO_2 deposition. This suggests that the Lewis acid sites in these samples were most likely not accessible to react with large TEOS molecules.

3.3.3. Catalytic testing of toluene methylation over hierarchical materials

The turnover rates of toluene at different reaction temperatures and the apparent energy of activation are shown in Table 3.3 (turnover rates of methanol and the conversions of both reactants shown in Tables 3.S3-3.S4). The reaction orders of toluene methylation were between zero and one with respect to methanol and one with respect to toluene under the reaction conditions used [38]. In general, desilication and subsequent dealumination increased and surface modification decreased the toluene turnover rates. This trend was especially pronounced at lower temperatures. The apparent activation energy for toluene methylation decreased slightly with desilication and dealumination, but increased significantly with surface modification by an external SiO_2 overlayer deposition, e.g., from 81 to 101 kJ mol^{-1} with H-ZSM5 and after surface modification, respectively (Arrhenius plot shown in Figure 3.S12).

Table 3.3: Turnover rates of toluene at different reaction temperatures and the apparent energy of activation for toluene methylation.

	573 K	623 K	673 K	723 K	
	Toluene turnover rate[a] (10^{-2} mol [s mol H]$^{-1}$)	Toluene turnover rate (10^{-2} mol [s mol H]$^{-1}$)	Toluene turnover rate (10^{-2} mol [s mol H]$^{-1}$)	Toluene turnover rate (10^{-2} mol [s mol H]$^{-1}$)	E_{app}[b] (kJ mol^{-1})
HZSM5	2.1	7.5	14	20	81
DS	2.7	8.9	16	20	75
DS-DA	3.7	11	19	25	68
SM	0.84	4.5	12	19	101
DS-SM	0.92	4.2	12	20	90
DS-DA-SM	1.5	6.5	15	24	87

[a]Measured based on the toluene consumption ($p_{toluene}$ = 6.0 kPa, $p_{methanol}$ = 1.5 kPa, 10 mg of catalyst and total flow rate = 2.3 cm^3 s^{-1}). [b]Apparent energy of activation based on the toluene turnover rates measured between 548 - 623 K.

The reaction of toluene methylation is diffusion limited because the turnover rates were affected by changes of mesoporosity/diffusivity in the catalyst (Table 3.3) and the estimated values of Thiele modulus were somewhat larger than unity, i.e., ~2-6 at 723 K and 1-2 at 573 K (Table 3.S5; effectiveness factor also calculated) [39]. Consequently, an increase in toluene turnover rates was observed from desilication and subsequent dealumination, because the effective diffusion length (determined by assuming an unchanged diffusivity inside the micropores) decreased by ~9 and 35 %, respectively [18]. After the surface modification by SiO_2 overlayer deposition, the diffusivity of large aromatic molecules decreased significantly from partial blocking of the pore openings [15,18] and resulted presumably in higher relative concentration of aromatic products, such as trimethylbenzenes (TriMBs), compared to the reactant (toluene) in the zeolite pores. The surface coverage with these species over H-ZSM5 and SM samples during toluene methylation increased from ~20 to 40 % at 573 K, respectively (see Figure 3.S13 [40]). This led to higher probability for the aromatic product methylation relative to the toluene and, consequently, lowered the toluene turnover rates (vide infra). In addition, the increase of aromatic products in the zeolite pores also led to a lower fraction of methanol being adsorbed/activated for methylation and reduced the overall rate of methylation. Note that the turnover rate increased significantly with the dealuminated sample compared to the sample after desilication, despite of the unchanged mesopore volume (Table 3.1). This indicates that the EFAl species formed on the external surface after desilication (Figure 3.7) block the micropore entrances and/or interact with the aromatic reactant and product molecules [18].

The diffusional limitation of this reaction most likely results from the slow transport of the large product molecules (e.g., m-xylene and TriMBs) out of the zeolite pores, rather than from the transport of the reactant molecules (toluene) to the active sites, because diffusivities of the methylated products inside the ZSM-5 pores were much lower compared to the reactant molecules. For example, m-xylene diffuses at least two orders of magnitude slower than toluene [18,41] and the difference should be even greater for larger products, such as TriMBs. Toluene must replace large aromatic products on the activated methanol [42] during the methylation and, thus, the turnover rates of toluene methylation are strongly influenced by residence time (therefore the relative concentration) of the large aromatic product molecules inside the zeolite pores under the steady state reaction conditions.

The limitation from diffusion of large aromatic products suggests that the surface concentration of reactants, i.e., toluene and methanol, and p-xylene (similar diffusivity compared to toluene [41]), should be independent of the diffusion length during toluene methylation over H-ZSM5. These species were nearly absent from the zeolite surface at reaction temperatures, but was covered with large aromatics, e.g., m-xylene and TriMBs, at much higher concentrations than that of the gas phase [43] (see section 3.3.2). In addition, the measured surface coverage of large aromatic products was much higher than the predicted coverage at equilibrium [40], also indicating that the reaction is limited by diffusion of these molecules.

The relative concentration of large aromatic products of toluene (e.g., m-xylene and TriMBs) compared to the reactant (toluene) should be higher for the samples with a longer effective diffusion length, e.g., SM compared to H-ZSM5 or H-ZSM5 compared to DS-DA sample. The apparent energy of activation shown in Table 3.3, thus, increased significantly with surface modification and slightly decreased with desilication-dealumination, because the average apparent activation energy of diffusion during the reaction (E_{diff}) presumably reflects more of the larger product molecules over the zeolites with longer effective diffusion length, i.e., the fraction of TriMBs used when defining the average E_{diff}, relative to xylenes, should be higher with SM than with H-ZSM5 sample [40]. The E_{diff} increases as molecules become larger [18,41] and the measured E_{app}, thus, increases because E_{app} in a diffusion limited reaction is proportional to the activation energy of diffusion, i.e., $E_{app} = \frac{E_{rxn}}{2} + \frac{E_{diff}}{2}$ [44]. Note that the activation energy of reaction, E_{rxn}, should be constant for all catalysts because the framework is the same and the acid strength between the hierarchical samples is similar.

The significant presence of aromatic products from toluene methylation in the zeolite pores [43] also leads to competitive methylation reactions, i.e., toluene methylation to xylene and xylene (or TriMB) methylation to TriMB (or Tetramethylbenzene (TetraMB)). The latter (xylene and TriMB) methylation reaction should be more significant for zeolites with longer effective diffusion length because the relative concentration of larger aromatic products to toluene is higher. The relative formation rate of xylenes to TriMBs, however, were not affected significantly (Table 3.S6) by changing the effective diffusion length because of product shape selectivity [38]. Note that the methylation of larger aromatic products is also favored compared to toluene because the activation energy of methylation reactions decreases with number of methyl substitutions (~ 10 kJ mol^{-1} between xylene and toluene methylation

[45,46]). The reaction rates are proportional to $\exp(\frac{-E_{app}}{R \cdot T})$ [47] and the differences in the rates caused by lower activation energy should be more pronounced at lower reaction temperatures (Table 3.3, see also section 3.3.3).

3.3.3.1. Influence of hierarchical pores and reaction temperature on methanol usage

The methanol usage during toluene methylation, in particular, the fraction of methanol used for formation of light hydrocarbons (LH), was determined previously by examining the *fraction of MeOH for LH formation* [38]. The fraction was defined based on the formation or consumption rates as follows:

$$\textit{Fraction of MeOH for LH formation} = \frac{2 \times C_2 + 3 \times C_3 + 4 \times C_4 + \ldots}{Methanol_{in} - (Methanol + 2 \times DME)_{out}} \quad (1)$$

Methanol and dimethyl ether (DME) were treated as one reactant (accounting for the stoichiometry of ½ for DME), because methanol can dehydrate to DME during the reaction, which could also methylate aromatic molecules via a similar mechanism [48,49]. The *fraction of MeOH for LH formation* (Equation 1) describes how much methanol was used for the formation of light hydrocarbons. A fraction of unity would indicate that methanol was used only for formation of light hydrocarbons and none for the methylation of aromatics. A fraction of zero, vice versa, would indicate that methanol was entirely used for the methylation of aromatic molecules and none for the formation of light hydrocarbons.

The fractions of methanol used for the formation of light hydrocarbons over H-ZSM5 and the hierarchical zeolites are summarized in Table 3.4. A higher methanol usage towards formation of light hydrocarbons was observed with decreasing the reaction temperature, e.g., the *fraction of MeOH for LH formation* increased from 0.23 to 0.52, as the temperature decreased from 723 to 573 K with H-ZSM5 (Table 3.4). Note that the products of toluene methylation, e.g., xylenes and TriMBs, could methylate further and eventually dealkylate light hydrocarbons from highly-methylated aromatics [50,51] from product shape selectivity, i.e., highly-methylated aromatic molecules cannot exit the pores (Scheme 3.2) [38]. The methylation of xylenes or TriMBs was favored relative to toluene methylation, because the activation energy of toluene methylation was higher than that of xylenes or TriMBs and this

influence was, therefore, more pronounced at lower reaction temperatures (vide supra). This led to higher probability for product methylation and dealkylation of light hydrocarbon reactions to take place at lower reaction temperatures and resulted, consequently, in higher methanol usage towards light hydrocarbons.

Table 3.4: Fraction of methanol (MeOH) used for the formation of light hydrocarbons (LH)[a] at different reaction temperatures during toluene methylation for the parent H-ZSM5 and its hierarchical samples.

	573 K	623 K	673 K	723 K
H-ZSM5	0.52	0.45	0.33	0.23
DS	0.34	0.34	0.28	0.23
DS-DA	0.33	0.30	0.22	0.16
SM	0.76	0.65	0.50	0.39
DS-SM	0.68	0.62	0.49	0.38
DS-DA-SM	0.60	0.55	0.43	0.34

[a]Defined in equation 1. Data was obtain with measured during toluene methylation at $p_{toluene}$ = 6.0 kPa, $p_{methanol}$ = 1.5 kPa, 10 mg of catalyst and total flow rate = 2.3 cm^3 s^{-1}.

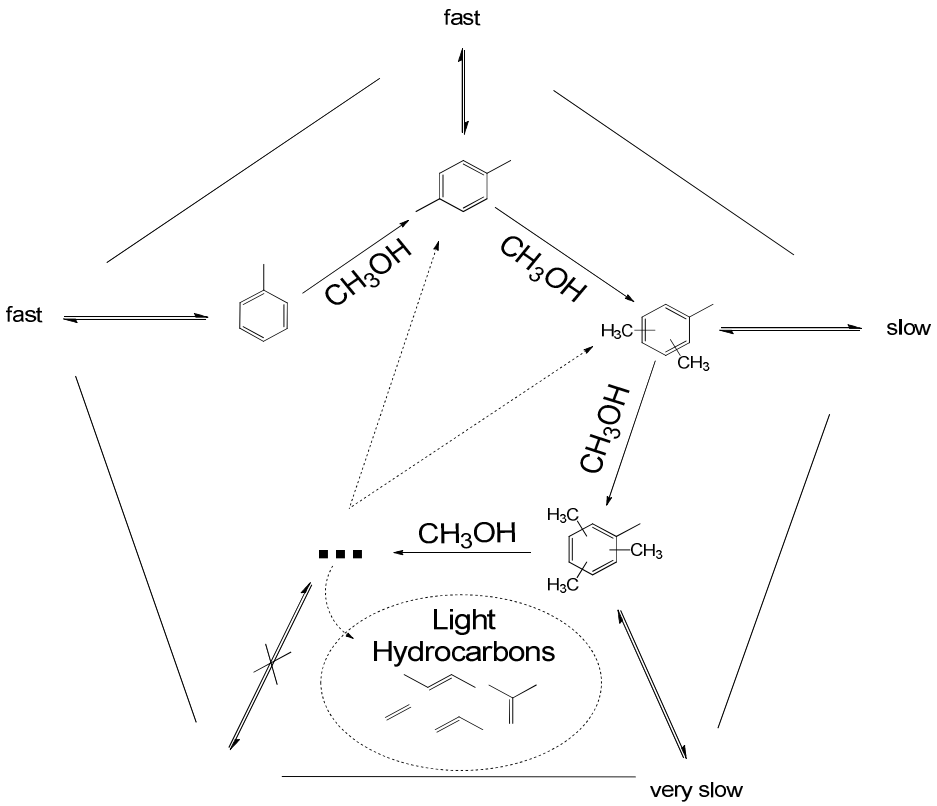

Scheme 3.2: Methylation and dealkylation of light hydrocarbons during the reaction of toluene with methanol inside H-ZSM5 zeolite. Toluene and p-xylenes diffuse in and out of zeolite pores fast relative to larger aromatic molecules, such as m- and o-xylenes, Tri- and TetraMBs. Most of the light hydrocarbons are formed from highly-methylated aromatic products before leaving the zeolite pores as less-methylated aromatic molecules.

The methanol usage toward formation of light hydrocarbons increased with longer effective diffusion length, because the residence time of large aromatic molecules in the zeolite pores, e.g., m-xylene and TriMBs, increased. Methylation and dealkylation of light hydrocarbon reactions (Scheme 3.2) occurred more frequently as the highly-methylated aromatic molecules spent more time inside micropores of the zeolites with longer effective diffusion length [38]. Consequently, the *MeOH for LH formation* fraction increased from 0.33 to 0.52 to 0.76, at 573 K with DS-DA, H-ZSM5 and SM samples, respectively (Table 3.4).

3.3.3.2. Influence of hierarchical pores and reaction temperature on selectivities

The selectivity of xylene isomers in xylenes, xylenes and TriMBs in aromatics are shown in Table 3.5. The selectivity of p-xylene decreased with desilication and dealumination, but increased significantly with deposition of an external SiO_2 overlayer. The increase in the reaction temperature increased the p-xylene selectivity with all catalysts (vide infra) [52]. Note that the xylenes and TriMBs selectivities in aromatics did not change significantly with the zeolite modifications or with reaction temperatures.

Table 3.5: Selectivity of xylene isomers in xylenes, xylenes and trimethylbenzenes (TriMBs) in aromatics during toluene methylation[a].

	573 K		623 K		673 K		723 K	
	Xylene selectivity p : m : o (%)	Xylenes (TriMBs) % in aromatics[b]	Xylene selectivity p : m : o (%)	Xylenes (TriMBs) % in aromatics	Xylene selectivity p : m : o (%)	Xylenes (TriMBs) % in aromatics	Xylene selectivity p : m : o (%)	Xylenes (TriMBs) % in aromatics
H-ZSM5	38 : 28 : 35	90 (5.8)	51 : 25 : 24	89 (8.3)	60 : 24 : 16	88 (9.2)	64 : 24 : 12	89 (8.8)
DS	33 : 29 : 38	92 (5.9)	42 : 29 : 29	87 (9.1)	52 : 29 : 19	86 (9.7)	56 : 30 : 14	87 (9.1)
DS-DA	33 : 28 : 39	92 (5.1)	41 : 29 : 31	90 (8.0)	49 : 29 : 22	89 (9.2)	52 : 31 : 17	89 (9.0)
SM	47 : 25 : 28	87 (8.0)	70 : 17 :13	88 (7.3)	81 : 13 : 6	89 (6.5)	85 : 11 : 4	92 (5.3)
DS-SM	41 : 27 : 32	86 (8.8)	60 : 21 : 18	85 (9.9)	76 : 15 : 9	87 (8.6)	84 : 12 : 5	90 (6.4)
DS-DA-SM	40 : 27 : 33	87 (8.0)	57 : 23 : 20	86 (9.8)	71 : 18 : 11	87 (9.2)	78 : 16 : 7	89 (7.6)

[a]Measured at $p_{toluene}$ = 6.0 kPa, $p_{methanol}$ = 1.5 kPa, 10 mg of catalyst and total flow rate = 2.3 cm^3 s^{-1}. [b]Rest are detected as 1,2,4,5-TetraMB.

The toluene conversion was generally lower for the surface modified samples compared to the non-modified ones by ~1-4 % (see Table 3.S4) at the same reaction conditions (space

velocity, temperature and partial pressures), because the concentration of Brønsted acid sites decreased after mesoporous SiO_2 overlayer deposition (Table 3.2). The selectivity of p-xylene decreased as the toluene conversion increased, but the selectivity to p-xylene was clearly higher for the surface modified materials (SM, DS-SM and DS-DA-SM) at the same toluene conversion level (Figure 3.8, at 723 K; p-xylene selectivity vs. C_1 conversion shown in Figure 3.S14). Note that the p-xylene selectivity decreased faster at toluene conversion levels above ~15 % (compared to the lower toluene conversion levels) for H-ZSM5 sample (Figure 3.8, empty square) because the methanol was nearly depleted at this point (conversion >90 %). Under these conditions the isomerization became the dominant reaction and the p-xylene selectivity started to approach the thermodynamic equilibrium. The disproportionation reaction was slow in these reaction conditions, i.e., <1% of the toluene converted went through disproportionation (not shown).

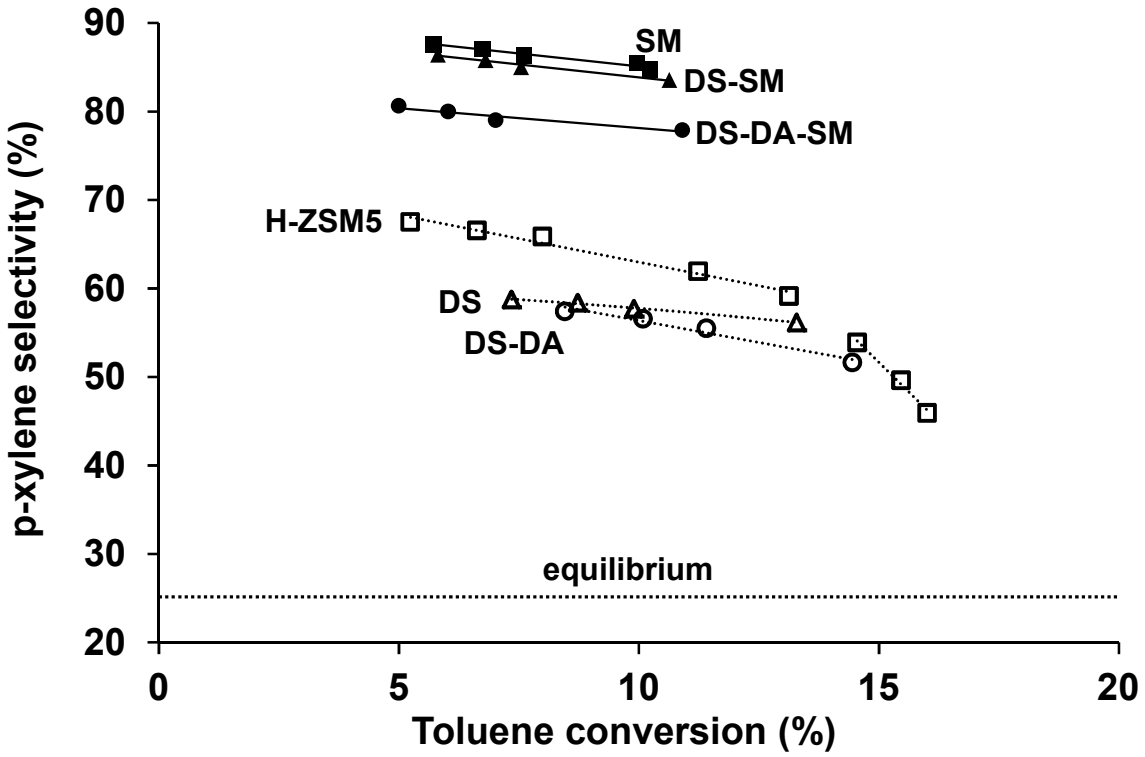

Figure 3.8: p-xylene selectivity vs. the conversion of toluene during toluene methylation, measured at 723 K ($p_{toluene}$ = 6.0 kPa, $p_{methanol}$ = 1.5 kPa, 4-25 mg of catalyst, total flow rate = 1.2-2.3 cm^3s^{-1}, C_1 (methanol and DME) conversion = 40-99 %). The filled symbols represent surface modified samples (SM (■), DS-SM (▲) and DS-DA-SM (●)) and unfilled the non-modified samples (parent H-ZSM5 (□), DS (Δ) and DS-DA (○)).

It was previously reported that the concentration of Brønsted acid sites located in the pore mouth region does not affect the p-xylene selectivity significantly [3,12,14]. This was

confirmed by comparing the Brønsted acid site concentrations (Table 3.2) with the selectivities (Table 3.5), where a correlation between the p-xylene selectivity and the concentration of Brønsted acid sites located in the pore mouth region was not found. The DS-SM sample had more acid sites accessible for 2,6-DTBPy (152 μmol g^{-1}) than the parent H-ZSM5 and DS-DA samples (90 and 131 μmol g^{-1}, respectively), but a higher p-xylene selectivity was observed for DS-SM.

During the reaction of toluene methylation, the xylene isomers can be generated by three major pathways, i.e., toluene methylation, xylene isomerization and dealkylation of highly-methylated aromatic molecules [38]. The isomerization reaction was found to be the most dominant pathway in controlling the selectivity of xylenes, as the reaction temperature increased and the product distribution were more strongly determined by the diffusivity of molecules (the reaction became more diffusion limited) [40,52,53]. The p-xylene diffuses an order of magnitude or faster than that of o-/m-xylenes (Table 6) and, thus, the p-xylene selectivity increased from 38 to 64 % with H-ZSM5 as the temperature increased from 573 to 723 K (Table 3.5). Likewise, the p-xylene selectivity increased significantly with surface modification by deposition of a mesoporous SiO_2 overlayer because the diffusivity of bulkier o-/m-xylenes decreased while it slightly increased for the p-xylene (Table 6). The difference in p-xylene after the SiO_2 overlayer increased from 7-9 to 21-26 % (Table 3.5), as the reaction temperature increased from 573 to 723 K and the reaction became more diffusion limited. This indicates that the diffusivity differences between p-xylene relative to o- and m-xylene play dominant role in controlling the p-xylene selectivity in these hierarchical materials under these reaction conditions.

Table 6: Apparent diffusion coefficients of xylenes at 373K and 0.1kPa over the parent H-ZSM5 and its surface modified sample (SM) by deposition of a mesoporous SiO_2 overlayer, from [15].

Catalyst	p-xylene (10^{-17} m^2 s^{-1})	o-xylene (10^{-18} m^2 s^{-1})	m-xylene (10^{-19} m^2 s^{-1})
H-ZSM5	4.7	6.3	3.8
SM	5.3	0.7	1.1

3.3.4. Impact of hierarchical materials on toluene methylation

The p-xylene selectivity as a function of the toluene turnover rates of the parent and the hierarchical materials at 723 K is shown in Figure 3.9 (similar figure as a function of gram of zeolite shown in Figure 3.S15 [40]). Desilication and subsequent dealumination increased the toluene turnover rate by ~2 and 25 %, respectively, but the surface modification by an external SiO_2 overlayer deposition on these materials decreased the rate by ~5 %. These modification procedures led to higher (DS and DS-DA) and lower (deposition of SiO_2 overlayer) toluene turnover rates by decreasing and increasing the concentration of highly methylated aromatic products in the pores, respectively, i.e., the coverage of activated methanol and the probability of toluene methylation relative to aromatic products increased with desilication-dealumination and decreased with SiO_2 overlayer. On the other hand, desilication and subsequent dealumination decreased the p-xylene selectivity within xylenes from ~65 to 55 and 50 % while the SiO_2 overlayer increased p-xylene selectivity significantly (from 50-65 to 75-85 %). Overall, the series of these zeolite modifications, i.e., desilication, dealumination and deposition of mesoporous SiO_2 overlayer, simultaneously enhanced the p-xylene selectivity and toluene turnover rate. The decrease in p-xylene selectivity (negative) and increase in toluene turnover rates (positive), to a different extent, from desilication-dealumination was compensated (and forfeited) after deposition of SiO_2 overlayer.

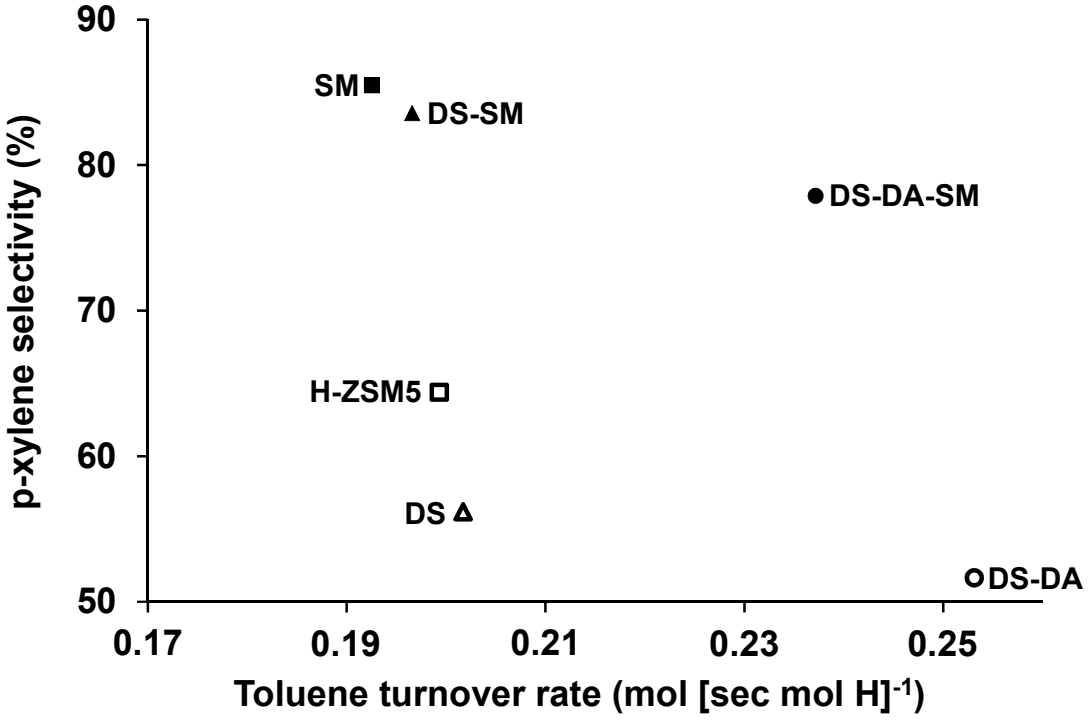

Figure 3.9: Selectivity of p-xylene within xylenes vs. toluene turnover rate (left) or consumption rate (right) during toluene methylation at 723 K ($p_{toluene}$ = 6.0 kPa, $p_{methanol}$ = 1.5 kPa, 10mg, total flow rate = 2.3 cm^3s^{-1}. The filled symbols represent surface modified samples (SM (■), DS-SM (▲) and DS-DA-SM (●)) and unfilled the non-modified samples (parent HZSM5 (□), DS (Δ) and DS-DA (○)).

Modification of the zeolite porosity is an effective method for simultaneously increasing both p-xylene selectivity and toluene turnover rates, however, only at relatively high reaction temperatures (compare Figure 3.9, at 723 K and Figure 3.S16, at 573 K). Deposition of an external SiO_2 overlayer increased the effective diffusion length and, consequently, the coverage of activated methanol decreased and the competitive reactions between methylation of the aromatic products (e.g., xylene and TriMB) and the reactant (toluene) increased. Higher reaction temperature decreased the effect of lower activation energies for the methylation of xylene to TriMB (and TriMB to TetraMB) compared to the methylation of toluene (vide supra). As a result, the difference in toluene turnover rates between the parent and the surface modified samples decreased as the temperature increased, e.g., SM sample from H-ZSM5 decreased the rate from 2.3 to 0.8 (10^{-2} mol [s mol H]$^{-1}$) at 573 K, but only from 20 to 19 at 723 K (Table 3.3). Therefore, a higher toluene turnover rate was observed for DS-DA-SM sample compared to the parent H-ZSM5 at high reaction temperatures as a result of relatively less-favored methylation of the aromatic products and higher coverage of activated methanol from shorter effective diffusion length.

3.4. Conclusions

Mesopores were generated in microporous H-ZSM5 by desilication with NaOH and chemical liquid deposition (CLD) of tetraethyl orthosilicate (TEOS) onto the zeolite surfaces. The Lewis and Brønsted acid site concentrations in the pore mouth region (accessible by 2,6-di-tert-butyl-pyridine) increased substantially after desilication, but these sites were effectively removed by subsequent dealumination with tartaric acid, without causing major changes to the mesoporosity. The surface modification by deposition of a mesoporous SiO_2 overlayer mainly decreased the concentration of Brønsted acid sites in the pore mouth region and decreased the diffusivity of the bulkier o- and m- xylene isomers, while increasing for p-xylene (desired product).

The toluene turnover rate and p-xylene selectivity increased simultaneously at relatively high reaction temperatures (>673 K) with H-ZSM5 after desilication, dealumination and subsequent SiO_2 overlayer deposition via CLD of tetraethyl orthosilicate. The turnover rate of toluene was strongly influenced by effective diffusion length because the reaction of toluene methylation was diffusion limited by the transport of large aromatic products. The selectivity of p-xylene among these hierarchical materials in these reaction conditions was predominantly controlled by the diffusivity differences between p-xylene relative to o- and m-xylenes and the Brønsted acid sites in the pore mouth region were determined to play only a minor role.

3.5. Acknowledgments

The financial support from the King Fahd University of Petroleum and Minerals (KFUPM) is acknowledged. Helpful technical discussions with Gary Haller, Jeongnam Kim, Mirek Derewinski, Oliver Gutiérrez, Stefan Schallmoser and Xianyong Sun, as well as Carolina Neudeck for dynamic light scattering experiments, Xaver Hecht for N_2 physisorption experiments and Martin Neukamm for AAS measurements are also acknowledged.

3.6. Supplementary materials

Table 3.S1: Integrated area counts from powder X-ray diffraction pattern in Figure 2 of the manuscript.

	5-10^{o}	22-25^{o}	Total	Relative crystallinity[a] (%)
H-ZSM5	37484	28246	65730	100
DS	36261	25443	61704	94
DS-SM	40013	26524	66537	101
SM	22697	34848	57545	88

[a]Determined by assuming that the parent H-ZSM5 has perfect crystallinity.

The pore distribution size of the parent (H-ZSM5), desilicated (DS) and subsequently dealuminated (DS-DA) samples are compared to the corresponding surface modified (SM) materials in Figures 3.S1-3.S3. The applicable diameter range with nitrogen adsorption measurement was 1.8nm (cylindrical pore, NLDFT equilibrium model).

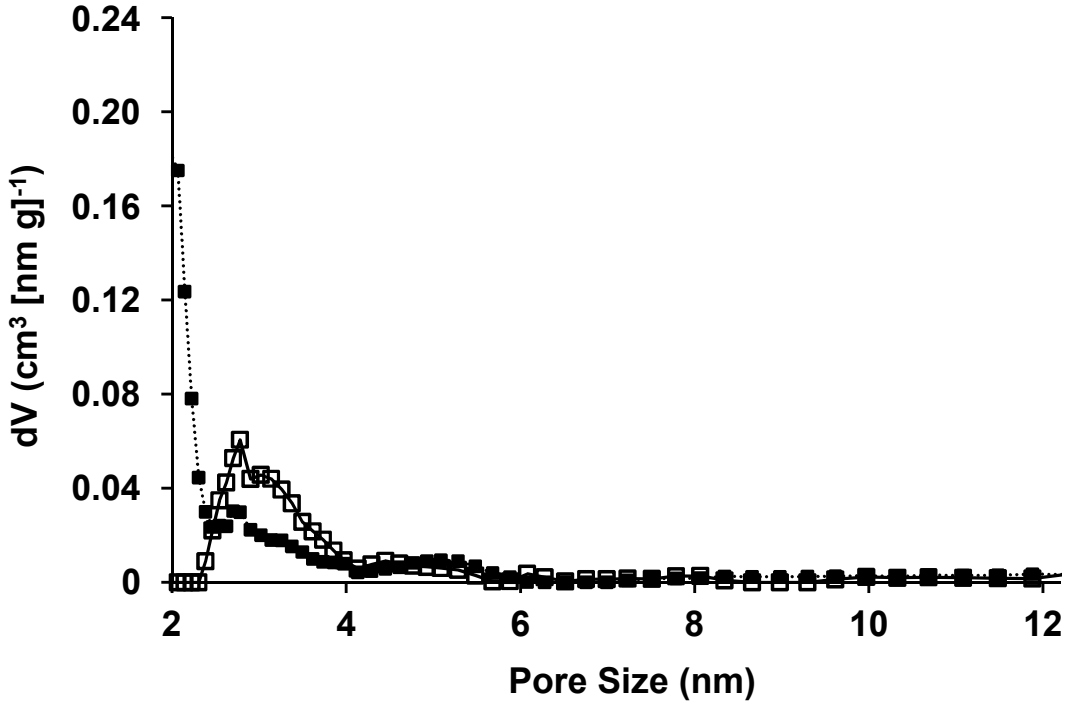

Figure 3.S1: Pore size distribution of the parent (H-ZSM5; □) and its surface modified sample by SiO_2 deposition (SM; ■), analyzed by DFT method (cylindrical pore, NLDFT equilibrium model).

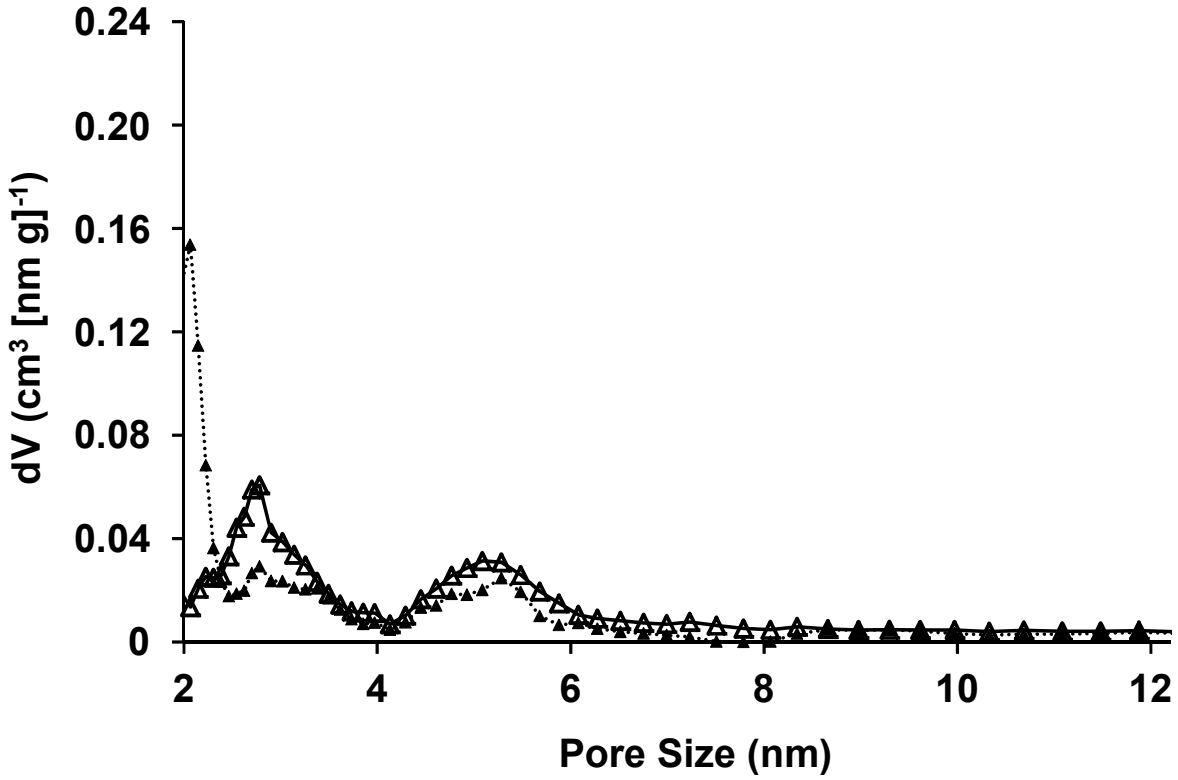

Figure 3.S2: Pore size distribution of the desilicated (DS; Δ) and its surface modified samples by SiO_2 deposition (DS-SM; ▲), analyzed by DFT method (cylindrical pore, NLDFT equilibrium model).

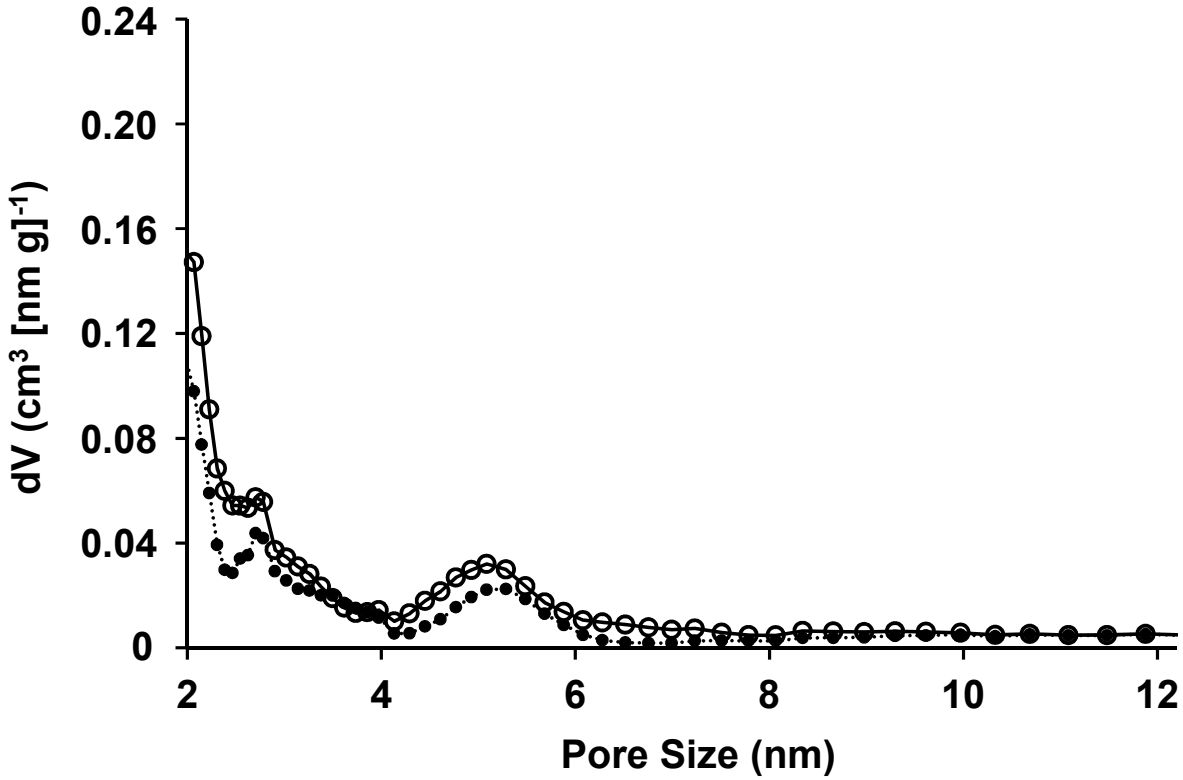

Figure 3.S3: Pore size distribution of the subsequent dealuminated (DS-DA; ○) and its surface modified samples by SiO_2 deposition (DS-DA-SM; ●), analyzed by DFT method (cylindrical pore, NLDFT equilibrium model).

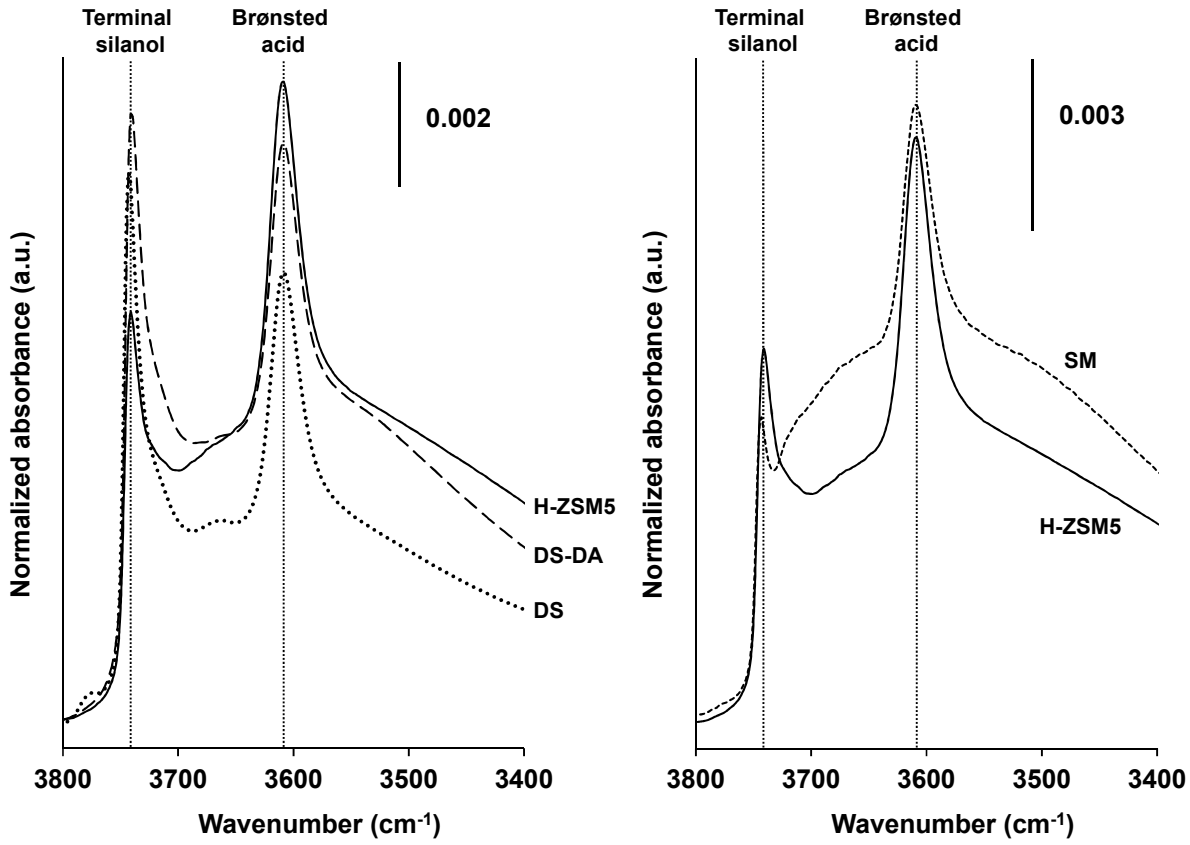

Figure 3.S4: Superimposed infrared (IR) spectra of H-ZSM5, DS and DS-DA (left) and H-ZSM5 and SM (right) measured at 423 K under vacuum (< 10^{-7} kPa) after activation at 723 K for 1 hour. The bands at 3745 cm^{-1} and 3610 cm^{-1} represents O-H vibration of the terminal silanol groups and the Brønsted acid sites, respectively. The spectra were normalized to the lattice vibrations and were superimposed onto H-ZSM5 spectrum.

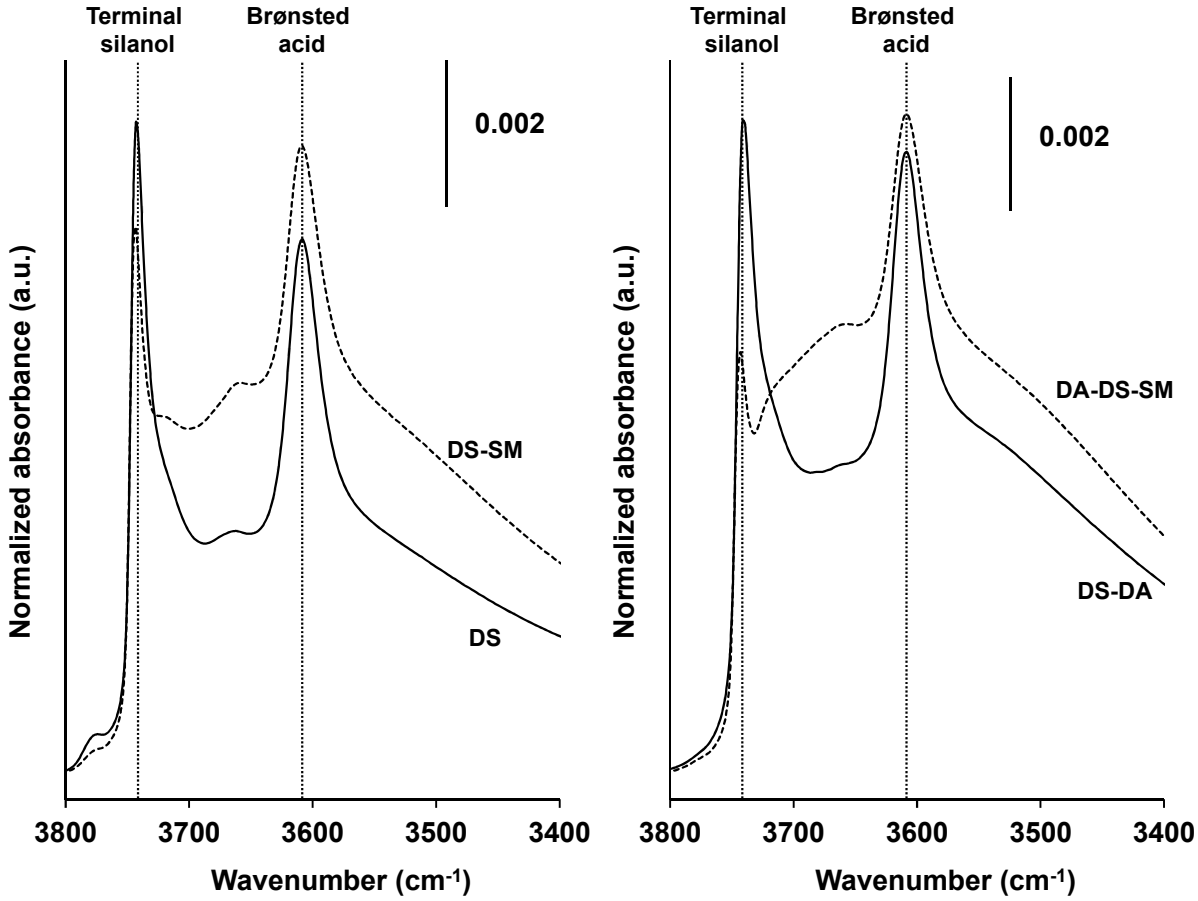

Figure 3.S5: Superimposed infrared (IR) spectra of DS and DS-SM (left) and DS-DA and DS-DA-SM (right) measured at 423 K under vacuum (< 10^{-7} kPa) after activation at 723 K for 1 hour. The bands at 3745 cm^{-1} and 3610 cm^{-1} represents O-H vibration of the terminal silanol groups and the Brønsted acid sites, respectively. The spectra were normalized to the lattice vibrations and were superimposed onto DS or DS-DA spectrum.

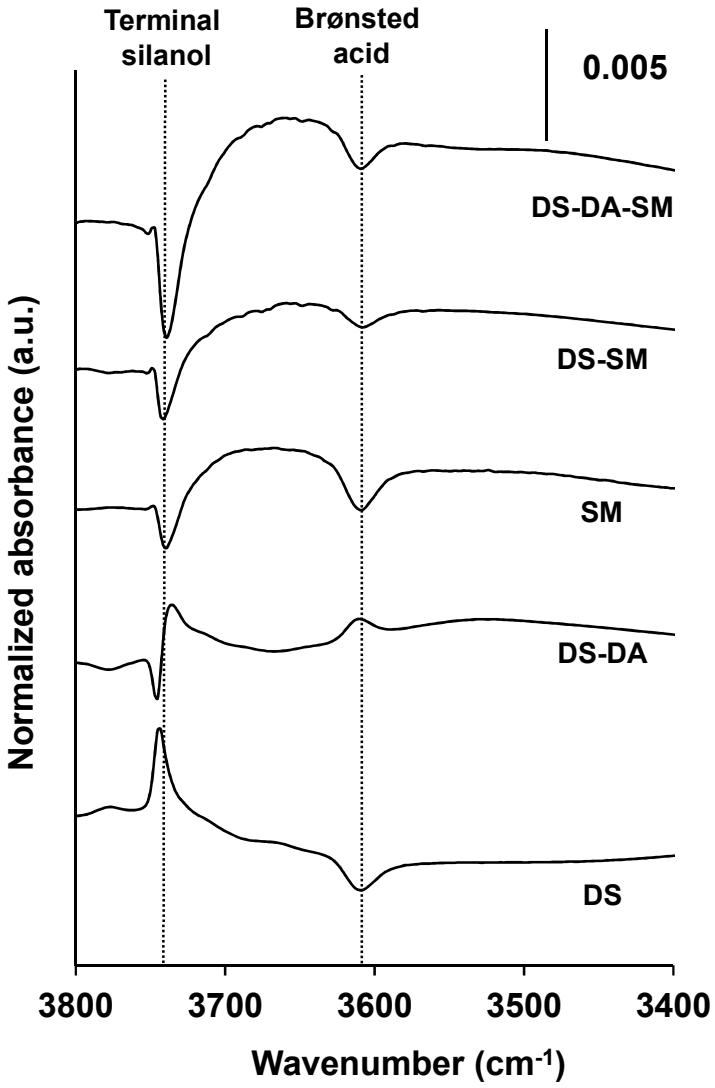

Figure 3.S6: Infrared (IR) spectra of activated samples (heated to 723 K for 1 hour) after subtraction of the spectra prior to the modification, i.e., DS = DS minus H-ZSM5, DS-DA = DS-DA minus DS, SM = SM minus H-ZSM5, DS-SM = DS-SM minus DS and DS-DA-SM = DS-DA-SM minus DS-DA. All spectra were measured at 423 K under vacuum (< 10^{-7} kPa) and normalized to the lattice vibrations. The bands at 3745 cm^{-1} and 3610 cm^{-1} represents O-H vibration of the terminal silanol groups and the Brønsted acid sites, respectively.

The distribution of the Lewis acid sites calculated by assuming similar extinction coefficient is summarized in Table 3.S2 (deconvoluted IR spectra of H-ZSM5 and DS are shown as an example in Figure 3.S7). The fraction of Lewis acid sites with hydrogen bond interactions from Brønsted acid site (1447 cm^{-1}) decreased significantly from 96 to 42% with desilication because relative concentration of the Brønsted to Lewis acid sites decreased by desilication (B/L; Table 3.S2). Consequently, there was less Brønsted acid sites available to interact with coordinately bonded pyridine on the Lewis acids sites generated by desilication. Subsequent dealumination removed more Lewis relative to Brønsted acid sites (Table 2) and

the fraction of the band at ~1447 cm^{-1} increased from 42 to 72 %. Note that the Brønsted to Lewis acid site ratio was slightly higher for the DS-DA sample compared to H-ZSM5 (6.3 to 5.7; Table 3.S2) but lower fraction of the band at ~1447 cm^{-1} was observed (71 vs. 96 % with DS-DA and H-ZSM5, respectively). This suggests that the Lewis acid sites with a nearby Brønsted acid site were selectively removed (or vice versa, Brønsted acid located near Lewis acid sites were removed) by subsequent dealumination using tartaric acid.

Deposition of mesoporous SiO_2 onto H-ZSM5 and DS-DA removed some Brønsted acids but slightly increased Lewis acid sites (Table 2). This decreased the Brønsted to Lewis acid site ratio and as a result, the fraction of Lewis acid sites with hydrogen bond interactions from a Brønsted acid site (1447 cm^{-1}) from 96 to 79 % and 71 to 62 % after depositing mesoporous SiO_2 overlayer on H-ZSM5 and DS-DA (Table 3.S2), respectively. In contrast, less Brønsted relative to Lewis acid sites were removed with DS sample, i.e., the ratio of Brønsted to Lewis acid sites increased with the DS sample, and, consequently, the fraction of band at 1447 cm^{-1} increased slightly after deposition of SiO_2 overlayer from 42 to 44 % (Table 3.S2). Note that decrease in the fraction of the band at 1447 cm^{-1} after heating the samples to 723 K was more pronounced compared to 1455 cm^{-1}, indicating that pyridine is less strongly bound to the sites with hydrogen bond from a Brønsted acid site. A linear correlation between the fraction of Lewis acid band at 1447 cm^{-1} and the fraction of Lewis acid sites remaining after heating to 723 K was observed (Figure 3.S8).

Table 3.S2: Distribution of Lewis acid sites determined from infrared spectral band deconvolution.

	Total[a]		Strong[b]		
	1455 cm^{-1} (%)[c]	1447 cm^{-1} (%)[c]	1455 cm^{-1} (%)[c]	1447 cm^{-1} (%)[c]	B/L[d]
H-ZSM5	4	96	39	61	5.7
DS	58	42	90	10	2.3
DS-DA	29	71	74	26	6.3
SM	21	79	78	22	4.6
DS-SM	56	44	91	9	2.8
DS-DA-SM	38	62	83	17	4.2

[a]After adsorption of pyridine at 423K and outgassing for 1 hour under vacuum. [b]After subsequently heating the samples to 723 K for 0.5 hour. [c]Similar molar extinction coefficients were assumed for bands at 1447 and 1455 cm^{-1}, which represent the coordinately bonded pyridine molecules on Lewis acid sites with and without hydrogen bond interactions from a Brønsted acid site, respectively. [d]B/L = Ratio of total Brønsted to Lewis acid sites, from Table 2.

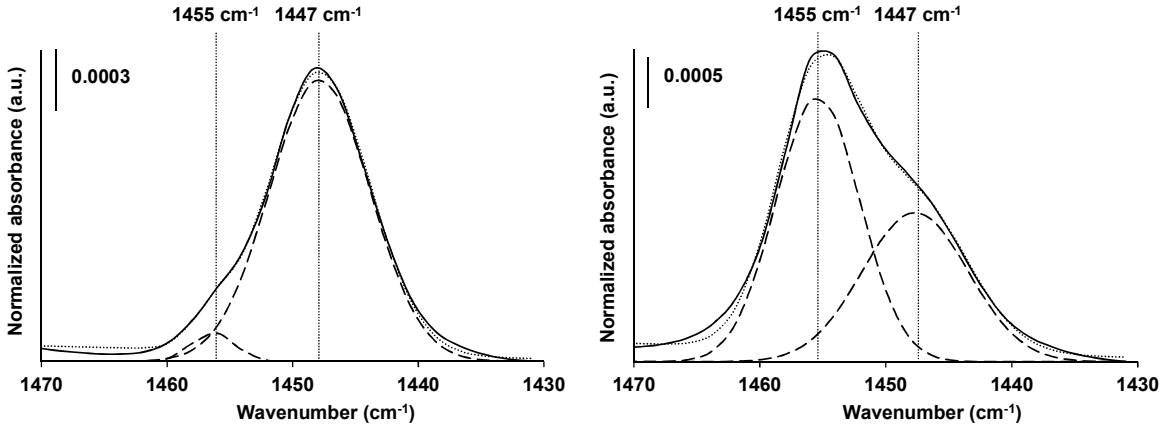

Figure 3.S7: Two bands centered at 1447 and 1455 ±1 cm^{-1} (dashed) represent the coordinately bonded pyridine molecules on Lewis acid sites with and without hydrogen bond interactions from a Brønsted acid site, respectively. Deconvoluted spectra of this region with H-ZSM5 (left) and DS (right) samples after adsorption of pyridine at 423 K and outgassing for 1 hour under vacuum (< 10^{-7} kPa) are shown above. The actual spectra and the fitted line are represented by solid and dotted line, respectively.

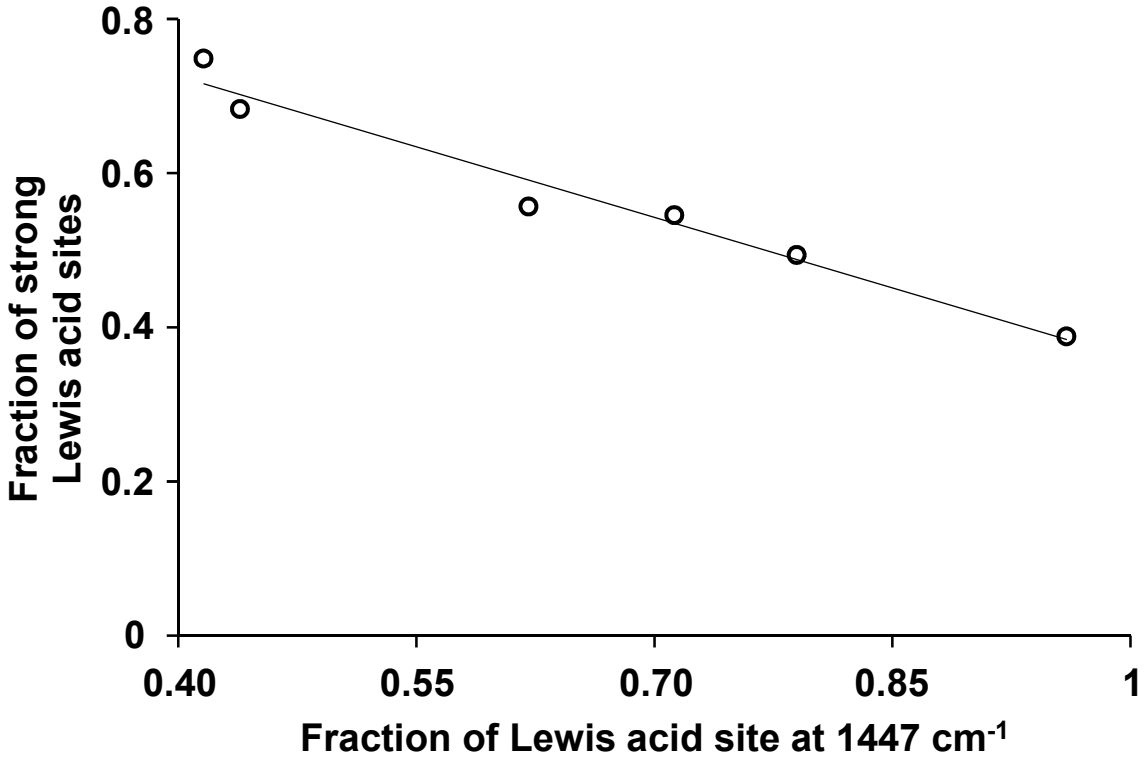

Figure 3.S8: The fraction of strong Lewis acid sites (defined by strong divided by total Lewis acid sites in Table 2) vs. fraction of Lewis acid sites with hydrogen bond interaction with a Brønsted acid site (1447 cm^{-1}, Table 3.S2).

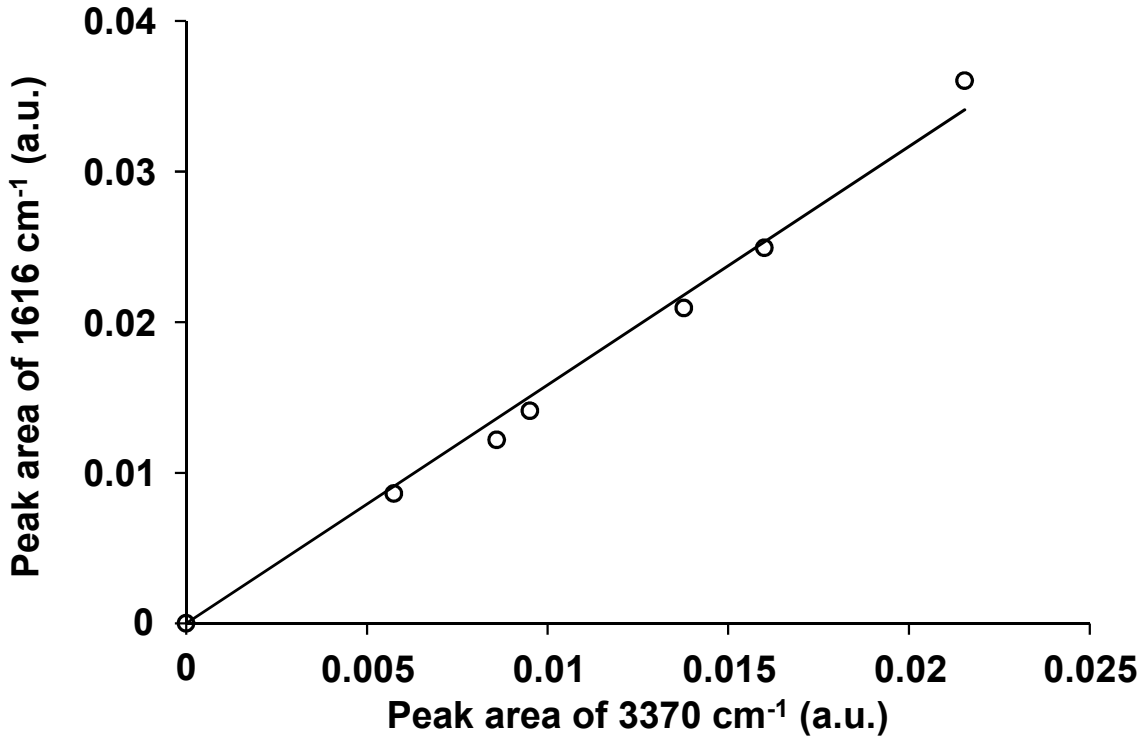

Figure 3.S9: Area counts of the band at 1616 cm^{-1} (C=C vibration) vs. 3367 cm^{-1} ($N\text{-}H^{+}$ vibration), after adsorption of 2,6-di-tert-butyl-pyridine at 423 K, 0.01 kPa and outgassing for 1 hour in vacuum (< 10^{-7} kPa).

The synthesis batch loses ~ 25 and 5 % of mass during desilication and subsequent dealumination procedure, respectively. The number (instead of concentration) of acid sites normalized to the initial 1 gram of parent H-ZSM5 sample are calculated, therefore, to keep track of the changes after each procedure more accurately. These numbers are determined as follows:

H-ZSM5:	*[Acid site] x 1g material*	*(2)*
DS:	*[Acid site] x 1g material x 0.75*	*(3)*
DS-DA:	*[Acid site] x 1g material x 0.75 x 0.95*	*(4)*
SM:	*[Acid site] x 1g material*	*(5)*
DS-SM:	*[Acid site] x 1g material x 0.75*	*(6)*
DS-DA-SM:	*[Acid site] x 1g material x 0.75 x 0.95*	*(7)*

where *[acid site]* denotes the concentration of sites per gram of zeolite (reported in Table 3 of the manuscript as μmol per gram of material). Figure 3.S10 shows the number of acid sites normalized by initial 1 gram of the parent H-ZSM5.

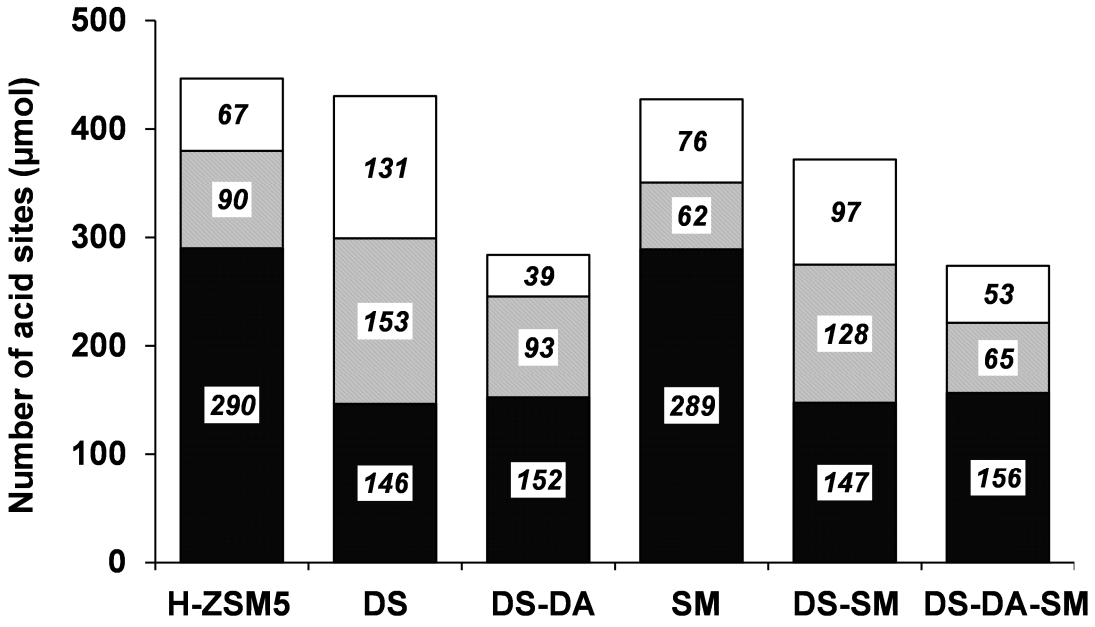

Figure 3.S10: Number of Brønsted and Lewis acid sites calculated from 1 gram of H-ZSM5 as a starting material. The material loses ~ 25 and 5 % of weight during desilication and subsequent dealumination, respectively, and gains ~ 12 % of mass after TEOS deposition onto the surface. White represents Lewis acid sites, grey and black the Brønsted acid site accessible and not accessible by bulky 2,6-DTBPy, respectively.

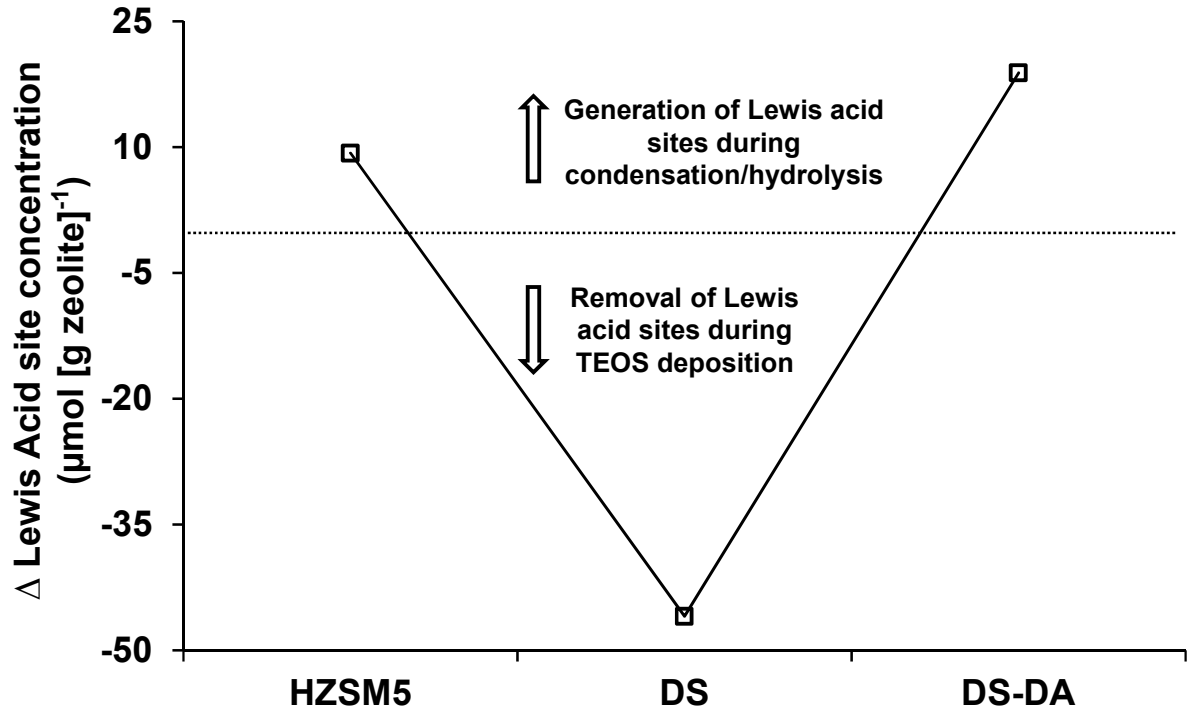

Figure 3.S11: Change in Lewis acid concentration after deposition of SiO_2 overlayer (from Table 2).

Table 3.S3: Turnover rates of C_1 at different reaction temperatures during toluene methylation.

	573 K	623 K	673 K	723 K
	C_1[a] turnover rate[b] (10^{-2} mol [s mol H]$^{-1}$)	C_1 turnover rate (10^{-2} mol [s mol H]$^{-1}$)	C_1 turnover rate (10^{-2} mol [s mol H]$^{-1}$)	C_1 turnover rate (10^{-2} mol [s mol H]$^{-1}$)
H-ZSM5	5.4	17	25	31
DS	4.5	16	27	32
DS-DA	6.1	18	29	35
SM	4.0	16	29	36
DS-SM	3.1	14	29	38
DS-DA-SM	4.5	18	32	42

[a]C_1 = methanol and DME (both are treated as the same reactant because methanol can be transformed into DME during the reaction and DME can also be used for methylation). [b]Measured at $p_{toluene}$ = 6.0 kPa, $p_{methanol}$ = 1.5 kPa, 10 mg of catalyst and total flow rate = 2.3 cm^3 s^{-1}.

Table 3.S4: Conversion of reactants (C_1 and toluene) at different reaction temperatures during toluene methylation.

	573 K		623 K		673 K		723 K	
	C_1[a] % conversion	Toluene % conversion[b]	C_1 % conversion	Toluene % conversion	C_1 % conversion	Toluene % conversion	C_1 % conversion	Toluene % conversion
H-ZSM5	15	1.4	45	4.8	68	8.7	84	13
DS	11	1.8	44	5.9	75	10	89	13
DS-DA	15	2.1	46	6.2	73	11	88	14
SM	8.5	0.4	39	2.4	65	6.2	82	10
DS-SM	5.5	0.5	31	2.3	67	6.4	88	11
DS-DA-SM	8.3	0.7	34	3.0	65	6.9	83	11

[a]C_1 = methanol and DME. [b]Measured at $p_{toluene}$ = 6.0 kPa, $p_{methanol}$ = 1.5 kPa, 10 mg of catalyst and total flow rate = 2.3 $cm^3 s^{-1}$.

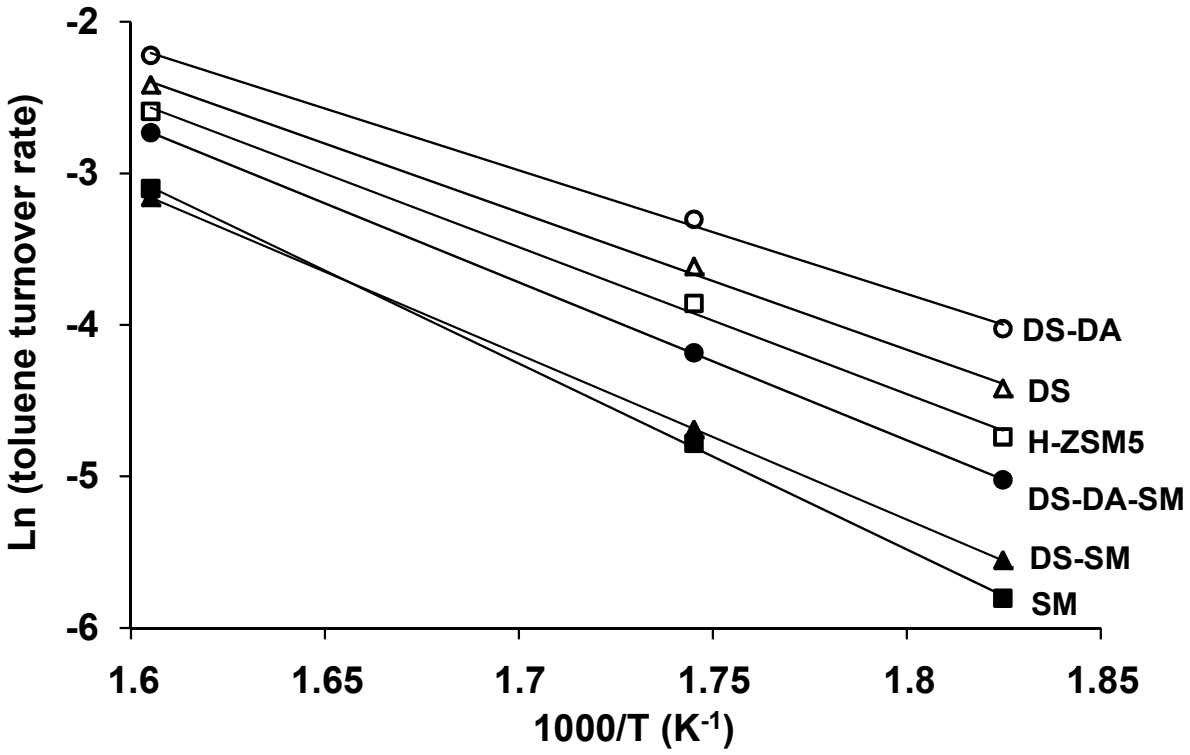

Figure 3.S12: Temperature dependence of toluene turnover rates between 548-623 K ($p_{toluene}$ = 6.0 kPa, $p_{methanol}$ = 1.5 kPa, 10 mg, total flow rate = 2.3 $cm^3 s^{-1}$.The filled symbols represent surface modified samples (SM (■), DS-SM (▲) and DS-DA-SM (●)) and unfilled the non-modified samples (parent HZSM5 (□), DS (Δ) and DS-DA (○)).

The Thiele modulus, Φ, for porous catalyst particles is estimated by the equation below [44]:

$$\Phi = L \sqrt{\frac{2 \times r_{obs}}{D_{toluene} \times R \times C_{toluene}}}$$

where L (m) is the radius of the zeolite crystal determined by dynamic light scattering method, r_{tol} (mol [m^2 s]$^{-1}$) is the observed turnover rate of toluene (Brunauer-Emmett-Teller surface area was used to normalize by the surface area), $D_{toluene}$ (m^2 s^{-1}) is the diffusion coefficient (extrapolated from [41] for H-ZSM5 sample and is scaled from zero length column measurements for hierarchical samples [18]), R (m) is the radius of the zeolite pore (i.e., of H-ZSM5 and assumed 0.27 nm for the calculation) and $C_{toluene}$ (mol m^{-3}) is the initial concentration of toluene. Estimated value of the Thiele modulus at various reaction temperatures on all samples are shown in Table 3.S5.

Table 3.S5: Estimated Thiele modulus and effectiveness factor at different reaction temperatures during toluene methylation.

	573 K		623 K		673 K		723 K	
	Φ[a]	η[b]	Φ	η	Φ	η	Φ	η
H-ZSM5	2.0	0.49	2.9	0.34	3.4	0.30	3.5	0.29
DS	1.5	0.61	2.1	0.46	2.3	0.43	2.2	0.45
DS-DA	1.3	0.66	1.8	0.52	2.1	0.47	2.0	0.47
SM	1.5	0.59	3.5	0.28	5.3	0.19	6.5	0.15
DS-SM	1.0	0.75	1.8	0.54	2.4	0.41	2.6	0.38
DS-DA-SM	1.3	0.66	2.4	0.41	3.3	0.30	3.8	0.26

[a]Φ = Thiele modulus. [b]η = effectiveness factor assuming cylindrical model, tanh (Φ) / Φ.

The in-situ infrared (IR) spectroscopy of toluene methylation with H-ZSM5 and SM samples was measured at 573 K using Thermo Nicolet 6700 FT-IR spectrometer (resolution of 4 cm^{-1}; cell volume of 1.5 cm^3). The catalyst in a self-supported wafer (~5 mg) was activated at 573 K (heating rate of 0.17 K s^{-1}) for 1.5 hours under flowing helium (2.2 cm^3 s^{-1}; 99,996%, Westfalen). After collecting the spectra of activated samples, the reaction mixtures were introduced by flowing saturated toluene (2.4 kPa, 2.0 cm^3 s^{-1}) and methanol (9.9 kPa, 0.11 cm^3 s^{-1}) at 288 K with helium (0.20 cm^3 s^{-1}). The spectra were measured every 60 seconds during the reaction and the spectra of H-ZSM5 and SM after activation and ~0.5 hour after introducing the reaction mixtures is shown in Figure 3.S13. The gas product distributions

and rates (all within factor of 2) trends were similar to the ones obtained from plug flow reactor at similar conditions. The areas of the O-H vibration region of Brønsted acid (~3610 cm^{-1}) in Figure 3.S13 were integrated to estimate the changes of surface coverage in the zeolites. About 20 and 40 % of Brønsted acid sites interacted with H-ZSM5 and SM samples, respectively (determined by change in the area counts of dashed from solid spectra in 3610 cm^{-1} region in Figure 3.S13).

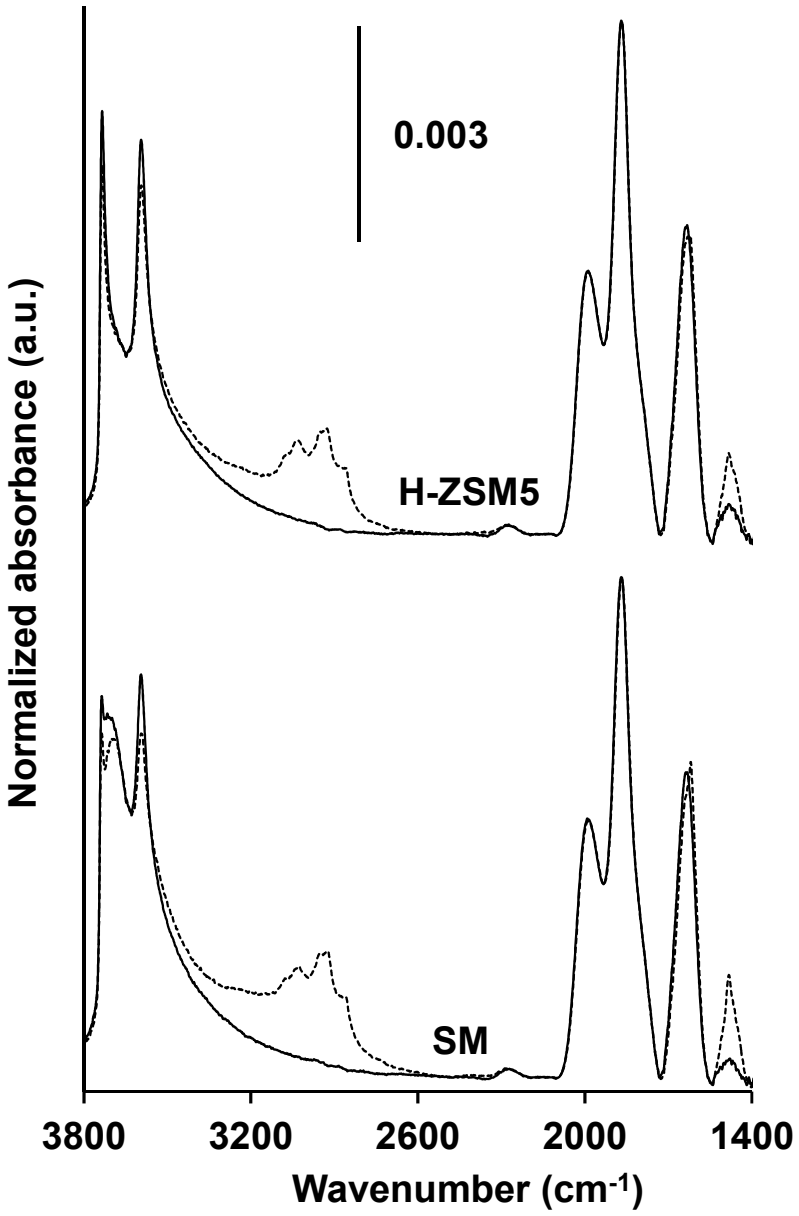

Figure 3.S13: Infrared spectra before (solid) and during the reaction of toluene methylation (dashed, after ~0.5 hour) at 573 K with H-ZSM5 (top) and SM (bottom; surface modified sampled derived from H-ZSM5 by depositing SiO_2 overlayer from tetraethyl orthosilicate) samples. The areas of O-H vibration region corresponding to Brønsted acid (~3610 cm^{-1}) were integrated to estimate the surface coverage in the zeolites.

Table 3.S6: Formation rate of xylenes and trimethylbenzenes (TriMBs) and the rate ratios at different reaction temperatures.

	573 K		623 K		673 K		723 K	
Formation rates[a]	Xylenes (TriMBs)[b]	X:T[c]	Xylenes (TriMBs)	X:T	Xylenes (TriMBs)	X:T	Xylenes (TriMBs)	X:T
H-ZSM5	2.1 (0.13)	16	6.8 (0.64)	11	12 (1.3)	10	18 (1.8)	10
DS	2.5 (0.16)	16	7.8 (0.81)	10	14 (1.5)	9	18 (1.8)	10
DS-DA	3.4 (0.19)	18	9.8 (0.87)	11	17 (1.8)	10	23 (2.3)	10
SM	0.7 (0.06)	11	4.1 (0.34)	12	11 (0.78)	14	18 (1.0)	17
DS-SM	0.8 (0.08)	10	3.6 (0.42)	9	10 (1.0)	10	18 (1.3)	14
DS-DA-SM	1.3 (0.12)	11	5.6 (0.64)	9	13 (1.4)	9	21 (1.8)	12

[a]Measured at $p_{toluene}$ = 6.0 kPa, $p_{methanol}$ = 1.5 kPa, 10 mg of catalyst and total flow rate = 2.3 cm^3 s^{-1}. The units of the rates are reported as 10^{-2} mol [s mol H]$^{-1}$. [b]Values inside the parenthesis are the TriMBs formation rates. [b]X:T = ratio of xylene to TriMBs formation rates.

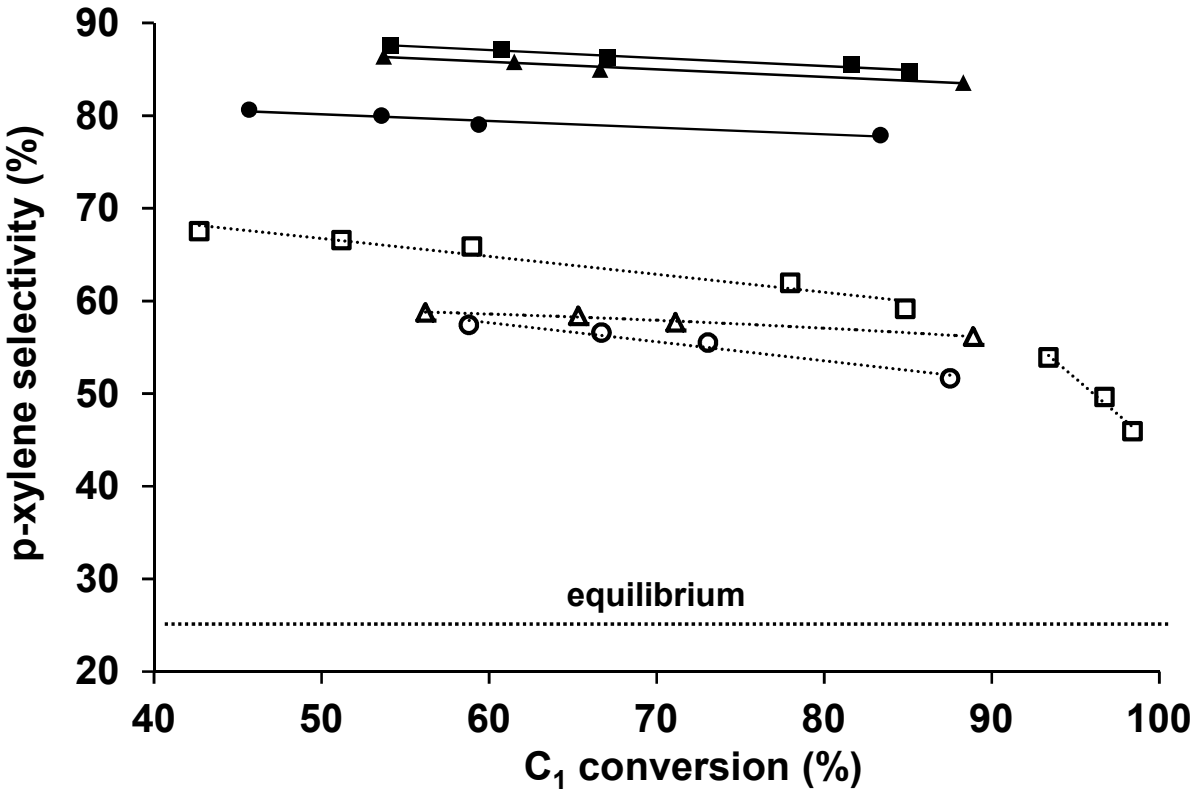

Figure 3.S14: p-xylene selectivity vs. the conversion of C_1 (methanol and DME) during toluene methylation, measured at 723 K ($p_{toluene}$ = 6.0 kPa, $p_{methanol}$ = 1.5 kPa, catalyst amount = 4-25 mg, total flow rate = 1.2-2.3 cm^3s^{-1}, toluene conversion = 5-16 %). The filled symbols represent surface modified samples (SM (■), DS-SM (▲) and DS-DA-SM (●)) and unfilled the non-modified samples (parent H-ZSM5 (□), DS (Δ) and DS-DA (○)).

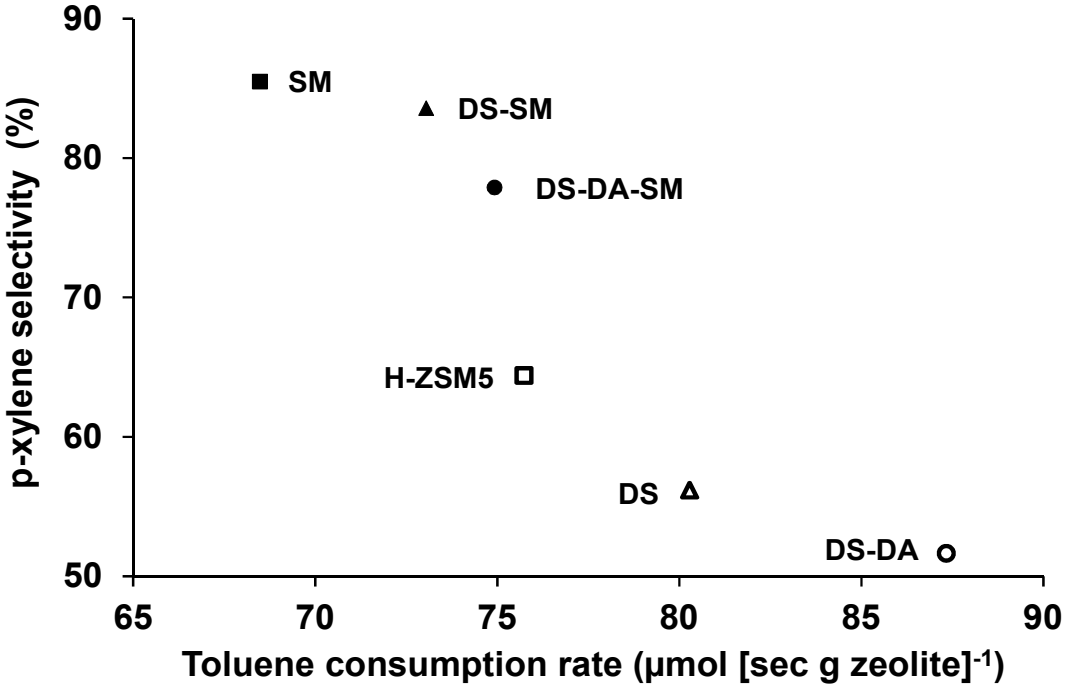

Figure 3.S15: Selectivity of p-xylene within xylenes vs. toluene consumption rate (per gram of zeolite) during toluene methylation at 723 K ($p_{toluene}$ = 6.0 kPa, $p_{methanol}$ = 1.5 kPa, 10mg, total flow rate = 2.3 cm^3s^{-1}. The filled symbols represent surface modified samples (SM (■), DS-SM (▲) and DS-DA-SM (●)) and unfilled the non-modified samples (parent HZSM5 (□), DS (Δ) and DS-DA (○)).

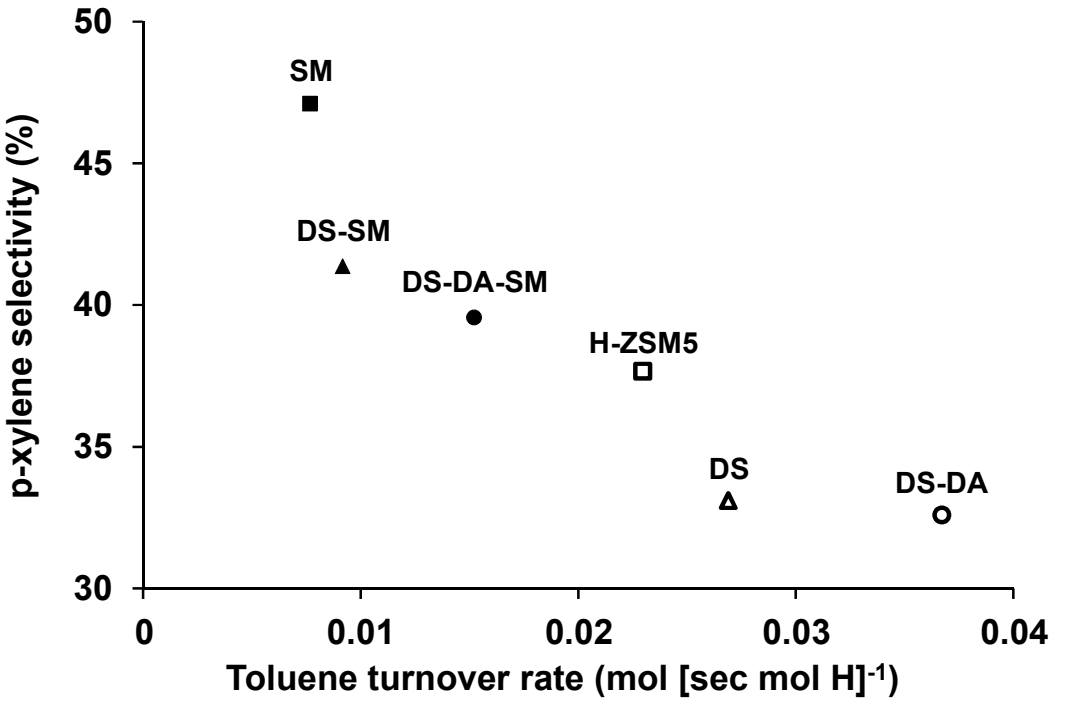

Figure 3.S16: Selectivity of p-xylene within xylenes vs. toluene turnover rate during toluene methylation at 573 K ($p_{toluene}$ = 6.0 kPa, $p_{methanol}$ = 1.5 kPa, 10mg, total flow rate = 2.3 cm^3s^{-1}. The filled symbols represent surface modified samples (SM (■), DS-SM (▲) and DS-DA-SM (●)) and unfilled the non-modified samples (parent HZSM5 (□), DS (Δ) and DS-DA (○)).

3.7. References

[1] W. Vermeiren, J.P. Gilson. Topics in Catalysis 52 (2009) 1131-1161.

[2] T. Tsai, S. Liu, I. Wang, Applied Catalysis A: General 181 (1999) 355-398.

[3] T. Hibino, M. Niwa, Y. Murakami, J. Catal. 128 (1991) 551-558.

[4] W.W. Kaeding, C. Chu, L.B. Young, B. Weinstein, S.A. Butter, J. Catal. 67 (1981) 159-174.

[5] H. Vinek, J.A. Lercher, J. Mol. Catal., 64 (1991) 23-39.

[6] R. D. Chirico, W.V. Steele, J. Chem. Eng. Data 42 (1997) 784-790.

[7] Y.S. Bhat, J. Das, K.V. Rao, A.B. Halgeri, 159 (1996) 368-374.

[8] L.B. Young, S.A. Butter, W.W. Kaeding, J. Catal. 76 (1982) 418-432.

[9] O. Mikkelsen, P.O. Rønning, S. Kolboe, Micropor. Mesopor. Mater. 40 (2000) 95-113.

[10] J.P. Breen, R. Burch, M. Kulkarni, D. McLaughlin, P.J. Collier, S.E. Golunski, Appl. Catal. A: General 316 (2007) 53-60.

[11] H. Vinek, G. Rumplmayr, J.A. Lercher, J. Catal. 115 (1989) 291-300.

[12] H.P. Röger, M. Krämer, K.P. Möller, C.T. O'Connor, Micropor. Mesopor. Mater. 21 (1998) 607-614.

[13] S. Zheng, H.R. Heydenrych, H.P. Röger, A. Jentys, J.A. Lercher, Top. Catal. 22 (2003) 101-106.

[14] J. Čejka, N. Žilková, B. Wichterlová, G. Eder-Mirth, J.A. Lercher, Zeolites 17 (1996) 265-271.

[15] S. Zheng, A. Jentys, J.A. Lercher, J. Catal. 241 (2006) 304-311.

[16] J.C. Groen, W. Zhu, S. Brouwer, S.J. Huynink, F. Kapteijn, J.A. Moulijn, J. Pérez-Ramírez, J. Am. Chem 129 (2007) 355-360.

[17] F.C. Meunier, D. Verboekend, J.P. Gilson, J.C. Groen, J. Pérez-Ramírez, Micropor. Mesopor. Mater. 148 (2012) 115-121.

[18] R. Kolvenbach, J. H. Ahn, S. S. Al-Khattaf, A. Jentys, J. A. Lercher, in preparation.

[19] C.H. Christensen, K. Johannsen, E. Törnqvist, I. Schmidt, H. Topsøe, C.H. Christensen, Cat. Today 128 (2007) 117-122.

[20] C.H. Christensen, K. Johannsen, I. Schmidt, C.H. Christensen, J. Am. Chem 125 (2003) 13370-13371.

[21] C. Fernandez, I. Stan, J.P. Gilson, K. Thomas, Aurélie Vicente, A. Bonila, J. Pérez-Ramírez, Chem. Eur. J. 16 (2010) 6224-6233.

[22] J.C. Groen, L.A.A. Peffer, J.A. Moulijn, J. Pérez-Ramírez, Colloids and Surfaces A: Physicochem. Eng. Aspects 241 (2004) 53-58.

[23] J. Kim, M. Choi, R. Ryoo, J. Catal. 269 (2010) 219-228.

[24] S. Brunauer, P. H. Emmett, E. Teller, J. Am. Chem. Soc. 60 (1938) 308-319.

[25] M. Kruk, M. Jaroniec, J. Choma, Carbon 36 (1998) 1447.

[26] S. J. Gregg, Adsorption Surface Area and Porosity, 2nd ed.; Academic Press Inc.: New York, 1982.

[27] A. Corma, V. Fornes, L. Forni, F. Marquez, J. Martinez-Triguero, D. Moscotti, J. Catal. 179 (1998) 451-458.

[28] Database of Zeolite Structures (http://www.iza-structure.org/databases/).

[29] N. Tøpsoe, K. Pedersen, E.G. Derouane, J. Catal. 70 (1981) 41-52.

[30] G. Qin, L. Zheng, Y. Xie, C. Wu, J. Catal. 95 (1985) 609-612.

[31] G. Lietz, K.H. Schnabel, C. Peuker, T. Gross, W. Storek, J. Volter, J. Catal. 148 (1994) 562-568.

[32] K. Yamagishi, S. Namba, T. Yashima, J. Phys. Chem. 95 (1991) 872-877.

[33] M. Kustova, M.S. Holm, C.H. Christensen, Y. Pan, P. Beato, T.V.W. Janssens, F. Joensen, J. Nerlov, Stud. Surf. Sci. Catal. 174A (2008) 117-122.

[34] D. Ma, F. Deng, R. Fu, X. Han, X. Bao, J. Phys. Chem. B 105 (2001) 1770-1779.

[35] R.A. Shaikh, S.G. Hegde, A.A. Behlekar, B.S. Rao, Catal. Today 49 (1999) 201-209.

[36] J.P. Marques, I. Gener, P. Ayrault, J.C. Bordado, J.M. Lopes, F. Ramôa Ribeiro, M. Guisnet, Micropor. Mesopor. Mater. 60 (2003) 251-262.

[37] E.P. Parry, J. Catal. 2 (1963) 371-379.

[38] J.H. Ahn, R. Kolvenbach, S.S. Al-Khattaf, A. Jentys, J.A. Lercher, ACS Catal. 3 (2013) 817-825.

[39] P.B. Weisz, Science 178 (1973) 433-440.

[40] J. H. Ahn, R. Kolvenbach, S. S. Al-Khattaf, A. Jentys, J. A. Lercher, to be submitted.

[41] O.C. Gobin, S.J. Reitmeier, A. Jentys, J.A. Lercher, J. Phys. Chem. C 113 (2009) 20435-20444.

[42] G. Mirth, J.A. Lercher, J. Phys. Chem. 95 (1991) 3736-3740.

[43] G. Mirth, J.A. Lercher, J. Catal. 132 (1991) 244-252.

[44] I. Chorkendorff, J.W. Niemantsverdriet, Concepts of Modern Catalysis and Kinetics, Wiley-VCH, Weinheim, Germany, 2003, p. 211-213.

[45] D. Lesthaeghe, B. De Sterck, V. Van Speybroeck, G.B. Marin, M. Waroquier, Angew. Chem. Int. Ed. 46 (2007) 1311-1314.

[46] D.M. McCann, D. Lesthaeghe, P.W. Kletnieks, D.R. Guenther, M.J. Hayman, V. Van Speybroeck, M. Waroquier, J.F. Haw, Angew. Chem. Int. Ed. 47 (2008) 5179-5182.

[47] S. Arrhenius, Z. physik. Chem. 4 (1989) 226-248.

[48] S. Svelle, S. Kolboe, O. Swang, U. Olsbye, J. Phys. Chem. B 109 (2005) 12874-12878.

[49] I.I. Ivanova, A. Corma, J. Phys. Chem. B 101 (1997) 547-551.

[50] Olsbye, U.; Bjørgen, M.; Svelle, S.; Lillerud, K.; Kolboe, S. Catal. Today 106 (2005) 108-111.

[51] Lesthaeghe, D.; Horré, A.; Waroquier, M.; Marin, G.B.; Van Speybroeck, V. Chem. Eur. J. 15 (2009) 10803-10808.

[52] J. H. Ahn, R. Kolvenbach, S. S. Al-Khattaf, A. Jentys, J. A. Lercher, in preparation.

[53] G. Mirth, J.A. Lercher, J. Catal. 147 (1994) 199-206.

Chapter 4

Influence of the reaction temperature on p-xylene selectivity in toluene methylation over medium pore-sized zeolites

The influence of the reaction temperature on p-xylene selectivity in toluene methylation was investigated over medium pore-sized zeolites with different frameworks (H-ZSM5, H-ZSM11 and H-NU10) as well as after structural modifications including deposition of tetraethyl orthosilicate on the surface, isomorphous substitution of aluminum in the framework with iron and the crystal size. An increase in the reaction temperature consistently resulted in a higher p-xylene selectivity from all three major reaction pathways for the formation of p-xylene during toluene methylation, i.e., methylation of toluene, isomerization of xylenes, further methylation and subsequent formation of xylenes after eliminating light hydrocarbons as byproducts. Among these reactions, the isomerization of xylenes influenced the xylene selectivity most strongly at high temperatures and enabled the diffusivity differences between xylene isomers to play a significant role in favoring high p-xylenes selectivity.

4.1 Introduction

Xylenes are important chemical intermediates for the production of polyesters and plasticizers [1,2]. The sources for the industrial production of xylenes are catalytic reforming and thermal cracking of naphtha, but alternative routes include the reaction from toluene by disproportionation and methylation [3]. The alkylation of toluene with methanol in particular, is an attractive route to produce xylenes because toluene is produced in surplus relative to the market demand [1, 4]. Furthermore, toluene methylation can be carried out at lower temperatures than toluene disproportionation [5,6] and methanol, used for the alkylation, should be widely available from the abundant resources of natural gas and potential increase in production for variety of uses in the future [7,8].

Among the three xylene isomers, p-xylene is the most valuable intermediate in the industry (~80 % of xylenes demand) for the production of terephthalate [1,4]. m-Xylene, however, is the thermodynamically favored isomer (~50 % [9]) and is typically the main product from various xylene production routes [3,5]. A catalyst with high para selectivity would therefore be desirable to reduce the costs of the expensive and energy intensive separation processes (e.g. crystallization or adsorption methods [1,3]) for the xylene isomers. Impregnation with phosphorous or boron compounds [10,11], tetraethyl orthosilicate (TEOS) deposition on the zeolite surface [12,13] or increasing the crystal size [5,6] are some of the known procedures in the literature to enhance the p-xylene selectivity during toluene methylation. Despite of a significant demand of p-xylene in the industry, detailed studies of the reaction conditions (e.g., temperature and pressure) and the zeolite properties governing diffusion on xylene selectivity were yet not reported in the literature.

Herein, we investigate the factors influencing the selectivity of p-xylene in toluene methylation over various medium pore-sized zeolites at different reaction temperatures. Three main reaction pathways for the formation of p-xylenes during toluene methylation were studied: methylation of toluene, isomerization of xylenes, further methylation and subsequent elimination of less-methylated aromatic molecules as xylenes (and light hydrocarbons) from highly-methylated aromatics [6,8,14,15]. In all these pathways, an increase of the reaction temperature consistently resulted in a higher p-xylene selectivity because the effect of differences in diffusivities between p-xylene and o-, m-xylenes [16] became more pronounced. This study demonstrates that high reaction temperatures are advantageous for the

methylation of toluene to p-xylenes because it enables both the formation rate of xylenes and the selectivity of p-xylene to increase simultaneously.

4.2 Experimental

4.2.1. Materials

H-ZSM5 (MFI framework), a medium pore zeolite with 3-dimensional structure comprised of two types of intersecting channels (one sinusoidal 0.51 x 0.55 nm and the other straight 0.53 x 0.56 nm [17]), was provided by Süd-Chemie (Si/Al = 36). The surface modified (H-ZSM5-SM) sample was prepared from H-ZSM5 by depositing 4 weight % (SiO_2 relative to the zeolite) of tetraethyl orthosilicate (TEOS; >99.0 %, Sigma-Aldrich) in hexane (>97 %, Sigma-Aldrich) under stirring for 1 hour [18]. This procedure was repeated three times and the total TEOS deposition amount was 12 weight %. H-ZSM11 (MEL framework), a medium pore zeolite with 3-dimensional structure comprised of straight intersecting channels (0.53 x 0.54 nm [17]), was synthesized by using tetrabutylammonium hydroxide (TBAOH; ≥99.0 %, 30-hydrate, Sigma-Aldrich) or 1,8-diamino-octane (DAO; 98 %, Sigma-Aldrich) as the organic templates for small (SC) and large crystal (LC) zeolites, respectively [19,20]. The detailed modification and synthesis procedures for H-ZSM5-SM and H-ZSM11 are described in ref. [14].

The isomorphously iron substituted ZSM5 (H-Fe-ZSM5) was synthesized similarly to the procedure described in ref. [21]. A sodium silicate (25.5-28.5 % SiO_2, 7.5-8.5 % Na_2O; Merck) solution was slowly added (drop-wise) to a uniform mixture of sulfuric acid (96 %) and iron (III) sulfate (21-23 % Fe basis; Sigma-Aldrich). After vigorous stirring, tetrapropylammonium bromide (98 %; Sigma-Aldrich) was added and the gel was aged overnight (~18 hours) before it was transferred into Teflon liners (~120 cm^3 capacity) and sealed inside autoclaves. The final gel composition was $150Na_2O : Fe_2O_3 : 150SiO_2 : 5200H_2O$: 25TPABr : $125H_2SO_4$. After 8 days of crystallization at 423 K under rotation (60 rpm) the solid was separated by centrifugation and washed 3 times with deionized water. The samples were dried in an oven at 353 K, grounded and treated at 753 K (heating rate of 0.05 K s^{-1}) for 10 hours in flowing synthetic air (1.67 cm^3 s^{-1}; 20.5% O_2 in N_2, Westfalen) to remove the organic templates. Ammonium ion exchange was carried out at 353 K under stirring for 2

hours in a 1 M NH_4NO_3 solution (30 cm^3 per gram of zeolite). This procedure was repeated twice. After the second ammonium exchange, the zeolites were separated by centrifugation, washed, dried and treated in synthetic air (flowing at 1.67 cm^3 s^{-1}) for 10 hours (heating rate of 0.083 K s^{-1}) at 753 K to obtain the protonic form of the zeolite.

H-NU10 (TON framework), a 1-dimensional zeolite with straight, nonintersecting elliptical shaped channels of 0.46 x 0.57 nm [17], was synthesized from aluminum sulphate (99.99 %, Sigma-Aldrich), potassium hydroxide (99.99 %, Sigma-Aldrich), silica sol (Ludox AS-30, Sigma-Aldrich) and DAO as the organic template, with the gel composition of 26DAO : Al_2O_3 : 90SiO_2 : 3580H_2O : 12K_2O [22]. The gel was aged ~1 hour before it was transferred into Teflon liners and sealed inside autoclaves. Note that this procedure for the H-NU10 synthesis was exactly the same as the large crystal H-ZSM11 synthesis, except for the rotation of the autoclaves (60rpm; static during H-ZSM11-LC synthesis) [23]. After the 72 hours of crystallization at 433 K, the materials were separated, washed, dried and treated in synthetic air (followed by ammonium exchange) as described above, except the treatment temperature in synthetic air was 823 K, instead of 753 K.

4.2.2. Catalyst characterization

Atomic absorption spectroscopy (AAS; Unicam M Series Flame-AAS equipped with an FS 95 auto-sampler and a GF 95 graphite furnace) was used to determine the elemental composition of the zeolites. The purity and crystallinity of the samples were examined by X-ray diffraction patterns (XRD; Philips X'Pert Pro system, $\lambda_{CuK\alpha}$ = 0.154056 nm, 40kV/40mA) recorded between 2 θ angles of 5-70° (step size of 0.017° and a scan speed of 115 seconds per step). The nitrogen physisorption experiments were carried out at 77 K on a PMI automated sorptometer after outgassing the samples under vacuum at 523 K for 2 hours. The BET surface area [24] was calculated from the adsorption data over a relative pressure range from 0.01-0.1, the pore volumes and external surface areas were evaluated by using the t-plot method [25] according to Halsey [26]. The scanning electron microscopy (SEM) images of all samples were recorded on a JEOL JSM 5900 LV microscope operating at 25 kV.

Diffuse Reflectance (DR) UV/Vis spectroscopy was used in order to check for the presence of Fe_xO_y species in H-Fe-ZSM5 catalyst. The powdered zeolite was placed in a sample cup of 10 mm diameter and 3 mm depth at ambient conditions and the UV/Vis spectra

were measured with Avantes avaspec 2048 spectrometer in diffuse reflectance mode. The DR UV/Vis spectra is shown in the form of the Kubelka-Munk function, i.e., $F(R) = (1 - R)^2 \times (2 \times R)^{-1}$, with $R = R_s/R_r$, where R_s is the reflectance of the H-Fe-ZSM5 sample and R_r the reflectance of the H-ZSM5 reference.

The temperature programmed desorption (TPD) of ammonia was used to compare the acid strength of the zeolite samples with aluminums in the framework and isomorphously substituted iron (H-Fe-ZSM5). About 50 mg of the samples (sieved to a particle size between 0.71-1.0 mm) were activated under a vacuum (10^{-4} kPa) at 723 K (heating rate of 0.17 K s^{-1}) for 1 hour before 0.1 kPa of NH_3 was adsorbed at 373 K for 1 hour. After outgassing the samples for 2 hours, the temperature was increased to 1043 K at 0.17 K s^{-1}, while desorption of NH_3 was monitored by mass spectroscopy (m/z+ = 16 signal).

Infrared spectroscopy (Thermo Nicolet 5700 FT-IR spectrometer, resolution of 4 cm^{-1}) with pyridine (99.8%, Sigma-Aldrich) as probe molecule was used to determine the total concentration of Brønsted and Lewis acid sites. The sample was first pressed into a self-supporting wafer (density of ~0.01 g cm^{-2}) and was activated for 1 hour at 723 K (heating rate of 0.17 K s^{-1}) under vacuum before the spectrum was collected. The pyridine was adsorbed onto the zeolite sample at 0.01 kPa, 423 K for 0.5 hour and outgassed for 1 hour under the vacuum to desorb weakly bounded species. The total number of Brønsted and Lewis acid sites was determined by integrating the peaks at 1546 and 1455 cm^{-1}, respectively.

4.2.3. Catalytic Testing

The zeolite samples (4-100 mg, 180-250 μm) were diluted with silicon carbide (F46, ESK-SiC GmbH) by 7 times the weight of the catalyst and were held in place by quartz wool inside a quartz plug flow reactor (inner diameter of 0.4 cm; 0.6 cm for the reactions with zeolite amount > 40 mg). The temperature was measured by a type K thermocouple in external contact to the reactor and was maintained constant by a stainless steel furnace connected to a Eurotherm controller (Series 2416). The catalysts were tested at atmospheric pressure in the temperature range of 573 to 723 K and the total flow rate was varied between 1.2 and 2.3 cm^3 s^{-1}. Prior to the reaction, the samples were treated for 0.5 hour under flowing helium (1.7 cm^3 s^{-1}; 99,996 %, Westfalen) at 823 K (0.17 K s^{-1}). Toluene methylation was carried out by flowing a premixed toluene (>99.9 %, Sigma-Aldrich) and methanol (>99.8 %,

Sigma-Aldrich) feed ($p_{toluene}$ = 6 kPa, $p_{methanol}$ = 1.5 kPa) into a vaporizer filled with silicon carbide. The isomerization reactions were carried out in a similar way by flowing o-, m- or p-xylene (all >99.0 %, Sigma-Aldrich) or a premixed feed of methanol and o- or m-xylene (p_{xylene} = 2.4 kPa, $p_{methanol}$ = 0 or 0.6 kPa) with same total gas flow rate through the reactor (1.2 and 2.3 cm^3 s^{-1}). The subsequent methylation and elimination of aromatic product molecules was tested by flowing premixed feed of 1,2,4-trimethylbenzene (1,2,4-TriMB; 98 %, Sigma-Aldrich) with methanol at $p_{1,2,4\text{-TriMB}}$ = 1.2 kPa, $p_{methanol}$ = 0.3 kPa. The reactor effluent was sampled 10 minutes after the start of the reactant flow into the reactor and was analyzed by on-line gas chromatography (Agilent 7820A) equipped with a DB-WAX column (30 m x 0.32 mm x 0.5 μm) and a flame ionization detector. All the rates were normalized by the total concentration of the Brønsted acid sites determined by adsorption of pyridine. The C_1 in the manuscript refers to methanol and dimethyl ether (DME) and they are treated as one reactant (accounting for the stoichiometry of ½ for DME) because methanol can readily dehydrate to form DME during the reaction and both molecules can methylate unsaturated aromatic/alkene molecules via a similar mechanism [27,28].

4.3. Results

4.3.1. Catalyst characterization

The chemical composition and textural properties of all the samples from AAS and nitrogen physisorption measurements are summarized in Table 4.1. Three different types of medium pore-sized (10-membered ring) zeolites i.e., H-ZSM5 (MFI), H-ZSM11 (MEL) and H-NU10 (TON), with similar Si/Al content (except for H-Fe-ZSM5) were used in this work. The MFI sample with isomorphously substituted iron in the framework (H-Fe-ZSM5) was synthesized with relatively low iron content, in order to avoid formation of Fe_xO_y clusters. The bands observed at ~215 and 240 nm in the UV/Vis spectrum of H-Fe-ZSM5 in Figure 4.1 (taken after treatment in synthetic air at 753 K for 10 hours) confirmed that the iron was incorporated as tetrahedral Fe^{3+} in the zeolite framework and the lack of broadening at λ > 300nm the absence (or only of a minor presence) of Fe_xO_y species [29,30].

Table 4.1: Chemical composition and textural properties of all the zeolites samples tested.

Catalyst	Si/Al ratio	S_{BET} (m^2 g^{-1}) [a]	S_{ext} (m^2 g^{-1}) [b]	V_{mi} (cm^3 g^{-1}) [c]	V_{tot} (cm^3 g^{-1})[c]
H-ZSM5	36	435	55	0.16	0.32
H-ZSM5-SM[d]	42	434	74	0.13	0.30
H-Fe-ZSM5	72[g]	443	66	0.16	0.25
H-ZSM11-SC[e]	34	445	110	0.13	0.30
H-ZSM11-LC[f]	33	427	2	0.16	0.17
H-NU10	39	282	37	0.08	0.16

[a]S_{BET} = BET surface area. [b]S_{ext} = external surface area. [c]V_{mi} and V_{tot} correspond to the micro- and total pore volume of the zeolites. [d]SM = surface modified by TEOS deposition. [e]SC = small crystal. [f]LC = large crystal. [g]Si/Fe ratio is reported for H-Fe-ZSM5 instead of Si/Al ratio.

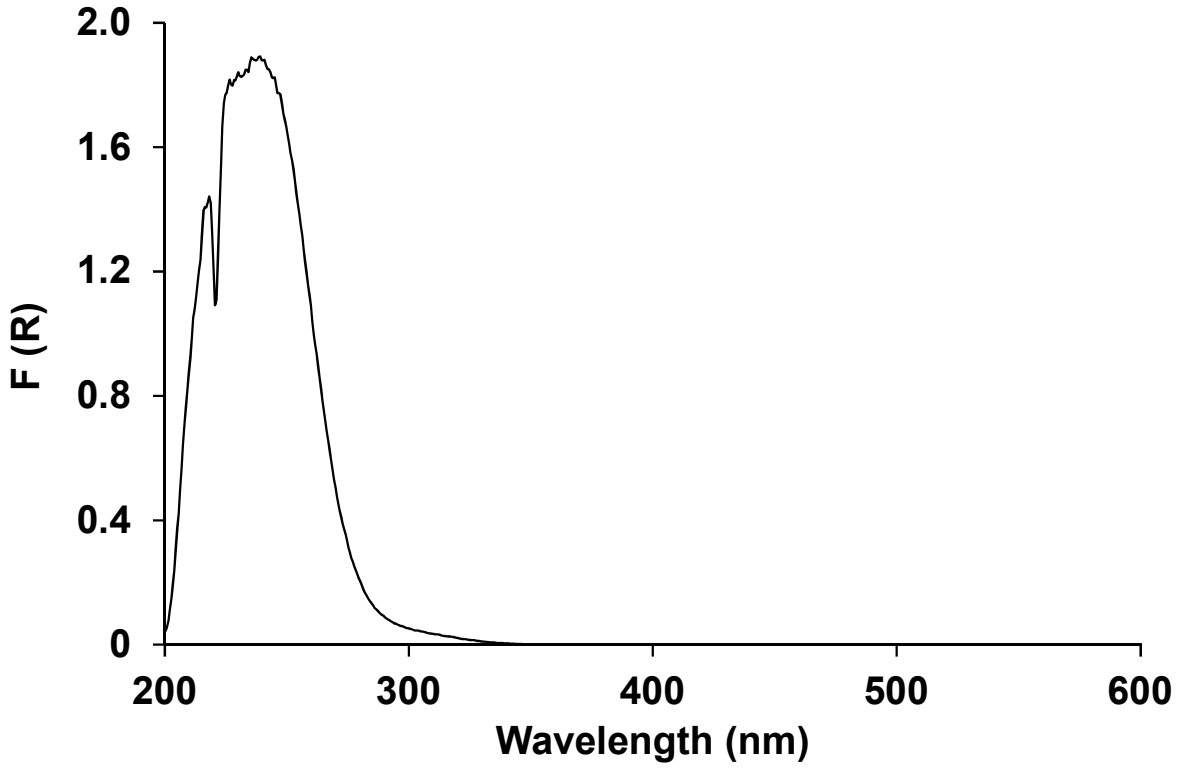

Figure 4.1: Diffuse reflectance UV/Vis spectra of H-Fe-HZSM5 sample (spectra taken after the sample was treated in synthetic air at 753K for 10 hours). The bands at ~215 and 240nm confirm that the iron was incorporated as tetrahedral Fe^{3+} in the zeolite framework and the lack of broadening at $\lambda > 300$nm verify that Fe_xO_y species are not present (or only in minor amount).

The modified and synthesized materials, i.e., H-ZSM5-SM, H-Fe-ZSM5, H-ZSM11-SC, H-ZSM11-LC, H-NU-10, were free of crystalline impurities, as indicated by XRD patterns shown in Figures 4.S1-4.S3. The H-ZSM11-SC sample had broader diffraction peaks

compared to the H-ZSM11-LC sample because the primary crystal size of H-ZSM11-SC is significantly smaller. The SEM images of all samples are shown in Figures 4.S4-4.S9. The particle sizes for all samples were about 0.5 μm or less except for the H-ZSM11-LC (~6 μm) and H-NU10 (long needle like structure with length of ~1μm and width of ~0.1 μm).

The temperature programmed desorption of ammonia and the concentrations of total acid sites calculated are shown in Figure 4.2 and Table 4.2, respectively. The temperature of the maximum in the NH_3 TPD traces reflects the activation energy of desorption and, thus, the relative acid strength of the materials. For the zeolites with aluminum in the framework (all except H-Fe-ZSM5), a desorption temperature of ~580 K was observed while the NH_3 desorption peak for the zeolite with iron in the framework occurred at a lower temperature (~520 K). This indicates that H-Fe-ZSM5 has weaker acid strength than the other zeolites [31,32] because the iron in the framework increases the deprotonation energy from lower polarizability [33].

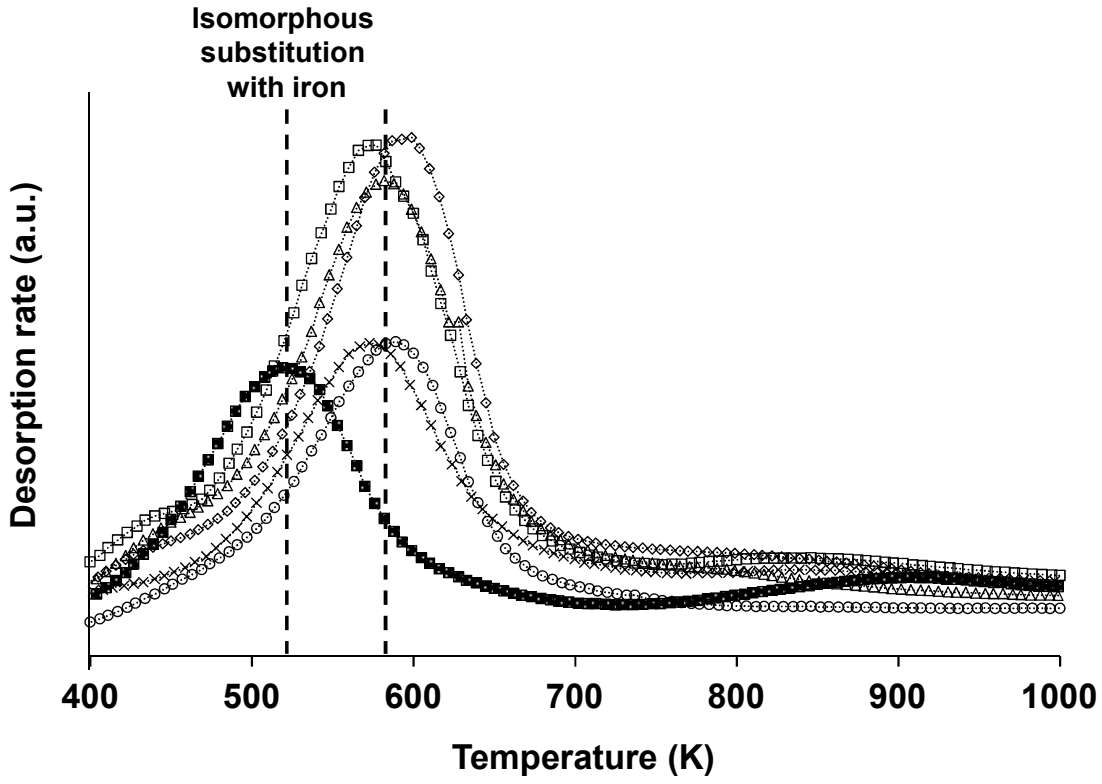

Figure 4.2: Temperature programmed desorption (TPD) of ammonia with H-ZSM5 (□), H-ZSM5-SM (x), H-Fe-ZSM5 (■), H-ZSM11-SC (Δ), H-ZSM11-LC (◊) and H-NU10 (○). The first and second vertical dashed line is placed at ~520 and 580 K, respectively.

Table 4.2: Total concentration of acid sites calculated from integrating the temperature programmed desorption (TPD) peak of ammonia and comparing it to the standard zeolite material (H-ZSM5 from Süd-Chemie, 360 μmol of acid sites g^{-1}).

Catalyst	Total Acid sites (μmol g^{-1})
H-ZSM5	405
H-ZSM5-SM	326
H-Fe-ZSM5	240
H-ZSM11-SC	397
H-ZSM11-LC	413
H-NU-10	324

The O-H stretching vibrations in the IR spectra of the activated samples are shown in Figure 4.3 (spectrum of H-ZSM11-LC is not shown because of low transmittance in this region). The band at 3745 cm^{-1}, characteristic for the O-H vibration of terminal silanol groups [34], was observed at the same wavenumbers on all samples. The band at ~3610 cm^{-1}, characteristic for the O-H vibration of SiOHAl groups (Brønsted acid sites) [31,35], was shifted to 3630 cm^{-1} for the iron containing sample because the acid strength of the SiOHFe sites was weaker (i.e. the O-H bond has a higher deprotonation energy). The O-H band from the Brønsted acid sites of H-NU10 sample, however, was shifted to lower wavenumbers compared to other aluminum containing samples. This was not because of increase in the acid strength (see TPD temperature in Figure 4.2), but most likely resulted from a weak perturbation of the O-H group inside the relative smaller pores in H-NU10. Note that for H-MOR, the O-H vibration of SiOHAl groups in the side pockets (8-membered ring) also had a lower wavenumber than the ones in the 12-membered ring channels [36,37].

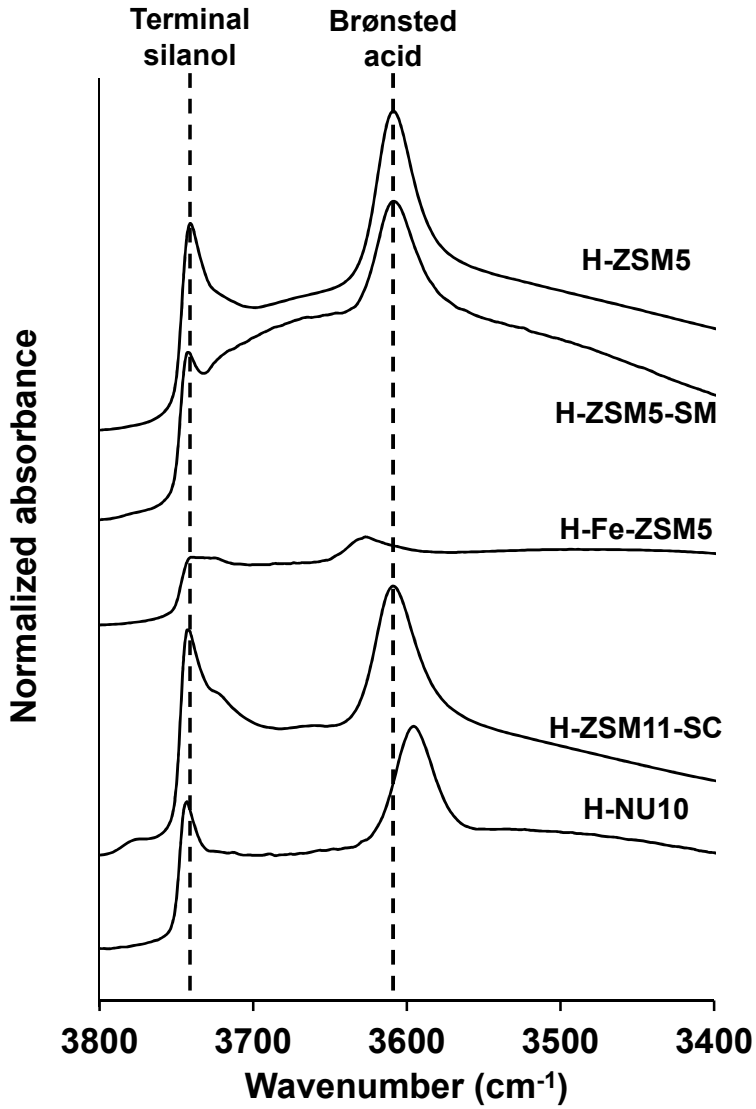

Figure 4.3: Infrared (IR) spectra of the samples (after heating to 723K for 1 hour for activation) measured at 423 K under vacuum. The bands at 3745 and ~3630-3590 cm^{-1} (the dashed line at 3610 cm^{-1}) represent O-H vibration of the terminal silanol groups and the Brønsted acid sites, respectively.

The concentrations of Brønsted and Lewis acid sites, determined by adsorption of pyridine, are summarized in Table 3 (the IR spectra of samples after the adsorption of pyridine are shown in Figure 4.S10-4.S11). H-ZSM5 (aluminum in the framework) retained >95 % of pyridine adsorbed on the Brønsted acid sites after outgassing at 723 K, while the isomorphously substituted iron sample retained only ~75 %, confirming that the acid strength of H-Fe-ZSM5 was weaker than H-(Al)-ZSM5. The total concentrations of Brønsted acid sites shown in Table 3 were used to normalize the rates.

Table 3: Concentration of Brønsted and Lewis acid sites determined by adsorption of pyridine.

Catalyst	Brønsted Acid sites (μmol g^{-1})		Lewis Acid Sites (μmol g^{-1})	
	Total[a]	Strong[b]	Total	Strong
H-ZSM5	380	371	67	26
H-ZSM5-SM[c]	313	292	68	34
H-Fe-ZSM5	162	122	42	27
H-ZSM11-SC[d]	387	357	100	78
H-ZSM11-LC[e]	393	342	104	76
H-NU10	331	288	48	36

[a]Measured at 423 K, after outgassing for 1 hour under vacuum. [b]Measured at 423 K, after heating the samples to 723K for 0.5 hour. [c]SM = surface modified by TEOS deposition. [d]SC = small crystal. [e]LC = large crystal.

4.3.2. Catalytic testing

The xylenes are produced from three main reaction pathways during toluene methylation (Scheme 4.1), i.e., methylation of toluene, isomerization of the xylene products and further methylation and elimination of less-methylated aromatic molecules as xylenes and light hydrocarbons from highly-methylated aromatics [14]. The disproportionation of toluene (calculated based on the formation rate of benzene, not shown) was not considered in this work because it was slow under these reaction conditions (e.g., less than 1% of the toluene converted went through disproportionation during toluene methylation).

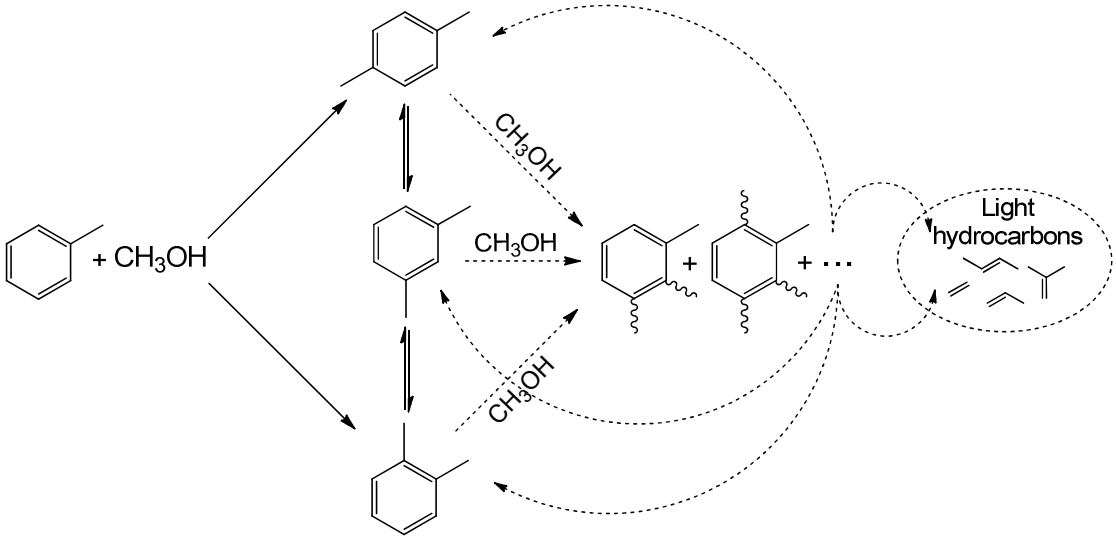

Scheme 4.1: Three main reaction pathways of generating xylenes during the reaction of toluene with methanol inside a medium pore-sized zeolite [14]. The solid, double half and dashed arrows represent toluene methylation, xylene isomerization and further methylation and elimination as xylenes (light hydrocarbons as byproducts), respectively.

The selectivity of xylenes and the toluene turnover rates from toluene methylation over different (framework, surface modification, acid strength and crystal size) medium pore-sized zeolites at similar C_1 (methanol and DME) conversion levels from 573-723 K are shown in Table 4.4 (conversions of C_1 and toluene are reported in Table 4.S1). The selectivity of p-xylene clearly increased over all medium pore zeolites (e.g., from 38 to 68 % with H-ZSM5) with increasing the reaction temperature, whereas the selectivity to m- and o-xylene decreased (e.g., from 28 to 20% for m-xylene and 35 to 12 % for o-xylene with H-ZSM5). H-Fe-ZSM5 had lower toluene turnover rates than H-ZSM5, because of the lower acid strength (e.g., from 0.30 to 0.10 mol [s mol H]$^{-1}$ at 723 K). H-NU10 had the lowest activity compared to the other zeolites (by an order of a magnitude), most likely because the relatively small and long 1-dimensional channels significantly decreased the transport of reactants to the Brønsted acid sites. Similarly, the toluene turnover rate of the large crystal H-ZSM11 decreased compared to the small crystal H-ZSM11 (e.g., from 0.42 to 0.15 mol [s mol H]$^{-1}$ at 723 K).

Table 4.4: Xylene selectivities (within xylenes) and toluene turnover rate at 573-723 K.

	573K		623K		673K		723K	
	Xylene selectivity p : m : o	Toluene turnover rate[a] (10^{-2} mol [sec mol H]$^{-1}$)	Xylene selectivity p : m : o	Toluene turnover rate (10^{-2} mol [sec mol H]$^{-1}$)	Xylene selectivity p : m : o	Toluene turnover rate (10^{-2} mol [sec mol H]$^{-1}$)	Xylene selectivity p : m : o	Toluene turnover rate (10^{-2} mol [sec mol H]$^{-1}$)
H-ZSM5	38 : 28 : 35	2.3	51 : 25 : 24	7.8	60 : 23 : 17	16	68 : 20 : 12	30
H-ZSM5-SM[b]	56 : 23 : 21	1.0	75 : 16 : 9	5.8	84 : 11 : 5	16	87 : 10 : 3	31
H-Fe-ZSM5	n/m[f]	n/m	40 : 24 : 36	3.1	46 : 23 : 30	6.2	52: 23 : 25	10
H-ZSM11-SC[c]	33 : 31 : 36	2.9	45: 30 : 25	11	55 : 28 : 18	25	63 : 24 : 12	42
H-ZSM11-LC[d]	52 : 25 : 23	0.2	72 : 17 : 11	1.4	87 : 9 : 3	7.7	92 : 7 : 2	15
H-NU10	n/m	n/m	72 : 13 : 15	0.1	82 : 9 : 9	0.4	85 : 8 : 7	1.0
Equilibrium[e]	*25 : 54 : 20*	-	*25 : 54 : 21*	-	*25 : 53 : 22*	-	*25 : 52 : 23*	-

[a]measured at $p_{toluene}$ = 6.0 kPa, $p_{methanol}$ = 1.5 kPa with 4-100 mg catalyst, total flow rate = 1.2-2.3 cm^3s^{-1} and C_1 (methanol and DME) conversion = 47-56 %, toluene conversion = 1.0-7.5 %. [b]SM = surface modified by TEOS deposition. [c]SC = small crystal. [d]LC = large crystal. [e]Xylene equilibrium distribution is from ref [9]. [f]Toluene methylation of H-Fe-ZSM5 and H-NU10 at 573K was not measured (n/m).

The rates of o- and m-xylene isomerization and methylation in the presence and absence of methanol over H-ZSM5 (chosen as a representative for typical medium pore zeolites) were measured at different reaction temperatures to observe the effect of temperature on p-xylene selectivity. The ratio of p- to m-xylene or p- to o-xylene formation rates increased with increasing the reaction temperature (see Table 4.5 and Table 4.6), with and without the presence of methanol, which agrees well with the trend observed in toluene methylation (see Table 4.4).

Table 4.5: p- and m- xylene formation rates, o-xylene methylation rate (when co-fed with methanol), conversion of o-xylene and p:m-xylene ratios at 573-723 K.

	o-xylene co-fed with methanol				o-xylene alone			
Temperature (K)	573	623	673	723	573	623	673	723
p-xylene formation rate[a] (10^{-3} mol [s mol H]$^{-1}$)	1.4	4.6	7.7	11	2.9	7.9	14	20
m-xylene formation rate (10^{-3} mol [s mol H]$^{-1}$)	4.0	9.1	12	16	9.3	15	19	23
o-xylene methylation rate (10^{-3} mol [s mol H]$^{-1}$)	3.9	9.5	17	20	-	-	-	-
o-xylene conversion (%)	3.5	3.1	3.3	3.2	4.0	3.6	3.9	3.4
p/m ratio	0.34	0.51	0.64	0.71	0.31	0.52	0.72	0.86

[a]Measured at $p_{o\text{-}xylene}$ = 2.4 kPa, $p_{methanol}$ = 0.6 kPa (when co-fed) with 4-25 mg of H-ZSM5 and total flow rate = 2.3 cm^3s^{-1}.

Table 4.6: p- and o- xylene formation rates, m-xylene methylation rate (when co-fed with methanol), conversion of m-xylene and p:o-xylene ratios at 573-723 K.

	m-xylene co-fed with methanol				m-xylene alone			
Temperature (K)	573	623	673	723	573	623	673	723
p-xylene formation rate[a] (10^{-3} mol [s mol H]$^{-1}$)	2.0	6.6	13	19	4.7	11	22	34
o-xylene formation rate (10^{-3} mol [s mol H]$^{-1}$)	1.3	3.3	5.2	6.9	3.2	5.9	8.8	10
m-xylene methylation rate (10^{-3} mol [s mol H]$^{-1}$)	3.2	9.8	18	22	-	-	-	-
m-xylene conversion (%)	3.0	2.7	2.9	3.2	2.8	2.9	3.3	3.5
p/o ratio	1.6	2.0	2.5	2.8	1.5	1.9	2.5	3.3

[a]Measured at $p_{m\text{-}xylene}$ = 2.4 kPa, $p_{methanol}$ = 0.6 kPa (when co-fed) with 4-23 mg of H-ZSM5 and total flow rate = 2.3 cm^3s^{-1}.

It was proposed that the xylenes formed from toluene methylation methylate further inside zeolite pores and that these bulky highly-methylated aromatic molecules eliminate light hydrocarbons and form less-methylated aromatic molecules, e.g., xylenes, because of product shape selectivity [14]. The reaction of 1,2,4-TriMB and methanol was therefore carried out at different reaction temperatures to observe the effect on the xylene selectivity from this elimination pathway (dashed arrows in Scheme 4.1). The formation rate of p-xylene strongly increased, whereas the m- and o-xylene formation rates did not change significantly as the temperature was increased (Table 4.7). Similar to the observation during toluene methylation (Table 4.4) and xylene isomerization (Table 4.5 and Table 4.6), the selectivity to p-xylene increased with higher reaction temperatures. Note that under these reaction conditions, the rate of the disproportionation [38,39,40] and of the demethylation reactions (reverse step of methylation) should be very slow compared to the methylation [15,41]. The formation rates of less-methylated products from highly-methylated aromatics, e.g., toluene from xylene and xylene from TriMB, increased significantly with the number of methyl groups on the aromatic ring [14]. This indicates that the xylenes in the reaction of 1,2,4-TriMB and methanol were most likely formed from methylated product of TriMBs after eliminating light hydrocarbons [8,14].

Table 4.7: Xylene formation, 1,2,4-Trimethylbenezene (1,2,4-TriMB) turnover rates and p-xylene selectivity (within xylenes) at 573-723 K.

Temperature (K)	573	623	673	723
p-xylene formation rate[a] (10^{-3} mol [s mol H]$^{-1}$)	0.21	0.30	0.39	0.60
m-xylene formation rate (10^{-3} mol [s mol H]$^{-1}$)	0.26	0.29	0.25	0.28
o-xylene formation rate (10^{-3} mol [s mol H]$^{-1}$)	0.06	0.08	0.07	0.09
1,2,4-TriMB turnover rate (10^{-3} mol [s mol H]$^{-1}$)	1.7	2.7	3.8	6.2
p-xylene selectivity (%)	40	45	55	62

[a]Mesaured at $p_{1,2,4\text{-TriMB}}$ = 1.2 kPa, $p_{methanol}$ = 0.3 kPa, 9-25 mg of H-ZSM5, total flow rate = 2.3 cm^3s^{-1}, C_1 (methanol and DME) conversion = 51-58 %, 1,2,4-TriMB conversion = 2.0-2.6 %.

4.4. Discussion

It is well known that the observed reaction rates (and therefore the selectivity of products) can be limited at low reaction temperatures by the reactions on the surface and at high reaction temperatures by the transport of reactants and products to the active sites. The acid catalyzed reactions on zeolites are especially susceptible to diffusion limitations because of the size of the micropores. As diffusion of reactants and products could determine the probability of a given reaction, tuning the residence time of the molecules (diffusion) relative to the catalyst activity (reaction rates) may lead to enhanced product selectivities. Here, we explored effect of the reaction temperature on the xylenes selectivities, in which, increasing the temperature should shift the reaction to a more diffusion-controlled regime (slower rate of diffusion relative to surface reactions). The reaction rates are influenced by the temperature more significantly than the diffusion because the activation energy is typically higher for the former.

The selectivity of p-xylene was enhanced by increasing the reaction temperature in all three main reactions (Table 4.4-Table 4.7) that take place during toluene methylation, i.e., methylation of toluene, isomerization of xylenes, and formation of xylenes from highly-methylated aromatic molecules (accompanied by formation of light hydrocarbons). The diffusivity of p-xylene is about two orders of magnitude faster than that of o- and m-xylenes

at the reaction temperature (Figure 4.4) and consequently, p-xylene has less probability to react further than o- and m-xylenes from relatively fast diffusion to the bulk. This indicates that the xylene selectivities are controlled by the diffusivity differences between the xylene isomers in the diffusion-controlled regime. Note that this increase of p-xylene selectivity with higher reaction temperatures cannot be from changes in the relative contribution of the three main reaction pathways towards formation of p-xylene, but from the lower probability of subsequent reactions of p-xylenes formed with respect to the other two xylene isomers. The dominant xylene isomer formed is not p-xylene from the toluene methylation, elimination from highly-methylated aromatics pathways (vide infra) and m-xylene is favored from xylene isomerization reactions [9].

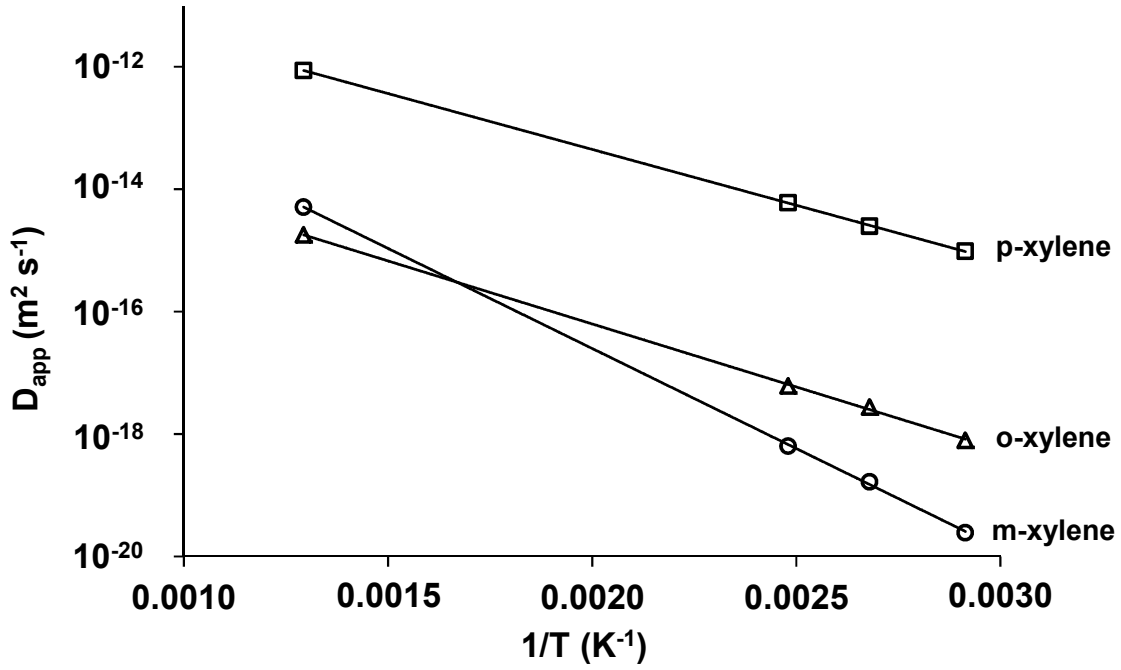

Figure 4.4: Arrhenius plot of p- (□), m- (○) and o-xylene (Δ) diffusion coefficients in the H-ZSM5 sample between 343 and 773 K. The diffusion coefficients were measured with frequency response method for p-xylene [42] and infrared uptake rates for m- and o-xylene [43] at 343, 373 and 403 K. The data measured were extrapolated to 773 K.

The xylene selectivities observed at low reaction temperature, on the other hand, should reflect more closely the primary product distribution from the reactions. In this temperature range, the individual rates are slow relative to the diffusion and, consequently, the product molecules have a higher chance of leaving the active sites in the zeolite pores before another reaction can take place. The o- and p-xylenes were the dominant products observed among the

xylenes at low temperatures during the reaction of toluene methylation (e.g., ~70 % at 573 K, see Figure 4.5 left) because these isomers were the primary xylene products from toluene methylation [44]. This observation is in accordance with the fact that the methyl addition is favored at o- and p- positions because the methyl group on the aromatic ring of toluene is an electron donating group (inductive effect) and the positive charge can be placed on the position of a methyl group to form tertiary carbocations (Scheme 4.2).

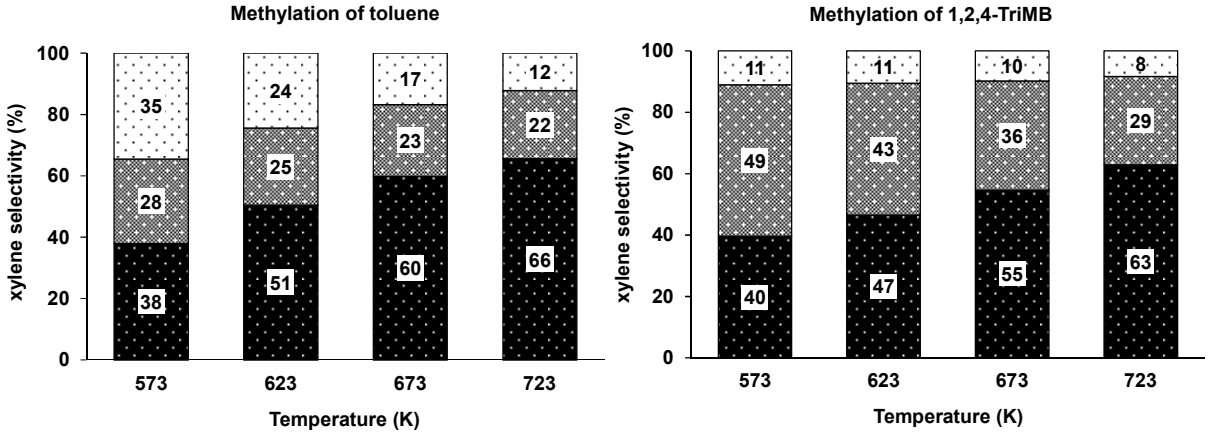

Figure 4.5: Selectivity of xylene isomers within xylenes at 573-723 K with the parent H-ZSM5. The reaction on the left with toluene and methanol ($p_{toluene}$ = 6.0 kPa, $p_{methanol}$ = 1.5 kPa, 4-10 mg, total flow rate = 1.2-2.3 cm^3s^{-1}, C_1 conversion = 47-55 %, toluene conversion = 4.3-6.5%) and on the right with 1,2,4-TriMB and methanol ($p_{1,2,4\text{-}TriMB}$ = 1.2 kPa, $p_{methanol}$ = 0.3 kPa, 9-25mg, total flow rate = 2.3cm^3s^{-1}, C_1 (methanol and DME) conversion = 51-58 %, 1,2,4-TriMB conversion = 2.0-2.6 %). Black, grey and white represents p-, m- and o-xylene selectivities. Data from Table 4.4 and Table 4.7.

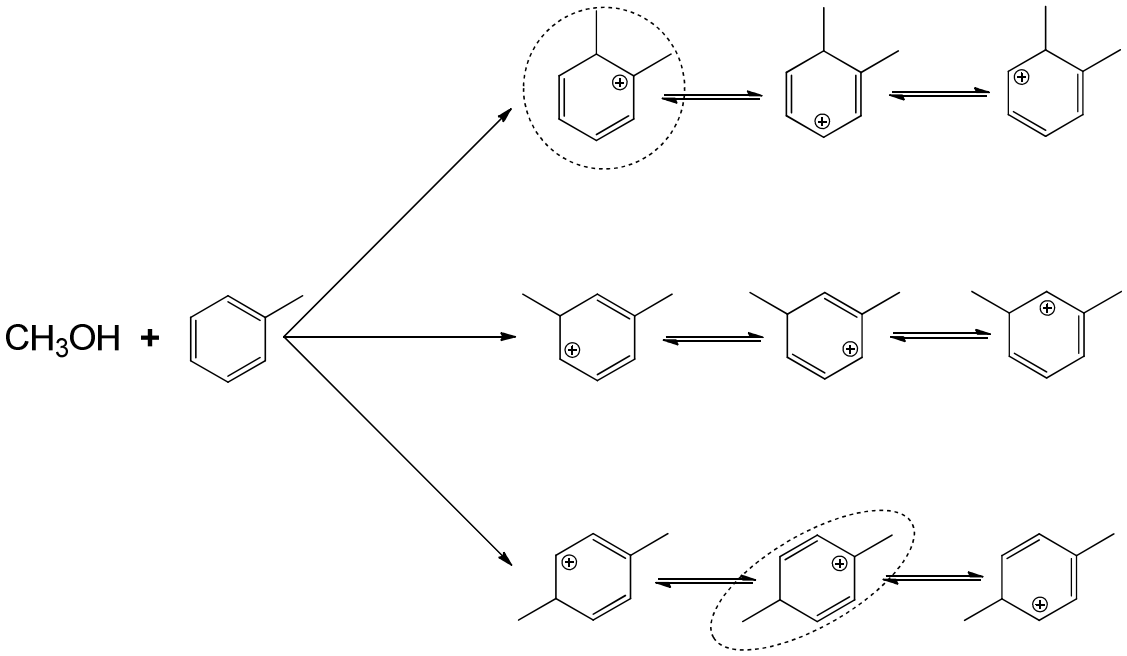

Scheme 4.2: Methylation of toluene via carbenium ion transition state in an acid catalyzed reaction. The dotted circled compounds (o- and p-xylene) represent the most favored resonance structures from inductive effect of the methyl groups.

The selectivity to o-xylene was lower during the reaction between 1,2,4-TriMB and methanol (8-11 %; Figure 4.5, right) than during the toluene methylation (12-35 %, Figure 4.5, left), while the selectivity to m-xylene was higher (29-49 % during the reaction of 1,2,4-TriMB and methanol and 22-28 % during the methylation of toluene, see Figure 4.5). The difference in the xylene selectivities between these two reactions was more pronounced at low reaction temperatures, where the selectivity of primary xylene products formed from the reactions would be observed. This indicates that m- or p-xylenes (~90 % at 573 K) were predominantly formed from the highly-methylated aromatics by the elimination pathway. Note that the experiments with ^{13}C-methanol and ^{12}C-toluene described in ref. [6] revealed that the m- and p-xylenes had higher ^{13}C content in the aromatic ring (from ring contraction and expansion [45] during the methylation and subsequent elimination of xylenes and light hydrocarbons) than o-xylene, also supporting that the primary products from further methylation and elimination pathway are m- and p-xylenes.

The primary reaction product distribution of xylenes observed at low reaction temperatures changed significantly as the temperature increased (e.g., p-xylene and o-xylene selectivity increased from 38-66 % and decreased from 12-35 % during toluene methylation,

respectively, Figure 4.5). The reaction kinetics shifted to a more diffusion-controlled regime as the surface reactions became faster relative to diffusion and the selectivity of xylenes became controlled more strongly by the differences in diffusivity between xylene isomers. The selectivity of p-xylene thus increased at high reaction temperatures because it diffuses faster than o- and m-xylenes by about two orders of magnitude (Figure 4.4). In addition, similar xylene selectivities are observed at high temperatures (see 723 K in Figure 4.5) between the toluene methylation and the elimination from highly-methylated aromatic reaction pathways, despite of the differences in the primary xylene products formed from these two reactions. This suggests that xylene isomerization is probably the most important reaction (among toluene methylation, xylene isomerization and xylene production from highly-methylated aromatic molecules) for determining xylene selectivity at high reaction temperatures.

The significance of isomerization on xylene selectivity was further examined by comparing the reaction of o- or m-xylene individually and by co-feeding the xylene isomer with methanol at different temperatures. Only isomerization reactions take place when o- or m-xylene reacts over the catalyst, whereas both isomerization and methylation-elimination reactions occur when xylene is introduced together with methanol in the feed (other reactions, e.g., disproportionation, were not significant under these reaction conditions). The selectivity to p-xylene increased (relative to o- or m-xylene) with increasing temperature for all reactions with and without the presence of methanol, i.e., higher p-/m-xylene and p-/o-xylene ratios were observed (Figure 4.6). At low reaction temperatures, the selectivity to p-xylene (relative to o- or m-xylene) was higher when o- or m-xylene was co-fed with methanol than without (e.g., at 573 K, the p:m and p:o ratios were 0.34 and 1.8 in the presence of methanol and 0.31 and 1.5 without methanol, respectively). This indicates that the methylation-elimination pathway (co-fed with methanol) generated more p-xylene as primary products compared to the isomerization reactions (vide supra). In contrast, a lower p-xylene selectivity was observed at high reaction temperatures, when o- or m-xylene reacted with methanol in the feed compared to the reaction without methanol (e.g., at 723 K, the p:m and p:o ratios were 0.69 and 2.8 in the presence of methanol and 0.86 and 3.3 without methanol, respectively). The relatively low p-selectivity in the presence of methanol at high reaction temperatures can be assigned to the decrease in the isomerization rates (Table 4.5 and Table 4.6), as some of o- or m-xylene in the feed were consumed for methylation reactions. This indicates that fast isomerization at higher reaction temperatures favors high p-xylene selectivity by shifting the

reaction to a more diffusion-limited regime and consequently enables the diffusivity differences in xylenes to become more important in determining the selectivity of xylenes.

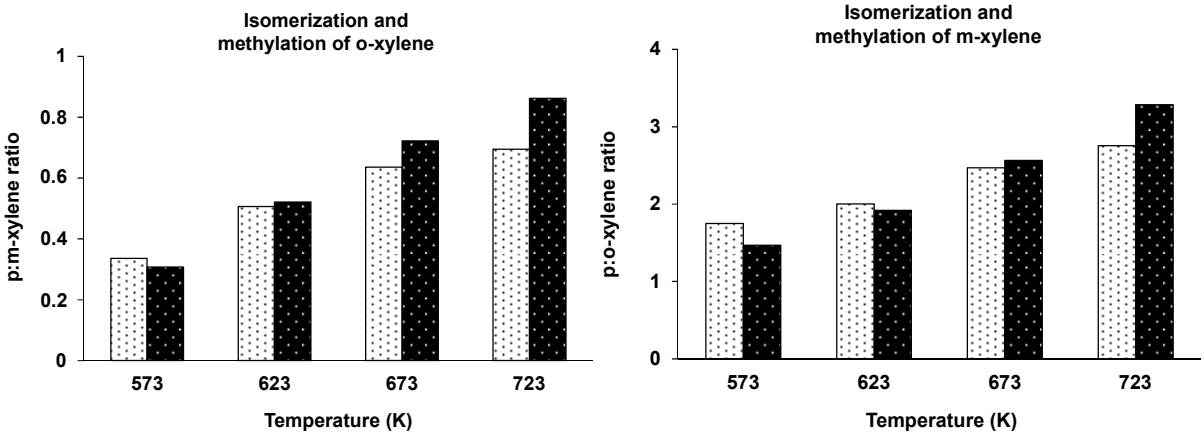

Figure 4.6: Ratios of xylene isomers within xylenes at 573-723 K with H-ZSM5 (p_{xylene} = 2.4 kPa, $p_{methanol}$ = 0.6 kPa, 4-25 mg, total flow rate = 2.3 cm^3s^{-1}) with o-xylene (left) and m-xylene (right) in the feed. The white represents the xylene ratios when xylene was co-fed with methanol and the black without. o-Xylene conversion = 2.7-4.0 %, m-xylene conversion = 1.6-3.5 % and C_1 (methanol and DME) conversion = 47-54 % (when co-fed with methanol). Data from Table 4.5 and Table 4.6.

The influence of xylene isomerization at high reaction temperatures on p-xylene selectivity was additionally investigated by comparing the H-ZSM5 and its iron substituted sample, H-Fe-ZSM5. The relative differences in diffusivity of the xylene isomers in these samples are similar because both samples have the same zeolite structure (MFI) and comparable crystal sizes (concluded from the SEM images in Figures 4.S4 and 4.S6, and analyzing the width of X-ray diffraction peaks in Figure 4.S1). The only difference between the two zeolites is the acid strength of the sites, which allows the direct assessment of the influence of isomerization rates on p-xylene selectivity during toluene methylation. Table 4.8 shows that the reaction rates, in particular p-xylene isomerization, decreased significantly over the iron containing zeolite (by about factor of 7) because of weaker acid strength of H-Fe-ZSM5 compared to H-ZSM5. Slower isomerization rates decreased the influence of the diffusivity differences of xylenes on p-xylene selectivity because the reaction became less diffusion limited (more reaction controlled) and consequently, a decrease in the p-xylene selectivity was observed, i.e., from 68 to 52 % with H-ZSM5 and H-Fe-ZSM5, respectively (Table 4.8). Note that this was not because of higher Si/Al ratio of H-Fe-ZSM5. The H-ZSM5

sample with lower aluminum content (Si/Al = 123) and crystal size resulted in higher p-xylene selectivity (77 %) at similar reaction conditions.

Table 4.8: p-Xylene isomerization rate and conversion at 723 K.

	H-ZSM5	H-Fe-ZSM5
p-xylene isomerization rate[a] (10^{-2} mol [s mol H]$^{-1}$)	21	3.0
p-xylene conversion[a] (%)	6.1	6.3
p-xylene selectivity[b]	68	52

[a]Measured at p_{xylene} = 2.4 kPa, 2-15 mg catalyst, total flow rate = 1.2-2.3 cm^3s^{-1}. [b]Selectivity of p-xylene (within xylenes) during methylation of toluene reported in Table 4.4.

4.5. Conclusions

The p-xylene can be generated in three different major reaction pathways during toluene methylation, i.e., methylation of toluene, isomerization of xylenes, further methylation and subsequent elimination of less-methylated aromatic molecules as xylenes (and light hydrocarbons) from highly-methylated aromatics. The selectivity to p-xylene increased in all three reactions over medium pore-sized zeolites as the reaction temperature was increased. At low temperatures the selectivity of xylenes more closely reflected the primary reaction products because rate of the surface reactions were slower relative to the diffusion (reaction-limited regime). With increasing temperatures, the reactions became faster relative to diffusion and differences in the transport rates between xylene isomers played a more significant role in determining the xylene selectivities. The diffusivity of p-xylene was about two orders of magnitude faster than o- and m-xylenes and a higher selectivity of p-xylene was observed in the diffusion controlled regime at higher reaction temperatures. In addition, when the aluminum in the framework was isomorphously substituted with iron, lower p-xylene selectivity was observed because the reaction rates decreased over the acid sites with weaker strength and thereby shifted the reaction to a less diffusion limited regime, i.e., xylene selectivity was less controlled by the relative xylene diffusivity differences which favored p-xylenes. High reaction temperature and strong acids should therefore, be used for methylation of toluene to p-xylene with medium pore-sized zeolites because both the activity (reaction rates) and the selectivity of p-xylene can be increased simultaneously.

4.6. Acknowledgments

The financial support from the King Fahd University of Petroleum and Minerals (KFUPM) is acknowledged. Helpful technical discussions with Jeongnam Kim and Oliver Gutiérrez, as well as the N_2 physisorption measurements by Xaver Hecht, SEM images and AAS measurements by Martin Neukamm are also acknowledged.

4.7. Supplementary Materials

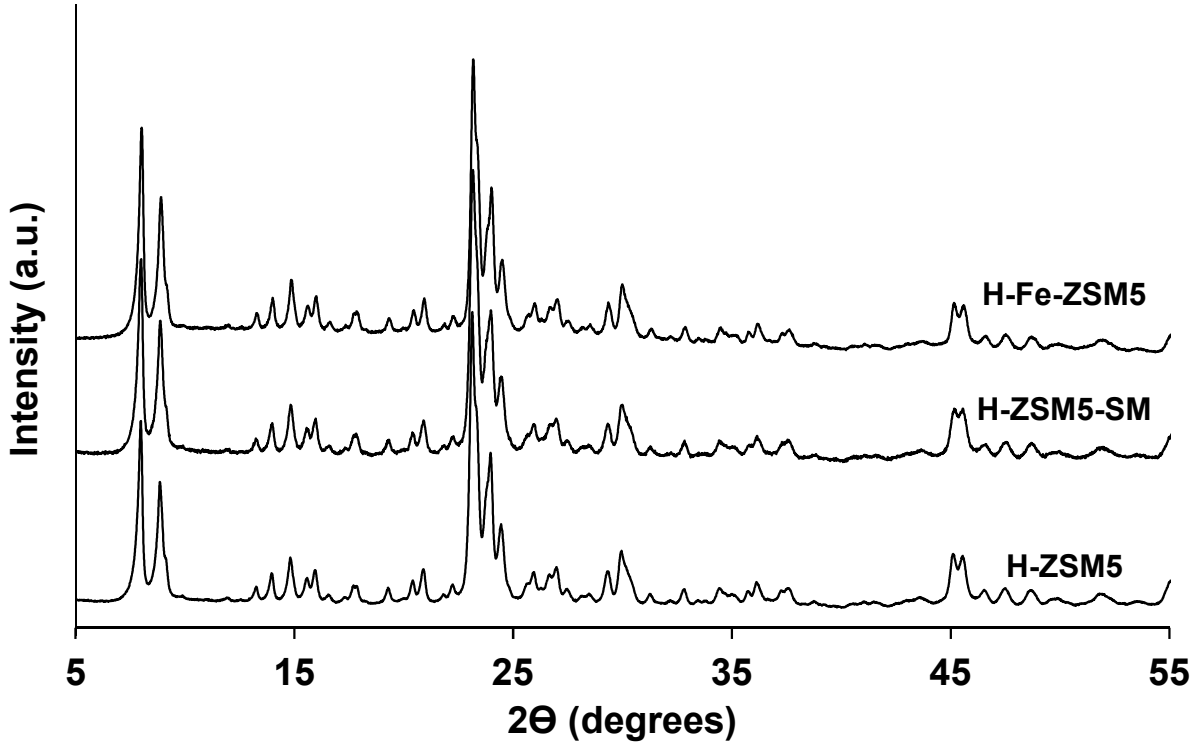

Figure 4.S1: Powder X-ray diffraction (XRD) patterns of H-ZSM5 samples. The spectra were taken in their final H-form of zeolite.

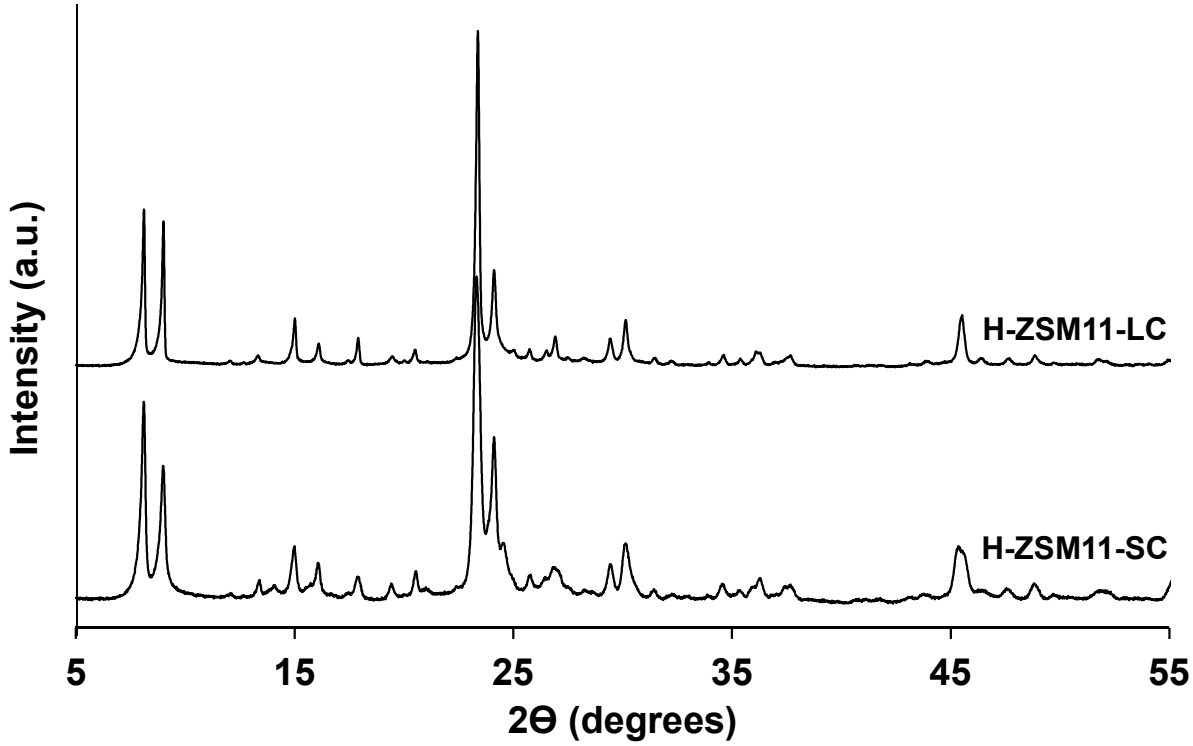

Figure 4.S2: Powder X-ray diffraction (XRD) patterns of H-ZSM11 samples. The spectra were taken in their final H-form of zeolite.

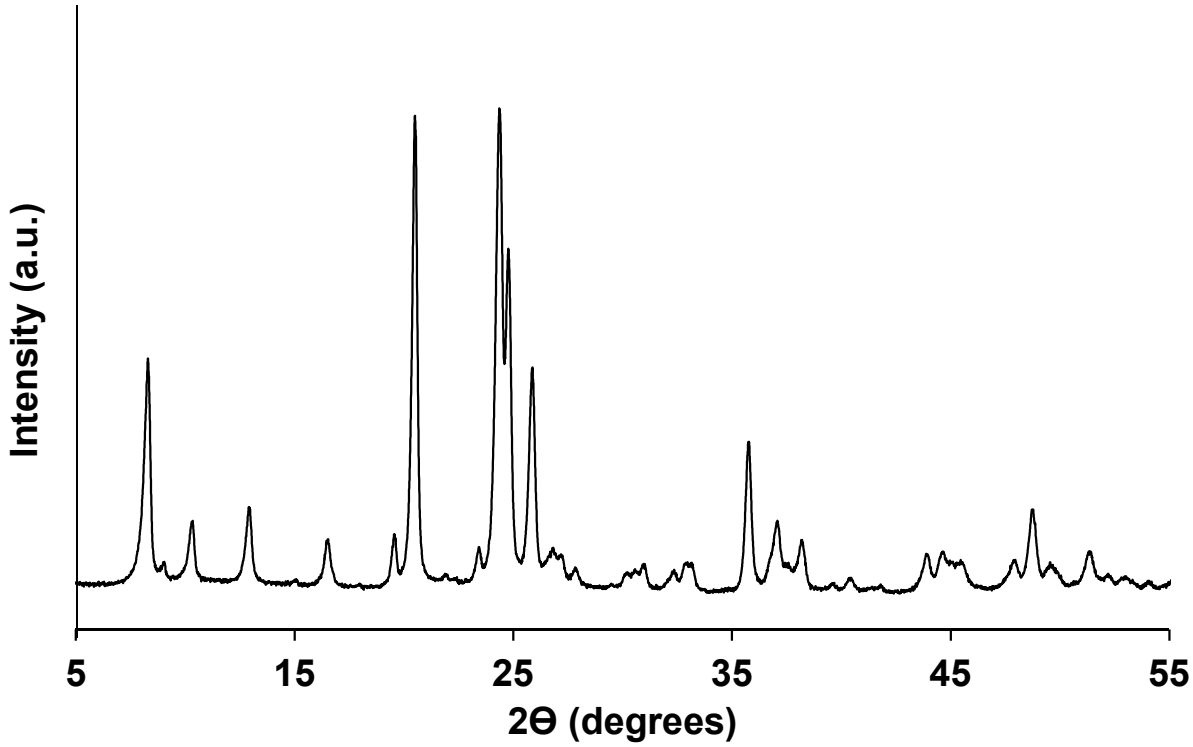

Figure 4.S3: Powder X-ray diffraction (XRD) patterns of H-NU10 sample. The spectrum was taken in its final H-form of zeolite.

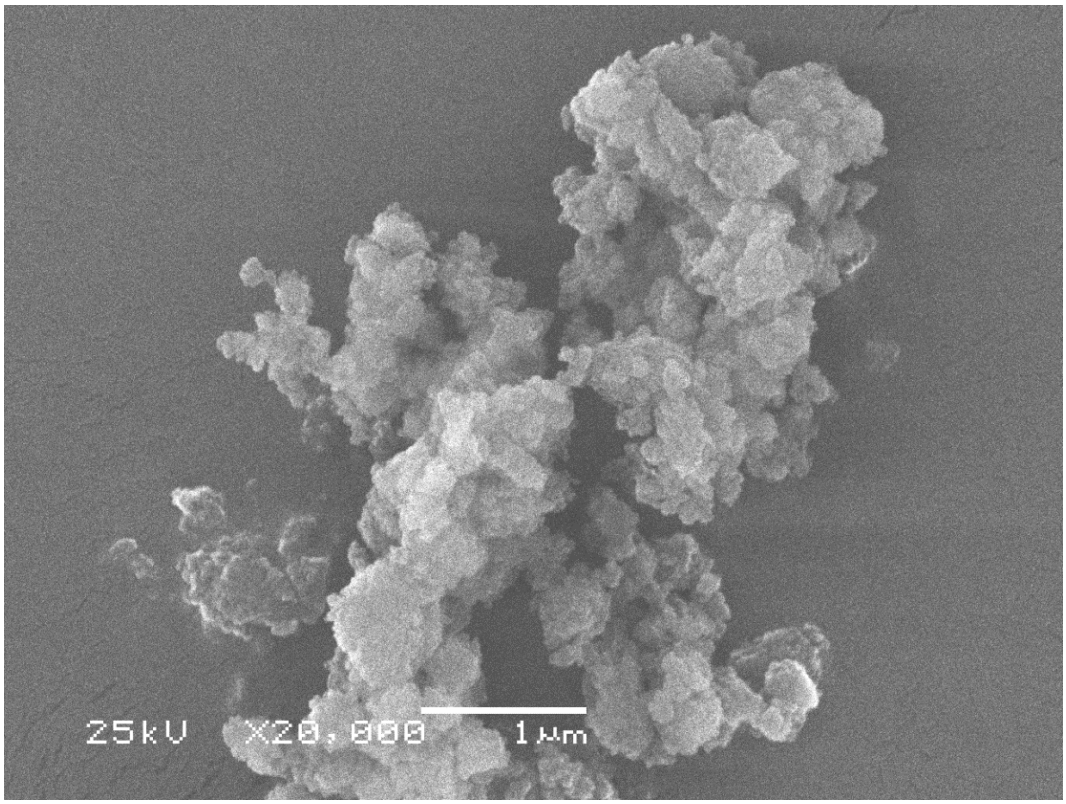

Figure 4.S4: Scanning electron microscope (SEM) image of H-ZSM5 sample.

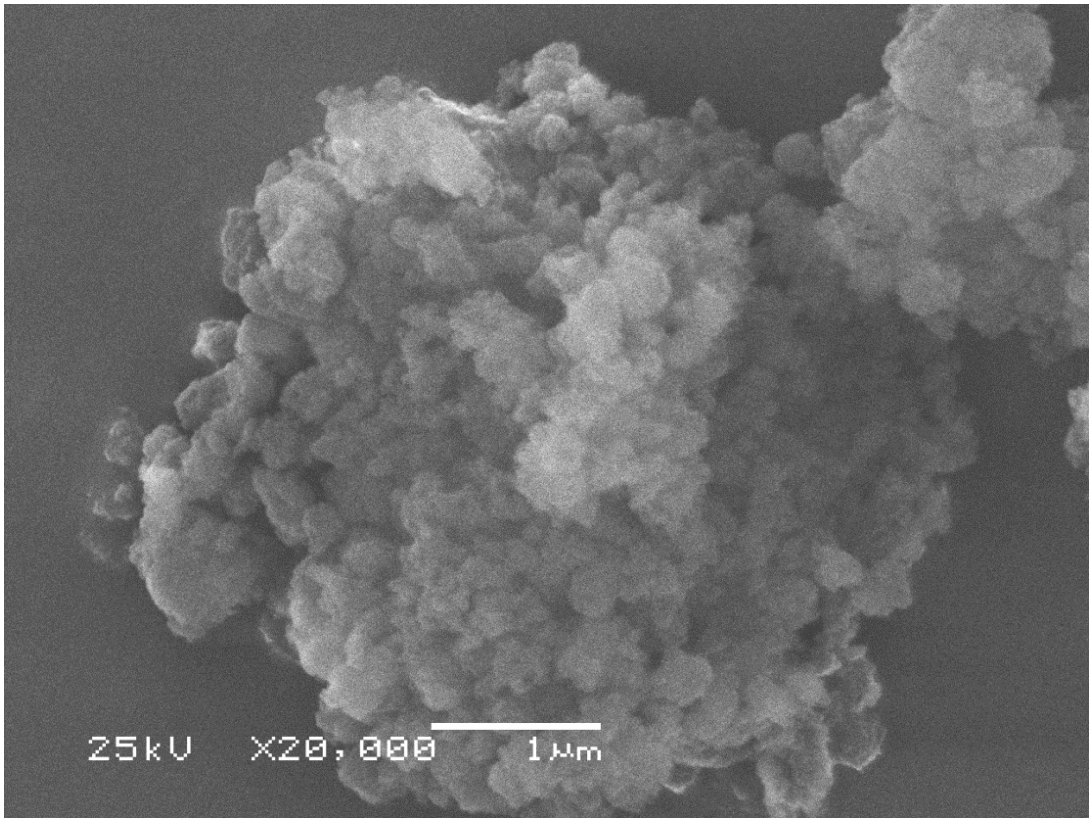

Figure 4.S5: Scanning electron microscope (SEM) image of H-ZSM5-SM sample (H-ZSM5 surface modified by tetraethyl orthosilicate (TEOS) deposition).

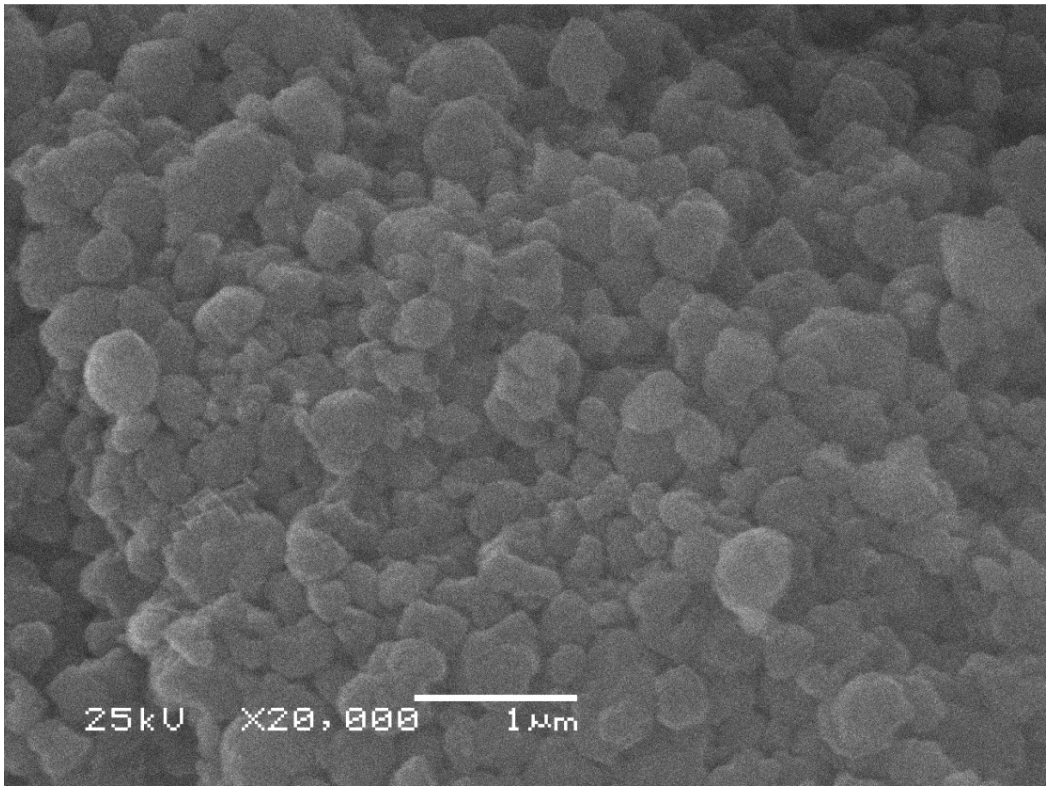

Figure 4.S6: Scanning electron microscope (SEM) image of H-Fe-ZSM5 sample (iron isomorphously substituted in the framework).

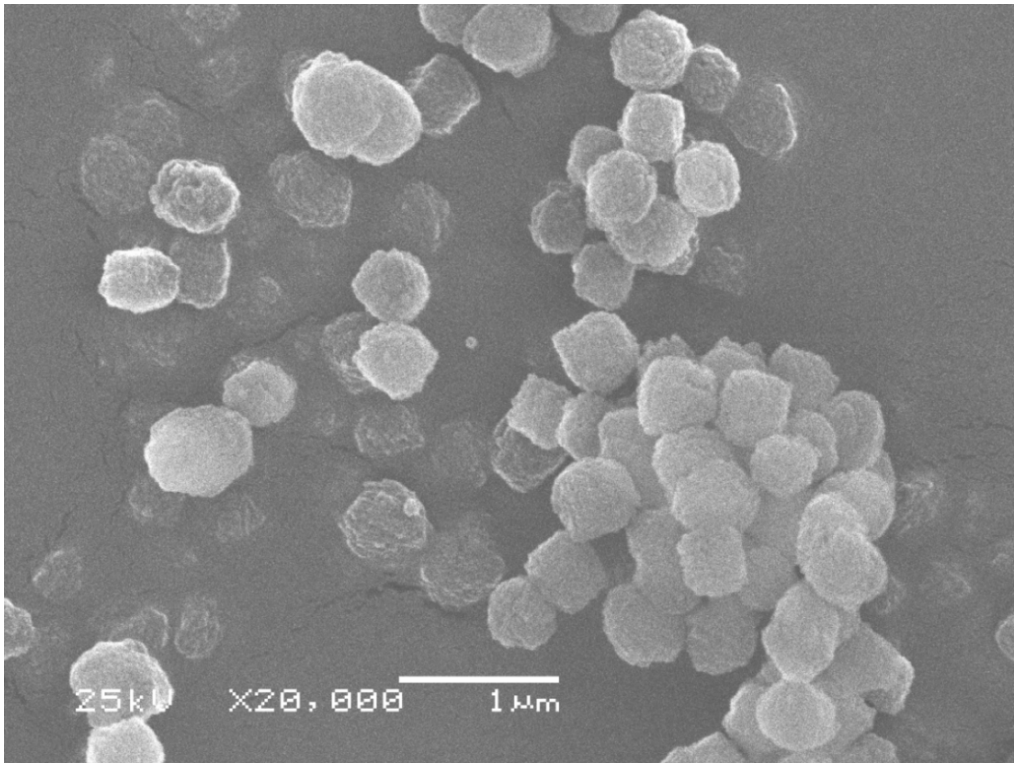

Figure 4.S7: Scanning electron microscope (SEM) image of H-ZSM11-SC sample (small crystal).

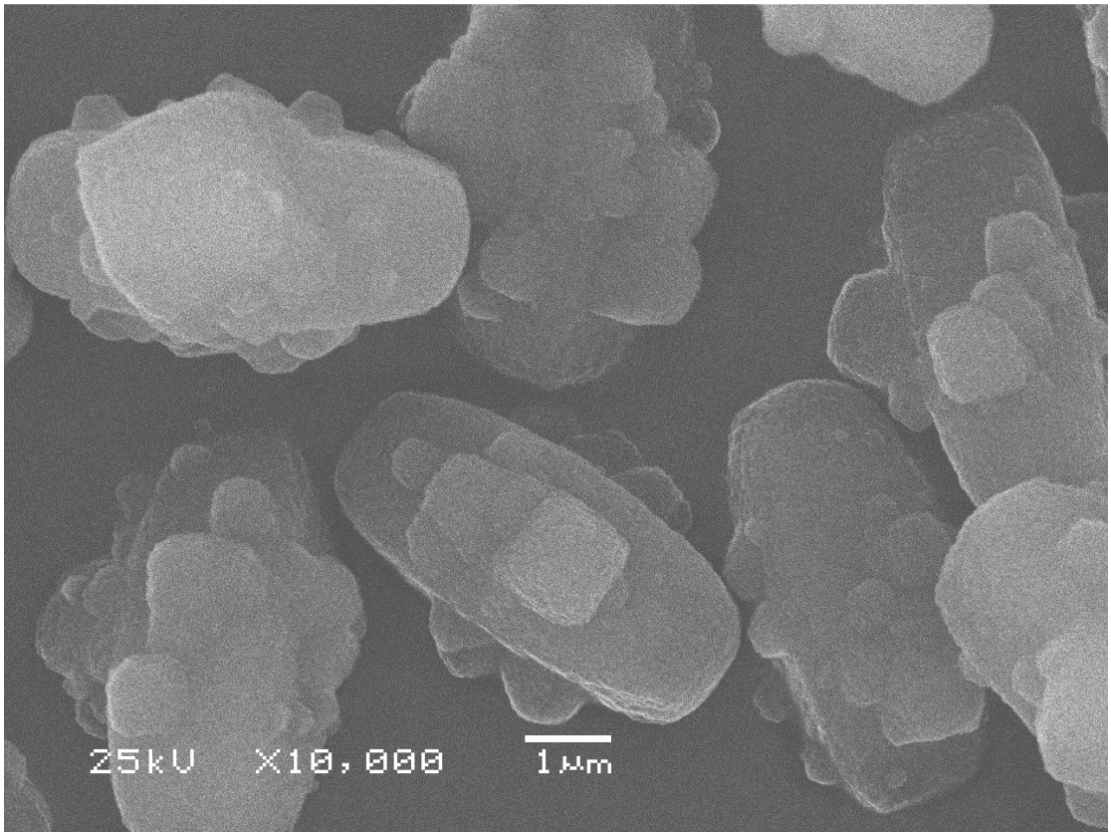

Figure 4.S8: Scanning electron microscope (SEM) image of H-ZSM11-LC sample (large crystal).

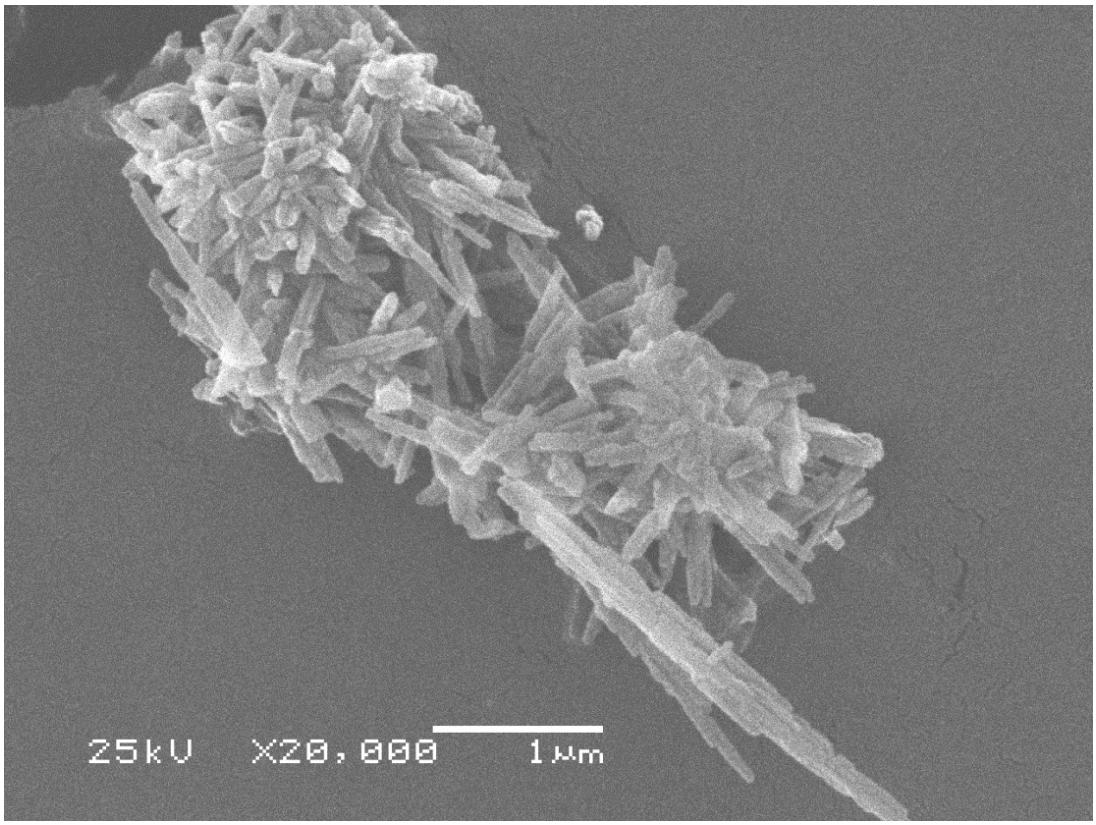

Figure 4.S9: Scanning electron microscope (SEM) image of H-NU10 sample.

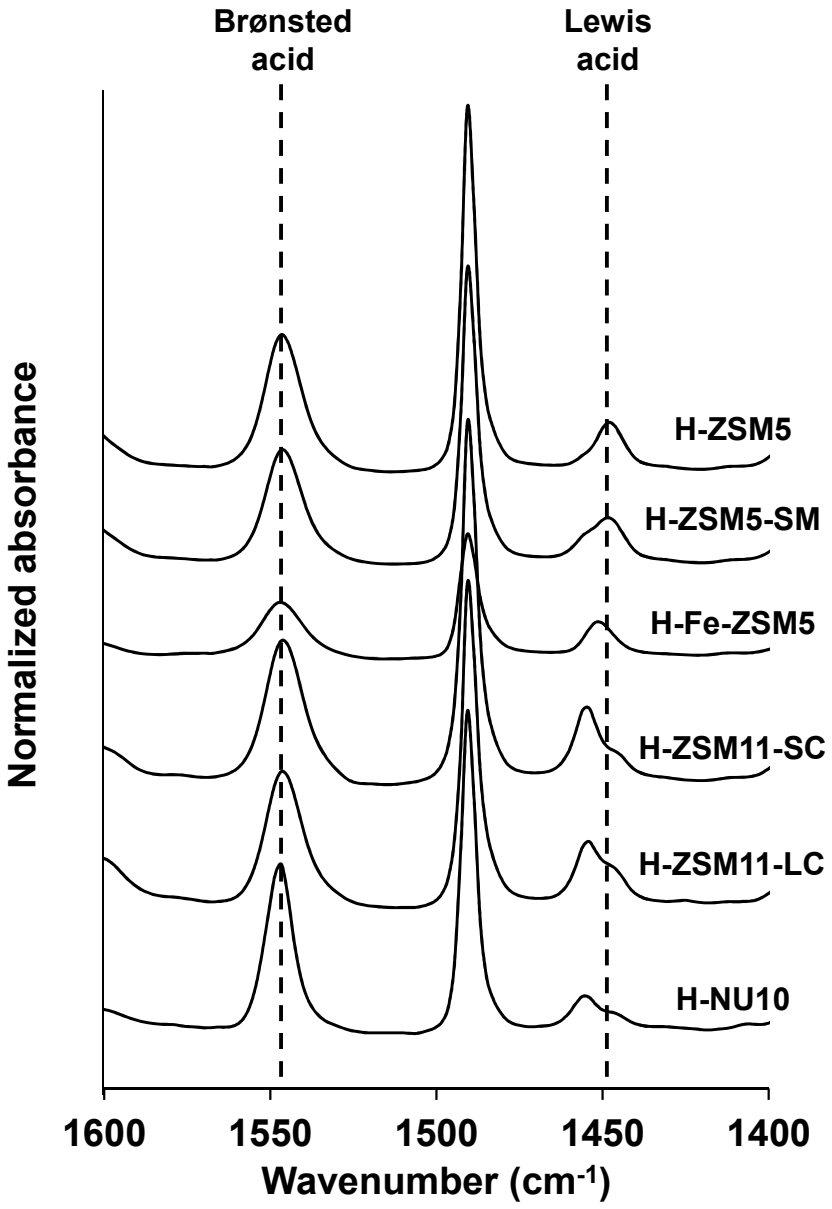

Figure 4.S10: Infrared (IR) spectra of all samples after adsorption of pyridine at 423 K, 0.01 kPa and outgassing for 1 hour under vacuum (spectra of the activated sample subtracted). The bands at 1545 cm^{-1} and ~1450 cm^{-1} represents Brønsted and Lewis acid site, respectively.

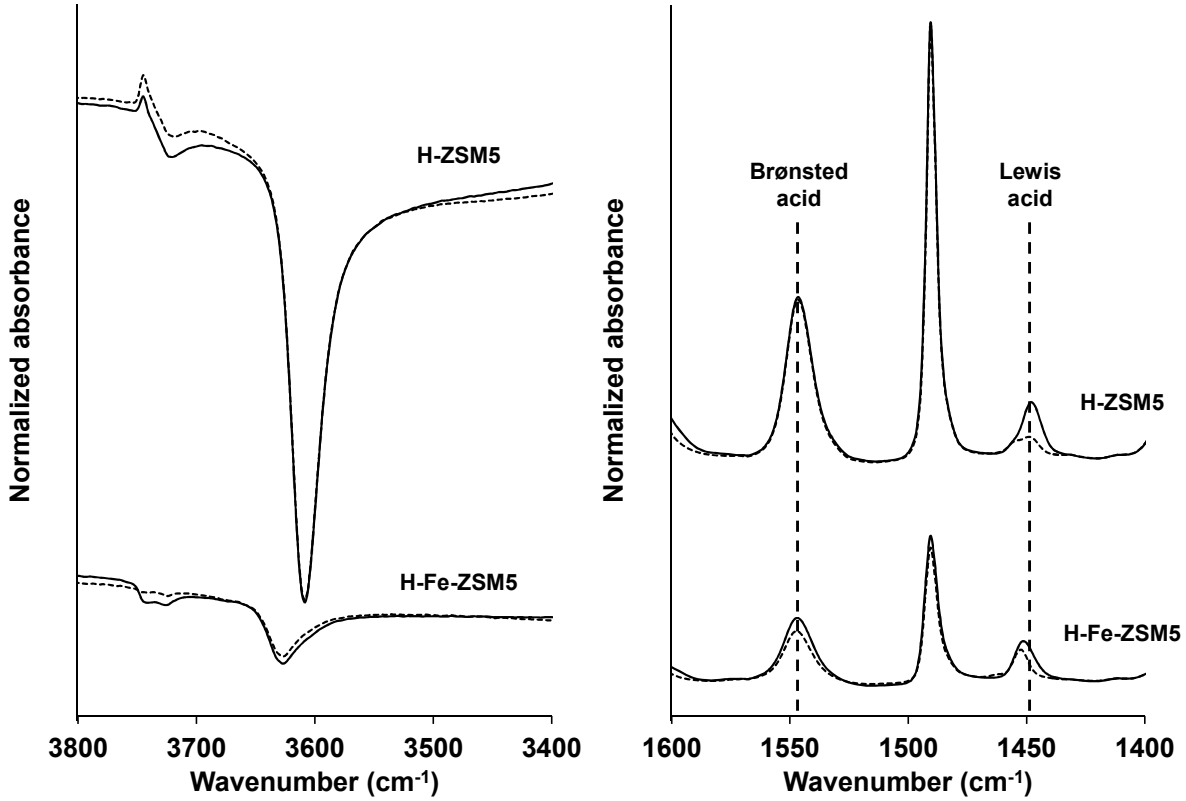

Figure 4.S11: Infrared (IR) spectra of H-ZSM5 and H-Fe-ZSM5 (iron isomorphously substituted in the framework). The solid lines represent the spectra after adsorption of pyridine at 423 K, 0.01 kPa and outgassing for 1 hour under vacuum. The dotted lines represent the spectra after additional outgassing at 723 K for 0.5 hour under vacuum. The spectra of the activated samples were subtracted from the spectra shown above. The bands at 1545 cm^{-1} and ~1450 cm^{-1} represents Brønsted and Lewis acid site, respectively.

Table 4.S1: C_1 (methanol and dimethyl ether) and toluene conversion at 573-723 K.

	573K		623K		673K		723K	
Conversion[a]	C_1	Toluene	C_1	Toluene	C_1	Toluene	C_1	Toluene
H-ZSM5	47	4.3	53	5.0	55	6.4	50	6.5
H-ZSM5-SM[b]	50	2.0	51	3.2	51	4.1	53	5.8
H-Fe-ZSM5	n/m[e]	n/m	52	4.8	54	4.9	52	5.2
H-ZSM11-SC[c]	50	6.3	53	6.5	51	7.1	52	7.5
H-ZSM11-LC[d]	52	1.1	51	2.0	56	3.4	53	5.1
H-NU10	n/m	n/m	53	1.0	48	2.3	50	3.3

[a]measured at $p_{toluene}$ = 6.0 kPa, $p_{methanol}$ = 1.5 kPa with 4-100 mg catalyst, total flow rate = 1.2-2.3 cm^3s^{-1}. [b]SM = surface modified by TEOS deposition. [c]SC = small crystal. [d]LC = large crystal. [e]Toluene methylation of H-Fe-ZSM5 and H-NU10 at 573K was not measured (n/m).

4.8. References

[1] T. Tsai, S. Liu, I. Wang, Applied Catalysis A: General 181 (1999) 355-398.

[2] S. Kulprathipanja, Zeolites in Industrial Separation and Catalysis, Wiley-VCH, Weinheim, 2010.

[3] W. Vermeiren, J.P. Gilson. Topics in Catalysis 52 (2009) 1131-1161.

[4] R.A. Meyers, Handbook of Petroleum Refining Processes, McGraw-Hill, USA, 2003.

[5] L.B. Young, S.A. Butter, W.W. Kaeding, J. Catal. 76 (1982) 418-432.

[6] O. Mikkelsen, P.O. Rønning, S. Kolboe, Micropor. Mesopor. Mater. 40 (2000) 95-113.

[7] G.A. Olah, Angew. Chem. Int. Ed. 44 (2005) 2636-2639.

[8] U. Olsbye, S. Svelle, M. Bjørgen, P. Beato, T.V.W. Janssens, F. Joensen, S. Bordiga, K.P. Lillerud, Angew. Chem. Int. Ed. 51 (2012) 2-24.

[9] R. D. Chirico, W.V. Steele, J. Chem. Eng. Data 42 (1997) 784-790.

[10] J.P. Breen, R. Burch, M. Kulkarni, D. McLaughlin, P.J. Collier, S.E. Golunski, Appl. Catal. A: General 316 (2007) 53-60.

[11] H. Vinek, G. Rumplmayr, J.A. Lercher, J. Catal. 115 (1989) 291-300.

[12] H.P. Röger, M. Krämer, K.P. Möller, C.T. O'Connor, Micropor. Mesopor. Mater. 21 (1998) 607-614.

[13] J.H. Ahn, R. Kolvenbach, S. S. Al-Khattaf, A. Jentys, J. A. Lercher, in preparation.

[14] J.H. Ahn, R. Kolvenbach, S. S. Al-Khattaf, A. Jentys, J. A. Lercher, submitted to ACS Catalysis.

[15] D.M. McCann, D. Lesthaeghe, P.W. Kletnieks, D.R. Guenther, M.J. Hayman, V. Van Speybroeck, M. Waroquier, J.F. Haw, Angew. Chem. Int. Ed. 47 (2008) 5179-5182.

[16] S. Zheng, A. Jentys, J.A. Lercher, J. Catal. 241 (2006) 304-311.

[17] Database of Zeolite Structures (http://www.iza-structure.org/databases/).

[18] S. Zheng, H.R. Heydenrych, A. Jentys, J.A. Lercher J. Phys. Chem. B 106 (2002) 9552-9558.

[19] P. De Luca, F. Crea, R. Aiello, A. Fonseca, J.B. Nagy, Stud. Surf. Sci. Catal. 105 (1997) 325-332.

[20] M. Derewinski, M. Machowska, Stud. Surf. Sci. Catal. 154 (2004) 349-354.

[21] A. Brückner, R. Lück, W. Wieker, B. Fahlke, H. Mehner, Zeolites 12 (1992) 380-385.

[22] A. Araya, B.M. Lowe, Zeolites 4 (1984) 280-286.

[23] M. Derewinski, M. Machowska, Stud. Surf. Sci. Catal. 154 (2004) 349-354.

[24] S. Brunauer, P. H. Emmett, E. Teller, J. Am. Chem. Soc. 60 (1938) 308-319.

[25] B.C. Lippens, B.G. Linsen, J.H. de Boer, J. Catal. 3 (1964) 32-37.

[26] G. Halsey, J. Chem. Phys. 16 (1948) 931-937.

[27] I.I. Ivanova, A. Corma, J. Phys. Chem. B 101 (1997) 547-551.

[28] S. Svelle, S. Kolboe, O. Swang, U. Olsbye, J. Phys. Chem. B 109 (2005) 12874-12878.

[29] S. Bordiga, R. Buzzoni, F. Geobaldo, C. Lamberti, E. Giamello, A. Zecchnia, G. Leofanti, G. Petrini, G. Tozzola, G. Vlaic, J. Catal. 158 (1996) 486-501.

[30] J. Pérez-Ramírez, J.C. Groen, A. Brückner, M.S. Kumar, U. Bentrup, M.N. Debbagh, L.A. Villaescusa, J. Catal. 232 (2005) 318-334.

[31] C.T.W. Chu, C.D. Chang, J. Phys. Chem. 89 (1985) 1569-1571.

[32] P. Mériaudeau, V.A. Tuan, L.N. Hung, V.T. Nghiem, C. Naccache, J. Chem. Soc., Faraday Trans. 94 (1998) 467-471.

[33] A. Chatterjee, T. Iwasaki, T. Ebina, A. Miyamoto, Micropor. Mesopor. Mater. 21 (1998) 421-428.

[34] N. Tøpsoe, K. Pedersen, E.G. Derouane, J. Catal. 70 (1981) 41-52.

[35] P.A. Jacobs, R. Von Ballmoos, J. Phys. Chem. 83 (1982) 3050-3052.

[36] F. Eder, M. Stockenhuber, and J. A. Lercher, J. Phys. Chem. B 101 (1997) 5414-5419.

[37] V.L. Zbolobenko, M.A. Makarova, J. Dwyer, J. Phys. Chem. 97 (1993) 5962-5964.

[38] W.W. Kaeding, C. Chu, L.B. Young, S.A. Butter, J. Catal. 69 (1981) 392-398.

[39] C. Fernandez, I. Stan, J. Gilson, K. Thomas, A. Vicente, A. Bonilla, J. Pérez-Ramírez, Chem. Eur. J. 16 (2010) 6224-6233.

[40] X. Cheng, X. Wang, H. Long, Micropor. Mesopor. Mater. 119 (2009) 171-175.

[41] D. Lesthaeghe, J. Van der Mynsbrugge, M. Vandichel, M. Waroquier, V. Van Speybroeck, Angew. ChemCatChem 3 (2011) 208-212.

[42] O.C. Gobin, S.J. Reitmeier, A. Jentys, J.A. Lercher J. Phys. Chem. C 113 (2009) 20435-20444.

[43] R. Kolvenbach, J. H. Ahn, S. S. Al-Khattaf, A. Jentys, J. A. Lercher, in preparation.

[44] P.B. Venuto, L.A. Hamilton, P.S. Landis, J.J. Wise, J. Catal. 4 (1966) 81-98.

[45] U. Olsbye, M. Bjørgen, S. Svelle, K. Lillerud, S. Kolboe, Catal. Today 106 (2005) 108-111.

Chapter 5

Summary and concluding remarks

Summary and concluding remarks

The reaction of toluene methylation has great potential to become a key process for increasing the production of p-xylenes in chemical industries. The endeavor of our work focused on investigating the technical challenges and improving the catalyst system by better understanding various limitations of this reaction. Herein, the topics regarding the utilization of methanol (Chapter 2), synthesis of hierarchical zeolites for simultaneous enhancement of catalyst activity and p-xylene selectivity (Chapter 3), and the influence of the reaction temperature on p-xylene selectivity (Chapter 4) during toluene methylation, were addressed in detail.

A significant fraction of methanol (i.e., >30%) was utilized to form products other than xylenes, e.g., light hydrocarbons, tri- and tetramethylbenzenes, during the toluene methylation reaction. Despite of using an excess of toluene relative to methanol (i.e., 4:1 molar ratios), the products of toluene methylation (e.g., xylenes and trimethylbenzenes) were readily methylated further inside the zeolite pores because the rate of methylation increased as the number of methyl substitution increased. These multi-methylated aromatic molecules eventually eliminated light hydrocarbons as a consequence of product shape selectivity. We therefore concluded from the work reported in chapter 2 that the inefficiency of methanol usage during toluene methylation was a consequence of the further methylation of the aromatic products of toluene, e.g., xylenes and trimethylbenzenes, and that the light hydrocarbons were unavoidable side-products from product shape selectivity.

A series of hierarchical materials were derived from a microporous MFI (H-ZSM-5) by desilication, dealumination and chemical liquid deposition of tetraethyl orthosilicate (TEOS) onto the zeolite surface. For the first time in the literature, the work in chapter 3 demonstrated that this sequence of zeolite modification can increase simultaneously the toluene consumption rate (per Brønsted acid site) and p-xylene selectivity. We concluded here that the consumption rate of toluene increased because the mesopores enhanced the diffusivity of the reactant and product molecules by decreasing the diffusion length. We further concluded that the increase in the selectivity of p-xylene within these hierarchical materials was not caused by the removal of unselective Brønsted acid sites in the pore mouth region, but predominantly by the diffusivity differences between p-xylene relative to o- and m-xylenes. TEOS deposition on the zeolite surface therefore, increased the p-xylene selectivity because diffusivity of the

bulkier o- and m- xylene isomers decreased, while it increased for p-xylene (the desired product).

The selectivity of p-xylene over medium pore-sized zeolites was further investigated in chapter 4 by examining three different major reaction pathways for the formation of p-xylene during toluene methylation, i.e., methylation of toluene, isomerization of xylenes, further methylation and subsequent elimination of less-methylated aromatic molecules as xylenes (and light hydrocarbons) from multi-methylated aromatics. In all these pathways, increasing the reaction temperature consistently resulted in higher p-xylene selectivity because the differences in diffusivities of xylenes i.e., between p-xylene and o-, m-xylenes, played more significant role in determining selectivity of xylenes, as the reactions (most importantly xylene isomerization) became faster at higher reaction temperature. We concluded, therefore, that the reaction of toluene methylation to p-xylene over medium pore-sized zeolites should be operated at high temperature because both the activity (reaction rates) and the selectivity of p-xylene can be increased simultaneously.